SRR-CWDA-2013-00062
Revision 2

FY2013 Special Analysis for the Saltstone Disposal Facility at the Savannah River Site

October 2013

Prepared by: Savannah River Remediation LLC
Closure and Waste Disposal Authority
Aiken, SC 29808

Prepared for U.S. Department of Energy Under Contract No. DE-AC09-09SR22505

REVISION SUMMARY

REV. #	DESCRIPTION	DATE OF ISSUE
0	Initial Issue to DOE-SR	June 11, 2013
1	Issue for LFRG Review	June 27, 2013
2	Issue with LFRG Comments Incorporated	October 2013

TABLE OF CONTENTS

LIST OF FIGURES

LIST OF TABLES

ACRONYMS/ABBREVIATIONS

ALARA	As Low As Reasonably Achievable
CBP	Cementitious Barriers Partnership
CFR	Code of Federal Regulations
CRESP	Consortium for Risk Evaluation with Stakeholder Participation
CSH	Calcium Silicate Hydrate
D&D	Deactivation and Decommissioning
DAS	Disposal Authorization Statement
DCF	Dose Conversion Factor
DLL	Dynamic Link Library
DOE	U.S. Department of Energy
DWPF	Defense Waste Processing Facility
ECN	Energy Research Center of the Netherlands
EPA	U.S. Environmental Protection Agency
FDC	Future Disposal Cell
GCL	Geosynthetic Clay Liner
GSA	General Separations Area
HDPE	High Density Polyethylene
HELP	Hydrologic Evaluation of Landfill Performance
IHI	Inadvertent Human Intruder
LHS	Latin Hypercube Sampling
LLW	Low-Level Waste
LXO	LeachXS/Orchestra
MCC	Moisture Characteristic Curve
MCL	Maximum Contaminant Level
MOP	Member of the Public
N/A	Not Applicable/Not Available
NDAA	National Defense Authorization Act
NIST	National Institute of Standards and Technology
NRC	U.S. Nuclear Regulatory Commission
PA	Performance Assessment
PRCC	Partially Ranked Correlation Coefficient
RAI	Request for Additional Information
SA	Special Analysis
SCDHEC	South Carolina Department of Health and Environmental Control
SRRC	Standardized Rank Regression Coefficient
SREL	Savannah River Ecology Laboratory
SRNL	Savannah River National Laboratory
SRS	Savannah River Site
SDF	Saltstone Disposal Facility
SDU	Saltstone Disposal Unit
SQAP	Software Quality Assurance Plan
SPF	Saltstone Production Facility
TER	Technical Evaluation Report

UTR	Upper Three Runs
UTRA-LZ	Upper Three Runs Aquifer-Lower Zone
UTRA-UZ	Upper Three Runs Aquifer-Upper Zone

Note: Figures and text throughout this document may abbreviate Special Analysis as SA.

EXECUTIVE SUMMARY

Special Analyses (SAs) are performed to evaluate the significance of new information or new analytical methods on the conclusions reached based on an approved performance assessment (PA). The evaluations documented in this SA provide further evidence to support that there is reasonable expectation/assurance that all applicable performance objectives associated with the operation and closure of the Savannah River Site (SRS) Saltstone Disposal Facility (SDF) will be met. Specific conclusions include that a roof slope variability of 1.5 % does not adversely impact dose results and that no restrictions on technetium-99 (Tc-99) disposal in Saltstone Disposal Units (SDU) 2, 3, and 5 outside the current PA envelope are required.

The SDF PA was prepared to assess whether there is reasonable expectation/assurance that the applicable performance objectives in the U.S. Department of Energy (DOE) Manual 435.1-1, Change 1, *Radioactive Waste Management Manual* as required by DOE Order 435.1, Change 1, *Radioactive Waste Management*, Chapter IV, and Title 10, of the Code of Federal Regulations (CFR) Part 61, *Licensing Requirements for Land Disposal of Radioactive Waste*, Subpart C as required by the *Ronald W. Reagan National Defense Authorization Act (NDAA) for Fiscal Year 2005*, Section 3116 will be met. [DOE M 435.1-1, DOE O 435.1, Chg. 1, 10 CFR 61, NDAA_3116] This SA has been prepared to evaluate new information that has been developed through the implementation of the Savannah River Site Liquid Waste Facilities Performance Assessment Maintenance Program (hereinafter referred to as SRS LW PA Maintenance Program) since the SDF PA was developed.

Requirements in DOE M 435.1-1 and 10 CFR 61 stipulate that there must be reasonable expectation/assurance that low-level waste (LLW) disposal facility operations and closure conditions must comply with specified performance objectives which include evaluation of impacts to hypothetical future members of the public (MOP) as well as inadvertent intruders. DOE M 435.1-1 also requires assessments for impacts to water resources. In both the SDF PA and this SA, evaluations focused on the DOE M 435.1-1 1,000-year compliance period. Evaluations of a 10,000-year performance period and model runs to 100,000 years after facility closure are also included to provide additional information in assessing compliance with performance objectives.

The evaluations contained within this SA take full advantage of new information that has been developed since the issuance of the SDF PA through the execution of the SRS LW PA Maintenance Program. This SA has been performed to evaluate the performance of the existing SDUs, SDU 1 and SDU 4 (referred to as Vaults 1 and 4 in the SDF PA), as well as the Future Disposal Cells (FDCs), in light of information not previously considered in analyses conducted to support the SDF PA, and in the responses to Requests for Additional Information (RAIs) issued by the U.S. Nuclear Regulatory Commission (NRC). [SRR-CWDA-2011-00044] Note that the term "Future Disposal Cell" was used in the SDF PA to describe the then newly designed cylindrical disposal cells (i.e., SDUs 2A/2B, 3A/3B, 5A/5B, and other future SDUs of this design). Since that time SDUs 2, 3 and 5 have been constructed and the cells of SDU 2 (Cells 2A and 2B) are actively receiving treated salt waste.

Information being considered in this SA includes SDU design features not previously considered, new information relating to the degradation of cementitious materials, new

information relating to the release of technetium from reducing environments within cementitious materials, and updated parameters relating to the dose pathway methodology. The radionuclide inventories used in this SA are based on the projected inventories presented in SDF PA, Tables 3.3-1, 3.3-3, and 3.3-5, (SRR-CWDA-2009-00017) as modified in the response to RAI PA-8 in SRR-CWDA-2011-00044, with no other constraints on the inventory of Tc-99 in SDUs 2, 3, and 5.

The radiological results presented in Sections 5 and 6 of this SA considered the new information through an Evaluation Case and other studies to confirm that the conclusions reached based on the SDF PA remain valid. The Evaluation Case was developed by selecting parameters values (creating a conservative operational envelope) that were most probable and defensible considering the new information available. The uncertainty and sensitivity analyses generally address the impact that variability surrounding key parameters has on dose results. The Evaluation Case and other sensitivity studies specifically address select NRC issues from the *Technical Evaluation Report (TER) For the Revised Performance Assessment for the Saltstone Disposal Facility at the Savannah River Site*, *South Carolina* and the associated Type IV Letter. [ML121170309, ML120650576] For example, the Evaluation Case in this SA considers explicit SDU design features not previously modeled (e.g., construction joints, columns within the saltstone monolith, presence of the roof support trusses in SDU 4), degradation of cementitious materials based on the latest models from the Cementitious Barrier Partnership (CBP) and other analytical models, and the latest laboratory testing results on saltstone hydraulic conductivity. In addition, in this SA, the release and transport of Tc-99 is based on solubility (1.0E-08 mol/L in the Evaluation Case) when the cementitious material is reduced and reverts to a K_d-controlled transport with a K_d value of 0.5 mL/g when the cementitious material is oxidized. The consumption of slag (reduction capacity) is modeled explicitly in PORFLOW by tracking the amount of oxygen and slag in each nodal element in the model as the dissolved oxygen from inflowing water consumes the reducing capacity in the cementitious material.

This SA provides updated individual dose results based on the Evaluation Case modeling using the SDU radiological inventories provided in the SDF PA, as amended in the response to RAI PA-8 provided in SRR-CWDA-2011-00044, and information following closure regarding radiological modeling. Additional sensitivity studies were performed based on a revised technetium waste release model and updated radiological transport parameters. The results of this SA can be used in concert with the SDF PA in subsequent documents to demonstrate that there is reasonable expectation/assurance that applicable performance objectives will be met within the DOE M 435.1-1 1,000-year compliance period. The NRC typically uses a 10,000-year performance period when evaluating the 10 CFR 61 performance objectives. Evaluations to 10,000 years and beyond are included in the SA for additional information. Table ES.0-1 provides a summary of dose results. Note that DOE M 435.1-1 results reflect a 1,000-year compliance period and 10 CFR 61 results reflect a 10,000-year performance period.

Table ES.0-1: Comparison of SA Dose Results with Performance Objectives

Performance Objective			Peak Dose
DOE M 435.1-1	All-Pathways Dose	25 mrem/yr	0.04 mrem/yr
DOE M 435.1-1	Intruder Dose-chronic	100 mrem/yr	0.4 mrem/yr
10 CFR 61.41	All-Pathways Dose	25 mrem/yr	12 mrem/yr
10 CFR 61.42	Intruder Dose	Normally 500 mrem/yr	39 mrem/yr

During the 1,000-year compliance period, the peak groundwater pathways dose to the MOP is 0.04 mrem/yr at the year 1,000, with the dose dominated by the release of I-129 and Tc-99 from SDU 4. The highest overall peak groundwater pathways dose in the 10,000-year performance period is 12 mrem/yr and is dominated by I-129 release from the cylindrical SDUs. Figure ES.0-1 presents the contributors to the 100-meter peak groundwater pathway doses for the 12, 100-meter sectors for 10,000 years following facility closure. Figure ES.0-2 shows the contributors to the 100-meter peak groundwater pathway doses from 10,000 to 20,000 years. As can be seen from these figures, I-129 is the peak dose driver at 10,000 years, with Tc-99 controlling at 20,000 years.

Figure ES.0-1: Contributors to the 100-Meter Peak Groundwater Pathways Dose within 10,000 Years

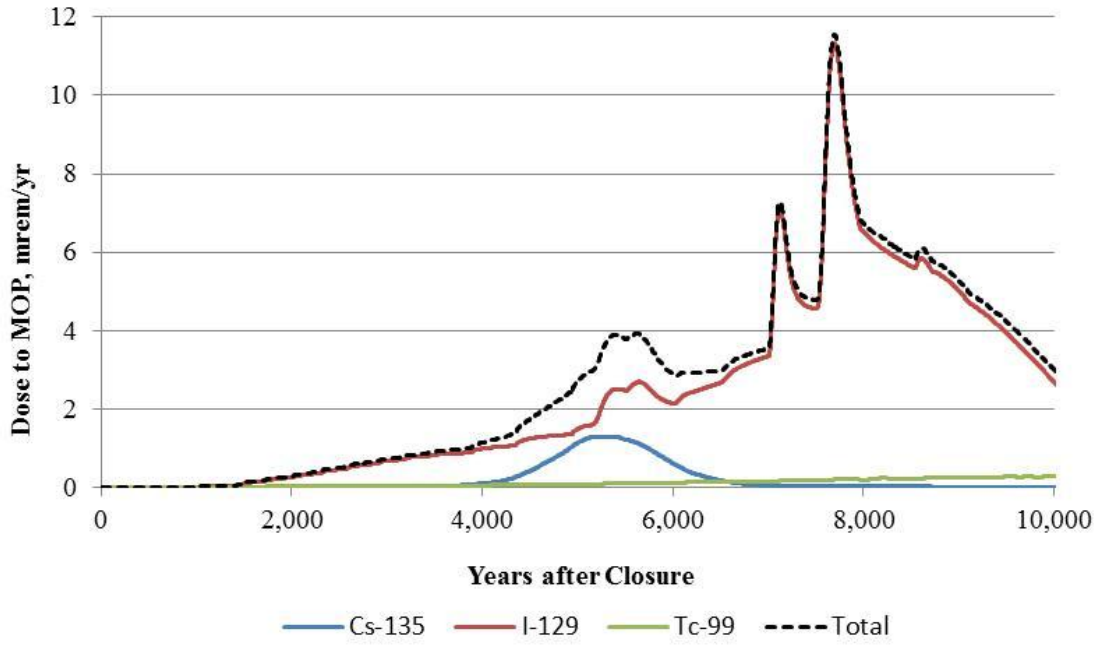

Figure ES.0-2: Contributors to the 100-Meter Peak Groundwater Pathways Dose, 10,000 Years - 20,000 Years

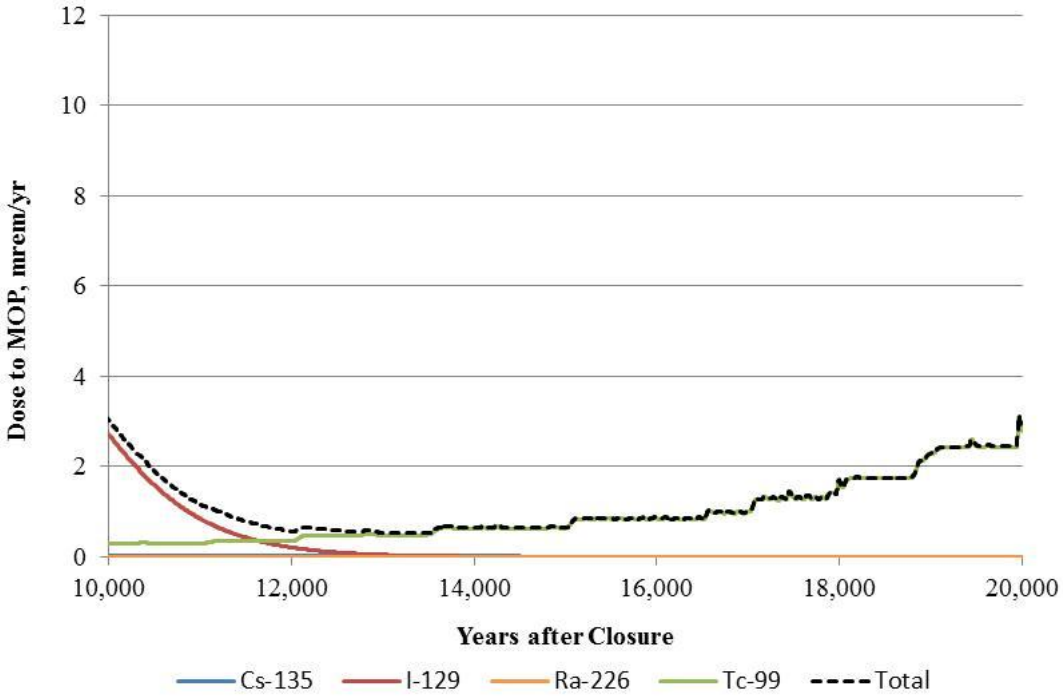

The various uncertainty and sensitivity analyses combine with the Evaluation Case to illustrate that the SDF dose results are not significantly impacted even using more conservative inputs, providing greater confidence that the results and conclusions remain valid. Uncertainty and sensitivity analyses were performed via probabilistic analyses using the GoldSim computer code. The probabilistic sensitivity analysis was supplemented with multiple deterministic sensitivity analyses using the PORFLOW code. The probabilistic sensitivity analysis identified important factors that affect the SDF dose results. In addition, the various deterministic sensitivity analyses included flow variability, roof slope variability, and Tc-99 parameter sensitivities. These analyses provide confidence that the SDF operation and closure, as modeled, will meet performance objectives. The roof slope variability analysis demonstrated that the dose results would not be adversely impacted by a roof slope of 1.5 %. The multiple sensitivity analyses performed regarding Tc-99 specific parameters demonstrate the dose results would meet performance objectives even assuming more conservative Tc-99 release assumptions. The analyses concerning Tc-99 also demonstrate no additional restrictions are needed on Tc-99 beyond the inventory currently considered in the SDF PA envelope.

The SA results provide reasonable expectation/assurance that compliance is maintained with the applicable requirements of DOE M 435.1-1 and 10 CFR 61. The additional sensitivity and uncertainty analyses performed using the lessons learned regarding radiological waste release modeling provide further confidence. The results presented in the SDF PA reflecting SDF final operational closure radiological inventories are not significantly impacted by new information and parameters presented in this SA; therefore, there is no driver to impose additional restrictions on the disposed inventory of Tc-99.

1.0 SPECIAL ANALYSIS HISTORY/PURPOSE

1.1 History

A PA was prepared and issued in October 2009 to support the operation and eventual closure of the SDF, located in Z Area in the central region of the SRS. [SRR-CWDA-2009-00017] The SDF PA was prepared to demonstrate compliance with the pertinent requirements of DOE O 435.1, Chg. 1, DOE M 435.1-1, and 10 CFR Part 61, Subpart C as required by NDAA Section 3116.

Requirements in DOE M 435.1-1 and 10 CFR 61 stipulate that a PA should provide reasonable expectation/assurance that LLW disposal will comply with specified performance objectives. DOE M 435.1-1 and 10 CFR 61 both require assessments of impacts to MOP and inadvertent human intruders. DOE M 435.1-1 also requires assessments for impacts to water resources.

After approval by DOE and upon initial review of the SDF PA, the NRC issued RAIs in March 2010 (ML100820097) for which DOE provided a response (SRR-CWDA-2010-00033) in July 2010. In December 2010, the NRC provided a second set of RAIs (ML103400571), for which responses (SRR-CWDA-2011-00044) were provided by DOE to the NRC in August 2011.

Subsequent to the review of the second set of RAI responses, the NRC issued a *Technical Evaluation Report (TER) For the Revised Performance Assessment for the Saltstone Disposal Facility at the Savannah River Site, South Carolina* (ML121170309). The NRC TER concludes that current proposed disposal activities for salt waste may result in releases that exceed the performance objective in §61.41 of 10 CFR Part 61, for the protection of the general population at a time much greater than 1,000 years, but within 10,000 years. Based on the results of this TER, in April 2012, the NRC issued a Type IV letter (ML120650576) of concern indicating that the performance objective in §61.41 may not be met.

The DOE issued a Disposal Authorization Statement (DAS) transmittal letter in May 2012 for the SDF, dated May 22, 2012, with a stipulation that a sensitivity analysis be performed to ensure that the performance objective in §61.41 of 10 CFR Part 61 is met. [WDPD-12-49] In response to the DAS, a sensitivity analysis (SRR-CWDA-2012-00103) was prepared that assumed the inventory of Tc-99 in the six newly constructed cylindrical SDUs to be approximately four times less than modeled in the SDF PA, based on anticipated salt waste processing and disposal activities. The sensitivity analysis also assumed that the Tc-99 inventory in SDU 1 was twice the current inventory to account for future potential disposal activities. The Tc-99 inventory in SDU 4 was assumed to be limited to the current Tc-99 inventories. DOE considered the actions defined in WDPD-12-49 complete as documented in WDPD-12-66.

1.2 Purpose

Through the SRS LW PA Maintenance Program, additional information has been collected and evaluated (e.g., solubility information) subsequent to the issuance of the SDF PA in 2009. Pursuant to DOE processes and based on the amount of new technical data generated as part of the SRS LW PA Maintenance Program, such as data related to technetium release mechanisms and cementitious material properties, it is appropriate to develop this SA. The SA does not repeat all information presented in the SDF PA, but will present and model changes to ensure the

requirements of DOE O 435.1 and its associated manual and guide and 10 CFR 61 are met. The primary purposes of this SA are to:

1. Justify disposal of Tc-99 inventory presented in the SDF PA (SRR-CWDA-2009-00017)
2. Address the NRC concerns as presented in the TER (ML121170309)

For this SA, the average modeled Tc-99 inventory for each of the future SDUs is assumed to be the same as projected in the SDF PA (i.e., 540 curies of Tc-99 per FDC). [SRR-CWDA-2009-00017] The release and transport of Tc-99 is controlled by solubility when the cementitious material is reduced, and reverts to a K_d-controlled transport when the cementitious material becomes oxidized. The consumption of slag (reduction capacity) is modeled explicitly in PORFLOW by tracking the amount of oxygen and slag in each nodal element in the model as the dissolved oxygen from inflowing water oxidizes the cementitious material.

In addition, this SA considers explicit design features that were not previously modeled. This includes features such as construction joints, columns within the saltstone monolith, and presence of the roof support trusses in SDU 4. This SA also incorporates new information related to the degradation of cementitious materials based on the latest models from the CBP and other analytical models, and the latest laboratory testing results on saltstone hydraulic conductivity.

In this SA, dose results are presented both deterministically and stochastically to support that reasonable expectation/assurance exists that the predicted dose to the MOP will meet all performance objectives in DOE M 435.1-1 and 10 CFR Part 61.

2.0 BASIS

The Maintenance Guide for U.S. Department of Energy Low-Level Waste Disposal Facility Performance Assessments and Composite Analyses (DOE_11-10-1999) recognizes that conduct of a PA is not a static process, and states that,

> *"Special analyses are expected to be needed as part of the routine maintenance of the performance assessment." As described in the maintenance guide, "special analyses are analyses performed to evaluate the significance of new information or new analytical methods to the results of the performance assessment, or to supplement or amend the analyses performed in the original performance assessment. A special analysis is not the same as a revision to the performance assessment, but the results of the special analysis may be used to determine whether a performance assessment revision is needed."*

As stated in the maintenance guide, a number of different factors may prompt a SA.

The guide also states that,

> *"the purpose of conducting special analyses can be thought of as similar to the process for resolving unreviewed safety questions described in the DOE Order 5480.21, Unreviewed Safety Questions. The intent of the process is to provide flexibility in day-to-day operations and to require those issues with a significant impact on the performance assessment's conclusions, and therefore the projected compliance with performance objectives, to be proper level for attention."* [DOE_11-10-1999]

Based on the amount of new technical data generated as part of the SRS LW PA Maintenance Program in areas such as technetium release mechanisms and cementitious material properties, it is appropriate to develop this SA. This SA does not repeat all information presented in the SDF PA, but will discuss any model changes to ensure the applicable requirements of DOE O 435.1 and its associated manual and guide and 10 CFR 61 are met.

3.0 DISPOSAL FACILITY BACKGROUND INFORMATION

3.1 Savannah River Site Characteristics

SRS is owned by the Federal government and is managed by the DOE. Construction of SRS started in the early 1950s to produce nuclear materials (Pu-239 and tritium). SRS is located in south-central South Carolina, approximately 100 miles from the Atlantic Coast. The major physical feature at SRS is the Savannah River, which serves as the southwestern boundary of the site along the South Carolina-Georgia border. SRS encompasses portions of Aiken, Barnwell, and Allendale Counties in South Carolina. SRS occupies an almost circular area of approximately 310 square miles and contains production, service, and research and development areas. The developed areas occupy less than 10 % of the SRS area while the remainder of the site is undeveloped forest or wetlands. The site is approximately 12 miles south of Aiken, South Carolina, and 15 miles southeast of Augusta, Georgia, as shown in Figure 3.1-1.

Figure 3.1-1: Physical Location of Savannah River Site

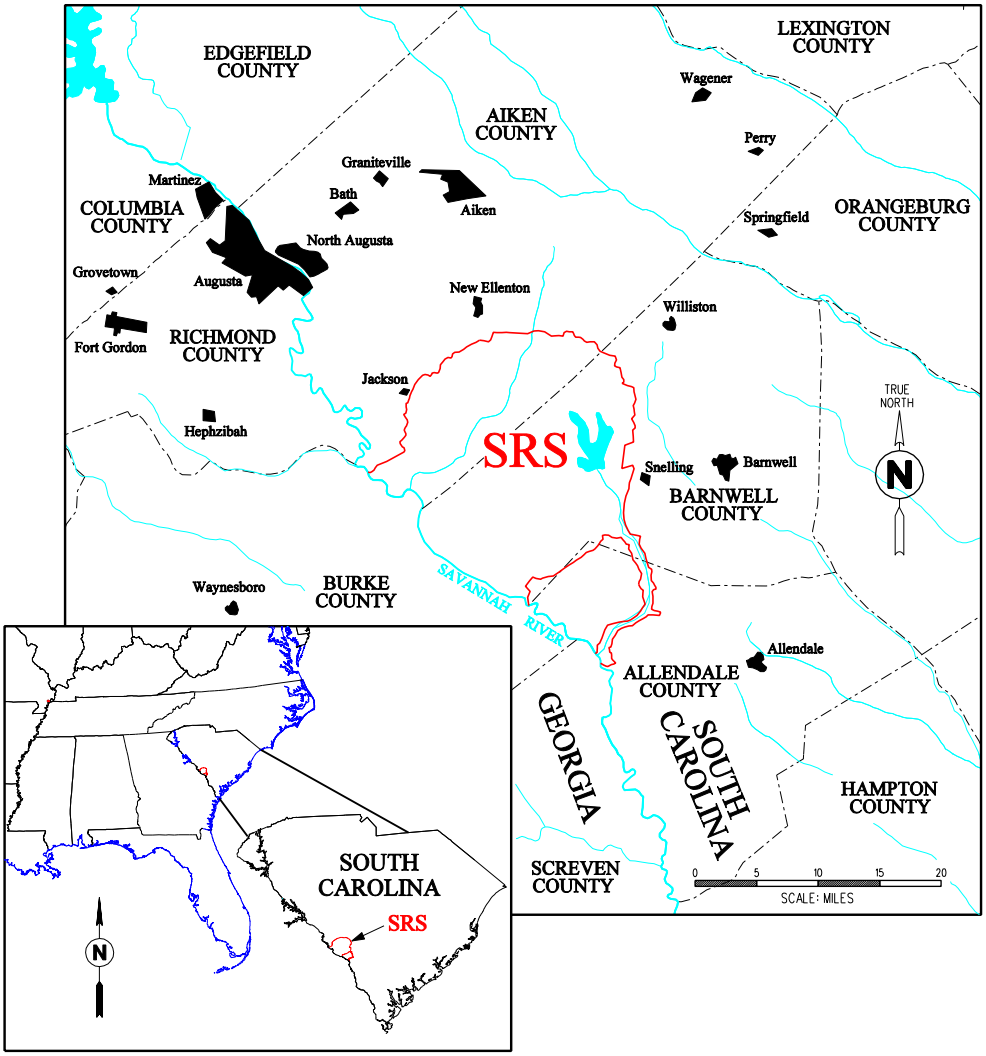

Prominent geographic features within 30 miles of SRS include the Savannah River and Thurmond Lake (also known as Clarks Hill Lake), shown in Figure 3.1-2. The Savannah River forms the southwest boundary of SRS and Clarks Hill Lake is the largest nearby public recreational area, which lies on the Savannah River approximately 40 miles upstream of the center of SRS.

Figure 3.1-2: Location of SRS and Adjacent Areas

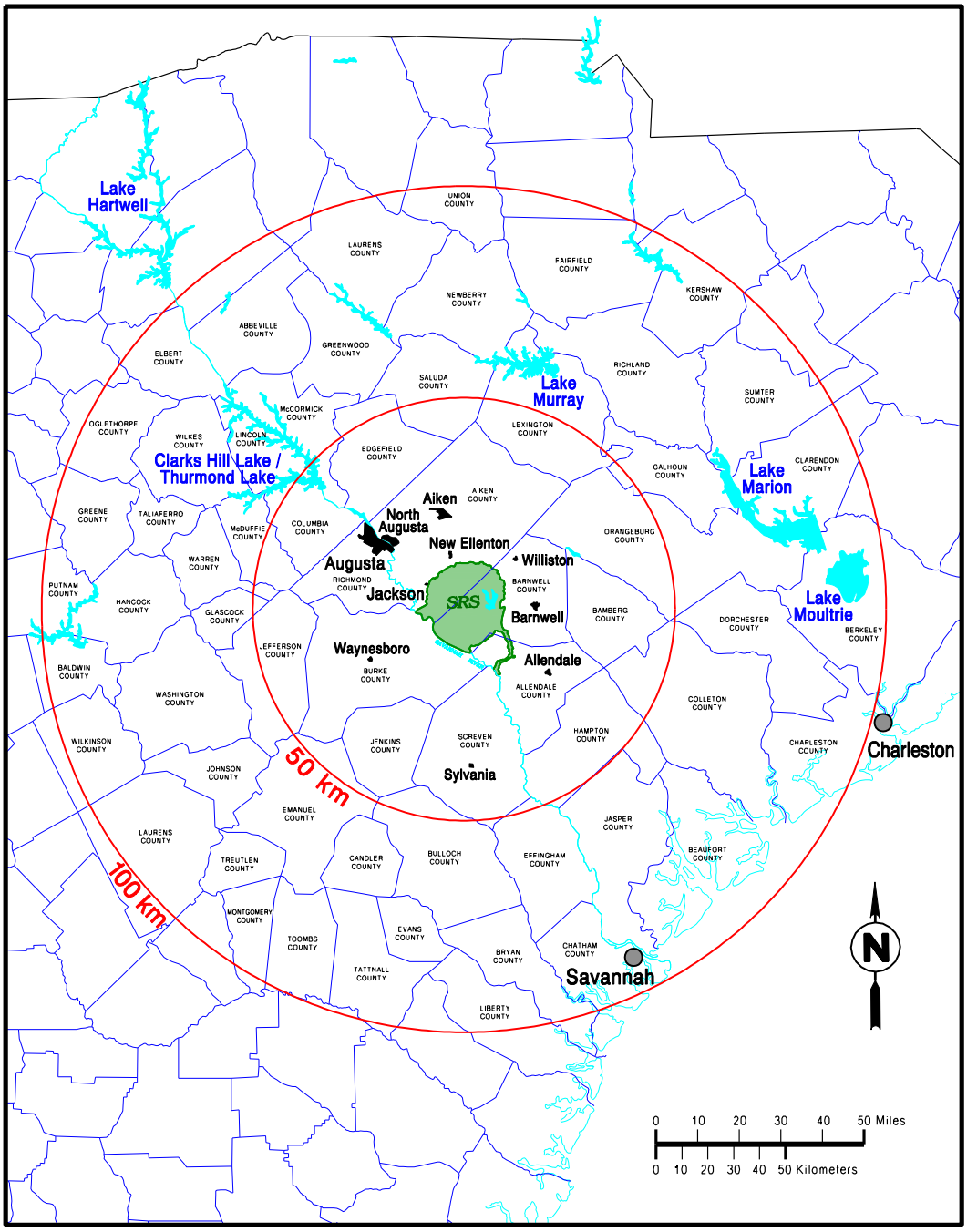

Within the SRS boundary, prominent water features include PAR Pond and L Lake, shown in Figure 3.1-3. PAR Pond, a former reactor cooling water impoundment, covers approximately 2,700 acres and lies in the eastern sector of SRS. L Lake, another former reactor cooling water impoundment, covers approximately 1,000 acres and lies in the southern sector of SRS.

Figure 3.1-3: SRS Operational Area Location Map

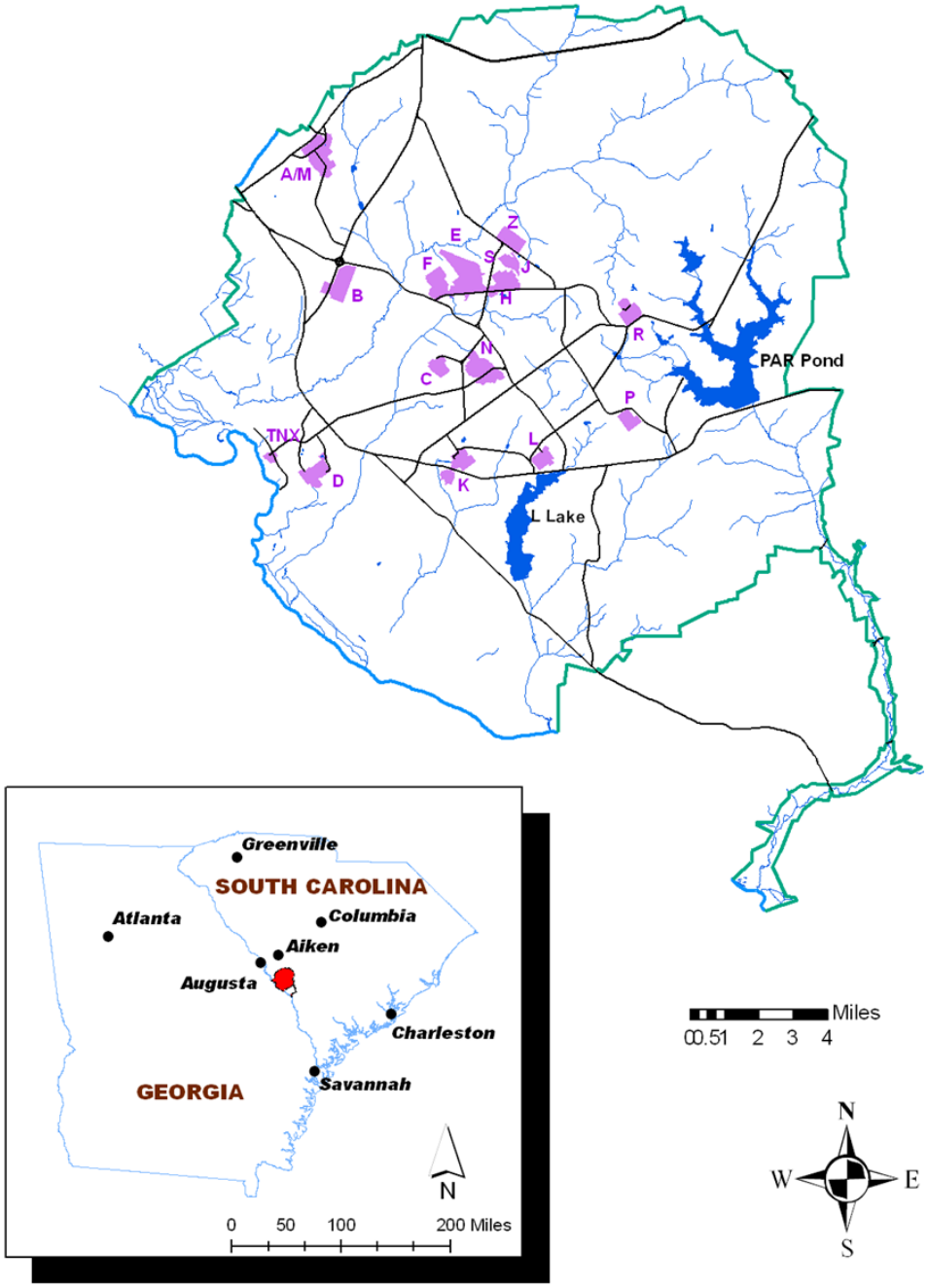

Figure 3.1-3 also shows the major operational areas at SRS. Prominent operational areas, both past and present, include Separations Areas (F and H), Waste Management Operations Areas (E, F, and H), Reactor Areas (C, K, L, P, R), and Defense Waste Processing Areas (S and Z). The Savannah River National Laboratory (SRNL) and Savannah River Ecology Laboratory (SREL) are located in A Area. Administrative and support services are located in B Area and construction administration activities are located in N Area. M Area, D Area, and TNX have undergone Deactivation and Decommissioning (D&D).

Additional site characteristics are addressed in Section 3.1 of the SDF PA. Topics addressed in Section 3.1 of the SDF PA include geography, demography, meteorology, climatology, ecology, geology, seismology, hydrogeology, geochemistry, and natural resources and have not significantly changed since publication. [SRR-CWDA-2009-00017]

3.2 Saltstone Disposal Facility Description

Evaluation of radionuclide transport from the SDF, and of human exposure resulting from the release of hazardous chemicals and radionuclides into the environment, requires careful consideration of factors affecting transport processes and exposure potential. Topographic features and hydrogeologic characteristics strongly affect the direction and flow of contaminants potentially released from the closure site. Projected land use and population distributions affect the estimation of human exposure. In this section, the relevant natural and demographic characteristics of Z Area as it relates to the SRS and the surrounding area are discussed.

The Saltstone Facility is located in Z Area, which is in the central region of SRS. Figure 3.2-1 presents the area known as the General Separations Area (GSA). The GSA is located atop a ridge running southwest-northeast that forms the drainage divide between Upper Three Runs (UTR) to the north and Fourmile Branch to the south. The GSA contains the F- and H-Area Separations Facilities, the S-Area Defense Waste Processing Facility (DWPF), the Z-Area Saltstone Facility, and the E-Area LLW Facility. Z Area consists of approximately 161 acres and is situated northeast of DWPF. The SDF is permitted as a Class 3 Landfill per South Carolina Department of Health and Environmental Control (SCDHEC) regulations. [DHEC_09-09-2008]

Figure 3.2-1: Layout of the GSA

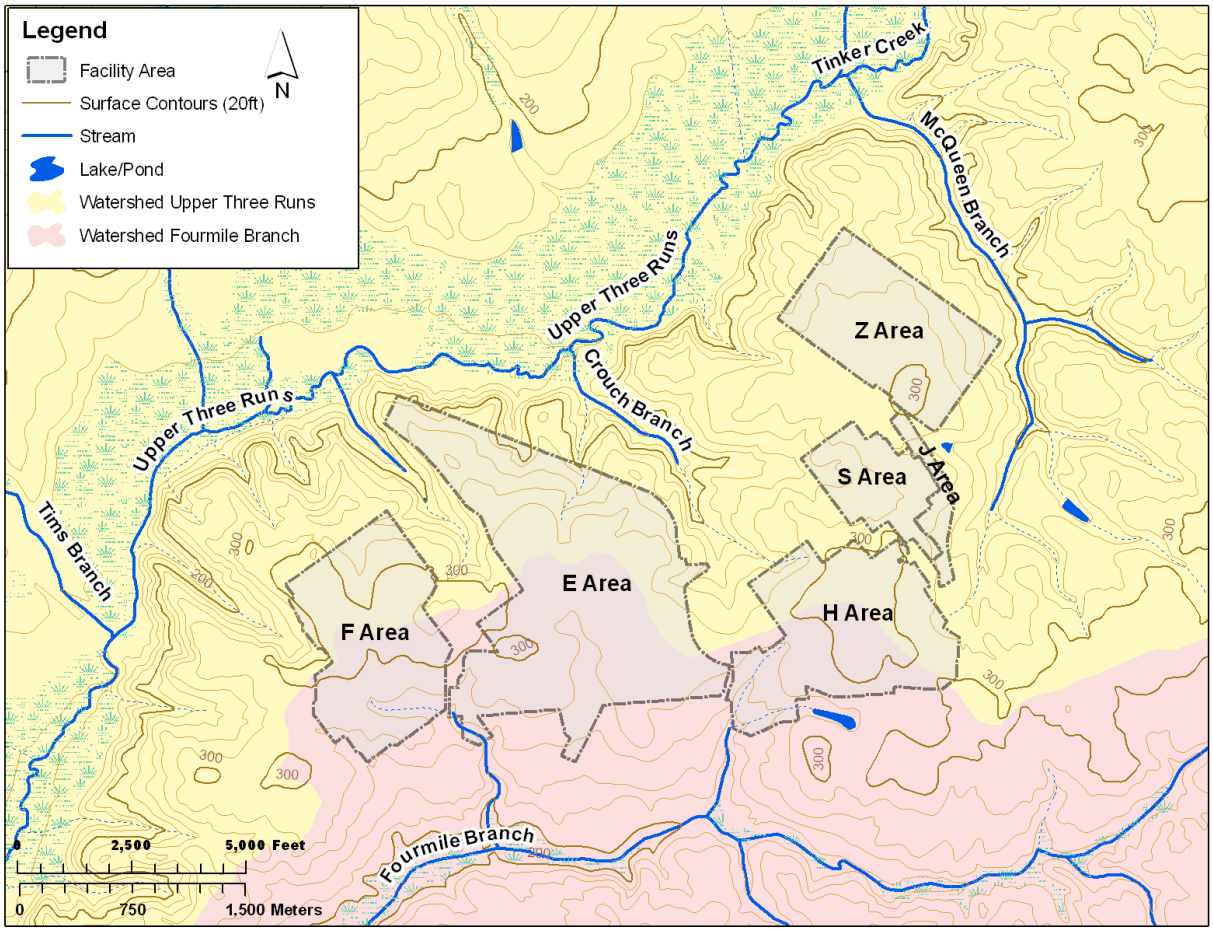

SDU capacities and configurations are subject to change prior to permitting and construction. If design changes are significant, SAs or a revised PA will be developed and approved prior to use to validate that there is still reasonable expectation/assurance performance objectives will be met. Figure 3.2-2 illustrates the layout of the SDF as it was modeled for the SDF PA and this SA. Note that while the figure presents anticipated configuration the design of the units serve as placeholders and may not match the final disposal cell configurations.

Figure 3.2-2: Layout of SDUs and FDCs as Modeled in SDF PA and SA

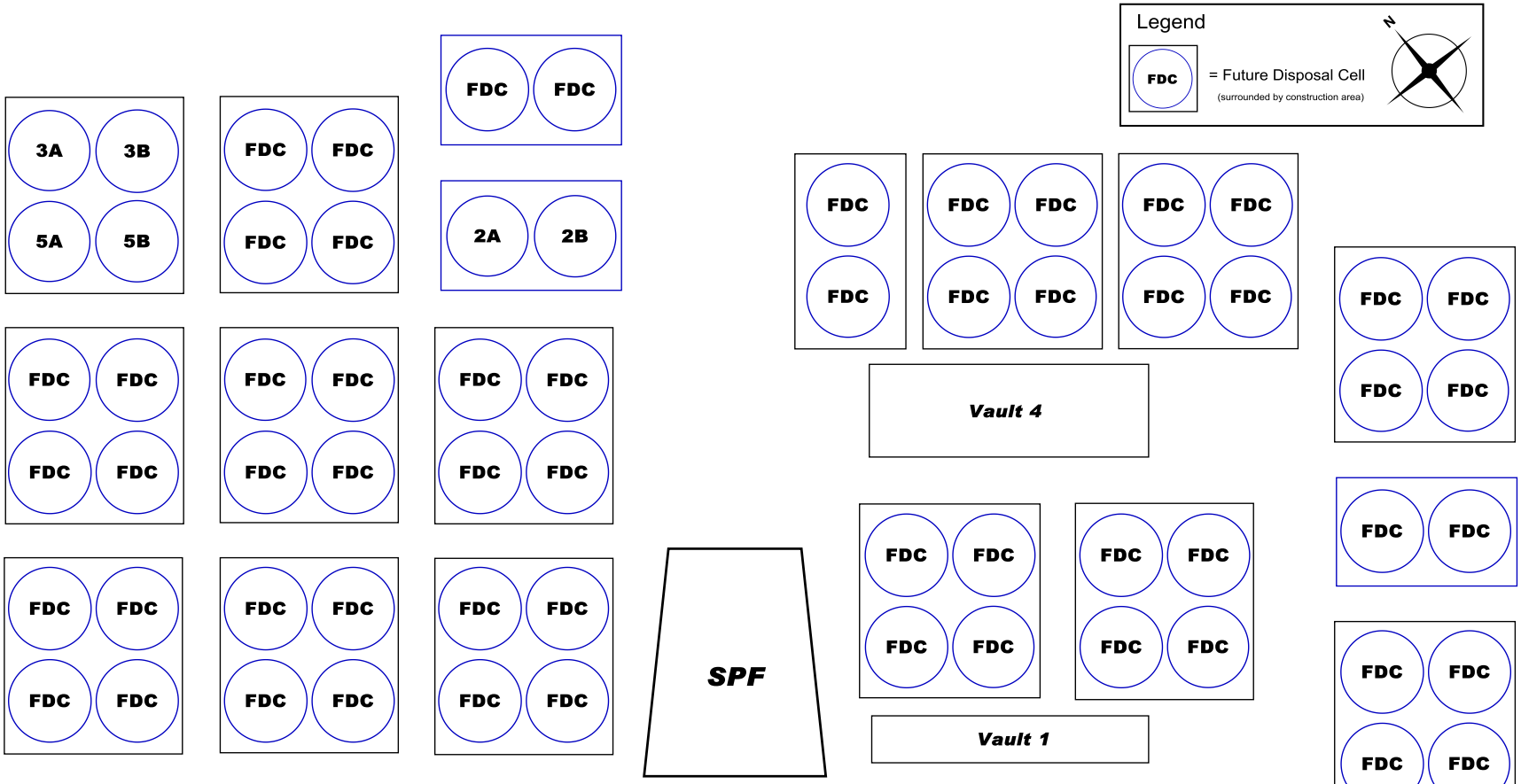

Note: Not to Scale - Figure presents the anticipated FDC locations, numbered disposal units are per existing construction

Surface drainage in Z Area, which includes the Saltstone Production Facility (SPF) and the SDF, is toward UTR, northwest to north, and toward McQueen Branch, northeast and southeast.

Z Area was chosen for the SDF site based on considerations of depth to the water table, available surface area, surface topography, proximity to the waste treatment facilities on site, and distance to surface water and the public.

3.3 Principal Design Features

The SDF consists of existing SDUs 1, 2, 3, 4, and 5 and is modeled to include additional SDUs. In the SDF PA, the SDUs are identified as Vault 1, Vault 4, and FDCs. SDUs 1 and 4 are rectangular vaults as described in the SDF PA Sections 3.2.1.1 and 3.2.1.2, respectively.

In this SA, design features are being considered that were not previously included in the evaluation of the performance of the SDUs. The FDCs described in SDF PA Section 3.2.1.3 are recently designed and constructed cylindrical disposal cells (SDUs 2, 3, and 5) as described in the SDF PA Section 3.2.1.3. SDU Cells 2A and 2B are operational, and SDU Cells 3A, 3B, 5A, and 5B are expected to be operational toward the end of 2013. In this SA, the designation FDC will be used as needed for clarity and refer to all the existing cylindrical SDUs and future SDUs of this design to be constructed as needed to coordinate with salt processing rates, with 64 total disposal cells assumed for the SDF PA. Any changes to future SDUs capacity and configuration, relative to what is analyzed herein, must be evaluated prior to obtaining operational approval.

3.3.1 SDU 1 Design Features

A design feature not previously included in the modeled performance of SDU 1 is the water stops used during the construction of the floors and the wall-to-floor interface.

Figure 3.3-1 presents a portion of the floor design for SDU 1. The grid shows half of the 60 constructed concrete floor sections. The total length of the floor construction joints in SDU 1 is approximately 3,000 feet ((4 × 301.5 feet) + (18 × 100 feet)). [W780625] Water stops are also included along the interface of the walls and the floor, which follows the perimeter of the SDU for approximately 1,400 feet plus the length of the walls separating the individual cells within the SDU, for an additional 600 feet. Thus, the total linear feet of construction joints is 5,012 feet. [SRR-CWDA-2013-00064] For this SA, the construction joints are modeled as fast-flow zones within the SDU 1 floor and the wall-to-floor interface, as described in Section 4.

Figure 3.3-1: SDU 1 Floor Construction Sections

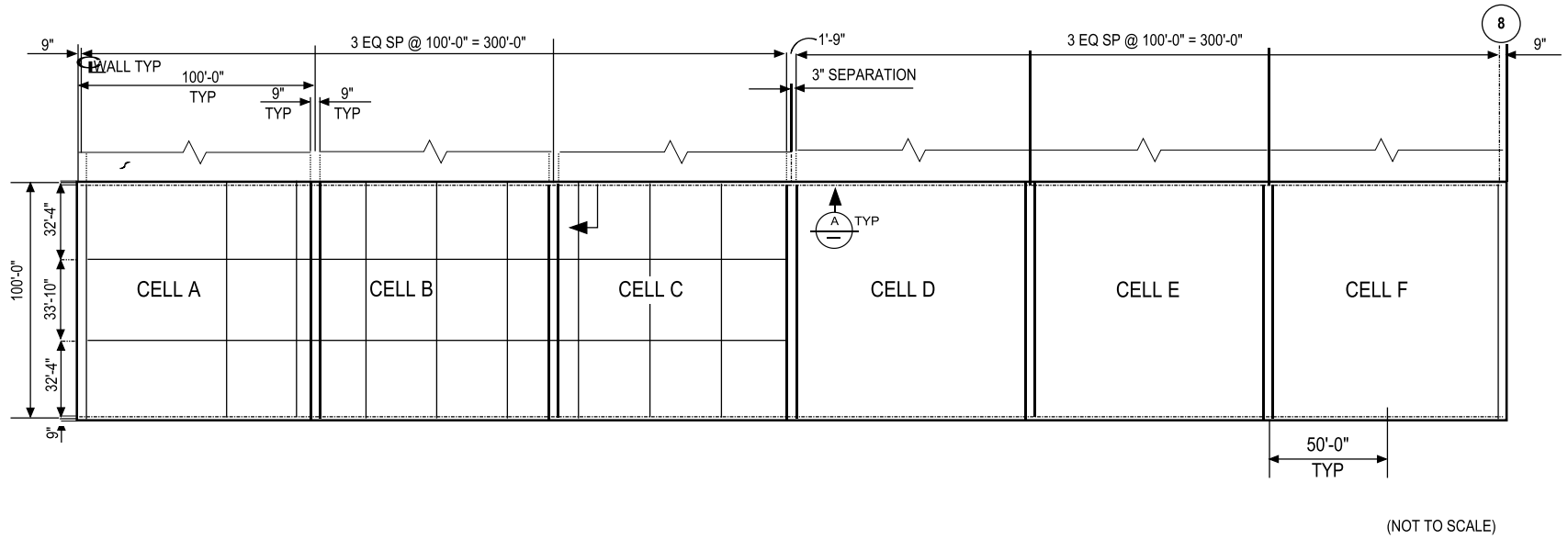

[W780625]

3.3.2 SDU 4 Design Features

Two features not previously considered in the evaluation of the modeled performance of SDU 4 are (1) the use of water stops in the construction of the floor and the wall-to-floor interface and (2) the roof support structures used within the cells (except Cell A).

Similar to the construction of SDU 1, SDU 4 also utilizes water stops during the construction of the floor. Figure 3.3-2 presents a portion of the floor design, showing the floor for six of the 12 cells within SDU 4. The gird shows half of the 120 constructed concrete floor sections. The total length of the floor construction joints in SDU 4 is 6,012 feet ((8 × 301.5 feet) + (18 × 200 feet)). [W828992] Water stops are also included along the interface of the walls and the floor, which follows the perimeter of the SDU for 1,606 feet plus the length of the walls separating the individual cells of the SDU, for an additional 1,200 feet. Thus, the total linear feet of construction joints is 8,818 feet in SDU 4. [SRR-CWDA-2013-00064] For this SA, the construction joints are modeled as fast-flow zones within the SDU 4 floor and wall-to-floor interface, as described in Section 4.

For SDU 4 (Cells B through L), the concrete roof is supported by girders, joists, and decking with all exposed steel being galvanized. The roof support structure is described in SDF PA Section 3.2.1.2.6 and is shown in SDF PA, Figures 3.2-11 and 3.2-12. Nine columns in a 3 by 3 array within each cell support the roof girder system. Each column is a 10-inch diameter steel pipe, filled with clean concrete. [C-CS-Z-0002] The clean cap that covers the saltstone will fill the volume from the top of the saltstone to the bottom of the roof and thus the clean cap and a portion of saltstone will fill the volume taken up by the roof girder system.

In this SA, the roof girder system will be considered as a means of degradation of the saltstone and clean cap via carbonation as described in Section 4. The columns will also be considered separate from the saltstone as they experience degradation via carbonation, as described in Section 4.

Figure 3.3-2: SDU 4 Floor Construction Sections

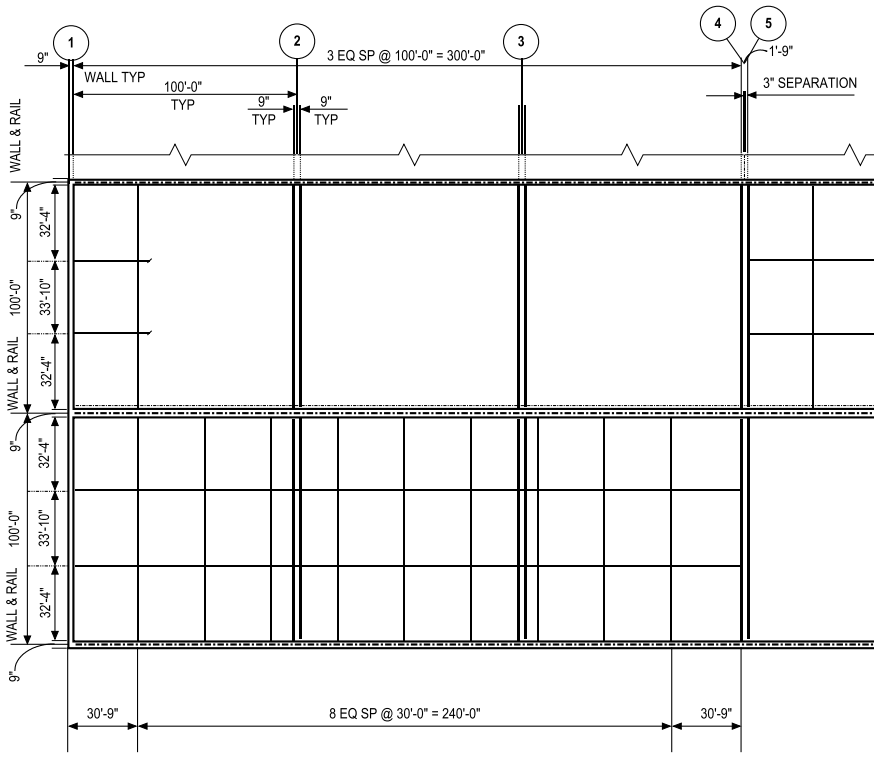

[W828992]

3.3.3 FDC Design Features

Two features not previously considered in the evaluation of the modeled performance of the FDCs are (1) the use of water stops in the construction of the floor and the wall-to-floor interface and (2) the roof support structures used within the cells.

As discussed in SDF PA Section 3.2.1.3.5, each FDC contains 48 roof support columns [08084SD, Sheet 3]. Each cylindrical column is comprised of rebar and Class III sulfate resistant concrete (same as the FDC wall/floor concrete) with an outer diameter of 14 inches. [08084SD, Sheet 6] Similar to the degradation of these SDU 4 columns, the FDC columns are modeled as degrading via carbonation, as described in Section 4, and modeled separate from the saltstone.

Not included in earlier evaluations of the performance of the FDC design was the potential flow path that could exist if water stops deteriorate. The FDC wall rests on a 2-inch thick by 6-inch wide bearing pad on the floor of FDC and this interfaces with an interior concrete curb as shown in Figure 3.3-3. [08084SD, Sheet 8] Other water stop materials exist to fill the area below the 8-inch thick wall. The interface of the concrete curb with the wall and the floor is covered with an epoxy adhesive/mortar and then covered by an overlay coating. Deterioration of the water stop has the potential to form a path that allows transport of contaminants through the bearing pad and the water stop material. This potential path, assumed to exist along the circumference of the 75-foot radius FDC, is 471 feet and is included in the model as described in Section 4. [SRR-CWDA-2013-00064]

Figure 3.3-3: FDC Wall-to-Floor Joint

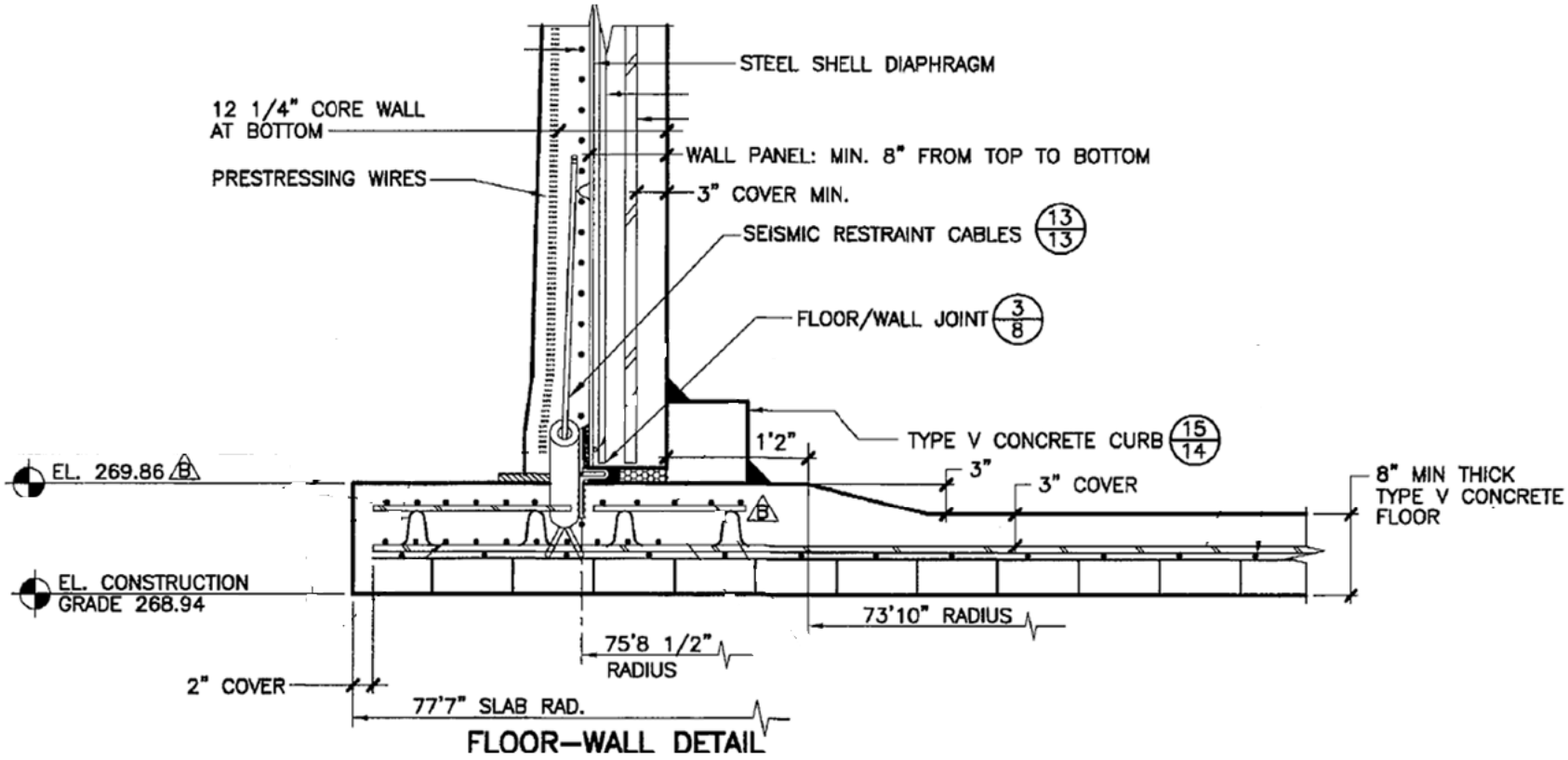

[08084SD]

3.3.4 Conceptual Closure Cap

The conceptual design of the closure cap remains unchanged. [SRR-CWDA-2009-00017] Figure 3.3-4 presents the conceptualization of the closure cap layers, as currently planned. These layers are described in the SDF PA, Section 3.2.2. [SRR-CWDA-2009-00017]

Figure 3.3-4: SDF Conceptual Closure Cap Layers

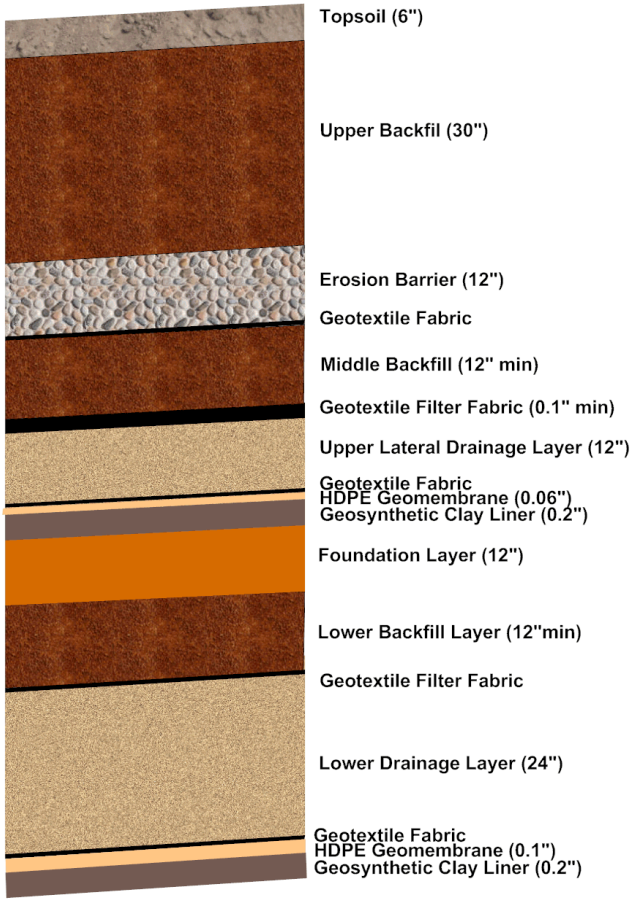

For this SA, the estimated infiltration rates through the closure cap, which are considered average (nominal) values, have been expanded to consider maximum and minimum estimated values. The intent of this expanded modeling approach is to provide greater understanding of the potential effects of infiltration variability.

The maximum, average, and minimum infiltration rates were obtained from Appendix K of WSRC-STI-2008-00244 are presented in Table 3.3-1 and shown graphically in Figure 3.3-5. These infiltration rates were used to estimate the degradation of the sand drainage layer that exists above each SDU

Table 3.3-1: Estimated Infiltration Rates through the Closure Cap

Time after Closure (years)	Infiltration Rate (in/yr)		
	Maximum	Average	Minimum
0	0.00269	0.00042	0.00007
100	0.0277	0.00333	0.0003
180	0.367	0.0452	0.00376
220	0.459	0.0568	0.0047
300	0.677	0.171	0.0414
380	1.652	0.472	0.117
460	2.207	0.723	0.187
560	2.759	1.021	0.276
1,000	4.647	2.264	0.679
1,800	8.280	4.340	1.465
3,200	10.629	6.795	2.998
5,412	12.450	10.606	5.303
5,600	12.450	10.606	5.302
> 10,000	12.450	10.606	5.410

[WSRC-STI-2008-00244]

Figure 3.3-5: Infiltration Rate through the Closure Cap

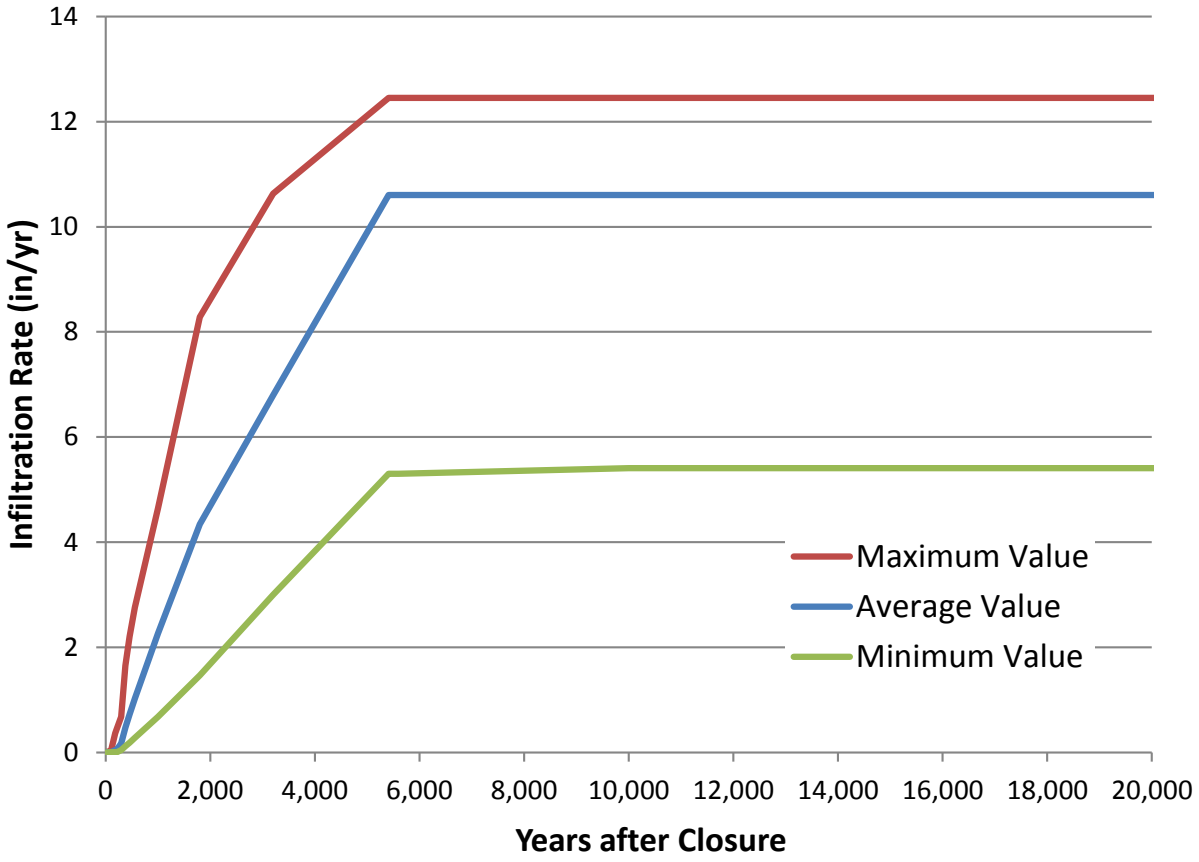

Figure 3.3-6 illustrates the degradation of the sand drainage layer based on the different infiltration rates based on the model presented in WSRC-STI-2008-00244. The maximum, average, and minimum infiltrate rates and degradation of the sand drainage layer are used in the various flow cases being considered in this SA, as described in Section 4.4. The Evaluation Case uses the average values and the sensitivity cases use the maximum, average, and minimum values.

Figure 3.3-6: Degradation of the Sand Drainage Layer above an SDU

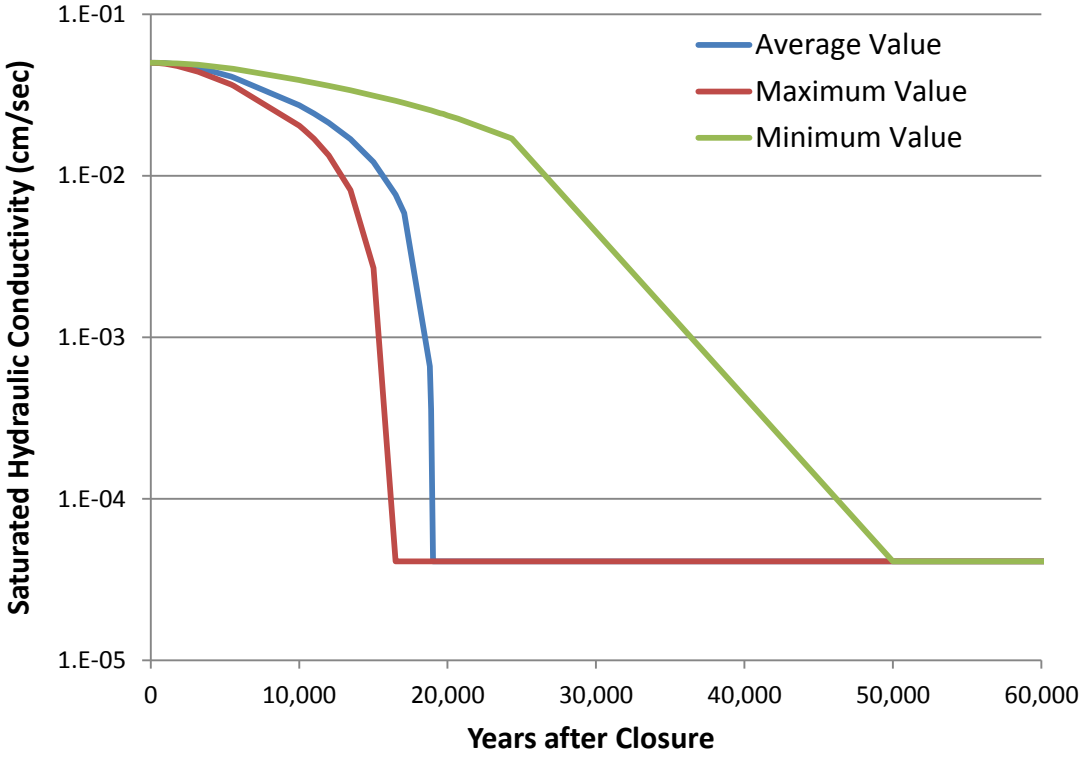

3.4 SDF Waste Inventory

The radionuclide inventories for this SA, in each SDU, are based on the projected inventories presented in SDF PA, Tables 3.3-1, 3.3-3, and 3.3-5 (SRR-CWDA-2009-00017), as modified in the response to RAI PA-8, in SRR-CWDA-2011-00044. Note that for SDU 1, the projected inventory is double the values presented in SDF PA, Table 3.3-1, to account for potential future disposal activities in the remaining three empty cells of the SDU, as was done in the modeling for the SDF PA. Table 3.4-1 presents the projected radionuclide inventory in each of the SDU/FDCs.

Table 3.4-1: Projected Radionuclide Inventory at Closure

Radionuclide (curies)	SDU 1	SDU 4	Each FDC	Radionuclide (curies)	SDU 1	SDU 4	Each FDC
Ac-227	Note	1.6E-05	1.7E-07	Pa-231	Note	9.3E-05	9.8E-07
Al-26	Note	3.4E-01	1.9E-01	Pd-107	3.8E-03	5.0E-02	5.6E-03
Am-241	9.4E-04	1.3E+02	1.4E+00	Pm-147	Note	4.1E-01	7.7E-02
Am-242m	Note	6.7E-02	5.9E-04	Pr-144	Note	1.8E-09	3.6E-10
Am-243	Note	1.8E+00	3.7E-02	Pt-193	7.4E-01	1.0E+01	1.1E+00
Ba-137m	8.2E+00	2.8E+05	2.2E+01	Pu-238	1.6E-02	1.0E+03	1.7E+02
Bk-249	Note	1.8E-28	1.8E-28	Pu-239	2.4E-02	3.8E+02	1.5E+01
C-14	2.6E+00	2.7E+01	2.0E+00	Pu-240	2.4E-02	1.2E+02	4.1E+00
Ce-144	Note	1.8E-09	3.6E-10	Pu-241	2.0E-02	2.4E+03	4.2E+01
Cf-249	Note	6.5E-13	6.7E-13	Pu-242	1.8E-03	8.1E-01	3.9E-03
Cf-251	Note	1.2E+00	2.3E-14	Pu-244	Note	1.6E-02	1.6E-05
Cf-252	Note	1.8E-18	1.8E-18	Ra-226	1.3E-06	1.0E-03	1.3E-05
Cl-36	1.5E-03	3.0E-03	4.2E-04	Ra-228	Note	1.6E-06	8.7E-05
Cm-242	Note	6.7E-02	6.3E-19	Rh-106	3.0E-10	9.1E-07	1.2E-06
Cm-243	Note	2.1E-01	2.1E-04	Ru-106	3.0E-10	9.1E-07	1.2E-06
Cm-244	Note	1.3E+02	9.5E-01	Sb-125	3.2E-01	5.7E+00	2.4E-01
Cm-245	Note	9.2E-01	2.4E-04	Sb-126	2.8E-01	9.0E-01	1.2E+00
Cm-247	Note	3.9E-06	7.1E-14	Sb-126m	2.0E+00	6.4E+00	8.2E+00
Cm-248	Note	1.2E-13	7.4E-14	Se-79	6.0E-01	4.6E+01	1.4E+00
Co-60	1.6E-04	4.6E-01	5.4E-02	Sm-151	Note	4.2E+01	5.9E+01
Cs-134	Note	5.2E-01	1.5E-05	Sn-126	2.0E+00	6.4E+00	8.2E+00
Cs-135	Note	5.4E+00	1.3E-04	Sr-90	1.4E-02	2.4E+05	3.7E+01
Cs-137	8.6E+00	3.0E+05	2.3E+01	Tc-99	2.2E+02	5.8E+02	5.4E+02
Eu-152	3.6E-03	9.7E-02	9.8E-02	Te-125m	7.6E-02	1.4E+00	5.8E-02
Eu-154	4.6E-04	1.2E+01	1.8E+00	Th-229	6.0E-01	2.5E+01	3.9E-02
Eu-155	Note	6.8E-01	1.3E-01	Th-230	8.2E-01	1.0E-02	1.3E-04
H-3	1.2E+01	2.6E+02	3.0E+01	Th-232	Note	3.2E-04	1.4E-03
I-129	2.2E-01	2.8E-01	3.8E-01	U-232	Note	4.4E-02	3.1E-04
K-40	1.5E-03	3.0E-03	4.2E-04	U-233	5.6E-01	2.4E+01	3.7E-02
Na-22	Note	1.5E-01	6.9E-02	U-234	5.6E-01	1.0E+01	1.3E-01
Nb-93m	5.0E-01	8.4E+00	3.7E-01	U-235	6.4E-03	4.7E-01	3.0E-03
Nb-94	5.0E-03	8.7E-02	3.8E-03	U-236	6.4E-03	7.7E-01	1.6E-02
Ni-59	7.0E-02	4.0E-01	8.4E-02	U-238	1.5E-02	5.9E-01	1.0E-01
Ni-63	1.6E+00	2.2E+01	2.4E+00	Y-90	1.4E-02	2.4E+05	3.7E+01
Np-237	9.0E-03	6.1E-01	5.0E-02	Zr-93	5.0E-01	8.4E+00	3.7E-01

[SRR-CWDA-2009-00017, Section 3.3 and response to RAI PA-8]

Note: Due to the smaller number of radionuclides analyzed during disposal operations, the SDU 1 inventory considers fewer radionuclides than SDU 4 and the other FDCs. The radionuclides not analyzed for SDU 1 are considered not significant to overall dose based on full characterization of subsequent salt solutions disposed in other SDUs.

4.0 ANALYSIS OF PERFORMANCE

The discussion presented in the SDF PA Section 4 remains essentially unchanged for this SA except for specific changes made to incorporate information developed during the responses to RAIs in SRR-CWDA-2011-00044 and to update information regarding the degradation of cementitious material, the release of technetium from reducing cementitious materials, distribution coefficients (K_d values), flow through joints, and dose pathway exposure methodology. These changes are discussed below.

4.1 Source Term Release

4.1.1 Chemical Transition Pore Volumes

As fluid moves through the pores within the cementitious materials, the E_h and pH properties of the materials transition to different states, thus influencing the performance of the materials with respect to contaminant releases. In the SDF PA model, the initial state of cementitious materials containing slag is Reduced Region II, which means that the material has a negative E_h potential and a high pH value. The quantity of slag within the cementitious materials is the primary indicator of the reducing capacity for the cementitious materials. For cementitious materials that do not contain slag, such as the roofs of SDU 1 and 4, and the lower mud mats of FDCs, the initial state is Oxidized Region II, meaning that the material has a positive Eh potential while retaining the high pH value. Oxidized Region III, in which cementitious material has a positive E_h value and a lower pH value, is the final chemical condition, in which cementitious materials reach equilibrium with the surrounding environment.

The total volume of pore spaces within a modeled region of cementitious material is referred to as the region's pore volume, and the amount of fluid moving through that region is measured by the count of its pore volumes. Analyses in support the SDF PA estimated the number of pore volumes required to transition the cementitious materials from Reduced Region II to Oxidized Region II, and finally from Oxidized Region II to Oxidized Region III. [SRNL-TR-2008-00283] The results from this initial evaluation, considered as the pore flush model, are provided in SDF PA, Table 4.2-9. [SRR-CWDA-2009-00017] The determination of pore volumes needed to initiate chemical transition is dependent on the infiltrating water chemistry. For saltstone, the infiltrating water is groundwater equilibrated with Calcium Silicate Hydrate (CSH) associated with Oxidized Region II cementitious material. For the SDU and FDC concrete, the infiltrating water is assumed to be groundwater.

In the response to the RAI SP-8, provided in SRR-CWDA-2011-00044, the required pore volumes for chemical transitions were revised to reflect updated parameters from the initial evaluation. For this SA, the most recent recommended values for the reduction capacity in the cementitious materials will be used. [SRNL-STI-2009-00637; SRNL-STI-2012-00596] Table 4.1-1 summarizes the parameters and the results of estimated pore volumes needed to initiate chemical transitions for the RAI response to SP-8 and for this SA. As shown, this SA uses the same transition volumes as was calculated for RAI SP-8 except for the pore volumes required to transition from Reduced Region II to Oxidized Region II. This transition is considered proportional to the reducing capacity of the material when all other parameters

are the same. Thus, the pore volume for transition from Reduced Region II to Oxidized Region II was lowered to reflect the lower value in the reducing capacity.

The total flow through each region in the PORFLOW model is accumulated during each time step and the count of pore volumes is tracked for each region. Each modeled region transitions to its next chemical state once the required number of pore volumes is reached. Table 4.1-2 identifies the times for the transitioning of the modeled regions of interest in the SDUs and in an FDC for the Evaluation Case described in Section 4.4.1.4.

Table 4.1-1: Pore Volumes Required for Chemical Transitions

Parameter	RAI SP-8	This SA
Saltstone and Clean Cap		
Bulk Density, g/mL	1.01	1.01
Porosity, unitless	0.58	0.58
Reduction Capacity, meq e-/g	0.822	0.607
Pore Volumes, unitless		
Reduced Region II to Oxidized Region II	1,653	1,220
Oxidized Region II to Oxidized Region III	11,213	11,213
SDU and FDC Concrete (Note 1)		
Bulk Density, g/mL	2.21	2.21
Porosity, unitless	0.12	0.12
Reduction Capacity, meq e-/g	0.240	0.178
Pore Volumes, unitless		
Reduced Region II to Oxidized Region II	4,953	3,673
Oxidized Region II to Oxidized Region III	6,446	6,446

Note 1: The concrete containing slag (from SRR-CWDA-2009-00017, Section 4) are:
SDU 1 and SDU 4 walls and floor
FDC roof, wall, floor, and upper mud mat
[SRR-CWDA-2013-00064]

Table 4.1-2: Transition Times in the SDUs and in an FDC (Years)

Modeled Region	SDU 1	SDU 4	FDC
Saltstone (a)			
Reduced Region II →Oxidized Region II	33,882	Top portion 5,930 Bottom portion 23,840	33,064
Oxidized Region II →Oxidized Region III	> 100,000	Top portion 23,961 Bottom portion > 100,000	> 100,000
Wall			
Reduced Region II →Oxidized Region II	14,707	10,330	5,935
Oxidized Region II →Oxidized Region III	22,312	17,688	8,431
Floor			
Reduced Region II →Oxidized Region II	7,035	4,488	5,540
Oxidized Region II →Oxidized Region III	9,624	5,544	7,468
Upper Mud Mat			
Reduced Region II →Oxidized Region II	NA	NA	3,802
Oxidized Region II →Oxidized Region III	NA	NA	5,091
Lower Mud Mat			
Oxidized Region II →Oxidized Region III	NA	NA	6,979

(a) For SDU 4 the saltstone region is divided between a top portion and a bottom portion as described in Section 3.3.2.

NA = Not applicable

4.1.2 Radionuclide Release and Transport

Radionuclide release and transport through the cementitious materials (except Tc-99) in reduced form and soil is controlled by the distribution coefficients (K_d values), which are dependent on the chemical conditions of the cementitious materials and soil. Table 4.1-3 presents the K_d values for the elements of concern in clayey and sandy soils.

Based on recent studies, the K_d values in soil can be impacted by the presence of pore water that has been chemically altered by leaching of cementitious materials. This cementitious pore water is highly basic (pH > 12) and has a high ionic strength (10.0E-02 molar). [SRNL-STI-2009-00473] Thus, Table 4.1-3 also presents K_d values for cementitious leachate impacted soils. Due to the large volume of saltstone within the SDUs and FDCs, the K_d values for leachate-impacted clayey and sandy soil are used in the vadose zone (i.e., the area above the aquifer).

Table 4.1-3: Distribution Coefficients (K_d Values) for Elements in Soils

Element	Clayey Soil (Backfill) (mL/g)				Sandy Soil (Vadose) (mL/g)			
	Without Leachate	Ref.	Leachate Impacted	Ref.	Without Leachate	Ref.	Leachate Impacted	Ref.
Ac	8,500	a	12,750	a	1,100	a	1650	a
Ag	30	b	96	g	10	b	32	g
Al	1,300	a	1,950	a	1,300	a	1,950	a
Am	8,500	a	12,750	a	1,100	a	1,650	a
As	200	a	280	a	100	a	140	a
At	0.9	a	0.1	a	0.3	a	0	a
Ba	101	c	303	g	15	c	45	g
Bk	8,500	a	12,750	a	1,100	a	1,650	a
C	400	a	2,000	a	10	a	50	a
Cd	30	a	90	a	15	a	45	a
Ce	8,500	a	12,750	a	1,100	a	1,650	a
Cf	8,500	a	12,750	a	1,100	a	1,650	a
Cl	8	b	0.8	g	1	b	0.1	g
Cm	8,500	a	12,750	a	1,100	a	1,650	a
Co	100	a	320	a	40	a	128	a
Cr	400	b	560	g	1,000	b	1,400	g
Cs	50	a	50	a	10	a	10	a
Cu	70	a	224	a	50	a	160	a
Eu	8,500	a	12,750	a	1,100	a	1,650	a
Fe	400	a	600	a	200	a	300	a
Fr	50	a	50	a	10	a	10	a
Gd	8,500	a	12,750	a	1,100	a	1,650	a
H	0	a	0	a	0	a	0	a
Hg	1,000	a	3,200	a	800	a	2,560	a
I	0.9	a	0.1	a	0.3	a	0	a
K	25	a	25	a	5	a	5	a
Mn	200	a	280	a	15	a	21	a
N	0	a	0	a	0	a	0	a
Na	25	a	25	a	5	a	5	a
Nb	900	e	1260	g	160	e	224	g
Ni	30	a	96	a	7	a	22	a
Np	9	a	180	c	3	a	60	c
Pa	9	a	180	c	3	a	60	c
Pb	5,000	a	16,000	a	2,000	a	6,400	a
Pd	30	a	96	a	7	a	22	a
Pm	0	f	0	f	0	f	0	f
Po	5,000	a	10,000	a	2,000	a	4,000	a
Pr	0	f	0	f	0	f	0	f
Pt	30	a	96	a	7	a	22	a

Table 4.1-3: Distribution Coefficients (K_d Values) for Elements in Soils (Continued)

Element	Clayey Soil (Backfill) (mL/g)				Sandy Soil (Vadose) (mL/g)			
	Without Leachate	Ref.	Leachate Impacted	Ref.	Without Leachate	Ref.	Leachate Impacted	Ref.
Pu	5,950	a	11,900	a	650	d	1,300	g
Ra	185	c	555	c	25	c	75	c
Rb	50	a	50	a	10	a	10	a
Re	1.8	a	0.2	a	0.6	a	0.1	a
Rh	0	f	0	f	0	f	0	f
Rn	0	a	0	a	0	a	0	a
Ru	0	f	0	f	0	f	0	f
Sb	2,500	a	3,500	a	2,500	a	3,500	a
Se	1,000	a	1,400	a	1,000	a	1,400	a
Sm	8,500	a	12,750	a	1,100	a	1,650	a
Sn	5,000	a	15,000	a	2,000	a	6,000	a
Sr	17	c	51	c	5	c	15	c
Tc	1.8	a	0.2	a	0.6	a	0.1	a
Te	1,000	a	1,400	a	1,000	a	1,400	a
Th	2,000	a	4,000	a	900	a	1,800	a
U	400	b	1,200	a	300	b	900	b
V	0	f	0	f	0	f	0	f
Y	8,500	a	12,750	a	1,100	a	1,650	a
Zn	30	a	90	a	15	a	45	a
Zr	2,000	a	4,000	a	900	a	1,800	a

a. SRNL-STI-2009-00473
b. SRNL-STI-2010-00493
c. SRNL-STI-2011-00011
d. SRNL-STI-2011-00672
e. ML073510127
f. Assigned a value of zero
g. Multiplied the "cement leachate impact factor" from SRNL-STI-2009-00473 to the "without leachate" value

Table 4.1-4 presents the distribution coefficients for cementitious materials under Reduced Region II, Oxidized Region II, and Oxidized Region III conditions. Technetium release, specifically the release of Tc-99, from saltstone and transport through concrete is modeled as a shrinking core, as described in the SDF PA Section 4.2.3.2.4. Unlike the SDF PA model, however, the release of Tc-99 in a reducing environment is controlled by solubility rather than by the K_d value. Once the cementitious material transitions to oxidizing conditions, the transport is controlled by the K_d value. The solubility value for technetium has been estimated to be 1.0E-08 mol/L for saltstone, clean cap grout, and for concrete containing slag based on a study that compared thermodynamic modeling results to recent laboratory measurements. [SRNL-STI-2012-00769] Calculations were conducted to evaluate the various solid phases that may control technetium solubility, and therefore aqueous technetium concentrations under reducing conditions. In addition to evaluating likely solid phases, this study also evaluated different thermodynamic databases.

The thermodynamic calculations captured the data trends and the magnitude of the experimental data reasonably well. The calculations suggested that in the first two experiments, TcO2·1.6H2O (solubility is 6.3E-07 M) or $TcO_2 \cdot 2H_2O$ (solubility is 9.5E-07 M) were most likely controlling technetium concentrations in the reducing saltstone leachates, but not TcO2(c) (solubility is 6.0E-11 M).

The solubility of hydrated $TcO_2 \cdot xH_2O$ (likely $TcO_2 \cdot 1.6H_2O$) controlled the technetium concentration in reducing saltstone leachates as long as the Eh remained < -0.38 V. However, as the Eh increased just above -0.35 V, the highly soluble Tc(VII) species, TcO_4^-, became the much more dominant species due to the re-oxidation of Tc(IV) in the aqueous and solid phases. Under the more oxidized environmental conditions, the TcO_4^- concentration increased dramatically to millimolarity. The influence of pH on technetium solubility was evaluated because it is used to define the "age of the saltstone" in the PA; such that the saltstone is initially at pH 12 or larger, then as it ages, the evolving mineral assemblage of the saltstone and air and recharge water that contacts the saltstone buffer the pH to ~10.5. After extensive leaching/weathering, the saltstone is expected to degrade and eventually take on the pH of the background sediment at pH 5.5. Under reducing conditions (Eh < -0.38 V), the calculated technetium solubility decreased as the pH decreased. For example, when pH changed from 12.7 to 10.5 (the approximate pH decrease between the young and moderately-aged saltstone stages used in the SA) at a fixed Eh of -0.38 V, the calculated solubility of $TcO_2 \cdot 1.6H_2O$ is predicted to significantly decrease from 6.3E-07 M to 5.2E-09 M.

During the two early stages of cement aging, the modeling indicated that solubility of $TcO_2 \cdot xH_2O$ was the controlling process of aqueous technetium concentration of saltstone. However, once the system became oxidized, generally anticipated to occur during the 2nd stage of cement aging, then solubility no longer controlled aqueous technetium concentrations. Under oxidizing conditions, technetium adsorption to solid phases becomes the predominant mechanism controlling the concentration of technetium in pore water, and thus the K_d construct is appropriate to use for predicting technetium concentrations. Similarly, once sufficient pore water has leached through the saltstone to advance the modeling into the 3rd and final stage of aged cement, a technetium K_d for an oxidized system would be appropriate to use.

Table 4.1-4: K_d Values for Elements in Cementitious Material

Element	Reduced Region II (mL/g)	Ref.	Oxidized Region II (mL/g)	Ref.	Oxidized Region III (mL/g)	Ref.
Ac	7,000	a	6,000	a	600	a
Ag	5,000	a	4,000	a	400	a
Al	7,000	a	6,000	a	600	a
Am	7,000	a	6,000	a	600	a
As	200	b	320	b	100	a
At	9	a	15	a	4	a
Ba	100	b	100	b	70	a
Bk	7,000	a	6,000	a	600	a
C	3,000	a	3,000	a	300	a
Cd	5,000	a	4,000	a	400	a
Ce	7,000	a	6,000	a	600	a
Cf	7,000	a	6,000	a	600	a
Cl	10	a	10	a	1	a
Cm	7,000	a	6,000	a	600	a
Co	5,000	a	4,000	a	400	a
Cr	1,000	a	10	a	1	a
Cs	20	a	20	a	10	a
Cu	5,000	a	4,000	a	400	a
Eu	7,000	a	6,000	a	600	a
F	10	a	10	a	1	a
Fe	7,000	a	6,000	a	600	a
Fr	20	a	20	a	10	a
Gd	7,000	a	6,000	a	600	a
H	0	a	0	a	0	a
Hg	5,000	a	300	a	100	a
I	9	a	15	a	4	a
K	20	a	20	a	10	a
Mn	100	a	100	a	10	a
N	10	a	10	a	1	a
Na	1	a	1	a	0.5	a
Nb	1,000	a	1,000	a	500	a
Ni	4,000	a	4,000	a	400	a
Np	10,000	a	10,000	a	5,000	a
Pa	10,000	a	10,000	a	5,000	a
Pb	5,000	a	300	a	100	a
Pd	5,000	a	4,000	a	400	a
Pm	0	d	0	d	0	d
Po	5,000	a	300	a	100	a

Table 4.1-4: K_d Values for Elements in Cementitious Material (Continued)

Element	Reduced Region II (mL/g)	Ref.	Oxidized Region II (mL/g)	Ref.	Oxidized Region III (mL/g)	Ref.
Pr	0	d	0	d	0	d
Pt	5,000	a	4,000	a	400	a
Pu	10,000	a	10,000	a	2,000	a
Ra	100	a	100	a	70	a
Rb	20	a	20	a	10	a
Re	5,000	a	0.8	a	0.5	a
Rh	0	d	0	d	0	d
Rn	0	a	0	a	0	a
Ru	0	d	0	d	0	d
Sb	1,000	a	1,000	a	100	a
Se	300	a	300	a	150	a
Sm	7,000	a	6,000	a	600	a
Sn	5,000	a	4,000	a	2,000	a
Sr	15	a	15	a	5	a
Tc	Note 1	-	0.5	a	0.5	a
Te	300	a	300	a	150	a
Th	5,000	a	10,000	a	2,000	a
U	2,500	a	1,000	c	100	c
V	0	d	0	d	0	d
Y	7,000	a	6,000	a	600	a
Zn	5,000	a	4,000	a	400	a
Zr	5,000	a	10,000	a	2,000	a

Note 1: In reducing cementitious materials technetium release is via solubility controls and for this SA the K_d value of 0.5 is used in all oxidized regions

a. SRNL-STI-2009-00473
b. SRNL-STI-2010-00667
c. SRNL-STI-2010-00493
d. Assigned a value of zero

4.2 Cementitious Material Properties

Of importance in the transport of radionuclides are the hydraulic properties of the cementitious materials. The intact or undegraded hydraulic properties of the cementitious materials presented in SDF PA, Table 4.2-16, remain unchanged, except for the intact hydraulic properties of saltstone and the clean cap. The intact properties of saltstone and the clean cap are discussed in Section 4.2.1 and the degradation of the cementitious material is discussed in Section 4.2.2. The hydraulic properties of the cementitious materials are described in Section 4.2.3.

4.2.1 Intact Properties of Saltstone and Clean Cap

Saltstone is pumped into the SDUs and FDCs to a specified level and then a clean cap is placed above the saltstone to fill the remainder of the free volume in the SDU or FDC. In preparing the saltstone and clean cap, the same dry mix is used for both. For saltstone, the water medium is a decontaminated salt solution, containing radionuclides and chemicals, whereas the clean cap uses well water. Thus, the hydraulic performance of the saltstone and clean cap are expected to be similar.

The average saturated hydraulic conductivity from a recent study considered various process water-to-premix ratios with two different curing temperature profiles. [SRNL-STI-2012-00558] The hydraulic conductivity of intact saltstone and clean cap, as used in this SA, is bounded by the operating bands of current facility data. Based on analysis of current production runs at the SPF that were conducted prior to SPF upgrades (Figure 4.2-1) and after SPF upgrades (Figure 4.2-2), the operating band for the water-to-premix ratio would be bounded by a low value of 0.59 and a high value of 0.64. [X-CLC-Z-00050]

Table 4.2-1 provides the measured values for the saturated hydraulic conductivity for the water-to-premix ratio, bounded by 0.59 and 0.64, and for saturated conditions and a high humidity exposure for two different curing temperature profiles. [SRNL-STI-2012-00558] The average value for these runs is 6.4E-09 cm/s and this value is considered the nominal value for the saturated hydraulic conductivity of intact saltstone and clean cap in the SDUs and FDCs. Alternative flow sensitivity cases, discussed in Section 4.4, consider two other values for the initial saturated hydraulic conductivity of saltstone and the clean cap. At the higher end of the spectrum, 10 times the maximum reported value in Table 4.2-1, or 4.5E-07 cm/s, is used to ensure conservatism. At the lower end of the spectrum, the lower bound value is taken to be the minimum value reported in Table 4.2-1, 3.9E-10 cm/s.

The relatively high initial saturated hydraulic conductivity for saltstone of 4.5E-07 cm/s is not indicative of how high the initial saturated hydraulic conductivity can be. Rather, this high value was chosen to ensure a large variability of flow in the sensitivity cases analyzed in this SA. Review of the data reported in SRNL-STI-2012-00558 shows that of the seventy-two saltstone simulant samples analyzed, only three of the samples had a measured saturated hydraulic conductivity greater than 1.0E-07 cm/s. All three of those samples were formulated with a water-to-premix ratio much greater than the current facility operating band analyzed in this SA.

Another important mechanism to transport is the diffusion coefficient. Recent testing on simulated saltstone indicates that the intrinsic diffusion coefficient (analogous to the effective diffusion coefficient used in PORFLOW) is less than 1.0E-08 cm^2/s. [SRNL-STI-2010-00515] This value of 1.0E-08 cm^2/s will be used as the effective diffusion coefficient for intact saltstone and the clean cap.

Finally, the recommended moisture characteristic curves (MCCs) for saltstone grout are presented in Figure 4.2-3. This MCC was developed using data based on recent testing of simulants cured at 20 °C. [SRNL-STI-2011-00661]

Figure 4.2-1: Water-to-Premix Ratio for Production Runs Prior to SPF Upgrades

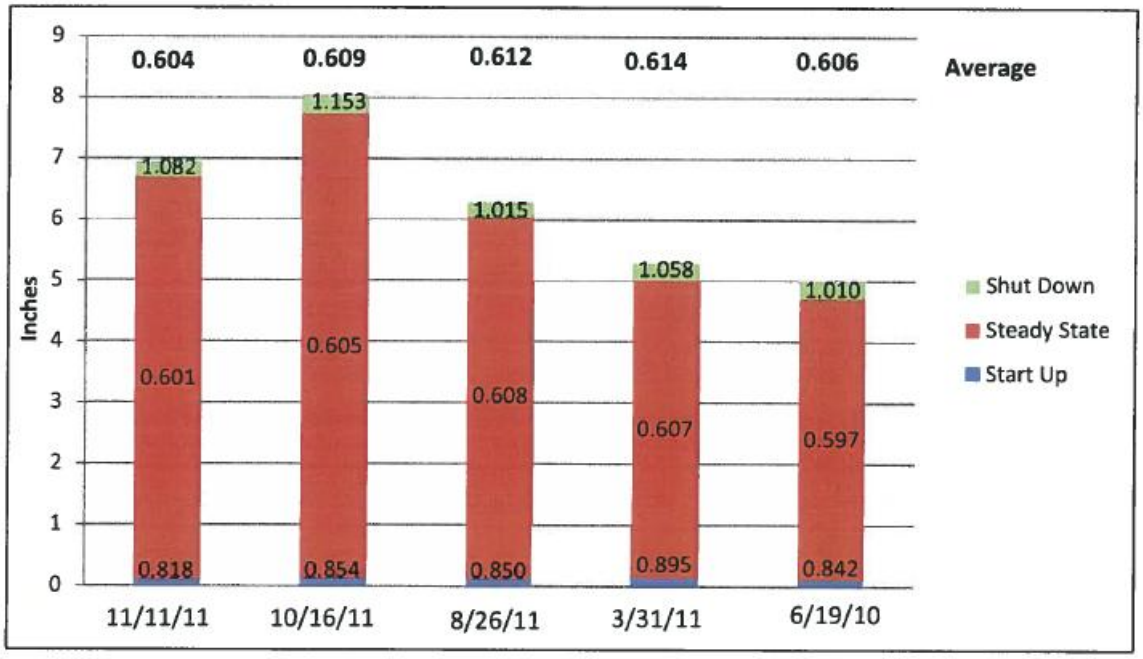

Figure 4.2-2: Water-to-Premix Ratio for Production Runs After SPF Upgrades

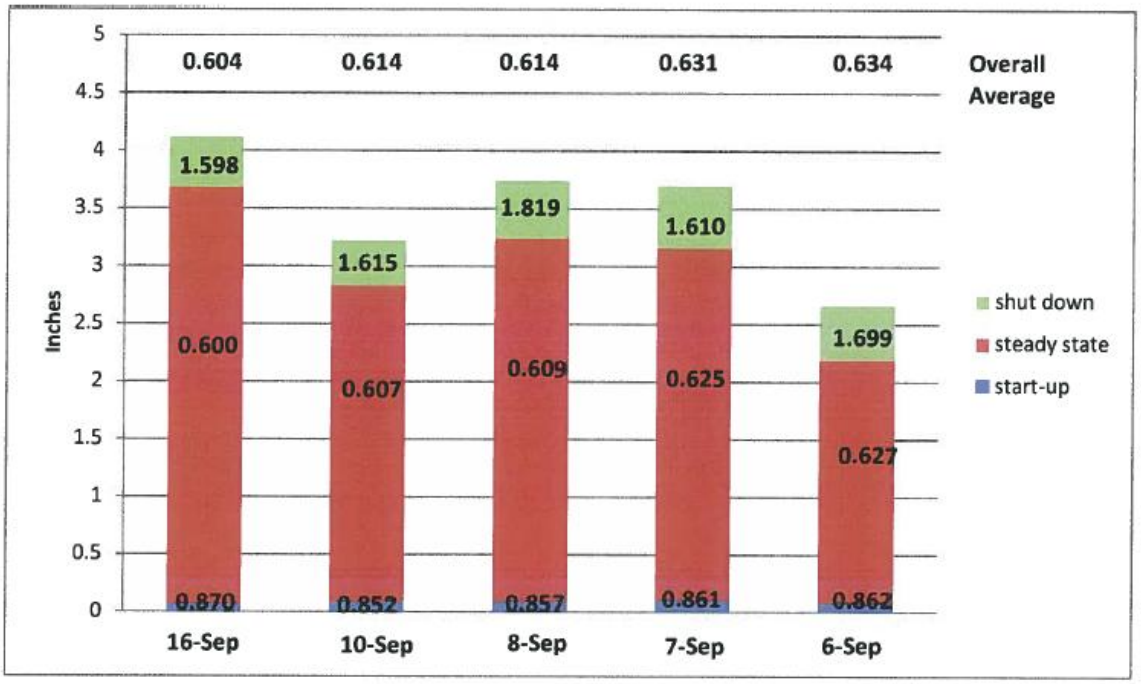

Table 4.2-1: Measured Hydraulic Conductivity from SRNL-STI-2012-00558

Final w/p ratio	Hydraulic Conductivity (cm/s)			
	Cell K Temperature Profile		Cell F Temperature Profile	
	Saturated	Exposed Surface	Saturated	Exposed Surface
0.59	1.7E-09	4.5E-09	1.4E-09	4.3E-09
0.59	1.9E-09	3.9E-10	3.6E-09	1.6E-09
0.6	1.7E-09	1.7E-09	4.1E-09	2.1E-09
0.6	2.1E-09	2.2E-09	3.7E-09	1.3E-09
0.64	3.2E-08	4.5E-08	7.0E-09	1.3E-09
0.64	9.6E-09	1.3E-08	5.0E-09	3.1E-09
Maximum	3.2E-08	4.5E-08	7.0E-09	4.3E-09
Average	8.2E-09	1.1E-08	4.1E-09	2.3E-09
Maximum	4.5E-08		7.0E-09	
Average	9.7E-09		3.2E-09	
Maximum	4.5E-08			
Average	6.4E-09			

Note: "Saturated" indicates that measurements were taken from grout in which the surfaces were covered with liquid to maintain saturated conditions. "Exposed Surface" refers to measurements taken from grout in which the sample surfaces were exposed to the humid environment. [SRNL-STI-2012-00558]

Figure 4.2-3: Moisture Characteristic Curve for Saltstone

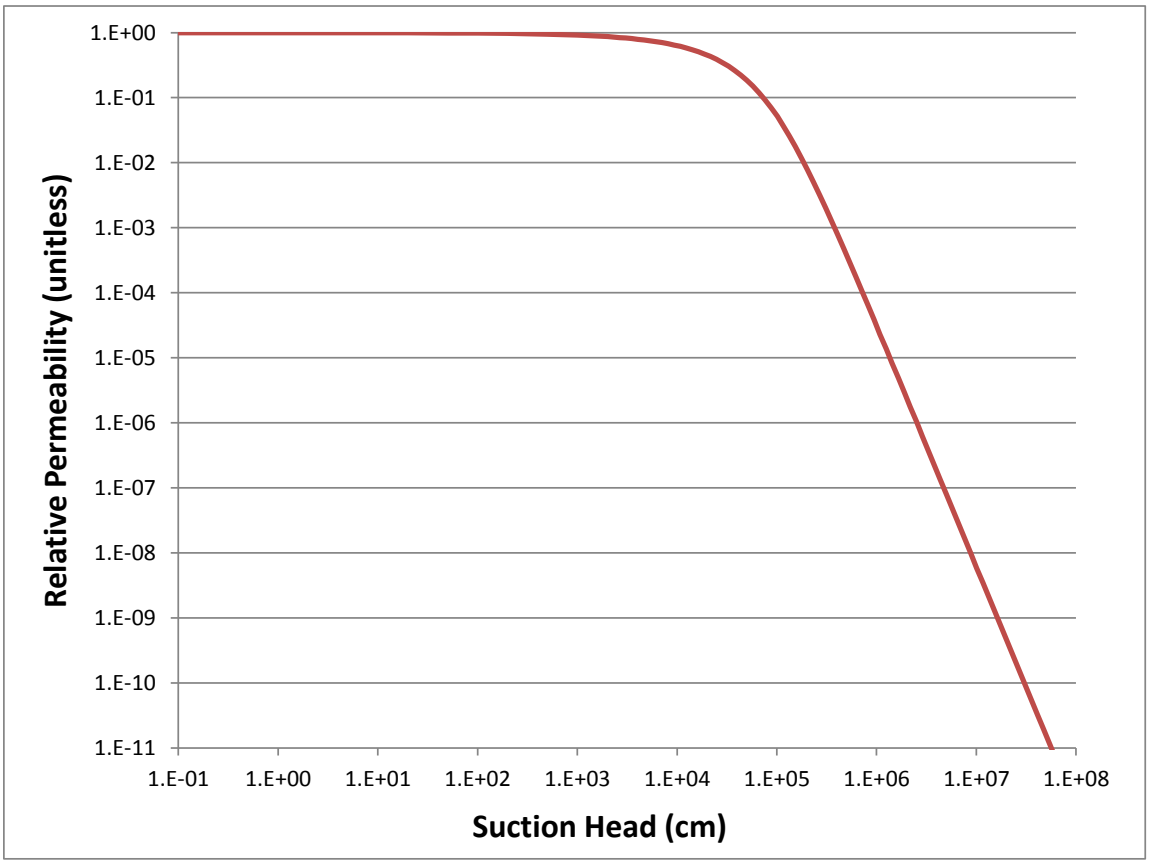

4.2.2 Degradation of SDF Cementitious Materials

This section summarizes the analysis and results of recent testing related to the degradation of SDF cementitious materials. Three mechanisms were analyzed for the degradation of SDF cementitious materials: sulfate attack, carbonation, and decalcification. [SRNL-STI-2013-00118]

Once SDF cementitious materials are fully degraded, they are generally assigned the same hydraulic properties as the surrounding soil or backfill. Exceptions to this are the fully degraded floor, upper mud mat, and lower mud mat of the FDCs, which are assigned the same hydraulic properties as the lower vadose zone (native soil) when they are fully degraded. Also, due to the current condition of the walls in SDU 1 and SDU 4, these are modeled as being initially degraded (i.e., no credit is taken for the hydraulic properties of the walls in SDU 1 and SDU 4). The properties for backfill and the lower vadose zone are provided in Table 4.2-2.

Table 4.2-2: Soil Properties

Material Zone	Saturated Effective Diffusion Coefficient D_e (cm^2/s)	Average Total Porosity (%)	Average Dry Bulk Density (g/cm^3)	Average Particle Density (g/cm^3)	Saturated Horizontal Hydraulic Conductivity (cm/s)	Saturated Vertical Hydraulic Conductivity (cm/s)
Backfill	5.3E-06	35	1.71	2.63	7.6E-05	4.1E-05
Lower Vadose Zone	5.3E-06	39	1.62	2.66	3.3E-04	9.1E-05

[SRR-CWDA-2009-00017 Table 4.2-14]

4.2.2.1 Cementitious Material Degradation from Sulfate Attack

Pore water in the saltstone waste form is expected to contain approximately 0.1 M sulfate. Over time, as sulfate ions migrate into the cement barrier surrounding the waste they react with calcium hydroxide (Portlandite) to form calcium sulfate (Gypsum) according to the reaction:

$$Ca(OH)_2 + SO_4^{2-} + 2H_2O \rightarrow CaSO_4 \bullet 2H_2O + 2OH^-$$

Calcium sulfate reacts with calcium/aluminum oxide minerals to form calcium aluminum sulfates such as ettringite according to the overall reaction:

$$3CaO \bullet Al_2O_3 \bullet 6H_2O + 3CaSO_4 + 20H_2O \rightarrow 3CaO \bullet Al_2O_3 \bullet 3CaSO_4 \bullet 26H_2O$$

These reactions alter the mineral content of the concrete. Products of the sulfate reactions have a greater volume than the reactants. The resulting expansion of the solid phase can lead to cracking which has a deleterious impact on structural integrity and the ability of the cementitious barrier to contain the radioactive waste.

The CBP Project has released a Software Toolbox that includes two models that can be used to assess sulfate attack on Saltstone SDUs and FDCs. The CBP Project is a multi-disciplinary, multi-institutional collaboration supported by the DOE Office of Tank Waste

Management with the objective of developing a set of tools to improve understanding and prediction of the long-term performance of cementitious barriers used in nuclear applications. The CBP is a partnership of federal, academic, private sector, and international expertise. In addition to the DOE, the CBP partners are the SRNL, Consortium for Risk Evaluation with Stakeholder Participation (CRESP) at Vanderbilt University, Energy Research Center of the Netherlands (ECN), and SIMCO Technologies, Inc. The NRC is providing support under a Memorandum of Understanding. The National Institute of Standards and Technology (NIST) is providing research under an Interagency Agreement.

One model in the CBP Software Toolbox is a version of the STADIUM code developed by SIMCO, Inc., which models the transport of chemical ions and water through porous materials and reactions between the chemical and mineral species. The model solves a set of coupled differential equations describing one-dimensional transport processes while simultaneously evaluating local diffusion coefficients and equilibrium chemical and mineral compositions in the materials. STADIUM can model systems with one (concrete), two (concrete and saltstone) or three (concrete, saltstone and soil) layers of material. One limitation of STADIUM modeling is that structural changes and damage to the concrete have no direct impact on the diffusion and transport properties.

The other model included in the CBP Software Toolbox for sulfate attack is based on LeachXS/Orchestra (LXO) developed at the ECN and Vanderbilt University with CRESP funding. Similar to STADIUM, LXO calculates transport rates of species through porous media and chemical equilibrium between local chemical and mineral phases. However, the LXO sulfate attack module also performs a damage calculation and modifies transport properties where damage is predicted. LXO models the material as a network of interconnected cells within which chemical equilibrium is maintained while transport of chemical species between cells occurs by diffusion and convection. The version of LXO released with the initial CBP Toolbox only allows modeling a single material. Because of its capability to perform damage calculations the LXO model predicts faster degradation and thus has been used in this SA to develop rates for cementitious materials degradation from sulfate attack.

The use of Orchestra (the modeling component of LXO) to model sulfate attack on cementitious material requires the use of a parameter designated as the “fractional porosity” which is defined to be the fraction of the pore volume that must be filled with mineral products from the chemical reactions that occur during concrete aging before cracking and concrete damage occurs. The larger the fractional porosity the more pore volume available for solid product deposition and the less damage occurs.

Based on model calibration and literature review the optimal value for fractional porosity is 0.3. [SRNL-STI-2013-00118] The main effect of fractional porosity in the model is to cause an increase in the diffusion coefficient, which accelerates delivery of sulfate to the reaction front and ettringite penetration. The model implicitly assumes saturated conditions for this calculation. However, any cracks that form during sulfate attack are expected to be unsaturated under SDF conditions. Such “dry” cracks would likely cause a smaller increase in diffusion coefficient compared to saturated cracks, or even impede diffusion. Unsaturated cracks and slower diffusion compared to saturated conditions can be approximately

accounted for by increasing fractional porosity above 0.3. Based on engineering judgment, the nominal value for the fractional porosity is assumed to be 0.45 with a conservative estimate of 0.3 and a best estimate of 0.6. [SRNL-STI-2013-00118] The progression of an ettringite mineral front into the concrete coincides with the extent of concrete damage according to the LXO sulfate attack model. After an initial period of rapid penetration, the rate of progression of the ettringite front predicted by LXO was found to be approximately linear, in contrast to a square root of time dependence for a fixed diffusivity. Mineralogy for SDUs 1 and 4 and FDC concretes were selected through the CBP Toolbox interface. Table 4.2-3 presents the results of the LXO sulfate attack model for the SDF concrete.

Table 4.2-3: Results of LXO Sulfate Attack Calculations

Concrete	Thickness (inches)	Estimated Time for Complete Degradation (years)		
		Fractional Porosity		
		0.3	0.45	0.6
FDC Roof and Walls	8	757	961	1,872
FDC Floor and upper mud mat	12	1,135	1,442	2,807
SDUs 1 and 4 Floor	24	1,325	1,648	3,958
SDU 1 Roof	6	331	412	990
SDU 4 Roof	4	221	275	660

[SRNL-STI-2013-00118]

4.2.2.2 Cementitious Material Degradation from Carbonation

Carbonation commonly refers to the reaction of carbon dioxide with calcium hydroxide (Portlandite) to form calcium carbonate (calcite):

$$Ca(OH)_2 + H_2O + CO_2 \rightarrow CaCO_3 + 2H_2O$$

More generally, carbonation in the context of concrete may include other reactions of carbon dioxide with calcium-bearing minerals, such as CSH. Carbonation increases mechanical strength and decreases alkalinity to a pH around 8.5 in cementitious materials. While the former is generally beneficial, corrosion of embedded steel accelerates as pH approaches carbonated conditions, approximately pH < 10. The volume of the corrosion products far exceeds that of the uncorroded steel, which typically introduces sufficient internal pressure to cause cracking and spalling of the surrounding concrete. Most FDC concrete components contain reinforcing steel, notable exceptions being the upper mud mat and lower mud mat in the FDC design. Saltstone and the clean cap also contains embedded steel in the form of support columns (in SDU 4 and FDCs) and roof trusses (in SDU 4), as discussed in Sections 3.3.2 and 3.3.3.

This analysis considers the transport of carbon dioxide through the gas phase, which is appropriate for unsaturated concrete, as well as the delivery of dissolved carbon dioxide under fully saturated conditions. The saturation state of the cementitious material strongly affects the rate of carbonation, particularly near full saturation. The anticipated saturation states for SDF cementitious materials can be assessed from estimated soil suction and relative humidity values.

Once buried under a low-permeability cover system, the soil conditions at the SDF will initially approach gravity equilibrium (no infiltration), where matric suction prevents water from infiltrating to the water table. Soil moisture contains dissolved solids, but the concentrations are dilute such that osmotic suction is negligible compared to that within cementitious materials. Any amount of infiltration produces lower capillary suction levels than gravity equilibrium. Thus as the cover system degrades over time, soil suction levels will decrease. With this consideration, the maximum suction head anticipated for the FDCs is roughly 1,500 centimeters (15 meters), the approximate height of the FDCs above the water table. The air entry head is observed to exceed 1,000 centimeters for saltstone and 10,000 centimeters for SDF concrete (see Figure 4.2-4). Thus, the concrete is expected to be saturated at all times. Ignoring osmotic effects, saltstone would be slightly unsaturated immediately after cap placement, and then would become saturated when the soil suction levels fall below approximately 1,000 centimeters. With osmotic effects, saltstone would be expected to be saturated.

Figure 4.2-4: Water Retention Curves for SDF Concrete and Grout

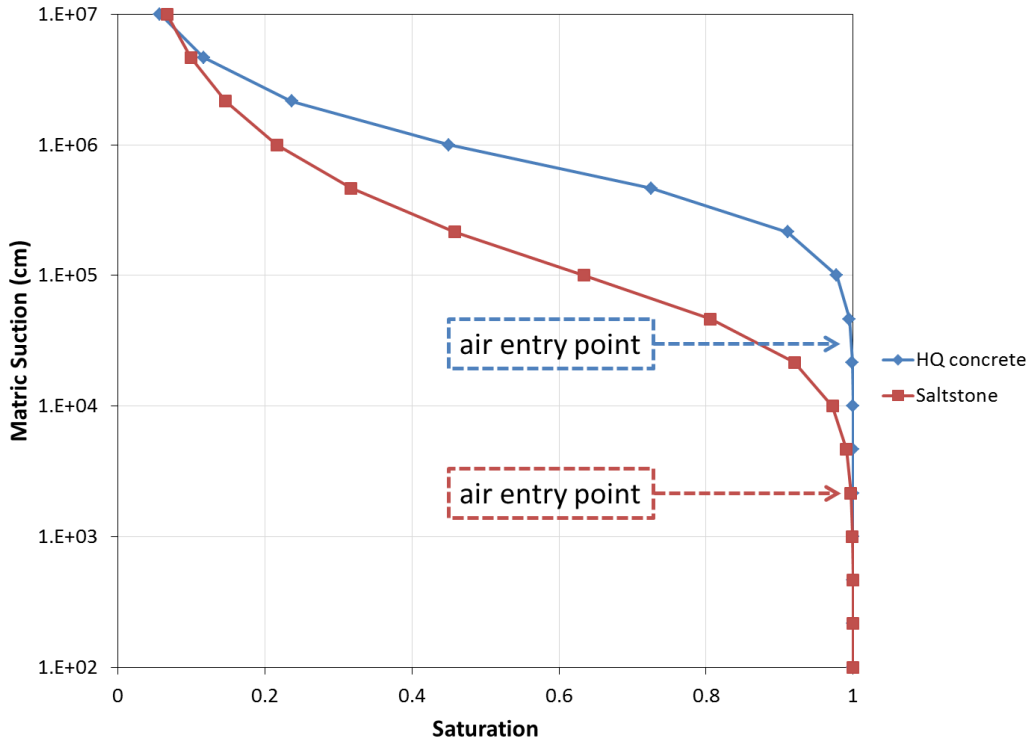

The best estimate for the rate of cementitious degradation is calculated by assuming a capillary suction of 1,500 centimeter and pure water occupying pore space (i.e., neglecting osmotic effects). Under these conditions concrete is fully liquid saturated and saltstone is liquid 99.8 % saturated. The conservative estimate rate implicitly assumes that connected fractures or similar unsaturated macro-porous features are present such that an equivalent of 5 % of the pore space is open for gas-phase transport (i.e., 5 % gas saturation). As a nominal rate, an intermediate setting of 2 % gas saturation is chosen. Table 4.2-4 presents the

intermediate results of the carbonation rate constant for these three values using an analytic solution.

As a point of reference, detailed simulations were performed for the carbonation of representative FDC concrete, using LXO in a developmental CBP Software Toolbox carbonation module. These simulations considered various carbon dioxide concentrations based on 30 % porosity (rather than 11 %), 90 % liquid saturation (rather than 95 %), and a diffusion coefficient of 1.0E-06 m^2/s (rather than 5.0E-10 m^2/s). At these settings, with a partial pressure of carbon dioxide of 0.01 atmosphere, roughly equivalent to the estimated average and median partial pressure of carbon dioxide in the SRS vadose zone soil, the equivalent carbonation rate constant is A = 0.083 cm/√yr. This value is significantly lower than the conservative estimate shown in Table 4.2-4 of 0.27 cm/√yr. This suggests that the analytic solution is biased in the conservative direction.

Table 4.2-4: Selected Input and Carbonation Rate Constants

Parameter	FDC Concrete	SDU 1/4 Floor	SDU 4 Roof	SDU 1 Roof	Saltstone
CO2 partial pressure in soil (atm)	0.01	0.01	0.01	0.01	0.01
Porosity (%)	11	12	13.6	14.5	58
Particle density (g/mL)	2.22	2.24	2.21	2.20	1.01
Diffusion coefficient (cm^2/s)	5.0E-08	5.0E-08	1.0E-07	1.0E-07	1.0E-08
Best Estimate					
Gas saturation (%)	0	0	0	0	0.2
Carbonation Rate Constant (cm/√yr)	0.0090	0.0077	0.0124	0.0138	0.21
Nominal Value					
Gas saturation (%)	2	2	2	2	2
Carbonation Rate Constant (cm/√yr)	0.17	0.18	0.21	0.24	0.72
Conservative Estimate					
Gas saturation (%)	5	5	5	5	5
Carbonation Rate Constant (cm/√yr)	0.27	0.28	0.33	0.37	1.1

[Extracted from Table 3-1 of SRNL-STI-2013-00118]

Implicit in the analysis is the assumption of a constant diffusion coefficient. If physical damage is occurring as a result of carbonation, then the diffusion coefficient may increase and the front penetrates deeper than indicated by a √t dependence. The √t dependence is a result of increasing distance between the exposure boundary and the reaction front. If damage occurs around the reaction front, then the diffusion distance may effectively not increase beyond some maximum distance, δ [cm], and penetration will be proportional to time instead of √t. A reasonable assumption for the maximum diffusion distance, δ [cm], is the depth of concrete cover over reinforcing steel, approximately 5 centimeter in typical construction based on concrete code ACI 318. To account for the feedback effects of physical damage on diffusion rates, the minimum is taken as the estimated failure time t_0 for a specified material thickness x_0, as shown below.

$$t_0 = min\left[\frac{x_0^2}{A^2}, \frac{\delta x_0}{A^2}\right]$$

Table 4.2-5 provides the estimated time for complete degradation from carbonation for the various SDF cementitious materials. Note that saltstone is included in Table 4.2-5 to address the potential degradation of saltstone from carbonation for the support columns in FDC and SDU 4 and the roof truss system in SDU 4. To eliminate the potential for unwanted flow impacts within the saltstone monolith in SDU 4 and FDC from the degradation of the columns, the columns are assumed to consist of saltstone rather than Type II concrete for the SDU 4 and Type V cement in Class III concrete for the FDCs. Again, these assumptions are biased in the conservative direction.

Table 4.2-5: Results of Carbonation Analysis for SDF Cementitious Materials

SDF Cementitious Material	Thickness (inches)	Estimated Time for Complete Degradation (years)		
		Conservative Estimate	Nominal Value	Best Estimate
FDC Roof and Walls	8	1,393	3,477	1,241,804
FDC Floor and upper mud mat	12	4,178	10,430	3,725,412
SDU 1 and 4 Floor	24	3,855	9,628	5,135,311
SDU 1 Roof	6	683	1,705	499,174
SDU 4 Roof	4	455	1,137	332,782
SDU 4 Saltstone (and clean cap)	41.4[(a)]	403	1,008	11,923
FDC and SDU 4 Columns	24[(b)]	234	585	6,917

(a) Estimated depth, 3.45 feet, of saltstone and clean cap impacted by the roof support truss system employed in SDU 4

(b) Columns are assigned initial properties of saltstone to minimize impact of flow through the saltstone monolith, degradation is based on 2 foot length segments

4.2.2.3 Cementitious Material Degradation from Decalcification

Decalcification in this application refers to leaching of Ca^{2+} in pore water to exterior soil, where the concentration is assumed to be zero. [WSRC-STI-2007-00607; SRNL-STI-2010-00035] Leaching may occur through diffusion and/or advection. For diffusion-controlled release between a sharp dissolution front and a soil interface, the penetration depth is:

$$x = \left[\frac{2\theta D_e c_{Ca^{2+}} t}{c_{Ca}}\right]^{1/2} = At^{1/2}$$

Where:

x = penetration depth [cm]

θ = liquid content, [cm^3 liquid / cm^3 total]

D_e = effective diffusion coefficient for liquid phase, τD_m [cm^2/yr]

t = elapsed time [yr]

$c_{Ca^{2+}}$ = dissolved Ca^{2+} concentration [mol / cm^3 liquid]

c_{Ca} = calcium concentration in solid phase [mol / cm^3 total]

The decalcification rate is given by the following expression:

$$A \equiv \left[\frac{2\theta D_e c_{Ca^{2+}}}{c_{Ca}}\right]^{1/2}$$

Table 4.2-6 summarizes the input parameters for determining the rate of decalcification via diffusion. The concentration of Ca^{2+} varies through the leaching process; alkali metals leach first, followed by hydroxide, and then CSH, calcium silicate hydrate. In this analysis, dissolution of CSH is assumed to control the concentration of Ca^{2+} over most of the leaching process, considering that little or no Portlandite, $Ca(OH)_2$, is expected in SDF cementitious materials. The CSH dissolves incongruently in that calcites leach preferentially in comparison to silicates. SRNL-STI-2013-00118 reports measured $c_{Ca^{2+}}$ = 1.8 - 2.0 mmol/L in SDF concrete; thus, a value of 2.0E-06 mol/cm^3 is assumed in Table 4.2-6. The rate constants for decalcification controlled by diffusion are low indicating a slow process. Comparing the nominal value carbonation rate constants in Table 4.2-5 to the nominal value decalcification rate constants in Table 4.2-6, carbonation is more than twice as fast as decalcification. Thus, for relatively thin concrete barriers decalcification will not be further considered.

Table 4.2-6: Selected Input and Rate Constants for Diffusion-Limited Decalcification

Parameter	FDC	SDU 1/4	SDU 4 Roof	SDU 1 Roof	Saltstone
Porosity	0.11	0.12	0.136	0.145	0.58
Particle density (g/cm^3)	2.22	2.24	2.21	2.20	1.01
$c_{Ca^{2+}}$ (mol/cm^3 liquid)	2.0E-06	2.0E-06	2.0E-06	2.0E-06	2.0E-06
$[Ca(OH)_2]$ (g/kg)	0	7.2	-	-	0
$c_{Ca(OH)_2}$ (mol/cm^3 total)	0	2.18E-04	-	-	0
$[CSH]$ (g/kg)	81.2	118.8	-	-	147.4
c_{CSH} (mol/cm^3 total)	9.90E-04	1.46E-03	-	-	8.18E-04
c_{Ca} (mol/cm^3 total)	1.63E-03	2.63E-03	2.11E-03	1.82E-03	1.35E-03
S_ℓ (cm^3 liquid / cm^3 void)	1	1	1	1	0.9983
θ_ℓ (cm^3 liquid / cm^3 total)	0.110	0.120	0.136	0.145	0.579
Best Estimate Value					
Diffusion coefficient (cm^2/s)	5.0E-08	5.0E-08	1.0E-07	1.0E-07	1.0E-08
Decalcification Rate (cm/√yr)	0.021	0.017	0.028	0.032	0.023
Nominal Value (10 times Best Estimate)					
Diffusion coefficient (cm^2/s)	5.0E-07	5.0E-07	1.0E-06	1.0E-06	1.0E-07
Decalcification Rate (cm/√yr)	0.065	0.054	0.090	0.10	0.074
Conservative Estimate (100 times Best Estimate)					
Diffusion coefficient (cm^2/s)	5.0E-06	5.0E-06	1.0E-05	1.0E-05	1.0E-06
Decalcification Rate (cm/√yr)	0.206	0.170	0.285	0.317	0.233

[SRNL-STI-2013-00118]

While diffusion may control the decalcification of thinner features at earlier times, specifically in concrete barriers, advection is more likely to control decalcification of saltstone because of its greater dimension and hydraulic conductivity. Considering downward flow, a quasi-steady state advective mass balance for decalcification is:

$$U \cdot c_{Ca^{2+}} \cdot t = c_{Ca} \cdot h$$

Where:

U = Darcy velocity (volumetric water flux) [cm/yr]

t = elapsed time [yr]

h = monolith height [cm]

The above expression assumes that advection occurs uniformly through the entire thickness, the dissolution front advances uniformly, and the exit concentration coincides with Ca^{2+} solubility. Solving for time yields:

$$t = \frac{c_{Ca}}{c_{Ca^{2+}}} \cdot \frac{h}{U}$$

The hydraulic head gradient in vadose zone soil tends to be one or less, such that the flow rate is equal to or less than the saturated hydraulic conductivity, per Darcy's Law. For saltstone placed in the vadose zone, the head gradient can be higher as infiltration flows around the lower permeability monolith. The assumptions for the best estimate, nominal value, and conservative estimate scenarios are U = 1, 10, and 100 times the saturated conductivity, respectively. Table 4.2-7 presents the estimated times for complete degradation of saltstone based on the three values for *U* from decalcification via advection.

Table 4.2-7: Saltstone Degradation from Decalcification via Advection

Parameter	SDU 1	FDC	SDU 4
c_{Ca} (mol/cm^3 total)	1.35E-03	1.35E-03	1.35E-03
$c_{Ca^{2+}}$ (mol/cm^3 liquid)	2.0E-06	2.0E-06	2.0E-06
Hydraulic conductivity (cm/s)	6.4E-09	6.4E-09	6.4E-09
Hydraulic conductivity (cm/yr)	0.202	0.202	0.202
Saltstone height (feet)	24.5	22	22.75[(a)]
Best estimate (U = 1)			
Time for complete degradation (years)	2,495,499	2,240,856	2,317,249
Nominal value (U = 10)			
Time for complete degradation (years)	249,550	224,086	231,725
Conservative estimate (U = 100)			
Time for complete degradation (years)	24,995	22,409	23,172

(a) The first 2 feet of saltstone is included in the portion that is degraded via carbonation

4.2.2.4 Performance of Other Barriers to Delay Cementitious Material Degradation

The FDCs have a High Density Polyethylene (HDPE) liner along the exterior of the walls and a composite layer of HDPE and a Geosynthetic Clay Liner (GCL) that covers the roof and separates the upper mud mat and lower mud mat. The degradation of these barriers must occur prior to the diffusion of carbon (in the air), for degradation by carbonation, or calcium (in the groundwater), for degradation by decalcification, into the concrete. The degradation data for these barriers is provided in Table 4.2-8.

Table 4.2-8: Degradation of HDPE and HDPE-GCL

Time Period (years)	HDPE Hydraulic Conductivity		HDPE-GCL Hydraulic Conductivity	
	Value (cm/s)	Ratio to Initial Value	Value (cm/s)	Ratio to Initial Value
0 - 50	5.87E-10	1	2.19E-11	1
900 – 1,000	6.04E-08	103	1.50E-09	68.5
1,400 – 1,600	9.69E-08	165	2.31E-09	105
9,500 – 10,000	6.44E-07	1,097	1.09E-08	498

[SRNL-STI-2009-00115, Appendix E]

To conservatively assess the performance of the HDPE and the HDPE-GCL, the initiation of the degradation of the FDC wall and the roof is assumed to occur after 900 years and 1,400 years, respectively (corresponding to the time that the effectiveness of the barrier is reduced by a factor of approximately 100). Because the lower mud mat is initially assumed to have soil properties, the degradation of the floor and upper mud mat starts after 1,400 years, when the HDPE-GCL is assumed degraded.

4.2.2.5 Summary of SDF Cementitious Material Degradation

Using the results from the previous sections, summary tables are developed and presented below which provide the mechanisms of degradation, time for complete degradation, and delay times (if any) for the various cementitious materials in the SDUs and FDCs. Where competing mechanisms for degradation exist, the time for complete degradation occurs when the sum of the depths of penetration from each degradation mechanism equals the thickness of the material. For example, the 8-inch thick FDC wall degrades externally from carbonation and internally from sulfate attack. Once the depth of the carbonation front (starting from the outside) plus the depth of sulfate attack front (starting from the inside) equals the thickness of the wall, the wall is considered fully degraded.

Table 4.2-9 presents the results of the analysis described for SDU 1 in SRNL-STI-2013-00118. The internal roof degradation is delayed from sulfate attack by the time it takes for the six-inch thick clean cap to degrade by sulfate attack from saltstone. The delay for the degradation of saltstone and clean cap is the degradation of the roof.

Table 4.2-9: Degradation Analysis Summary for SDU 1

SDU 1 Feature (thickness)	Mechanism(s) for Degradation					
	Best Estimate		Nominal Value		Conservative Estimate	
Roof (8 inches)	Sulfate	Carbonation	Sulfate	Carbonation	Sulfate	Carbonation
Degradation (inches)	5.77	0.23	3.86	2.14	2.82	3.18
Degradation (years)	952	1,761	265	489	156	292
Delay (years)	809	0	224	0	136	0
Elapsed time (years) [a]	1,761		489		292	
Floor (24 inches)	Sulfate	Carbonation	Sulfate	Carbonation	Sulfate	Carbonation
Degradation (inches)	23.8	0.2	20.5	3.5	17.9	6.1
Degradation (years)	3,927	3,927	1,407	1,407	986	986
Delay (years)	0	0	0	0	0	0
Elapsed time (years)	3,927		1,407		986	
Saltstone (24.5 feet) [b]	Decalcification		Decalcification		Decalcification	
Degradation (feet)	24.5		24.5		24.5	
Degradation (years)	2,495,499		249,550		24,955	
Delay (years)	1,761		489		292	
Elapsed time (years)	2,497,260		250,039		25,247	

[Data obtained from Table 5-3 of SRNL-STI-2013-00118]

a. Because of a transcription error the elapsed time for the degradation of the roof used in the flow runs was 507 years for the nominal value and 1,765 years for the best estimate value. This small variation has no appreciable impact on the analyses.

b. The 24.5 feet thickness includes the 6-inch thick clean cap.

Table 4.2-10 presents the results of the analysis described for SDU 4 in SRNL-STI-2013-00118. The internal roof degradation is delayed from sulfate attack by the time it takes for the minimum thickness of the clean cap (17.4 inches, SRR-CWDA-2009-00017, Table 4.4-2) to degrade via sulfate attack from saltstone. The delay for the degradation by carbonation of the top portion of saltstone (clean cap and 2 feet of saltstone) is the degradation of the roof. The delay for the degradation of the remaining saltstone is the degradation of the top portion of saltstone and clean cap. The degradation of the column is analyzed by 2-foot length segments and starts from the top of the column and from the bottom of the column. The degradation of the column is initially delayed by the degradation of the roof, or the floor, whichever is sooner. Each subsequent column segment starts degrading once the upper (or lower) adjacent segment has degraded.

Table 4.2-10: Degradation Analysis Summary for SDU 4

SDU 4 Feature (thickness)	Mechanism(s) for Degradation					
	Best Estimate		Nominal Value		Conservative Estimate	
Roof (4 inches)	Sulfate	Carbonation	Sulfate	Carbonation	Sulfate	Carbonation
Degradation (inches)	3.58	0.42	0	4	0	4
Degradation (years)	591	7,375	0	1,137	0	455
Delay (years)	6,784	0	1,879	0	1,141	0
Elapsed time (years)	7,375		1,137		455	
Floor (24 inches)	Sulfate	Carbonation	Sulfate	Carbonation	Sulfate	Carbonation
Degradation (inches)	23.8	0.2	20.5	3.5	17.9	6.1
Degradation (years)	3,927	3,923	1,407	1,407	986	986
Delay (years)	0	0	0	0	0	0
Elapsed time (years)	3,923		1,407		986	
Top Saltstone (3.45 feet) [a]	Carbonation		Carbonation		Carbonation	
Degradation (feet)	3.45		3.45		3.45	
Degradation (years)	11,923		1,008		403	
Delay (years)	7,375		1,137		455	
Elapsed time (years)	19,297		2,145		859	
Saltstone (22.75 feet) [b]	Decalcification		Decalcification		Decalcification	
Degradation (feet)	22.75		22.75		22.75	
Degradation (years)	2,317,249		231,725		23,172	
Delay (years)	19,297		2,145		859	
Elapsed time (years)	2,336,546		233,869		24,031	
Column (2 feet, length)	Carbonation		Carbonation		Carbonation	
Degradation (feet)	2		2		2	
Degradation (years)	6,917		585		234	
Delay (years)	3,923		1,137		455	
Elapsed time (years)	10,839		1,721		689	

[Data obtained from Table 5-2 of SRNL-STI-2013-00118]

a. Top of saltstone includes the minimum clean cap thickness and the top 2 feet of saltstone.

b. The remaining saltstone thickness is 2 feet less than the total saltstone thickness shown in SDF PA, Table 4.4-2.

Table 4.2-11 presents the results of the analysis described for FDC in SRNL-STI-2013-00118. The internal roof degradation is delayed from sulfate attack by the time it takes for the 2-foot thick clean cap to degrade via sulfate attack from saltstone. The external roof degradation is delayed until the HDPE-GCL has degraded, estimated to be 1,400 years. The external degradation of the wall is delayed until the HDPE has degraded, estimated to be 900 years. The external degradation of the floor and upper mud mat is delayed until the HDPE-GCL has degraded, estimated to be 1,400 years. The delay for the degradation of the saltstone and clean cap is the degradation of the roof. The degradation of the column is analyzed by 2-foot length segments and starts from the top of the column and from the bottom of the column. The degradation of the column is initially delayed by the degradation of the floor, which occurs sooner than the degradation of the roof. Each subsequent column segment starts degrading once the upper (or lower) adjacent segment has degraded.

Table 4.2-11: Degradation Analysis Summary for FDCs

FDC Feature (thickness)	Mechanism(s) for Degradation					
	Best Estimate		Nominal Value		Conservative Estimate	
Roof (8 inches)	Sulfate	Carbonation	Sulfate	Carbonation	Sulfate	Carbonation
Degradation (inches)	7.59	0.41	2.32	5.68	2.29	5.71
Degradation (years)	1,775	13,325	279	2,466	216	994
Delay (years)	12,950	1,400	3,587	1,400	2,178	1,400
Elapsed time (years)	14,725		3,866		2,394	
Wall (8 inches)	Sulfate	Carbonation	Sulfate	Carbonation	Sulfate	Carbonation
Degradation (inches)	7.89	0.11	7.68	0.32	8	0
Degradation (years)	1,846	945	923	23	757	0
Delay (years)	0	900	0	900	0	900
Elapsed time (years)	1,845		923		757	
Floor + upper mud mat (12 inches)	Sulfate	Carbonation	Sulfate	Carbonation	Sulfate	Carbonation
Degradation (inches)	11.9	0.1	11.8	0.2	12	0
Degradation (years)	2,776	1,375	1,413	13	1,135	0
Delay (years)	0	1,400	0	1,400	0	1,400
Elapsed time (years)	2,775		1,413		1,135	
Saltstone (22 feet) [a]	Decalcification		Decalcification		Decalcification	
Degradation (feet)	22		22		22	
Degradation (years)	2,240,856		224,086		22,409	
Delay (years)	14,725		3,866		2,394	
Elapsed time (years)	2,255,581		227,952		24,803	
Column (2 feet, length)	Carbonation		Carbonation		Carbonation	
Degradation (feet)	2		2		2	
Degradation (years)	6,917		585		234	
Delay (years)	2,775		1,413		1,135	
Elapsed time (years)	9,691		1,998		1,369	

[Data from Table 5-1 of SRNL-STI-2013-00118]

4.2.3 Hydraulic Properties of Cementitious Materials

Using the times for degradation presented in Section 4.2.2.5, the hydraulic properties (i.e., the initial saturated hydraulic conductivities and the effective diffusion coefficients) of the cementitious materials are degraded linearly over time until the hydraulic properties are equal to the hydraulic properties of the surrounding soil. The use of soil properties as an end state is a conservative assumption. The intact and degraded hydraulic properties for the cementitious materials are shown in Table 4.2-12. When there are competing degradation mechanisms, the minimum delay time of the two mechanisms is used to delay the start of degradation and the "elapsed time" presented in the summary table, minus the delay time, is used to determine the linear rate of change of the hydraulic property.

Table 4.2-12: Intact and Degraded Hydraulic Properties of SDU Cementitious Materials

Feature	Saturated Hydraulic Conductivity (cm/s)		Diffusion Coefficient (cm^2/s)	
	Intact	Degraded	Intact	Degraded
SDU 1 and 4 Roof [a]	5.0E-09	4.1E-05	1.0E-07	5.3E-06
SDU 1 and 4 Floor [a]	3.1E-10	9.1E-05	5.0E-08	5.3E-06
SDU 1 and 4 Walls [a]	4.1E-05		5.3E-06	
FDC Roof and Wall [a]	9.3E-11	4.1E-05	5.0E-08	5.3E-06
FDC Floor and Upper Mud Mat [a]	9.3E-11	9.1E-05	5.0E-08	5.3E-06
FDC Lower Mud Mat [a]	9.1E-05		5.3E-06	
Column Concrete, Saltstone and Clean Cap [b]	6.4E-09	4.1E-05	1.0E-08	5.3E-06

a. SRR-CWDA-2009-00017, Table 4.2-16
b. Section 4.2.1

Figures 4.2-5 through 4.2-15 illustrate the increase in the saturated hydraulic conductivity of the cementitious materials for the FDCs and SDUs using the various degradation values.

Note that the assumption of linear degradation is conservative in early time. For example, the SDU 1 roof has an initial saturated hydraulic conductivity of 5.0E-09 cm/s, but because this value increases at a rate of 2.3E-08 cm/s per year, it increases to 2.8E-08 cm/s within a single year and to 2.3E-06 cm/s by the end of the 100-year institutional control period, shown in Figure 4.2-5.

Assuming linear degradation and applying the data from the summary tables in Section 4.2.2.5 (Tables 4.2-9, 4.2-10, and 4.2-11) showed no significant difference between the degradation times for the nominal values and the conservative values for the FDC concrete, as illustrated by Figures 4.2-12 through 4.2-14. For saltstone, Table 4.2-6 shows that the conservative estimate for degradation via decalcification was based on an assumed, but improbable, diffusion coefficient that was 100 times higher than the best estimate value, whereas the nominal degradation rate used a diffusion coefficient that was reasonably conservative at 10 times higher (as illustrated by Figure 4.2-15). Therefore, only the nominal and the best estimate values will be used to investigate the behavior of the SDUs and FDCs in this SA.

Figure 4.2-5: Saturated Hydraulic Conductivity for the SDU 1 Roof

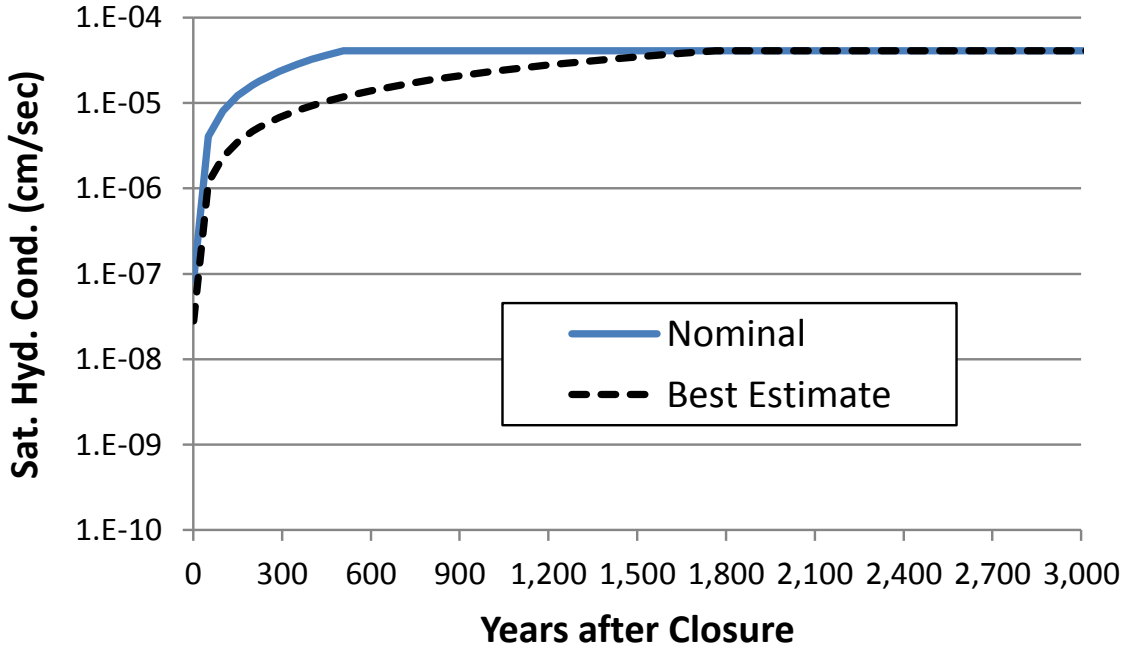

Figure 4.2-6: Saturated Hydraulic Conductivity for the SDU 1 Floor

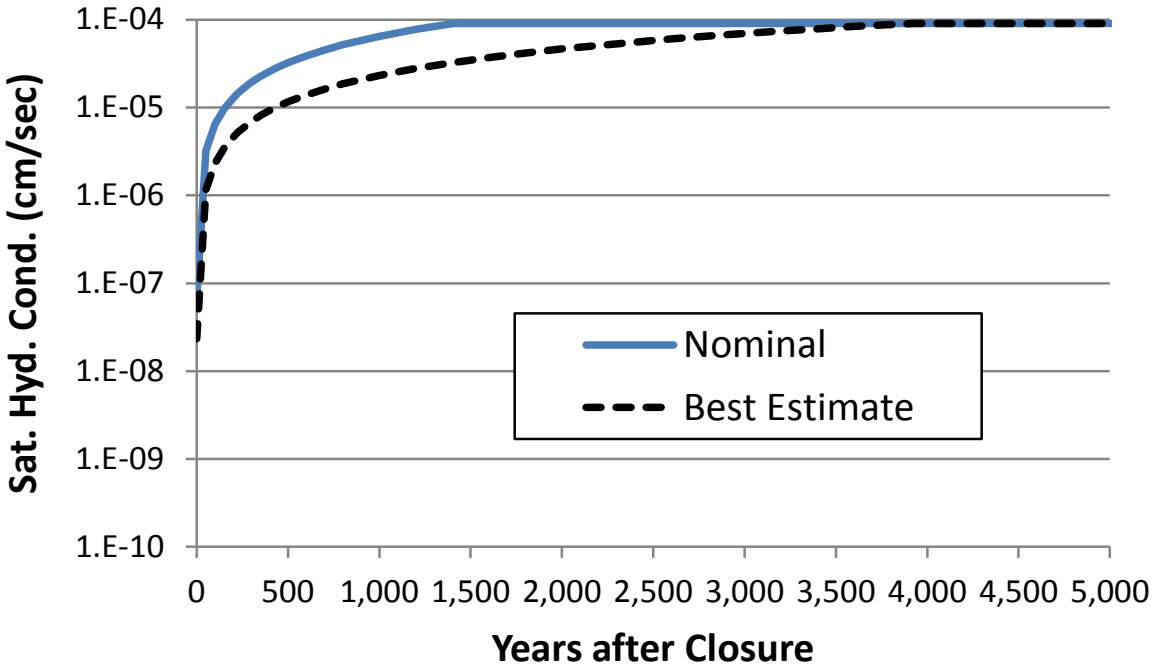

Figure 4.2-7: Saturated Hydraulic Conductivity for the SDU 1 Saltstone

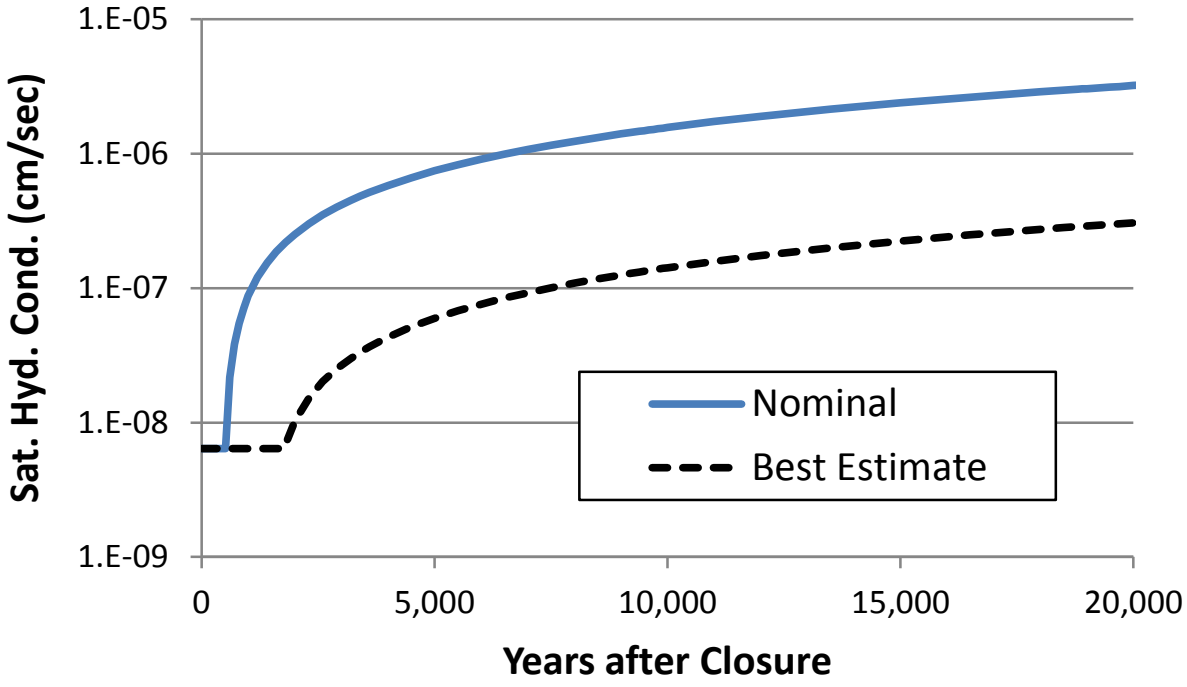

Figure 4.2-8: Saturated Hydraulic Conductivity for the SDU 4 Roof

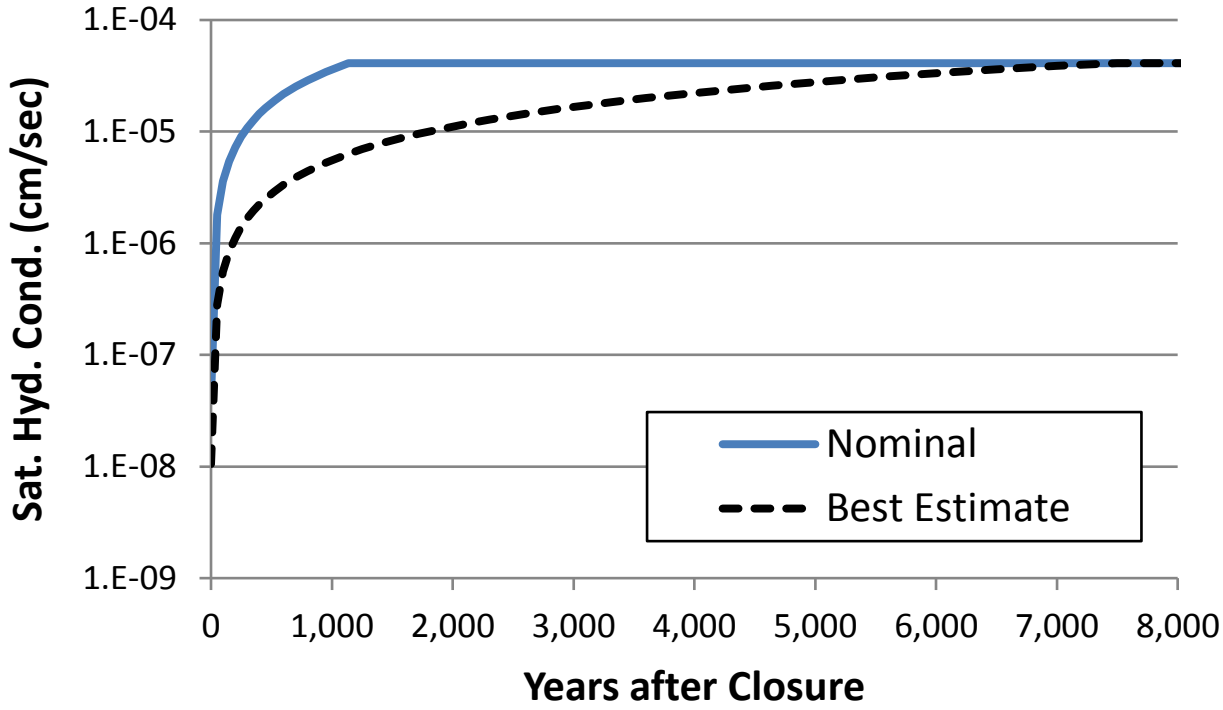

Figure 4.2-9: Saturated Hydraulic Conductivity for the SDU 4 Floor

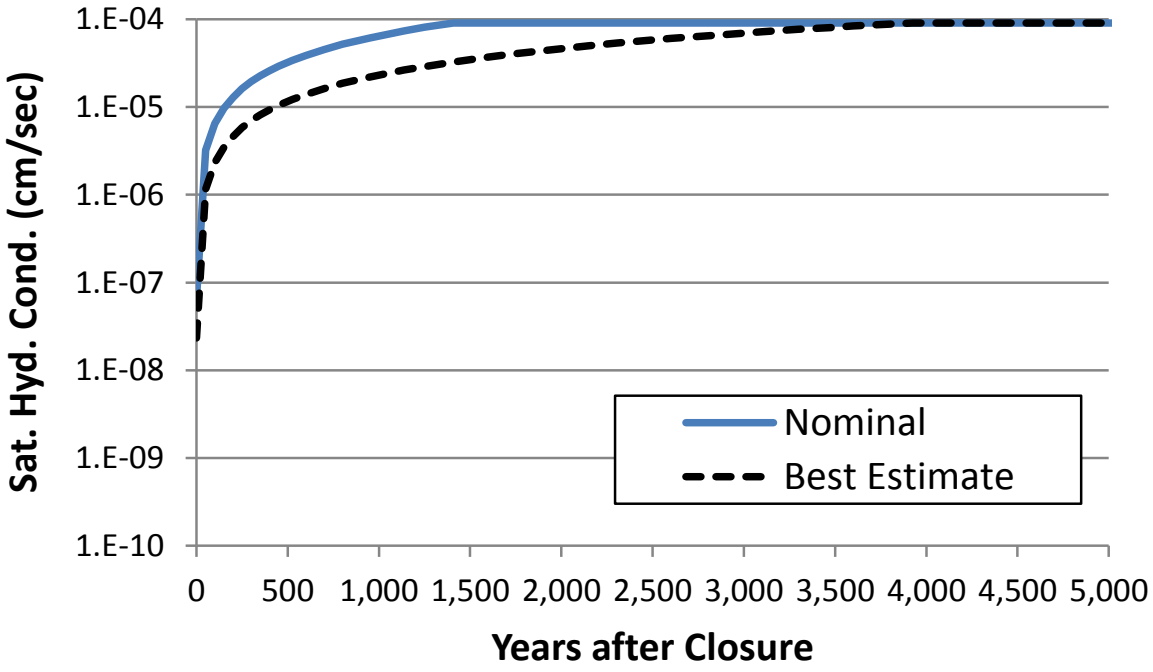

Figure 4.2-10: Saturated Hydraulic Conductivity for the SDU 4 Saltstone (Top)

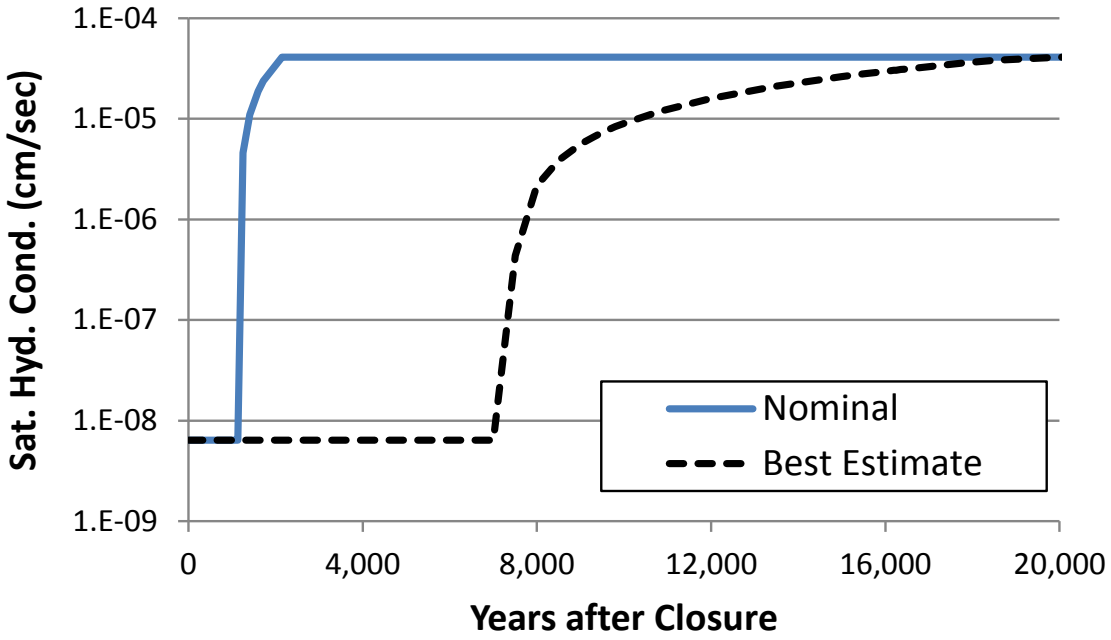

Figure 4.2-11: Saturated Hydraulic Conductivity for the SDU 4 Saltstone (Remaining)

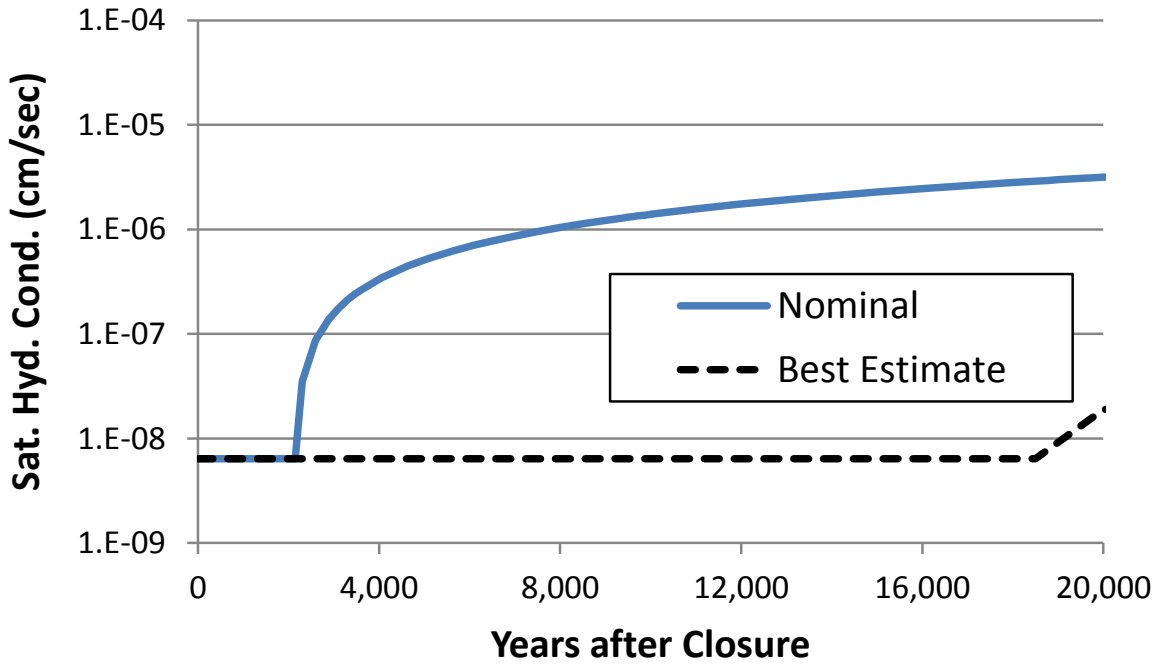

Figure 4.2-12: Saturated Hydraulic Conductivity for the FDC Roof

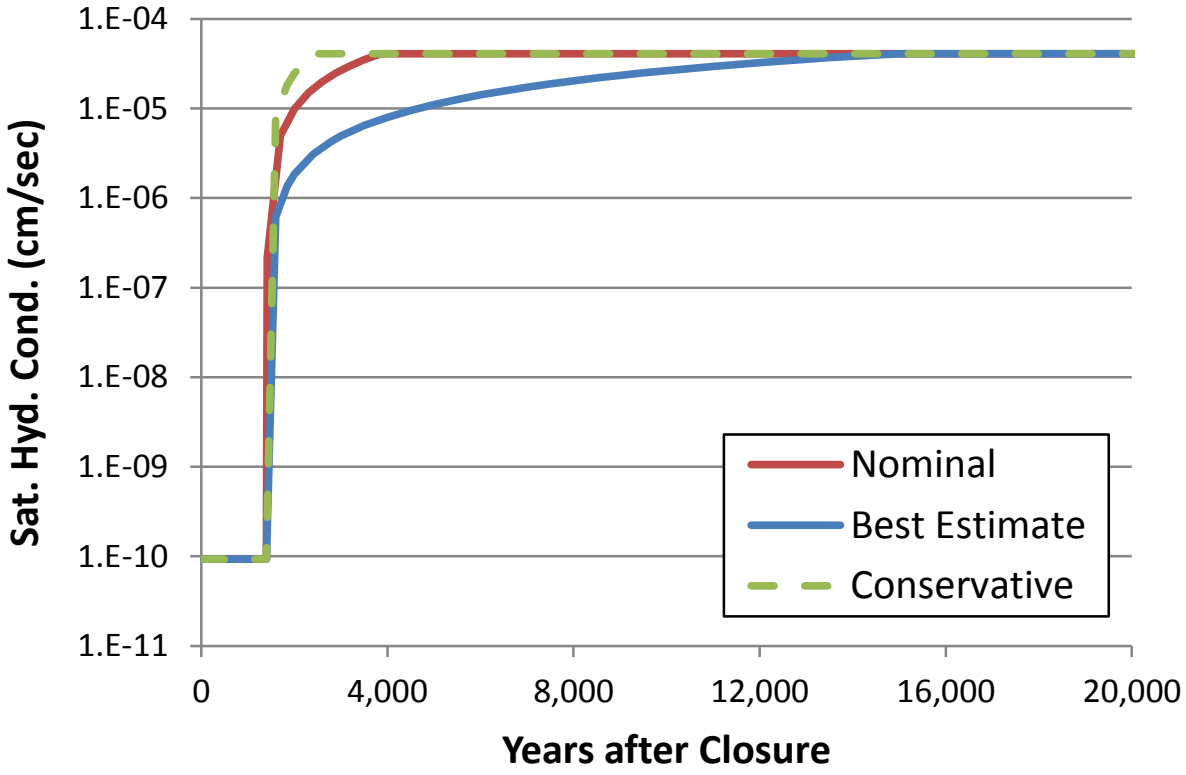

Figure 4.2-13: Saturated Hydraulic Conductivity for the FDC Wall

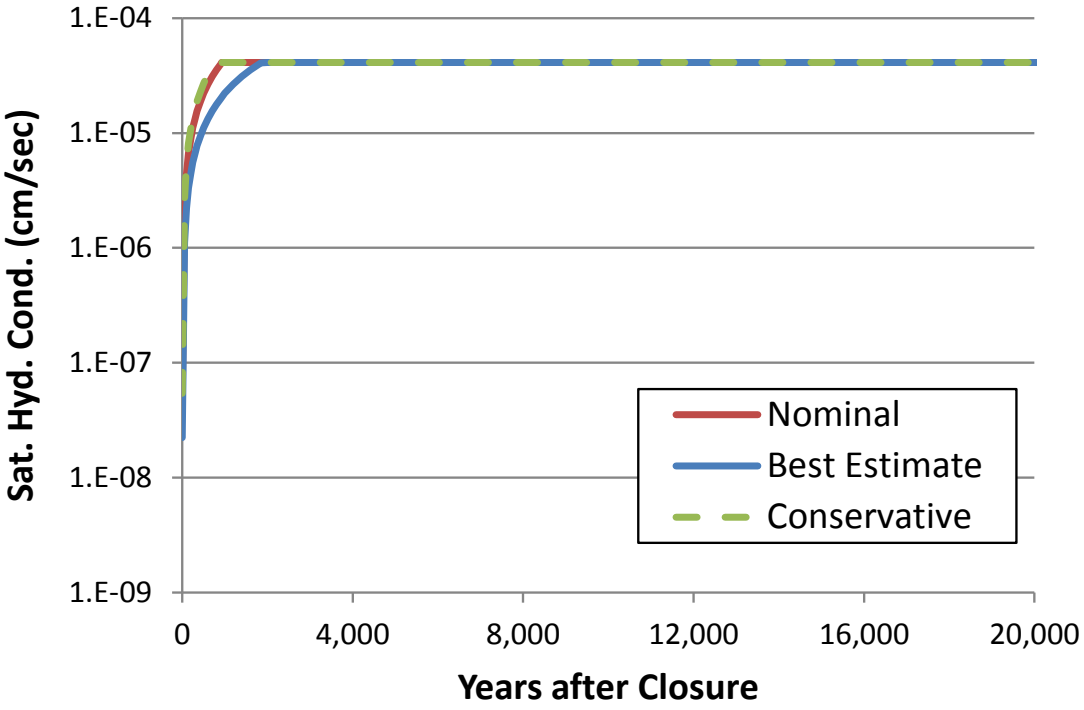

Figure 4.2-14: Saturated Hydraulic Conductivity for the FDC Floor

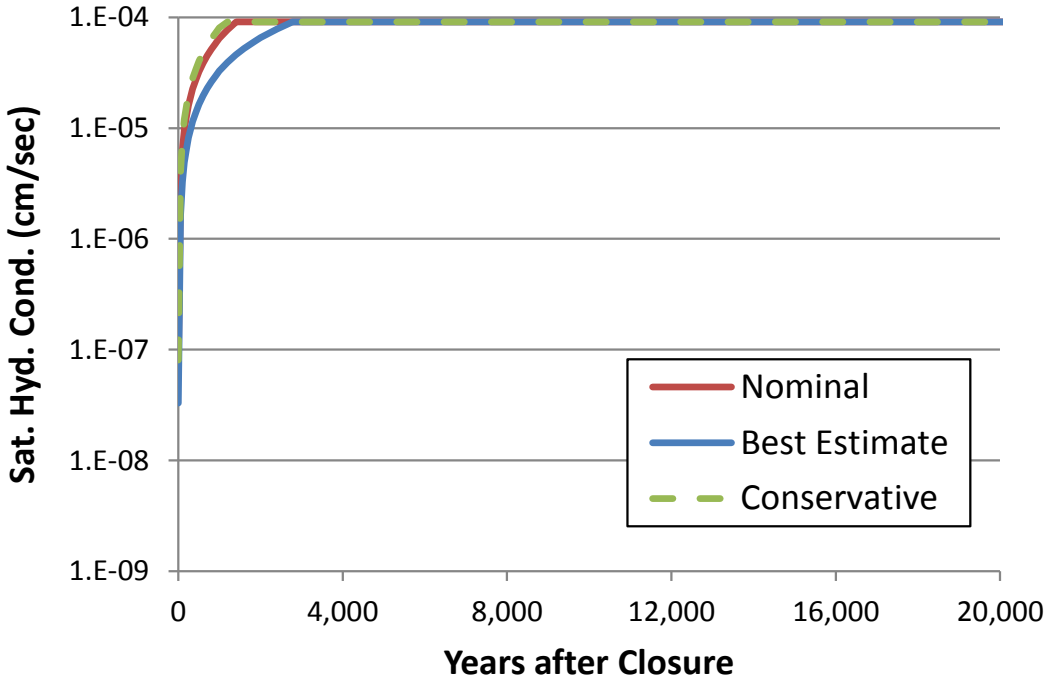

Figure 4.2-15: Saturated Hydraulic Conductivity for the FDC Saltstone

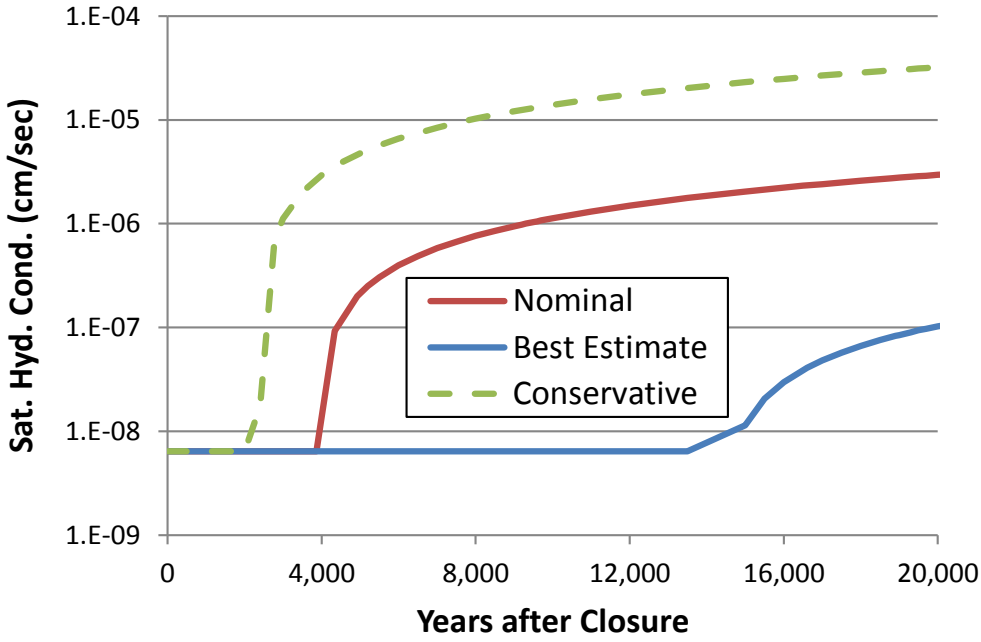

Figures 4.2-16 and 4.2-17 illustrate the change in saturated hydraulic conductivity for the columns in SDU 4 and FDCs for the nominal value case. The 2-foot length column segments in SDU 4 are numbered starting at 1 for the segment at the top of the clean cap and 12 for the segment on the floor. The 2-foot length column segments in FDC are numbered starting at 1 for the segment at the top of the clean cap and 11 for the segment on the floor.

Figure 4.2-16: Saturated Hydraulic Conductivity for the SDU 4 Columns

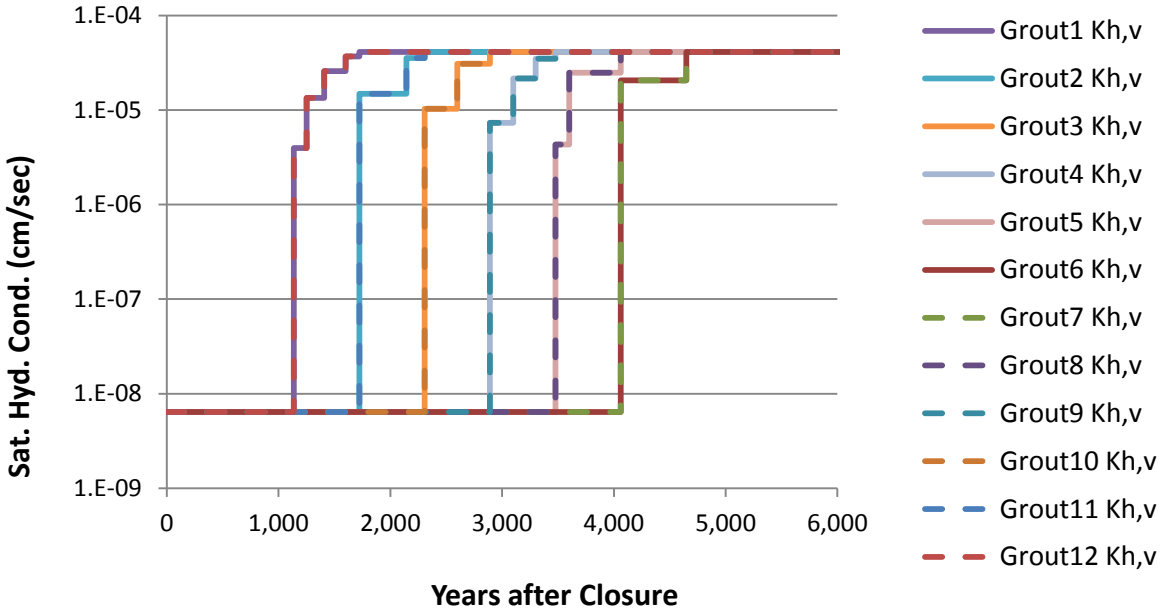

Figure 4.2-17: Saturated Hydraulic Conductivity for the FDC Columns

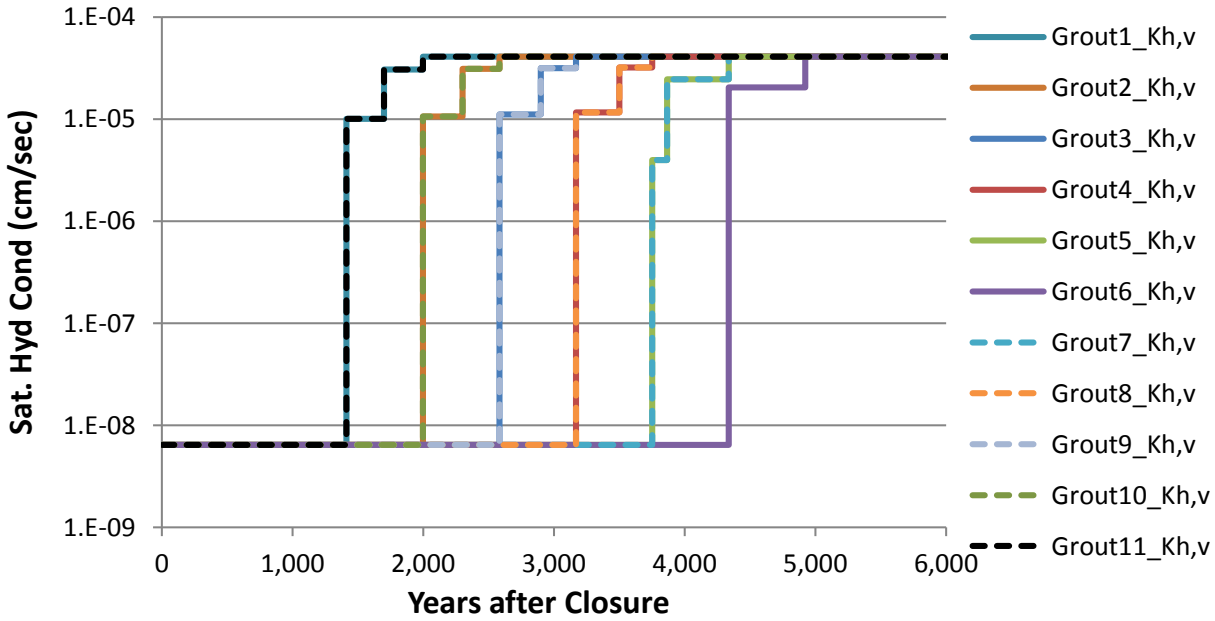

The change in hydraulic properties (saturated hydraulic conductivity and diffusion coefficient) of cementitious material to those of soil should also include a change in the MCCs associated with the cementitious material. Blended MCCs have been developed to simulate the behavior of the cementitious material as it degrades from cementitious material to soil. Figures 4.2-18 through 4.2-21 illustrate this blending of MCCs to effectively transition the cementitious material to soil properties. Figure 4.2-21 includes the MCC for saltstone generated from the data presented in SRNL-STI-2011-00661 for the 20 °C cured saltstone simulant (Section 4.2.1).

In addition to flow through cementitious materials, preferential flow may exist where there is a potential for a faster flow due to the loss of other non-cementitious material barriers, such as water stops in construction joints (described in Sections 3.3.2 and 3.3.3). These flow paths are assumed to have hydraulic properties associated with gravel. This represents a through-floor flow path (i.e., similar to a fracture). Table 4.2-13 provides the hydraulic properties of gravel obtained from SDF PA, Table 4.4-5.

The MCC associated with gravel is shown in Figure 4.2-22. Native soil and backfill are also included for comparison. To determine the sensitivity to flow in the joints from the selection of the MCC medium, flow cases are developed with the MCC associated with the joints to have a relative permeability of one for all suction levels to compare to the gravel MCC results.

Figure 4.2-18: Blended Moisture Characteristic Curves for FDC Roof

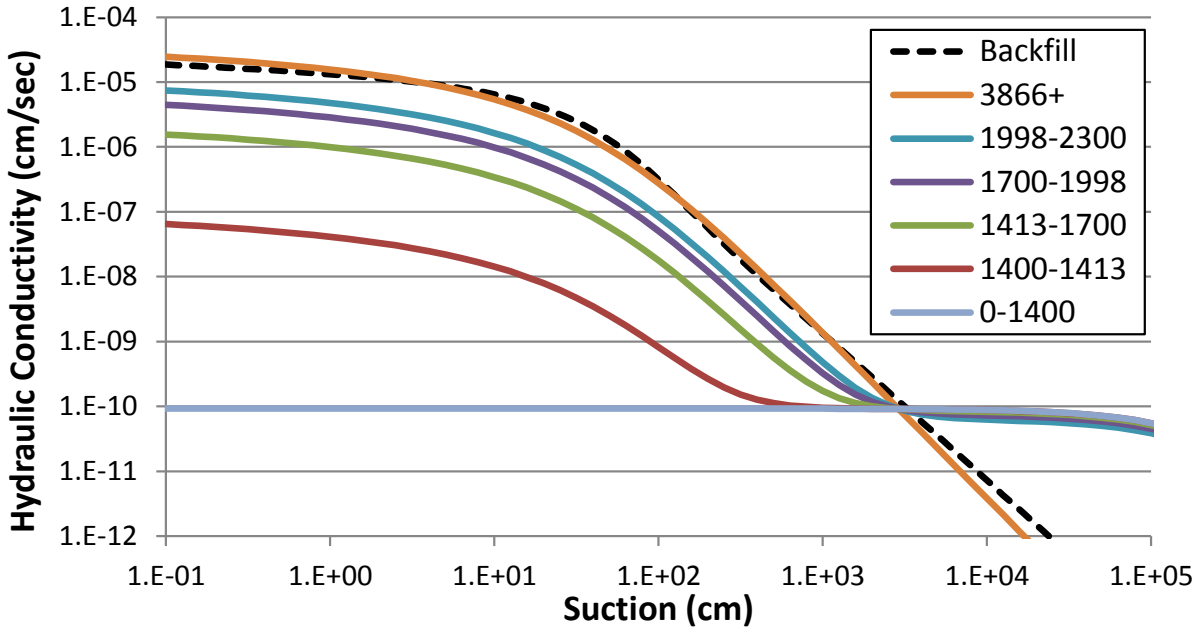

Figure 4.2-19: Blended Moisture Characteristic Curves for FDC Wall

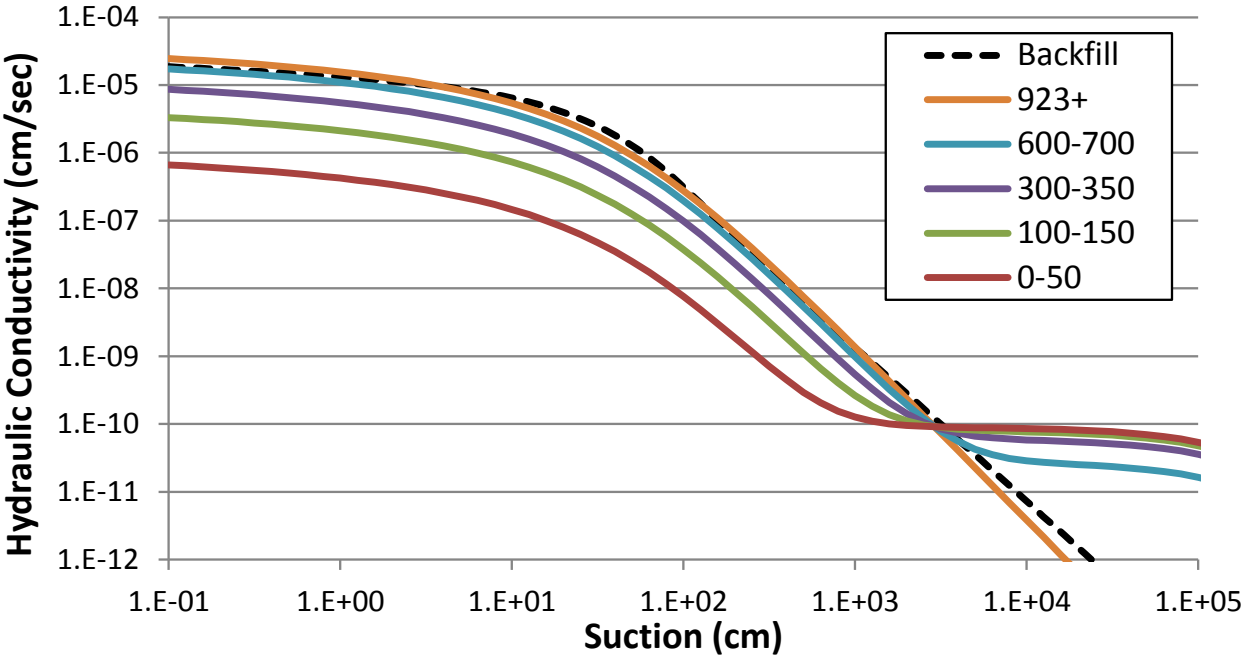

Figure 4.2-20: Blended Moisture Characteristic Curves for FDC Floor and Upper Mud Mat

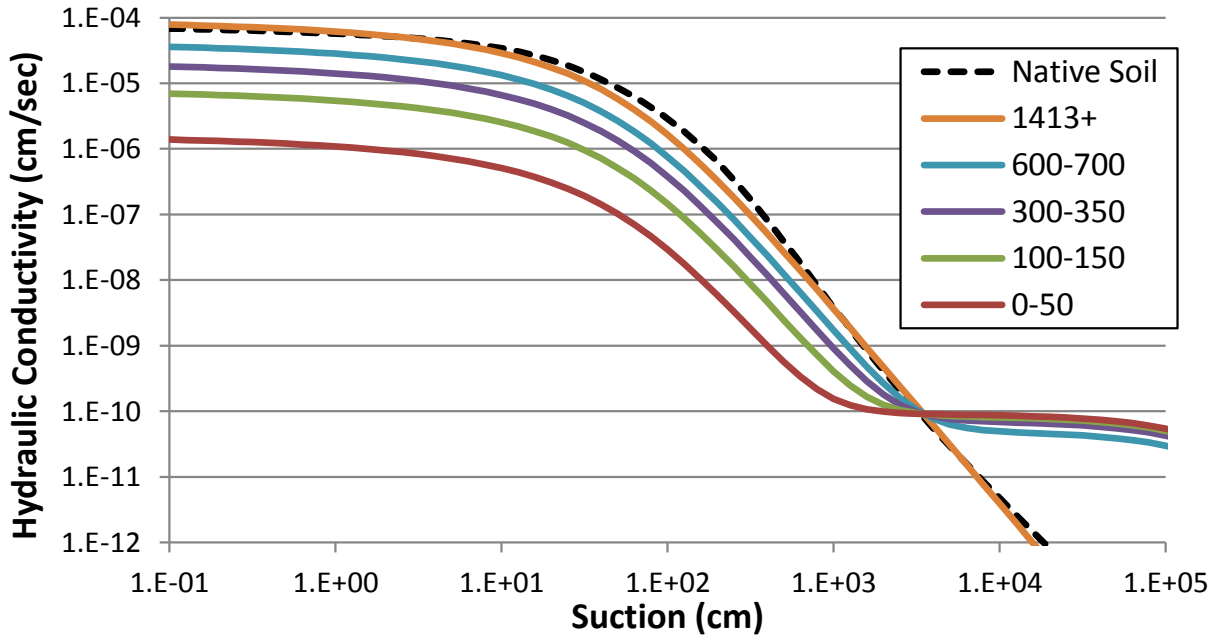

Figure 4.2-21: Blended Moisture Characteristic Curves for FDC Saltstone

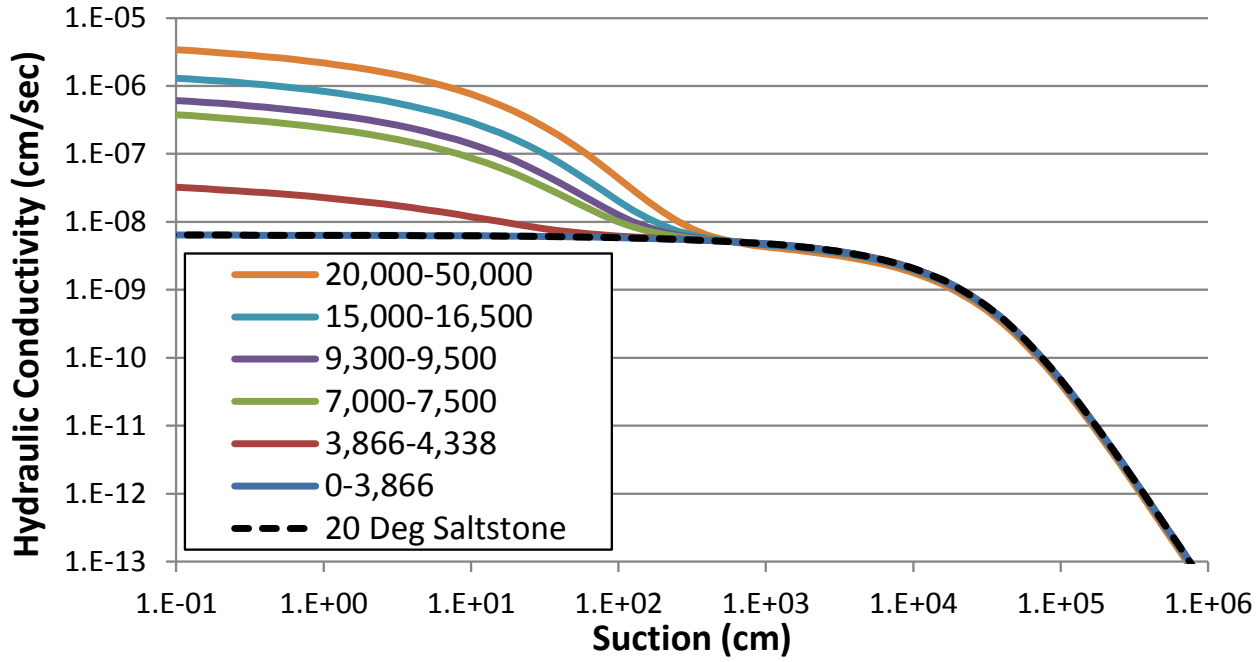

Figure 4.2-22: MCCs for Gravel, Native Soil, and Backfill

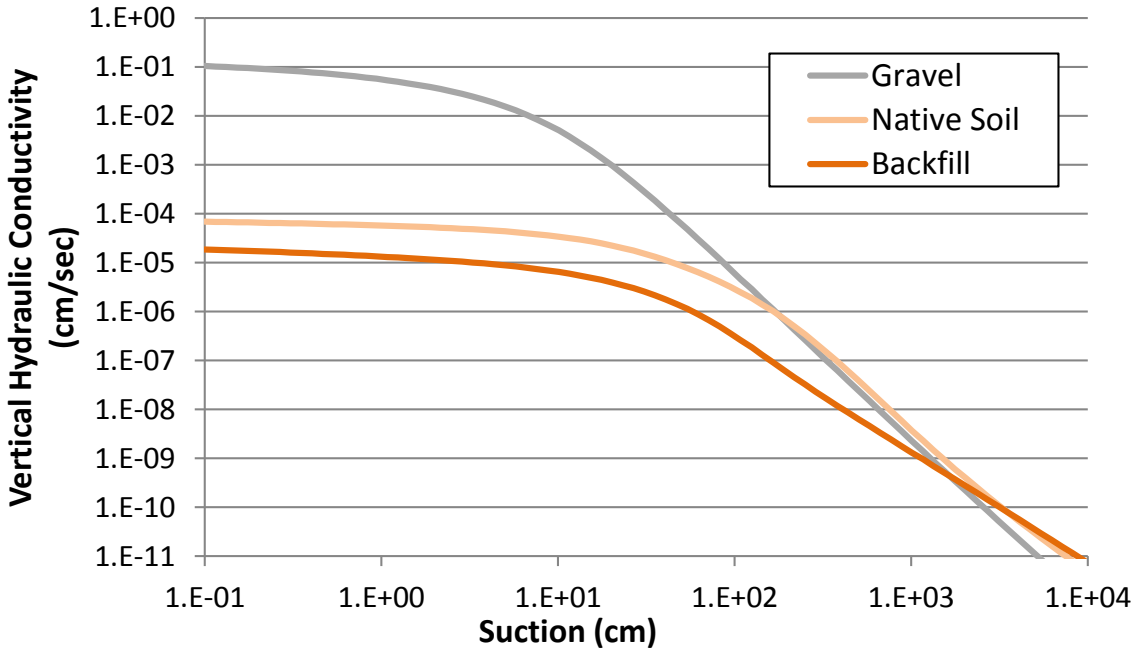

Table 4.2-13: Hydraulic Properties of Gravel

Saturated Effective Diffusion Coefficient D_e (cm^2/s)	Average Total Porosity (%)	Average Dry Bulk Density (g/cm^3)	Average Particle Density (g/cm^3)	Saturated Horizontal Hydraulic Conductivity (cm/s)	Saturated Vertical Hydraulic Conductivity (cm/s)
9.4E-06	30	1.82	2.60	1.5E-01	1.5E-01

[SRR-CWDA-2009-00017, Table 4.4-5]

4.3 Modeling Codes and Software Quality Assurance

Section 4.3 of SDF PA contains a discussion of the modeling codes. The Evaluation Case modeling was performed using the PORFLOW model as was done for the Base Case in the SDF PA. In general, the SDF PORFLOW Model was not changed for this SA; however, the model was rerun using a more recent version of the PORFLOW software and with a number of revisions to the modeling inputs as discussed throughout this text.

The SDF probabilistic modeling for the SA was performed using the GoldSim SDF Model version "SRS Saltstone v4.101." [SRR-CWDA-2013-00073]

Table 4.3-1 provides a summary of the software that was used to support this SA. Table 4.3-1 is not comprehensive as it only lists software that varies from those used in the SDF PA. Software that has not varied from its initial use in the SDF PA was omitted from this table. For example, the SA uses model data from the SDF PA (e.g., infiltration rates) that was developed using Hydrologic Evaluation of Landfill Performance (HELP) modeling software, described in Section 4.3.1.1 of the SDF PA.

Table 4.3-1: Summary of SA Software Used

Software Name	Version	Software Quality Assurance Documentation	Purpose/Use
GoldSim	10.50 (SP3)	*Software Quality Assurance Plan for GoldSim for the Savannah River Site's Liquid Waste Program* (B-SQP-C-00002)	Used for probabilistic modeling, benchmark testing, and dose calculations.
GoldSimFlows	N/A	*Software Quality Assurance Plan for PORFLOW Flow-Field Extraction Tool (GoldSimFlows)* (Q-SQP-A-00008)	Used to extract PORFLOW data and format it to be read by ReadPORFLOWData.dll.
MVIEW	4.00	*Software Quality Assurance Plan for mView* (B-SQP-C-00005)	Used for sensitivity analysis of probabilistic modeling results.
PORFLOW	6.30.2	*Software Testing and Verification of PORFLOW Versions 6.30.1 and 6.30.2* (SRNL-TR-2010-00213)	Used for deterministic modeling of flow and contaminant transport.
ReadPORFLOWData.dll	2.0	*Software Quality Assurance Plan for ReadPORFLOWData.dll for the Savannah River Site's Liquid Waste Program (*B-SQP-C-00003)	Dynamic linked library called by GoldSim software to read data from external files (i.e., PORFLOW result data).

All of the software listed above has undergone software qualification per SRS software qualification procedures (i.e., 1Q Manual, Procedure 20-1).

Quality assurance (e.g., verification of modeling inputs used) for these modeling input revisions is documented in the *SDF FY2013 Special Analysis for the Performance Assessment for the Saltstone Disposal Facility at the Savannah River Site Quality Assurance Report* (SRR-CWDA-2013-00087). This is also supplemented by an independent review of the PORFLOW modeling performed by SRNL, as documented in *Design Checking of PORFLOW Modeling Supporting the Saltstone FY13 Special Analysis* (SRNL-L3200-2013-00022).

4.4 Closure System Modeling

The modeling of the SDUs and FDCs in this SA is not different from that presented in the SDF PA Section 4.4.1, except for the additional features being analyzed, discussed in Section 3.3, and the changes in modeled properties discussed in Sections 4.1 and 4.2. In addition, this SA provides additional sensitivity cases. These additional cases were developed to evaluate various flow conditions that would be impacted by the infiltration rate, the rate of cementitious material degradation, the initial saturated hydraulic conductivity of saltstone, and the material medium of the joints.

4.4.1 Updates to PORFLOW Model

The PORFLOW model has been updated to reflect FDC design features not previously included in the model, to implement revised cementitious material degradation, and to model slag oxidation and Tc-99 release.

4.4.1.1 Modeling of FDC Design Features

Design features not previously included in PORFLOW modeling are joints in the FDCs, and columns in SDU 4 and FDCs. These joints and columns are described in Sections 3.3.

The floor joints in SDU 1 and SDU 4 and the wall-to-floor joints in FDCs are modeled as 2-inch bands of gravel extending through the floor of each disposal unit, and evenly spaced across the 2D model width. The 2-inch section of gravel equates to an open gap of 0.455 millimeter with respect to saturated hydraulic conductivity. Watertight structures are designed with a gap of less than 0.2 millimeter, so an equivalent gap size of 0.455 mm is reasonable and provides a convenient modeling dimension. The development of the various flow cases, presented in Section 4.4.3 include two considerations for moisture retention in the joints (1) using the MCC for gravel and (2) using a relative permeability of one at all suction levels (i.e., no retention) based on assumed 100 % saturation at all times.

The columns in SDU 4 and the FDCs are included in the model as discrete features that degrade over time in 2-foot segments as described in Section 4.2.2.5. As a modeling simplification, the columns are modeled as single structures: a vertical slab in SDU 4, and an annular ring in FDCs. Such representations are necessary due to the limitations of the PORFLOW software. The location and size of each column structure is determined to conserve the total surface area and volume of the number of columns associated with each FDC. Additional description of this modeling is provided in SRNL-STI-2013-00280.

4.4.1.2 Modeling of Cementitious Material Degradation

Section 4.2.2 summarizes the degradation of cementitious material. The blending of MCCs to simulate the expected moisture retention properties of the cementitious material as it degrades to soil conditions is addressed in Section 4.2.3. Even though the exact morphology of concrete or grout at its end-state is not known, a fully degraded material is assumed not to be any more permeable than the soil adjoining it.

For modeling purposes, each cementitious material degrades exactly to the adjoining soil, which makes the concrete or grout no longer a hydraulic barrier compared to the surrounding environment. The transition from an intact, low-permeability material to a fully degraded, soil-like material is assumed to occur linearly over the degradation time periods shown in Section 4.2.2.5. To avoid abrupt changes in properties through time, linear weighting is chosen to blend hydraulic properties smoothly between an intact initial matrix and a soil surrogate for the end-state. The development of this methodology is described in SRNL-STI-2013-00280.

4.4.1.3 Modeling of Slag Oxidation and Tc-99 Transport

Technetium-99 mobility varies strongly with redox conditions. Under reducing conditions technetium release from moderately-aged (i.e., Reduced Region II) cementitious materials is limited by a solubility of 1.0E-08 mol/L, whereas for oxidized conditions (i.e., Oxidized Region II and Region III) the release is controlled by sorption with a K_d value equal to 0.5 mL/g, as discussed in Section 4.1.2. By design, grouts and concretes, except SDU 1 and SDU 4 roof concrete, and the FDC lower mud mat concrete, contain ground blast furnace

slag to create reducing conditions that hinder Tc-99 release from the waste form and transport through cementitious barriers.

The reducing capacities of saltstone grout and concrete recommended for transport modeling are 0.607 and 0.178 meq e-/g, respectively, as stated in Section 4.1.1. Using these values for reducing capacity, the pore volumes required for a model region to transition from Reduced Region II to Oxidized Region II is determined using the pore flush model described in Section 4.1.1. In the pore flush model, a modeled region containing slag maintains its K_d value associated with Reduced Region II until the required number of pore volumes is reached to transition to Oxidized Region II. At that transition time, in that region, the K_d value for Oxidized Region II replaces the K_d value associated with Reduced Region II. This same step-wise change in the K_d value is utilized for the transition of the region from Oxidized Region II to Oxidized Region III.

For the release of Tc-99 a "shrinking core" model, rather than the pore flush model, is utilized. In the shrinking core model, the reducing capacity within each nodal element is evaluated. The reducing capacity of each nodal element is depleted by dissolved oxygen entering the nodal element and consuming (oxidizing) the slag via the infiltrating liquid. Until the reducing capacity of the nodal element is depleted, the release of Tc-99 is solubility controlled as discussed in Section 4.1.2. When the reducing capacity of the nodal element is depleted, the quantity of Tc-99 remaining in that nodal element is modeled with the K_d value of 0.5 mL/g.

As stated above, the reducing capacity of slag-bearing cementitious materials is consumed by dissolved oxygen entering the system through infiltrating liquid. Intact cementitious materials are expected to be fully saturated once buried under a facility closure cap, precluding oxidation by gas-phase transport of oxygen through the porous media. Soils surrounding FDCs will generally be unsaturated, such that soil moisture will be in contact with gas-phase oxygen. Slag oxidation via infiltrating dissolved oxygen is modeled with PORFLOW by defining liquid-phase oxygen and solid-phase slag concentrations and associated mass balance transport equations. The methodology employed in PORFLOW for slag oxidation is provided in SRNL-STI-2013-00280.

The dual dependency of Tc-99 solute transport on the redox state and the solid-phase concentration of Tc-99, via the solubility limit, are implemented within PORFLOW. [SRNL-STI-2013-00280] Sensitivity cases relating to technetium solubility, internal non-depleting oxygen sources within the saltstone monolith, and all concrete initially oxidized are presented in Sections 5.6.6.4 through 5.6.6.6.

The difference between the pore flush model and the shrinking core model on the release of Tc-99 can be illustrated as follows. As indicated in Table 4.1-2, the pore flush model shows that the saltstone in an FDC transitions from Reduced Region II to Oxidized Region II in 33,064 years and the transition from Oxidized Region II to Oxidized Region III does not occur for over 100,000 years. This would indicate that Tc-99 would be released from an FDC at its solubility value until 33,064 years and then the remaining Tc-99 would be released at the K_d value for Oxidized Region II (0.5 mL/g). Using the shrinking core model, Section 5.5.1.4 indicates that the peak Tc-99 release occurs at approximately 31,000 years

and releases continue for approximately 16,000 years until the slag in the floor is completely oxidized.

All of the radionuclides in the SDF PA model were analyzed to determine whether the use of the shrinking core model should be implemented for other radionuclides. This analysis was presented in the response to RAI SP-13 in SRR-CWDA-2011-00044, and concluded that Tc-99 is the only radionuclide that is appropriate to model its release with the shrinking core model.

4.4.1.4 Development of the Evaluation Case

The Evaluation Case was developed by selecting parameter values (creating a conservative operational envelope) that were most probable and defensible considering the new information available. The Evaluation Case considers explicit SDU and FDC design features not previously modeled (e.g., construction joints, columns within the saltstone monolith in SDU 4 and an FDC, presence of the roof support trusses in SDU 4), degradation of cementitious materials based on the latest models from the Cementitious Barriers Partnership (CBP) and other analytical models, and the latest laboratory testing results on saltstone hydraulic conductivity. The specific elements of the Evaluation Case are provided below.

4.4.1.4.1 Performance of the Closure Cap and Sand Drainage Layer

Section 3.3.4 discusses the performance of the closure cap with respect to the infiltration rate and identifies three different rates of infiltration based on results from the HELP code. The degradation of the sand drainage layer above each SDU and FDC is based on the infiltration rate as shown in Figure 3.3-6. For the Evaluation Case, the average value for the infiltration rate and the corresponding degradation of the sand drainage layer is selected to be consistent with the SDF PA.

4.4.1.4.2 Explicit SDU and FDC Design Features

Sections 3.3.1, 3.3.2, and 3.3.3 identify the design features of SDU 1, SDU 4, and an FDC, respectively, which have not been previously included in performance modeling. These design features include floor joints in SDU 1 and SDU 4, wall-to-floor joints in an FDC, the roof support girder system and columns in SDU4, and the roof support columns in an FDC. Flow through the joints is dependent on the material medium within the joint. For the Evaluation Case, so as not to inadvertently hinder flow through the joints, the relative permeability of the joints is assumed to be one for any suction level.

4.4.1.4.3 Initial Saturated Hydraulic Conductivity of Saltstone

Section 4.2.1 provides the results of the latest testing of saltstone simulants using various water-to-premix ratios and employing emplaced grout curing temperature profiles with either saturated conditions or high humidity conditions. Table 4.2-1 provides the results from this latest testing within the range of water-to-premix ratios bounded by the operating bands from current facility data. For the Evaluation Case, the average value of the saturated hydraulic conductivity (6.4E-09 cm/s), obtained from the twenty-four test results within the facility operating band, was selected to represent the initial saturated hydraulic conductivity of saltstone.

4.4.1.4.4 Degradation Rate of Cementitious Materials

The degradation of cementitious materials is discussed in Section 4.2.2 and considers sulfate attack, carbonation, and decalcification. Tables 4.2-9, 4.2-10, and 4.2-11 provide a summary of the degradation analysis for SDU 1, SDU 4, and an FDC, respectively. In these tables the rates of degradation for the various disposal unit features are provided based on best estimate, nominal, and conservative estimate parameters. Even though the best estimate parameters are considered expected parameters, the nominal parameters are selected to provide conservative and defensible estimates for the degradation of cementitious materials for the Evaluation Case.

4.4.2 Updates to the GoldSim Probabilistic Model

The SDF PORFLOW Model was updated to consider additional information regarding the degradation of cementitious material, the release of technetium from reducing cementitious materials, distribution coefficients (K_d values), flow through joints, and dose pathway exposure methodology (see Section 4.4.1). In a parallel effort, Version 3.02 of the SDF probabilistic GoldSim model was updated to consider the influence of the additional information in parameter sensitivity and parameter uncertainty simulations. Updates to the GoldSim model were also made to improve the computational efficiency of the model, and to allow for a probabilistic evaluation of the influence of the flow fields on the results. In addition, the Inadvertent Human Intruder (IHI) scenario analysis was updated to allow for a more rigorous evaluation of exposure levels.

This section briefly describes the updates to the SDF GoldSim Model 3.02, implemented in Version 4.101 to support this and future SAs. A more detailed description of these updates can be found in SRR-CWDA-2013-00073. The differences between the SDF GoldSim Model 3.02 and the SDF PA version are documented in SRR-CWDA-2011-00178. The major differences between SDF GoldSim Model, Version 4.101 and SDF GoldSim Model, Version 3.02 include:

- The replacement of K_ds by the latest SRS K_d data
- The use of leachate impacted K_ds in Version 4.101
- The implementation of solubility controls for Tc-99
- The inclusion of explicit flow paths in the SDU 1 and SDU 4 models to represent floor joints which may act as fast-flow paths through the floor
- The inclusion of an explicit flow path in the FDC model to represent wall-to-floor joints
- The inclusion of an explicit flow path in the SDU 4 and FDC models to represent segmented concrete columns that are subject to separate time-dependent deformation time-histories in each segment
- The updating of the model to allow for the importing (and sampling) of flow-field data and time-dependent diffusion coefficients from PORFLOW output files
- The updating of the model to allow for the importing (and sampling) of Tc-99 releases to the saturated zone from PORFLOW output files
- The updating of the model to allow for user identified grouping of FDCs to reduce the number of individual FDCs that have to be simulated

- The addition of a set of seven wells to be used in the IHI analysis
- The splitting of the floor into explicit floor, upper mud mat, and lower mud mat zones

4.4.2.1 Updates to GoldSim Model Associated with Additional Information Considered

This section describes the updates to the GoldSim model that were made for this SA and future special analyses that reflect the changes made to the SDF PORFLOW Model.

4.4.2.1.1 Linear Sorption Coefficients and Tc-99 Solubility Limits

Three types of changes relative to the process of the linear sorption were implemented in Version 4.101 of the SDF GoldSim Model. First, the K_d data in the model was updated to reflect the present SRS K_d data used in the SDF PORFLOW modeling studies. These updated values for both soils and cementitious materials are presented in Tables 4.1-2 and 4.1-3 of Section 4.1.2, respectively. The second change is concerned with the influence of leachate from the saltstone on the sorptive processes in the unsaturated zone. In the updated model, the leachate impacted soil K_d values presented in Tables 4.1-2 are utilized in the unsaturated zone until pH transition occurs. After transition, non-leachate-impacted values are used. The third model update is the implementation of solubility controls for Tc-99 in the modeling approach. As discussed in Section 4.1.2, the release of Tc-99, from the saltstone grout and transport through the SDU concrete is now modeled as a shrinking core where the release of Tc-99 in a reducing environment is controlled by solubility rather than by K_d value. Once the cementitious material transitions to oxidizing conditions the transport is controlled by the K_d value.

As noted in Section 4.1.2, the solubility value for technetium has been estimated to be 1.0E-08 mol/L for saltstone and for SDU concrete containing slag. [SRNL-STI-2012-00769] Because the evaluation of the shrinking core model is a computationally intensive calculation, Tc-99 releases to the saturated zone are derived outside the GoldSim model using the SDF PORFLOW Model. In Version 4.101 of the SDF GoldSim Model, time histories for Tc-99 release, are sampled from the results of a set of coupled PORFLOW oxygen/slag/Tc-99 simulations. For each realization, a time-history for Tc-99 release from each SDU type (SDU 1, SDU 4, and FDCs) is randomly selected, and imported into the GoldSim model. The sampling and importing process is discussed below in Section 4.4.2.3.

4.4.2.1.2 Floor Joints

In the SDF GoldSim Model, a single column of six mixing-cells linked in series now represents the floor joints, found in SDU 1 and the FDCs. The use of six mixing-cells is consistent with the vertical discretization used in the PORFLOW model. The vertical component of Darcy velocity used as the flow rate in the column of cells is the average of the vertical components of Darcy velocities for the all floor joints in the PORFLOW model. Leakage to the floor joint mixing-cell column from each saltstone mixing-cell above the floor is based on flow across a cross-sectional area defined as the product of the cell-bottom area and a joint-area factor. The joint-area factor is defined as the ratio of

the total cross-sectional area of all joints in the PORFLOW model to the total cross-sectional area of all the floor and joints combined.

4.4.2.1.3 Wall-to-Floor Joints

In the SDF GoldSim Model, wall-to-floor joints found in the FDCs are now explicitly modeled. The horizontal wall-to-floor joint, which separates the wall from the floor, is approximated using a single row of six mixing cells linked in series. The choice of six mixing cells is consistent with the discretization used in the PORFLOW model. In the wall-to-floor joint mixing cells, horizontal flow is modeled to account for leakage into to the backfill surrounding the FDC in addition to vertical leakage from the joint into the floor. The horizontal component of Darcy velocity used as the flow rate in the row of cells is the arithmetic average of the horizontal components of Darcy velocities for all wall-to-floor joint elements in the PORFLOW model.

4.4.2.1.3 Segmented Columns

For this SA, the PORFLOW model concrete column structure is divided from top to bottom into segments, and the model input was updated to reflect individual degradation time-histories within each segment of the column. The GoldSim model was also updated to consider the influence of the segmented column approach on radionuclide transport in SDU 4 and the FDCs. Because the cement columns in SDU 4 and the FDCs represent a potential fast-flow path, they were already included in Version 3.02 of the SDF GoldSim (and PORFLOW) Model. The changes implemented in GoldSim model Version 4.101 allow the model to consider the effects of segment specific degradation patterns. These changes include (1) the application of individual spatially averaged vertical flow rates for each segment of the column, and (2) the application of segment specific chemical transition times.

4.4.2.2 Improvements of Computational Efficiency

In order to reduce the time needed perform stochastic simulations with the SDF GoldSim Model the model was updated to allow for assembling FDCs into groups, which can be evaluated by solving the transport equations for a representative FDC, only. In other words, for each group, radionuclide releases from a representative FDC and transport through the saturated zone from that FDC to the 100-meter boundary would be evaluated. The resulting 100-meter boundary concentration from the representative FDC is then used in conjunction with the FDC-specific plume functions for individual FDCs in the group to generate concentrations for each member of the group to be used in dose calculations. When using the grouping option, the model automatically determines an average saturated zone path-length for each group and an average inventory. The FDC groups used in this SA are listed in Table 4.4-1.

4.4.2.3 Sampling of Data from External Files

A major weakness of previous SDF GoldSim Model versions was that although the model allowed for consideration of uncertainty in most parameters controlling the transport of radionuclides within the engineered barrier and Upper Three Runs Aquifer-Upper Zone (UTRA-UZ) beneath it, the model did not explicitly account for changes in flow fields within

the engineered barrier and UTRA-UZ. To enhance the probabilistic capabilities of the GoldSim model, the model was updated to allow it to read in flow rates and other data from external files containing time series assembled in table form.

Table 4.4-1: FDC Groups

FDC Name	FDC Number	Group Representative	FDC Name	FDC Number	Group Representative
V2A	1	1	V12C	33	31
V2B	2	1	V12D	34	31
V5A	3	3	V3A	35	35
V5B	4	3	V3B	36	35
V5C	5	3	V13A	37	37
V5D	6	3	V13B	38	37
V6A	7	7	V13C	39	37
V6B	8	7	V13D	40	37
V6C	9	7	V14A	41	41
V6D	10	7	V14B	42	41
V7A	11	11	V15A	43	43
V7B	12	11	V15B	44	43
V7C	13	11	V15C	45	43
V7D	14	11	V15D	46	43
V8A	15	15	V16A	47	47
V8B	16	15	V16B	48	47
V8C	17	15	V16C	49	47
V8D	18	15	V16D	50	47
V9A	19	19	V17A	51	51
V9B	20	19	V17B	52	51
V9C	21	19	V17C	53	51
V9D	22	19	V17D	54	51
V10A	23	23	V18A	55	55
V10B	24	23	V18B	56	55
V10C	25	23	V18C	57	55
V10D	26	23	V18D	58	55
V11A	27	27	V19A	59	59
V11B	28	27	V19B	60	59
V11C	29	27	V20A	61	59
V11D	30	27	V20B	62	59
V12A	31	31	V20C	63	59
V12B	32	31	V20D	64	59

For use with the SDF GoldSim Model, a set of flow fields and associated data for various flow scenarios (for each SDU type) were generated using the SDF PORFLOW Model. The SDF GoldSim Model randomly selects a flow scenario from the set of scenarios, and in turn reads the data associated with the selection. The GoldSim model also reads a correlated scenario specific file containing time histories of time-dependent diffusion coefficients. The diffusion-coefficient time histories reflect the influence of degradation on the diffusion coefficient. In addition, because the Tc-99 simulations are based on a coupled

oxygen/slag/Tc-99 transport analysis with very restrictive time stepping requirements, the SDF GoldSim Model does not explicitly simulate the release to Tc-99 from the SDUs and FDCs. Instead, a subset of the flow scenarios has been simulated using the SDF PORFLOW Model to generate time histories of Tc-99 releases. These time histories are sampled from and used as inputs to the SDF GoldSim Model's saturated zone analysis to be used for sensitivity or uncertainty. The Tc-99 release time histories are inputted to the model using the same methodology as the flow and diffusion data. The methodology implemented to read the data is discussed in Section 4.4.2.3.1 and the data used with this new implementation is discussed in Section 4.4.2.3.2.

4.4.2.3.1 Methodology

For this SA and future ones, the updated SDF GoldSim Model (Version 4.101) was restructured to allow flow rates and other associated data to be imported from external files as opposed to having the data reside in GoldSim data elements, where the data remains until it is updated and replaced. This change allows the model to sample from sets of data files that have been generated using PORFLOW (or another process model). The process of reading in the data is performed using a Dynamic Link Library (DLL) containing a FORTRAN-based function that accepts instructions from the SDF GoldSim Model, reads from an external file as per the instructions, and returns the data needed to the GoldSim model. The DLL, "ReadPORFLOWData.dll" (B-SQP-C-00003), is integrated into the SDF GoldSim Model using GoldSim External elements. Instructions pertaining to the file to be read and the locations of the data needed within the file are passed to the DLL through the External element interface.

The data passed back from the DLL to the SDF GoldSim Model (as listed in Table 4.4-2) include time series of zone–based Darcy velocities, saturations, infiltration rates, time-dependent diffusion coefficients, and Tc-99 mass flux rates, as well as scalar values of pH-based transition times and E_h-based transition times.

Table 4.4-2: Data Extracted from the PORFLOW Data Files

Data	Form	Units
Darcy Velocities	1-D Table	cm/yr
Saturations	1-D Table	N/A
pH Transition Times	Scalar	yr
E_h Transition Times	Scalar	yr
Infiltration Rate	1-D Table	cm/yr
Diffusion Coefficients	1-D Table	cm^2/s
Tc-99 Release Mass-Flux Rates	1-D Table	mol/yr

4.4.2.3.2 Data

The development of the flow cases used for sensitivity and uncertainty analyses is described in Section 4.4.3. The flow cases used are based on the Evaluation Case (Case F-1) flow parameters, with the following attributes varied:

- Three infiltration cases (minimum, average, maximum)

- Two degradation rates (nominal, best estimate)
- Two joint MCCs (gravel, relative permeability (K_{rel}) = 1))
- Three initial grout hydraulic conductivity values (6.4E-09 cm/s, 4.5E-07 cm/s, 3.9E-10 cm/s)

The maximum, average, and minimum infiltration rates were obtained from Appendix K of WSRC-STI-2008-00244 and were presented in Table 3.3-1 and Figure 3.3-5. The nominal and best estimate degradation rates for SDU 1, SDU 4, and the FDCs were extracted from Tables 4.2-9 through 4.2-11, respectively, in Section 4.2.2.5, wherein multiple degradation mechanisms were considered for each disposal unit feature. The surrogate MCC for joints (gravel medium MCC versus a relative permeability of 1 for all suction levels) was discussed in Section 4.2.3. Table 4.2-1, in Section 4.2.1, provided the measured values for the saturated hydraulic conductivity of saltstone. The average (nominal) value was 6.4E-09 cm/s. Bounding this parameter are the minimum reported value (3.9E-10 cm/s) and an assumed maximum value that is 10 times the highest reported value (4.5E-08 × 10 = 4.5E-07 cm/s). The development of these parametric flow cases from which the flow fields were sampled are described in more detail below in Section 4.4.3.

Analysis of these parametric PORFLOW-developed flow fields indicated that there were significant similarities among many of the sets of flow fields, such that sampling all 36 flow cases would create a sampling bias preferential to similar flow fields. Given the uncertainty inherent in the flows, it was determined that a subset of 12 of the 36 flow cases (as denoted by the superscript "C" in Table 4.4-3) provide a representative distribution that could be equally sampled from to ensure sufficient propagation of flow variability throughout the uncertainty sampling. A discussion of the selection process used to choose the 12 flow cases is presented in Section 5.6.6.7.

Figure 4.4-1 provides a statistical comparison of the 36 flow fields (All) generated in PORFLOW versus the 12 sampled flow fields (Selected) used for sampling uncertainty within the SDF GoldSim Model. This figure demonstrates that although the sampling approach is non-parametric, it is fully representative of potential future flows.

Figure 4.4-1: Statistical Comparison of Parametric Flow Cases Versus Representative Flow Cases

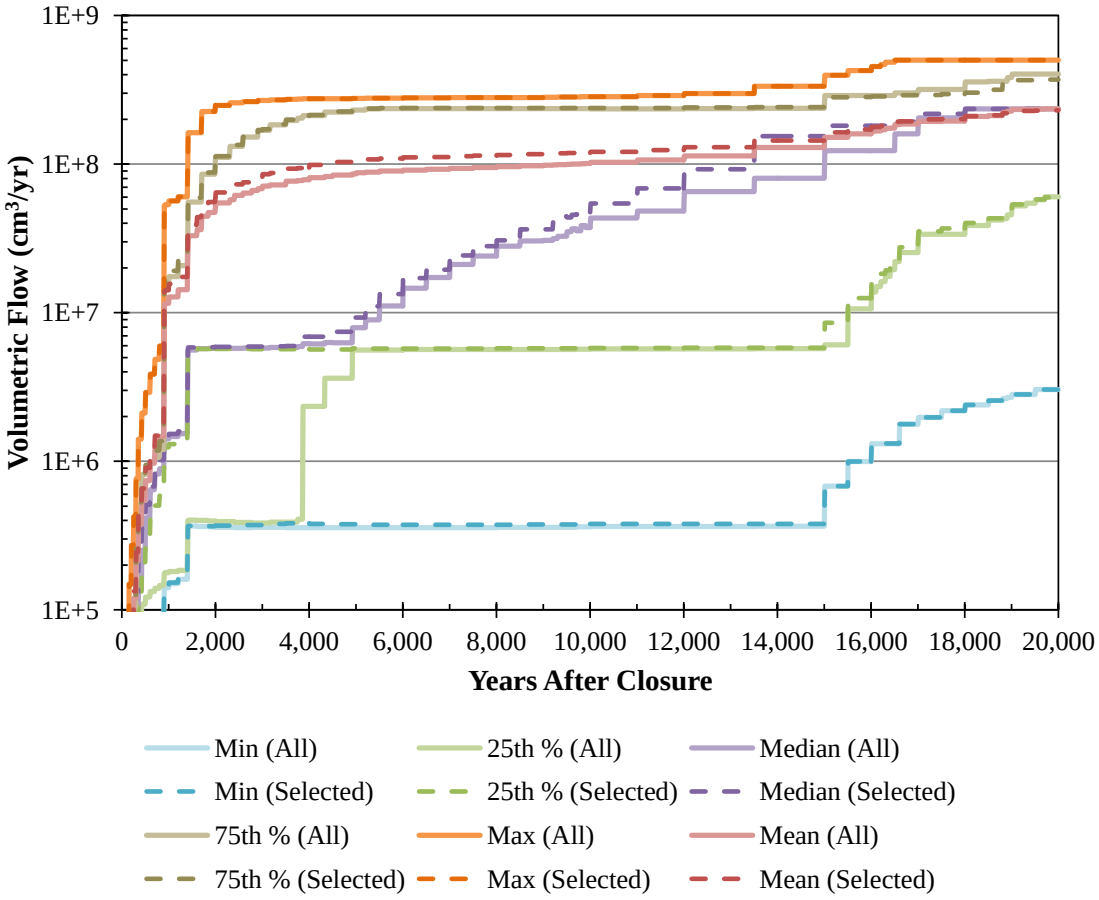

For each of the representative flow cases, three sets of Tc-99 releases were generated by PORFLOW, using varying values for solubility limits (1.0E-09 mol/L, 1.0E-08 mol/L, 1.0E-07 mol/L). When evaluating sensitivity or uncertainty with the full suite of radionuclides (including Tc-99), the subset of 12 flow cases and three solubility limits were used. In the stochastic sampling, each of the flow cases was given a 1 in 12 chance of occurring. The sampling for the solubility limit to be used with a sampled flow case is based on a discrete distribution with a 25 % chance of 1.0E-09 mol/L or 1.0E-07 mol/L occurring and a 50 % chance of 1.0E-08 mol/L occurring. The middle value (1.0E-08 mol/L) is consistent with conclusions from recent experiments; therefore, the higher probability was appropriate for this value. [SRNL-STI-2012-00769] Although the other two values (1.0E-09 mol/L and 1.0E-7 mol/L) do not reflect expected conditions, assigning the 25 % probability is intended to provide additional insights to the sensitivity of this parameter.

4.4.2.4 Inadvertent Human Intruder Scenario

This section describes the updates to the GoldSim model to improve the IHI exposure level analysis. For the IHI analysis, a set of seven wells was chosen to represent the possible location of a well, used by an IHI (see Figure 4.4-2). For each time step in a simulation, the maximum dose level produced by any of the seven wells is used to generate a single curve, which represents the time history of the IHI exposure level. Saturated zone radionuclide transport from the SDUs and FDCs to each of the seven wells is evaluated using the same methodology used to derive the MOP concentrations at the 100-meter boundary. [SRR-CWDA-2011-00178] For each disposal unit, in concert with the MOP concentrations along the 100-meter boundary, a set of concentrations at each of the seven wells is derived using release breakthrough curves as boundary conditions applied to GoldSim pipe elements. The outputs of the 1D pipe-element solutions (analytical solutions) for concentrations at the well are then multiplied by Green's Function based GoldSim plume-function factors, which superimpose the effects of horizontal and vertical transverse dispersion. Prior to the dose calculations, the final concentrations at each well are assembled by superposition of the contributions to the well from each of the SDU or FDC releases. Note that for computational efficiency, for releases that are not expected to reach a well (see the streamlines in Figure 4.4-2) the concentrations are set to zero and not evaluated.

Figure 4.4-2: SDF IHI Analysis Well Locations

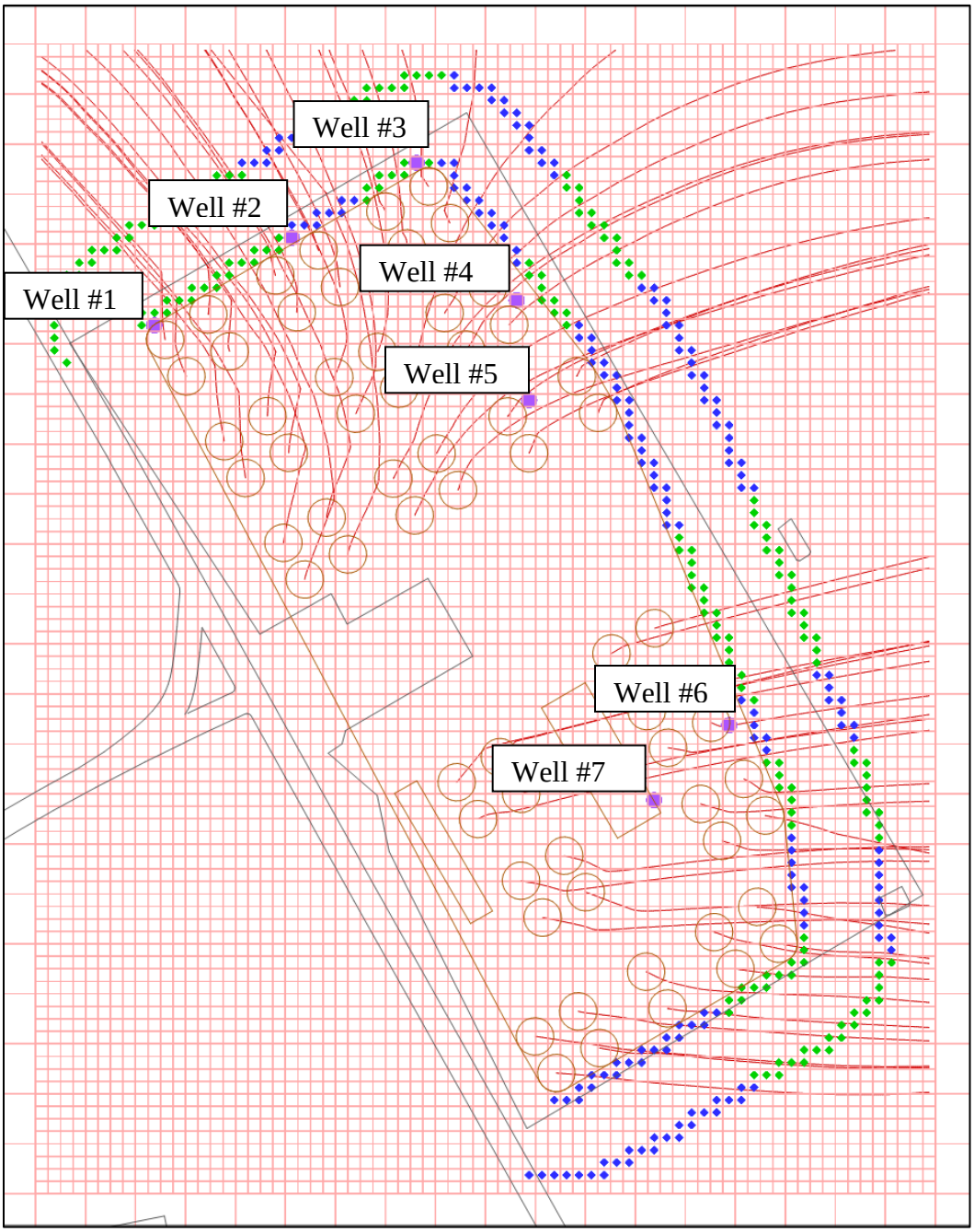

4.4.2.5 Floor Discretization

Version 4.101 of the SDF GoldSim Model explicitly models the floor, upper mud mat, and lower mud mat as individual layers, subject to their own flow rates and chemical transition times. Prior versions of the SDF GoldSim Model lumped these three layers into a single unit, the floor. Note that the HDPE layer sandwiched between the two mud mats is not explicitly model, but is implicitly considered in the PORFLOW-generated flow rates used in the model.

The floor/upper mud mat/lower mud mat system in Version 4.101 of the model is now represented by three parallel sets of 20 mixing cells linked in series. The top ten cells of each set represents the floor in each set, the next five, the upper mud mat and the bottom five, the lower mud mat. The three sets of mixing cells represent the floor system beneath the inner saltstone cylinder, the outer saltstone cylinder, and the wall (SRR-CWDA-2011-00178, Section 3.2.1). Note that a thin cylinder, approximating the influence of concrete columns, separates the inner and outer saltstone cylinders in the FDCs.

4.4.3 Development of the Flow Cases

A spectrum of flow cases was developed to ascertain the sensitivity to flow for selected parameters. These parameters are:

1. Infiltration rate and associated sand drainage layer degradation (maximum, average, or minimum values) provided in Section 3.3.4.
2. Cementitious material degradation (nominal or best estimate) provided in Section 4.2.2. (As noted in Section 4.2.3, there is no significant difference between the degradation times for the nominal values and the conservative values of the cement, thus nominal and best estimate values are sufficient for investigating the behavior of flow through the SDUs and FDCs in this SA.)
3. Initial saturated hydraulic conductivity of saltstone and clean cap (maximum, nominal, or best estimate) provided in Section 4.2.1.
4. MCC for joints (gravel medium or a relative permeability of 1 for all suction levels) discussed in Section 4.2.3.

Of these various flow cases, the Evaluation Case used to evaluate the performance of the SDUs and FDCs applies the following: the average infiltration rate, the nominal rate of cementitious material degradation, an initial saturated hydraulic conductivity of 6.4E-09 cm/s for saltstone, and the gravel medium for the MCC of the joints. Table 4.4-3 summarizes the 36 flow cases with Case F-1 representing the Evaluation Case.

Table 4.4-3: Summary of Flow Cases

Case	Infiltration Rate (Figure 3.3-4)	Cementitious Degradation Rate (Section 4.2.2.5)	Initial Saltstone Saturated Hydraulic Conductivity (cm/s)	Joint Material for MCC
F-1 [c]	Average	Nominal	6.4E-09	Gravel
F-2	Average	Nominal	4.5E-07	Gravel
F-3	Average	Nominal	3.9E-10	Gravel
F-4 [c]	Average	BE[a]	6.4E-09	Gravel
F-5 [c]	Average	BE[a]	4.5E-07	Gravel
F-6	Average	BE[a]	3.9E-10	Gravel
F-7	Average	Nominal	6.4E-09	Rel Per[b] = 1
F-8	Average	Nominal	4.5E-07	Rel Per[b] = 1
F-9	Average	Nominal	3.9E-10	Rel Per[b] = 1
F-10	Average	BE[a]	6.4E-09	Rel Per[b] = 1
F-11	Average	BE[a]	4.5E-07	Rel Per[b] = 1
F-12	Average	BE[a]	3.9E-10	Rel Per[b] = 1
F-13	Maximum	Nominal	6.4E-09	Gravel
F-14 [c]	Maximum	Nominal	4.5E-07	Gravel
F-15 [c]	Maximum	Nominal	3.9E-10	Gravel
F-16 [c]	Maximum	BE[a]	6.4E-09	Gravel
F-17 [c]	Maximum	BE[a]	4.5E-07	Gravel
F-18	Maximum	BE[a]	3.9E-10	Gravel
F-19	Maximum	Nominal	6.4E-09	Rel Per[b] = 1
F-20	Maximum	Nominal	4.5E-07	Rel Per[b] = 1
F-21	Maximum	Nominal	3.9E-10	Rel Per[b] = 1
F-22	Maximum	BE[a]	6.4E-09	Rel Per[b] = 1
F-23	Maximum	BE[a]	4.5E-07	Rel Per[b] = 1
F-24	Maximum	BE[a]	3.9E-10	Rel Per[b] = 1
F-25 [c]	Minimum	Nominal	6.4E-09	Gravel
F-26 [c]	Minimum	Nominal	4.5E-07	Gravel
F-27	Minimum	Nominal	3.9E-10	Gravel
F-28 [c]	Minimum	BE[a]	6.4E-09	Gravel
F-29 [c]	Minimum	BE[a]	4.5E-07	Gravel
F-30 [c]	Minimum	BE[a]	3.9E-10	Gravel
F-31	Minimum	Nominal	6.4E-09	Rel Per[b] = 1
F-32	Minimum	Nominal	4.5E-07	Rel Per[b] = 1
F-33	Minimum	Nominal	3.9E-10	Rel Per[b] = 1
F-34	Minimum	BE[a]	6.4E-09	Rel Per[b] = 1
F-35	Minimum	BE[a]	4.5E-07	Rel Per[b] = 1
F-36	Minimum	BE[a]	3.9E-10	Rel Per[b] = 1
F-37	For FDCs only – F-1 parameters with a roof slope of 1.5 % (rather than 2 %)			
F-38	For FDCs only – F-1 parameters with a roof slope of 2.5 % (rather than 2 %)			

[a] "BE" refers to best estimate values for cementitious degradation

[b] "Rel Per" refers to relative permeability at all suction levels

[c] Used for solubility limit sampling, as described in Section 4.4.2.3.

[SRR-CWDA-2013-00064]

PORFLOW is used to determine flow through the SDF closure system for these 36 flow cases. PORFLOW is also used to determine the time dependent change in the slag and oxygen content in the initially reduced cementitious materials to implement the shrinking core model for the release of technetium. For the Evaluation Case, PORFLOW is also used to determine the transport of radionuclides and the resulting concentrations in the aquifers at various locations inside and outside of the perimeter of the closed SDF. The GoldSim model is used to determine the transport and concentrations of the radionuclides for all of these cases as described in Section 4.4.4.2. Benchmarking of GoldSim to PORFLOW is conducted using the Evaluation Case, Flow Case F-1 of Table 4.4-3, as discussed in Section 5.6.2.

Two additional flow cases have been developed to investigate the sensitivity of the slope of the roof in FDCs. Using the parameters from Flow Case F1, Flow Case F37 considers a roof slope of 1.5 % and Flow Case F38 considers a roof slope of 2.5 %, rather than the nominal 2 % roof slope described in SDF PA Section 4.4.1.3. [SRR-CWDA-2009-00017]

These flow cases are discussed in detail in Section 4.4.4. Additionally, figures are included to provide greater insights into the effects of each of these parameters with respect to flow.

4.4.4 Analysis of the Flow Cases

The following figures present the volumetric flow rates (cm^3/yr) through the SDUs and FDCs for the Evaluation Case, F1 of Table 4.4-3. A detailed analysis of the volumetric flow through SDU 4 is provided in Section 4.4.4.1. Similarly, a detailed analysis of the volumetric flow through the FDCs is provided in Section 4.4.4.2. Because the potential releases from SDU 1 are not significant compared to the other FDCs, a detailed analysis of the volumetric flow through SDU 1 is not included.

Figure 4.4-3 presents the total (horizontal and vertical) volumetric flow rates through SDU 1 for the Evaluation Case. The curve for saltstone is dashed because it significantly overlaps the curve for the clean cap

Figure 4.4-3: Total Volumetric Flow Rates through SDU 1

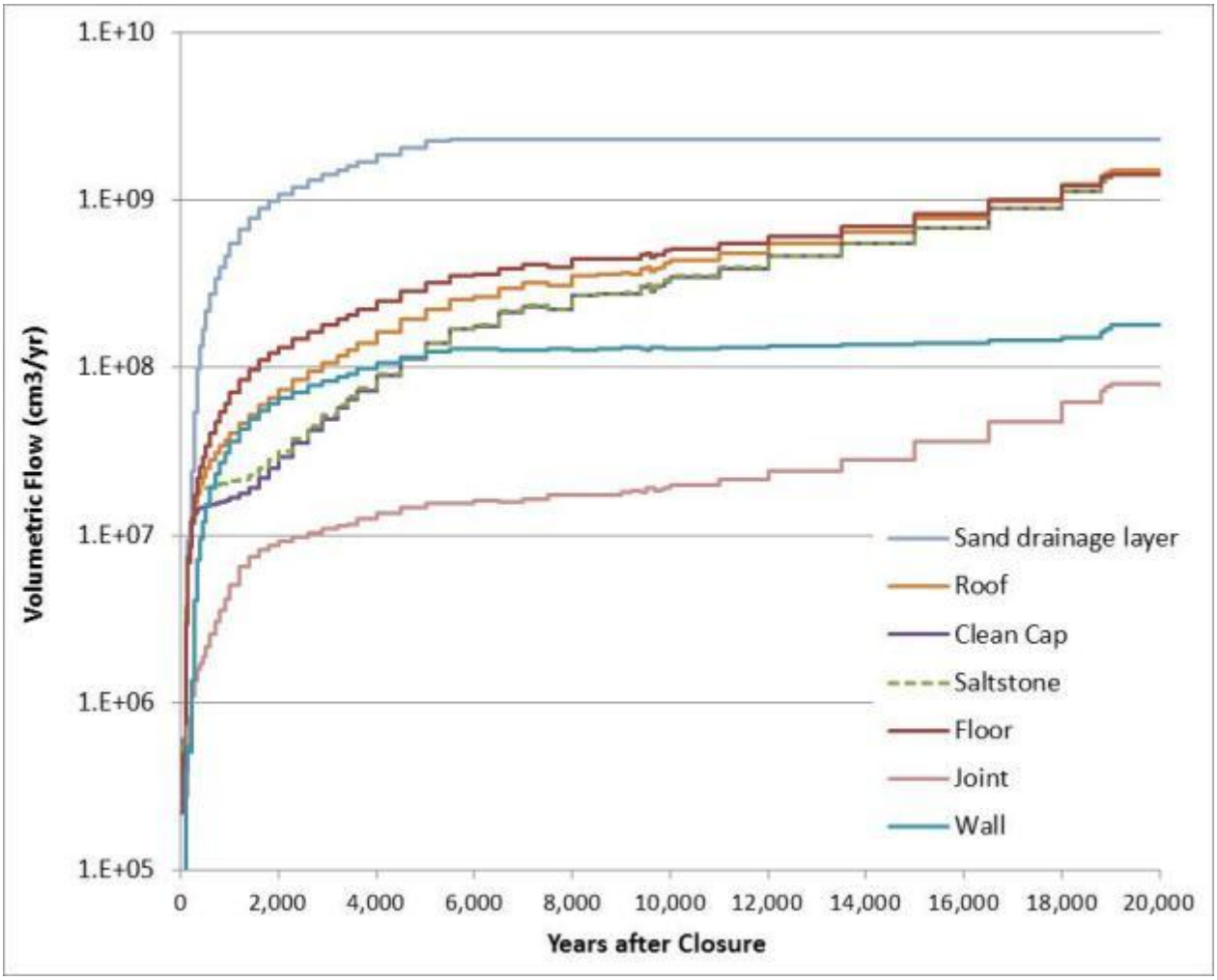

Figure 4.4-4 presents the Evaluation Case flow through SDU 4. The total (horizontal and vertical) volumetric flow rates for the roof, clean cap, top and remaining layer of saltstone and floor are essentially identical after approximately 5,000 years. Note that after approximately 3,000 years, volumetric flow through the wall of SDU 4 decreases. This is attributed to the differences in the degradation times between the wall and the saltstone. The wall degrades earlier than the saltstone, essentially creating a preferential path for flow; however, as the saltstone continues to degrade, the flow becomes less preferential until it reaches a relatively steady state at around 8,000 years.

Figure 4.4-4: Total Volumetric Flow Rates through SDU 4

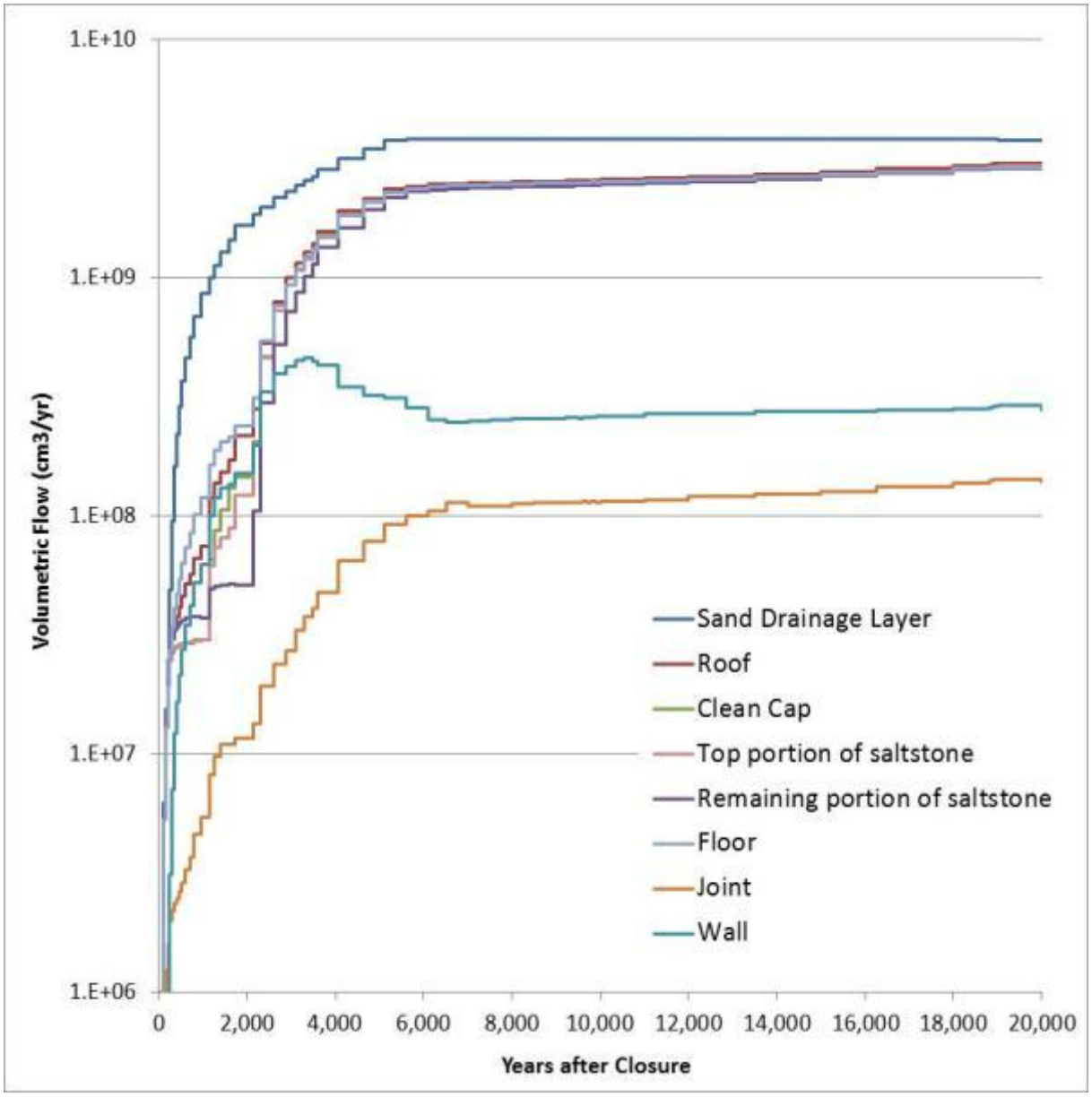

The flow through the columns in SDU 4 for the Evaluation Case is shown in Figure 4.4-5. Grout_1 is the top segment within the clean cap, Grout_2 is the segment within the 2 feet of saltstone degraded by carbonation, and Grout_3 through Grout_12 are the segments within the remaining saltstone monolith not degraded by carbonation; Grout_12 is the bottom segment within saltstone. As with the wall (in Figure 4.4-4), the top segments of the column degrade earlier, resulting in preferential flow. As other column segments degrade, and as the surrounding saltstone degrades, the preferential flows vary, resulting in the variability of the volumetric flow as shown.

Figure 4.4-5: Total Volumetric Flow Rates in SDU 4 Column Segments

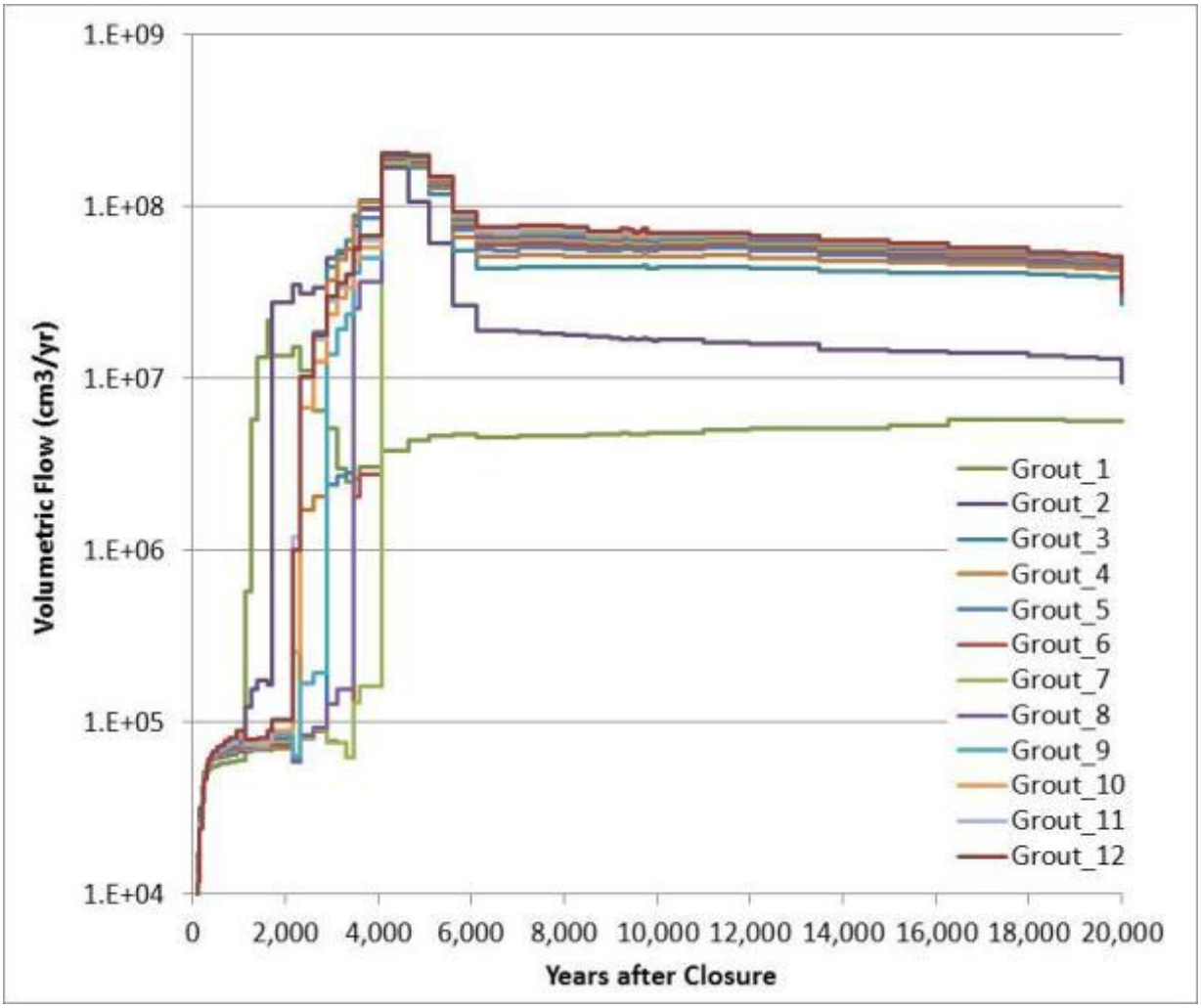

Figure 4.4-6 presents the total volumetric (horizontal and vertical) flow rates in an FDC. The degradation of the HDPE at 900 years is indicated by the step change of flow through the wall and the joint at that time. Similarly, the degradation of the HDPE-GCL at 1,400 years is indicated by the step change, at that time, of flow through the roof, clean cap, and saltstone for the HDPE-GCL covering the roof, and the step change of flow, at that time, through the floor, the upper mud mat, and the lower mud mat for the HDPE-GCL which separates the upper and the lower mud mats. The flow is steadily increasing through the roof, wall, floor, and the mud mats as the roof, wall, floor and the upper mud mat degrade. Not until the roof is fully degraded at 3,866 years does the flow through the clean cap and saltstone steadily increase.

Figure 4.4-6: Total Volumetric Flow Rates in FDCs

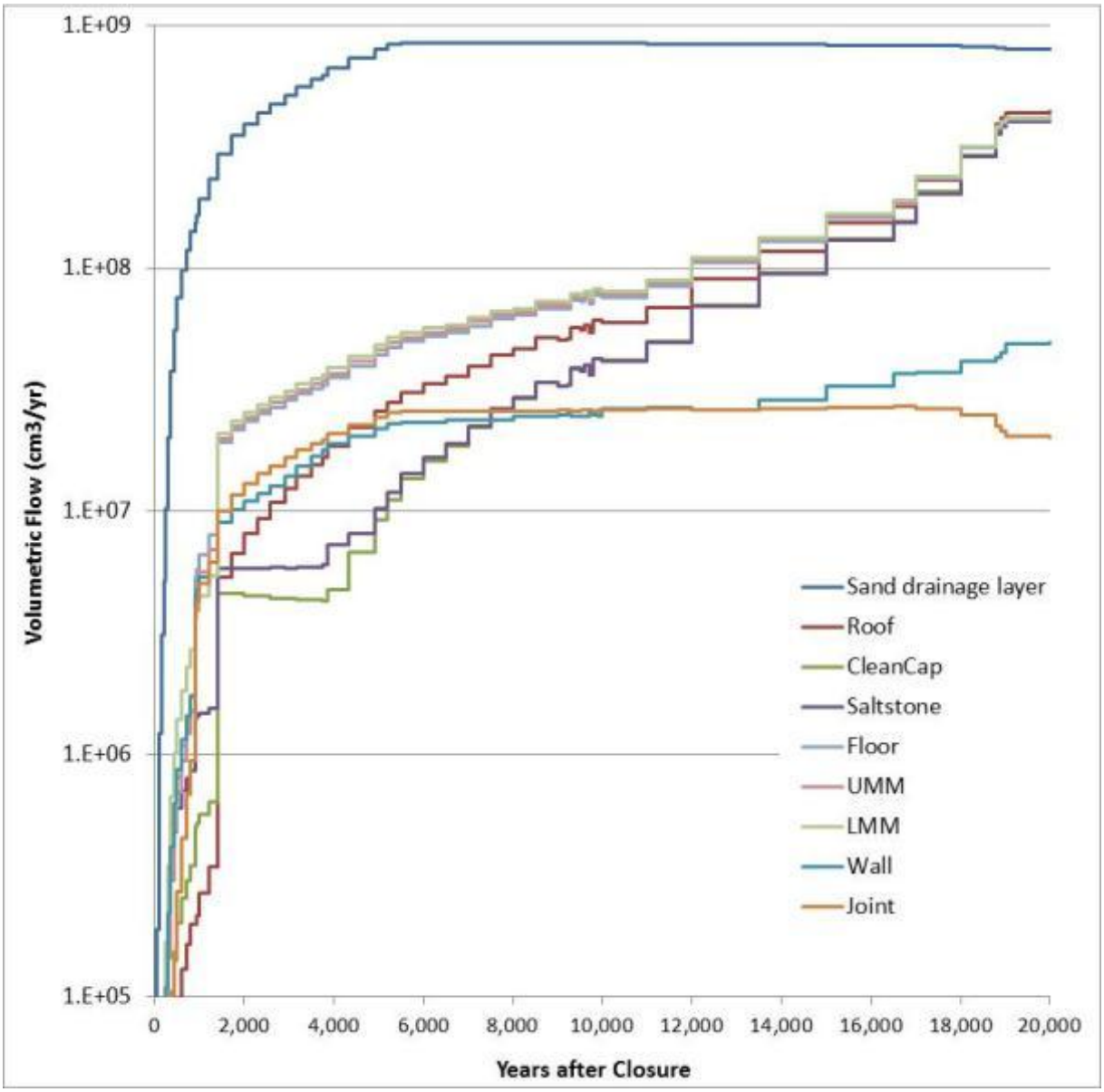

Figure 4.4-7 presents the volumetric flow through the columns in FDCs and shows the similar stair-stepping pattern shown in Figure 4.4-5 for SDU 4 because of the PORFLOW steady state flow fields at each individual time step.

Figure 4.4-7: Total Volumetric Flow Rates in FDC Column Segments

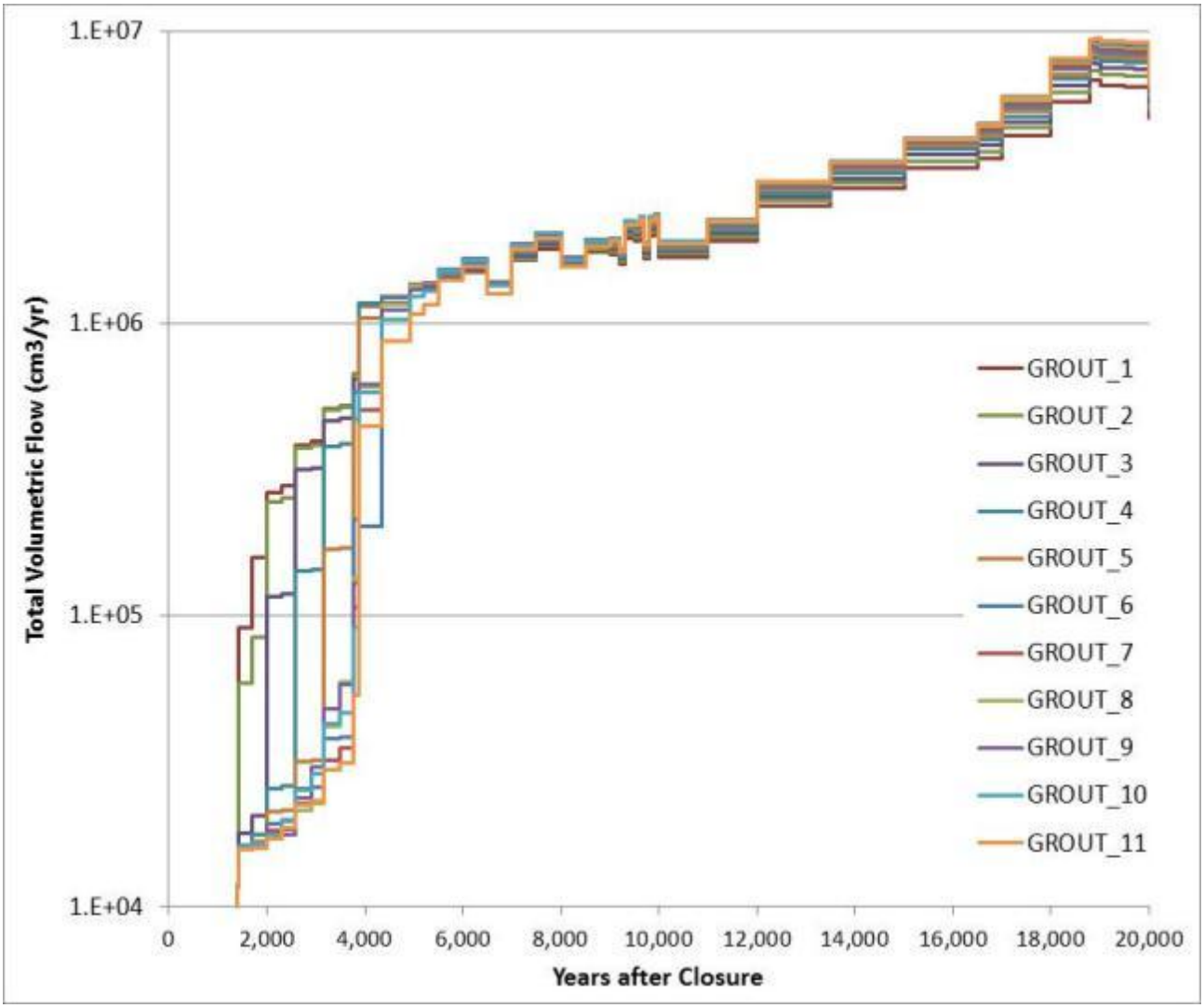

4.4.4.1 SDU 4 Evaluation (36 Flow Cases)

Figure 4.4-8 presents the total volumetric flow rates through saltstone in SDU 4 for the 36 flow cases. Of these 36 flow cases, half of them assume that the joints have MCCs associated with gravel and the other half of the cases assume that the relative permeability of material in the joint is set to one for all suction levels.

Figure 4.4-8: Total Volumetric Flow Rates in SDU 4 Saltstone (36 Cases)

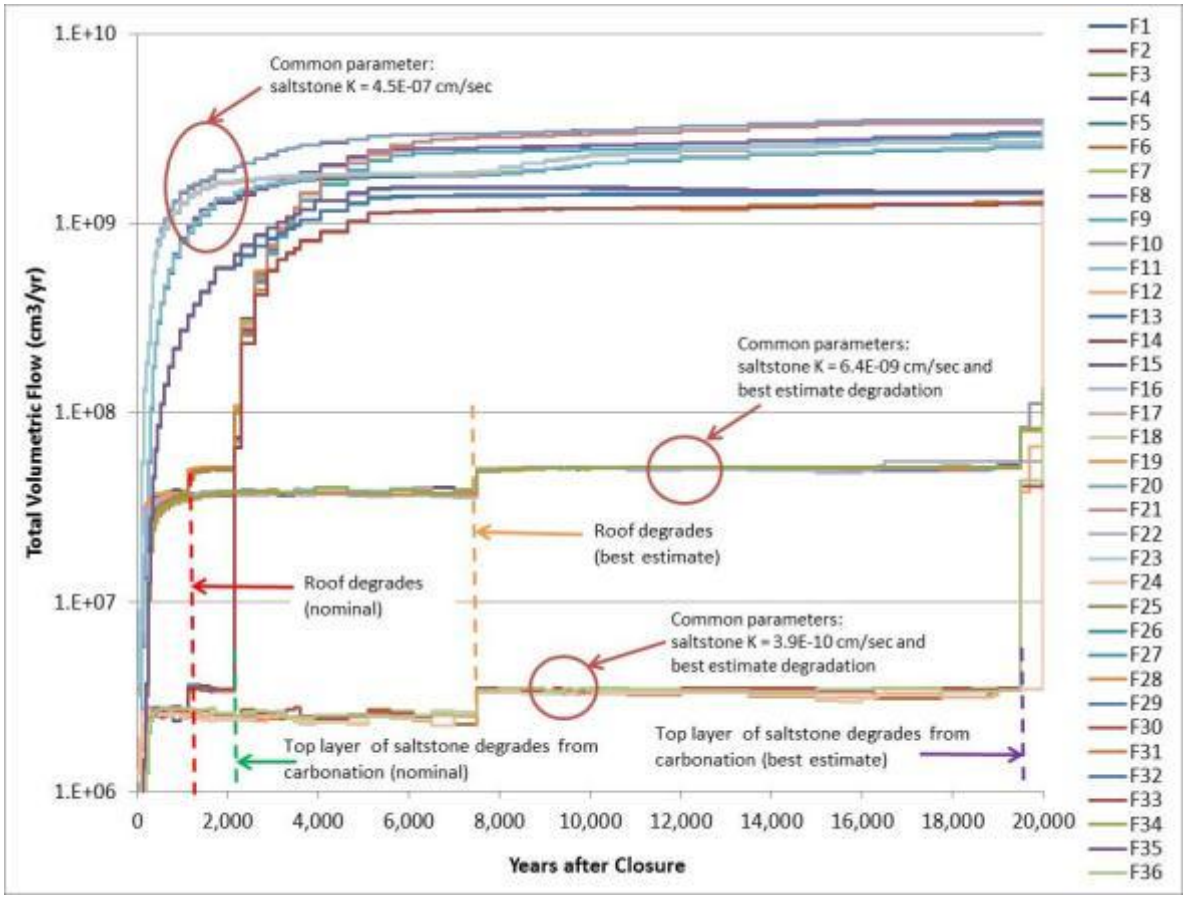

Figure 4.4-9 presents the same data, including all 36 flow cases, except each curve has been specifically colored based on (1) the initial hydraulic conductivity of saltstone (or K_{sat}) and (2) the cementitious degradation rate. Significant overlap within each group makes it difficult to distinguish all 36 flow curves, indicating that the hydraulic conductivity and the cementitious degradation rates have a much stronger influence over the flow behavior than infiltration or the MCCs of the joints. Inspection of these flow results indicates that the choice of MCCs for the joints has no impact on the flow through saltstone.

Figure 4.4-9: Total Volumetric Flow Rates in SDU 4 Saltstone (36 Cases, Grouped)

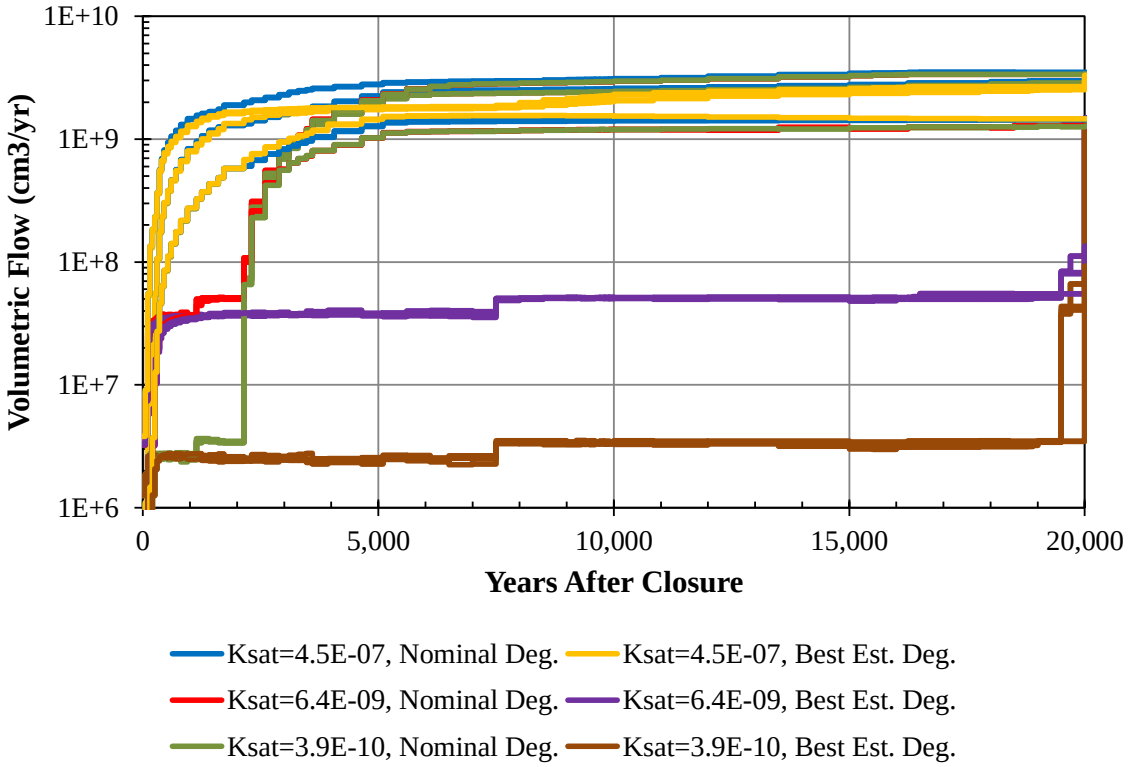

The early and rapid increase in volumetric flow rates, shown in Figures 4.4-8 and 4.4-9, at less than 2,000 years are associated with the eight flow cases having an initial saltstone hydraulic conductivity of 4.5E-07 cm/s (blue and yellow in Figure 4.4-9). Within 7,000 years, 24 flow cases have a saltstone volumetric flow rate between 3.0E+09 cm^3/yr and 1.2E+09 cm^3/yr. The only flow cases not included in these 24 cases are 12 flow cases with the best estimate cementitious degradation and initial saltstone hydraulic conductivities of either 6.4E-09 cm/s or 3.9E-10 cm/s (respectively, purple, and brown in Figure 4.4-9).

Figure 4.4-10 presents the total volumetric flow through the SDU 4 floor for the 36 flow cases. For the floor, there are four distinct flow case groupings by about year 6,000.

Figure 4.4-10: Total Volumetric Flow Rates through the SDU 4 Floor (36 Cases)

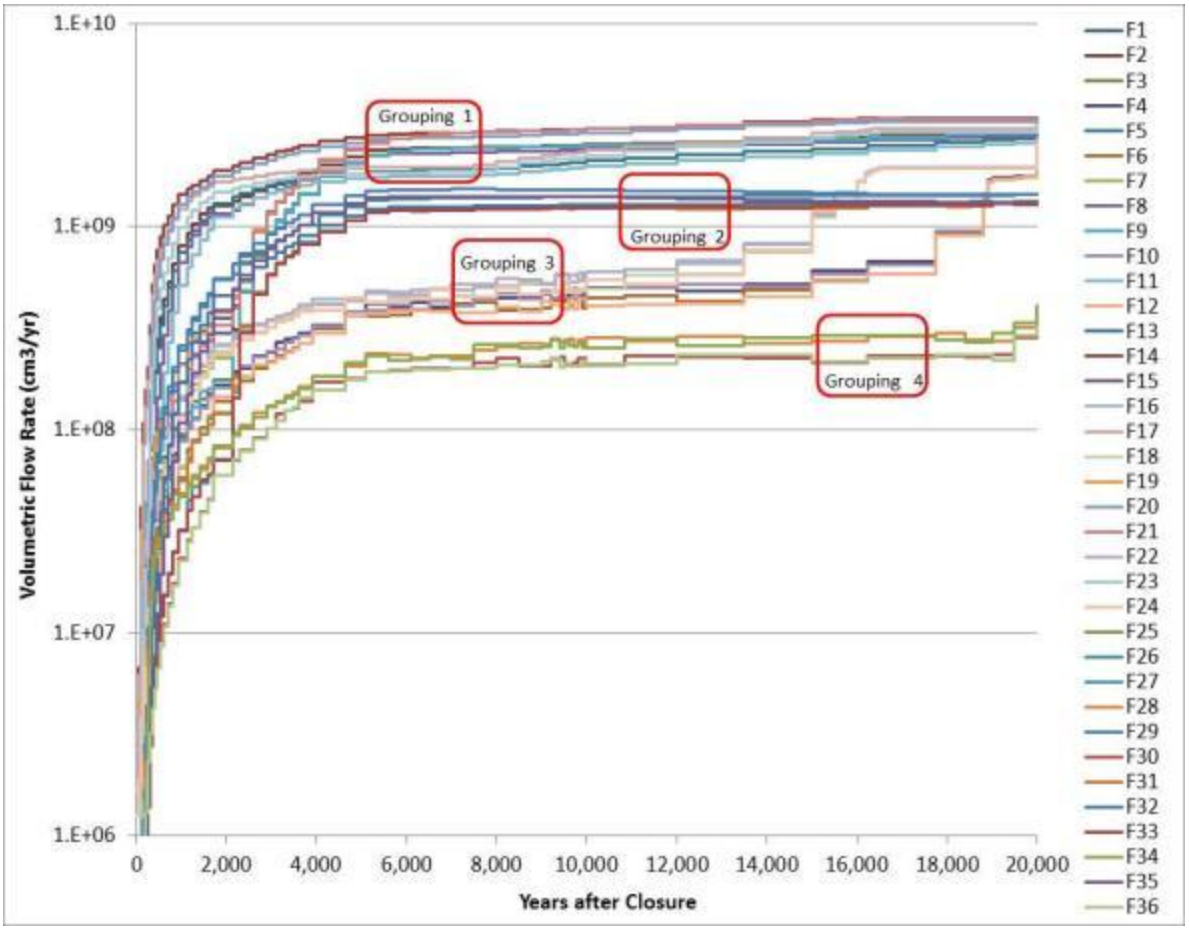

The first grouping, bounded by a volumetric flow rate of 2.9E+09 cm^3/yr and 1.8E+09 cm^3/yr, includes two sets. First, there are 12 flow cases having the nominal degradation rate and the maximum or average infiltration rate for the spectrum of initial saltstone hydraulic conductivity values. Second are the four flow cases that have the best estimate rate of degradation, maximum or average infiltration rate, and the maximum initial saltstone hydraulic conductivity value.

The second grouping contains eight flow cases and is bounded by volumetric flow rates of 1.5E+09 cm^3/yr and 1.2E+09 cm^3/yr. This second grouping includes six flow cases having the nominal degradation rate and the minimum infiltration rate for the spectrum of initial saltstone hydraulic conductivity values. The other two flow cases in this grouping have the best estimate degradation rate, the minimum infiltration rate, and an initial saltstone hydraulic conductivity of 4.5E-07 cm/s.

The third grouping, bound by volumetric flow rates of 4.9E+08 cm^3/yr and 3.9E+08 cm^3/yr, consists of eight flow cases. The flow cases in this grouping have the best estimate degradation rate, the maximum or average infiltration rate, and an initial saltstone hydraulic conductivity value of either 6.4E-09 cm/s or 3.9E-10 cm/s.

The fourth grouping, bounded by volumetric flow rates of 2.2E+08 cm^3/yr and 2.0E+08 cm^3/yr consists of four flow cases. These four cases have the best estimate degradation rate and minimum infiltration rate and an initial saltstone hydraulic conductivity value of either 6.4E-09 cm/s or 3.9E-10 cm/s. Again, inspection of the volumetric flow rates for the various flow cases found that the choice of MCC for the joints has no appreciable impact on the volumetric flow rates through the floor.

Figure 4.4-11 shows the same data (i.e., all 36 flow curves) as shown in Figure 4.4-10, but following the same grouping that was used in Figure 4.4-9. This figure illustrates that while the initial hydraulic conductivity of saltstone is still the prominent variable, infiltration is now more important than the cementitious degradation, such that it is now easier to distinguish individual curves than in Figure 4.4-9.

Figure 4.4-11: Total Volumetric Flow Rates through the SDU 4 Floor (36 Cases, Grouped)

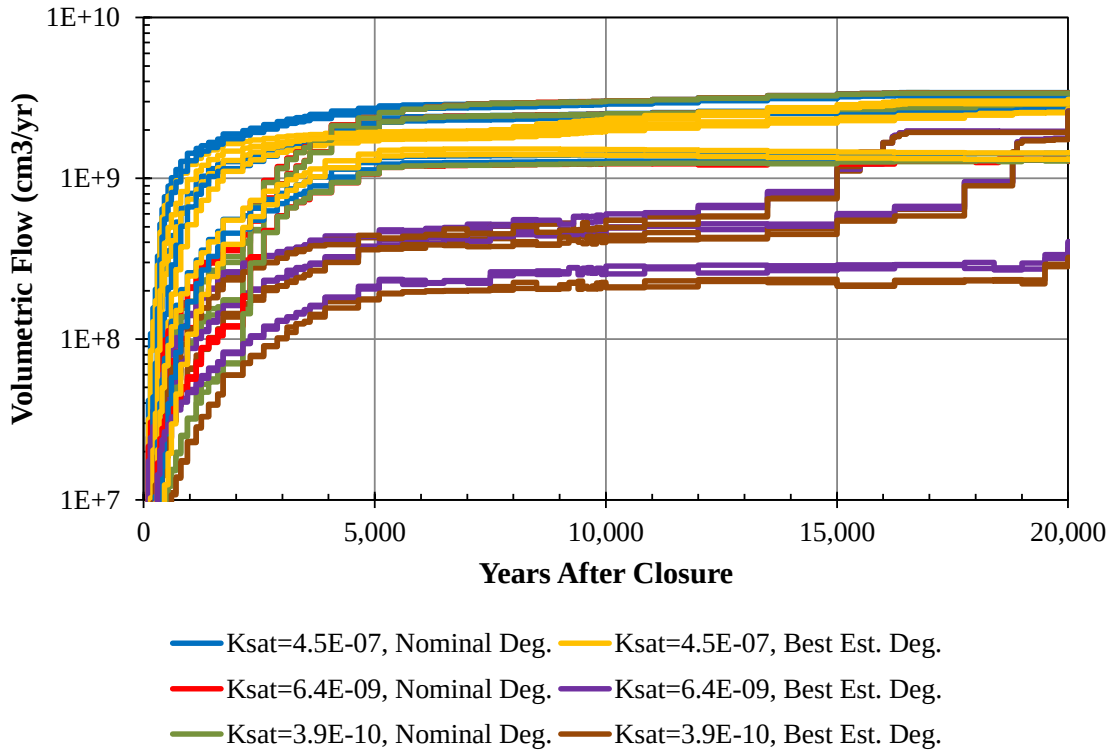

Figure 4.4-12 presents the total volumetric flow rates through the SDU 4 wall for the 36 flow cases. The highest volumetric flow rates between 7.2E+08 cm^3/yr and 7.0E+08 cm^3/yr shown around year 3,300 include four flow cases having the maximum infiltration rate, nominal rate for degradation, and the lower values for the initial saltstone hydraulic conductivity. The highest volumetric flow rates shown in Figure 4.4-12, 3.2E+09 cm^3/yr, occur around year 17,000 and include four flow cases having the maximum infiltration rate, the best estimate rate for degradation, and the lower values for the initial saltstone hydraulic conductivity. There are two flow cases with volumetric flow rates of 2.8E+09 cm^3/yr at about year 17,000. These two flow cases have the maximum infiltration rate, the best estimate rate for degradation, and the highest value for the initial saltstone hydraulic

conductivity. Near 20,000 years four additional flow cases appear with volumetric flow rates of approximately 2.8E+09 cm^3/yr. These flow cases have the average infiltration rate, the best estimate rate for degradation, and the lower values for the initial saltstone hydraulic conductivity.

Figure 4.4-12: Total Volumetric Flow Rates through the SDU 4 Wall (36 Cases)

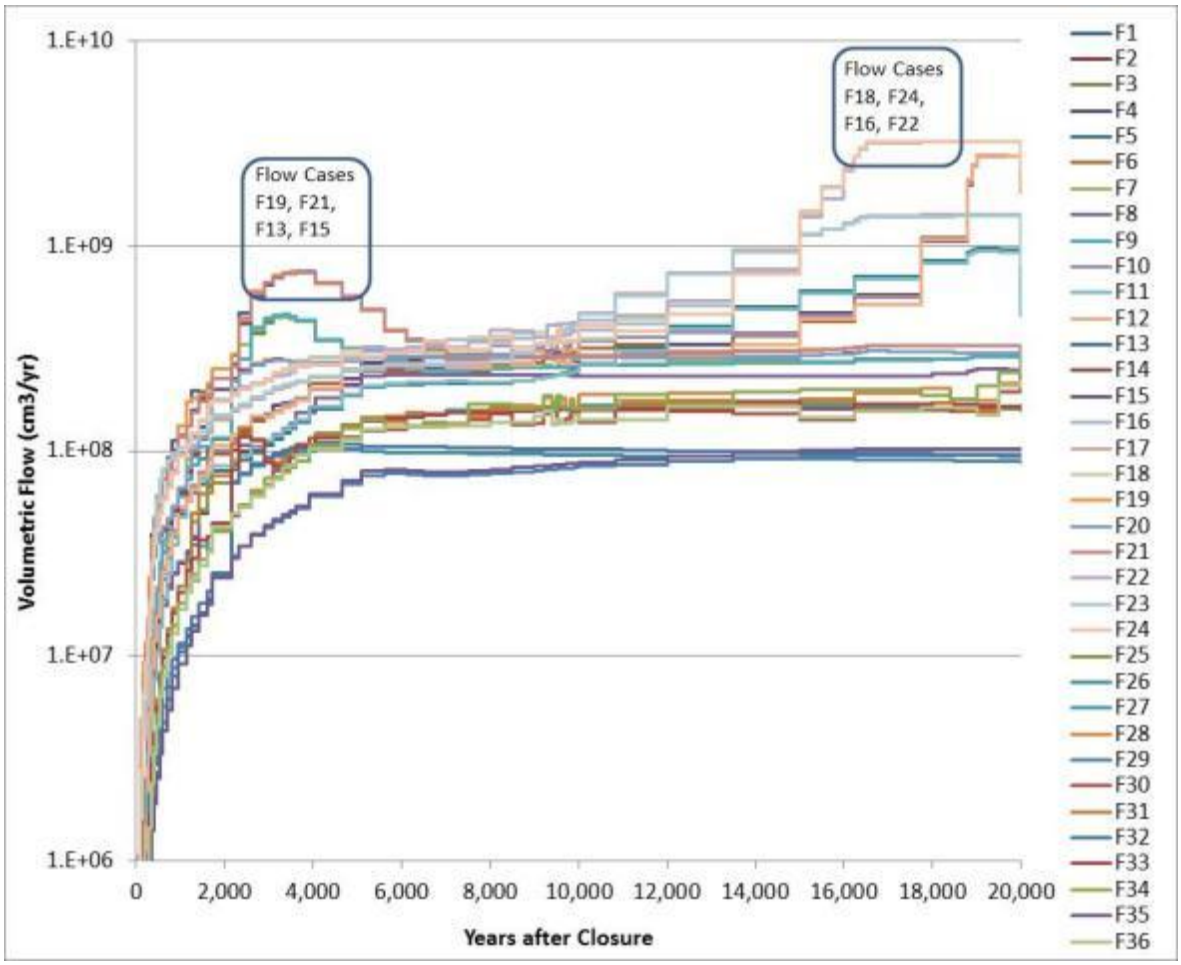

Of interest is the impact that the choice of MCC material may have on the flow through the joints in SDU 4. Figure 4.4-13 presents the volumetric flow rate through the joints when gravel is used as the material for the MCC. Figure 4.4-14 presents the volumetric flow rate through the joint when the relative permeability of the material in the joint is set equal to 1, regardless of the suction level.

Figure 4.4-13: Total Volumetric Flow through SDU 4 Joints (Using the Gravel MCC)

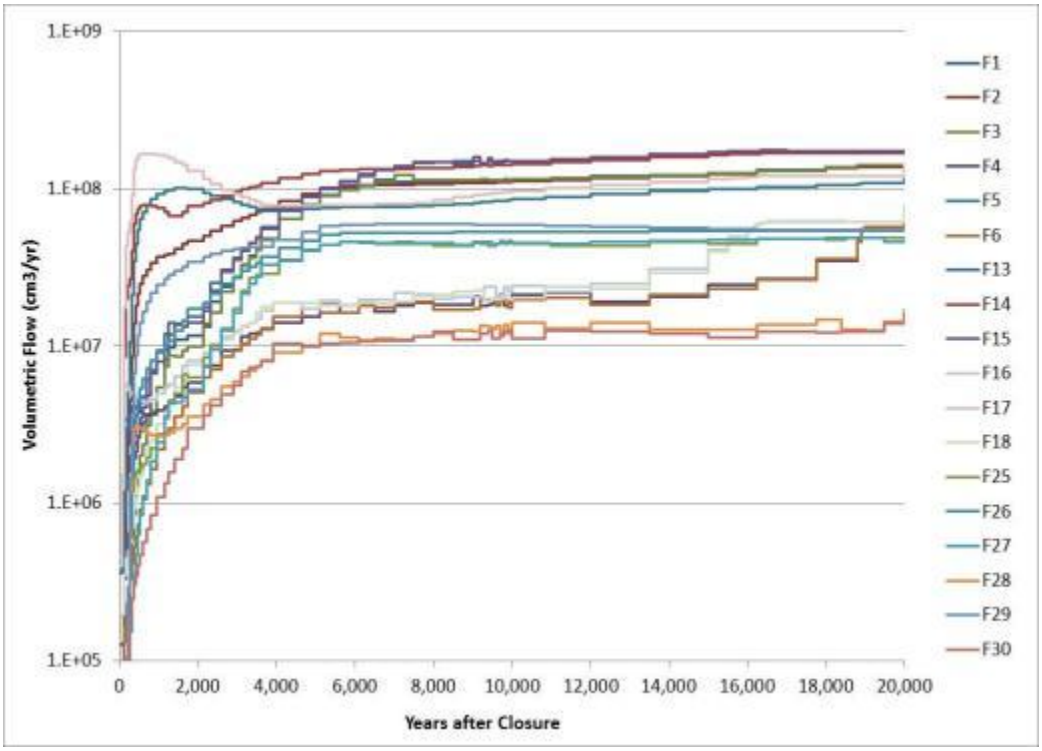

Figure 4.4-14: Total Volumetric Flow through SDU 4 Joints (Using MCC for Relative Permeability = 1)

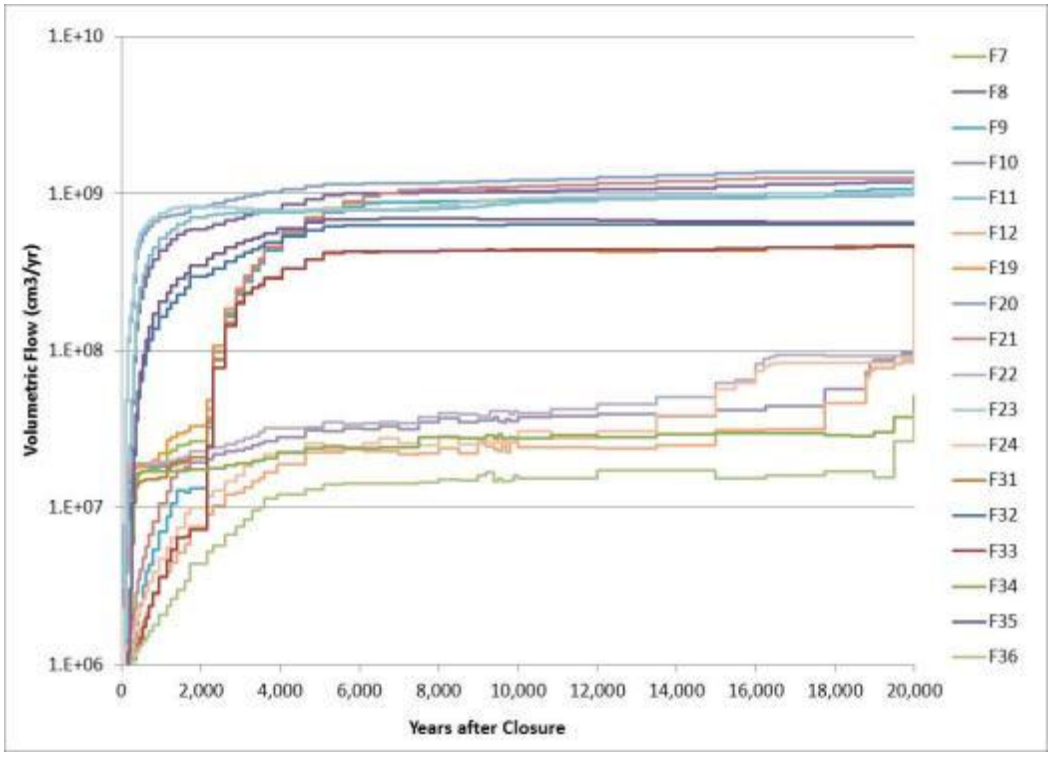

Comparison of Figures 4.4-13 and 4.4-14 shows that the choice of material chosen for the joint may have a significant impact on the flow through the joint based on a particular flow case. Table 4.4-4 presents the total flow for each flow case at 20,000 years after facility closure and the volumetric flow rate ratio between the flow cases with the same parameters except for the choice of joint MCC material. Table 4.4-4 indicates that the use of a constant relative permeability of 1 may cause as much as a 12 times increase in the flow through the joint when compared to the same case with a joint having an MCC of gravel.

Table 4.4-4: Comparison of Volumetric Flow Rates through SDU 4 Joints at 20,000 Years

Gravel MCC		Relative Permeability = 1		Ratio
Flow Case	**Flow at 20,000 Years (cm^3/yr)**	**Flow Case**	**Flow at 20,000 Years (cm^3/yr)**	**RP=1 to Gravel MCC**
F1	1.41E+08	F7	1.06E+09	7.53E+00
F2	1.38E+08	F8	1.19E+09	8.62E+00
F3	1.41E+08	F9	1.06E+09	7.52E+00
F4	5.69E+07	F10	8.68E+07	1.53E+00
F5	1.09E+08	F11	9.70E+08	8.93E+00
F6	5.71E+07	F12	7.73E+07	1.35E+00
F13	1.75E+08	F19	1.26E+09	7.21E+00
F14	1.68E+08	F20	1.37E+09	8.19E+00
F15	1.75E+08	F21	1.26E+09	7.21E+00
F16	6.17E+07	F22	9.34E+07	1.51E+00
F17	1.21E+08	F23	1.00E+09	8.30E+00
F18	6.20E+07	F24	8.38E+07	1.35E+00
F25	4.88E+07	F31	4.68E+08	9.58E+00
F26	5.43E+07	F32	6.42E+08	1.18E+01
F27	4.61E+07	F33	4.58E+08	9.94E+00
F28	1.42E+07	F34	3.77E+07	2.66E+00
F29	5.50E+07	F35	6.54E+08	1.19E+01
F30	1.38E+07	F36	2.65E+07	1.93E+00

4.4.4.2 FDC Evaluation (36 Flow Cases)

An evaluation of the various flow cases for FDCs is provided in this section.

Figure 4.4-15 presents the total volumetric flow rates (horizontal and vertical) in FDC saltstone for the 36 flow cases. This figure illustrates that the maximum flow in saltstone between approximately 7,000 years and 12,000 years lies within a relatively narrow band between 2.8E+08 cm^3/yr and 2.3E+08 cm^3/yr. The common parameter among the 12 cases comprising this band is the initial saltstone saturated hydraulic conductivity of 4.5E-07 cm/s, regardless of the infiltration rate and the degradation rate of cementitious material and the choice of MCC for the joints. Thus, the initial saltstone saturated hydraulic conductivity has much more impact on the volumetric flow rate in saltstone within the first 12,000 years than the other flow parameters.

Figure 4.4-15: Total Volumetric Flow Rates in Saltstone for FDCs (36 Cases)

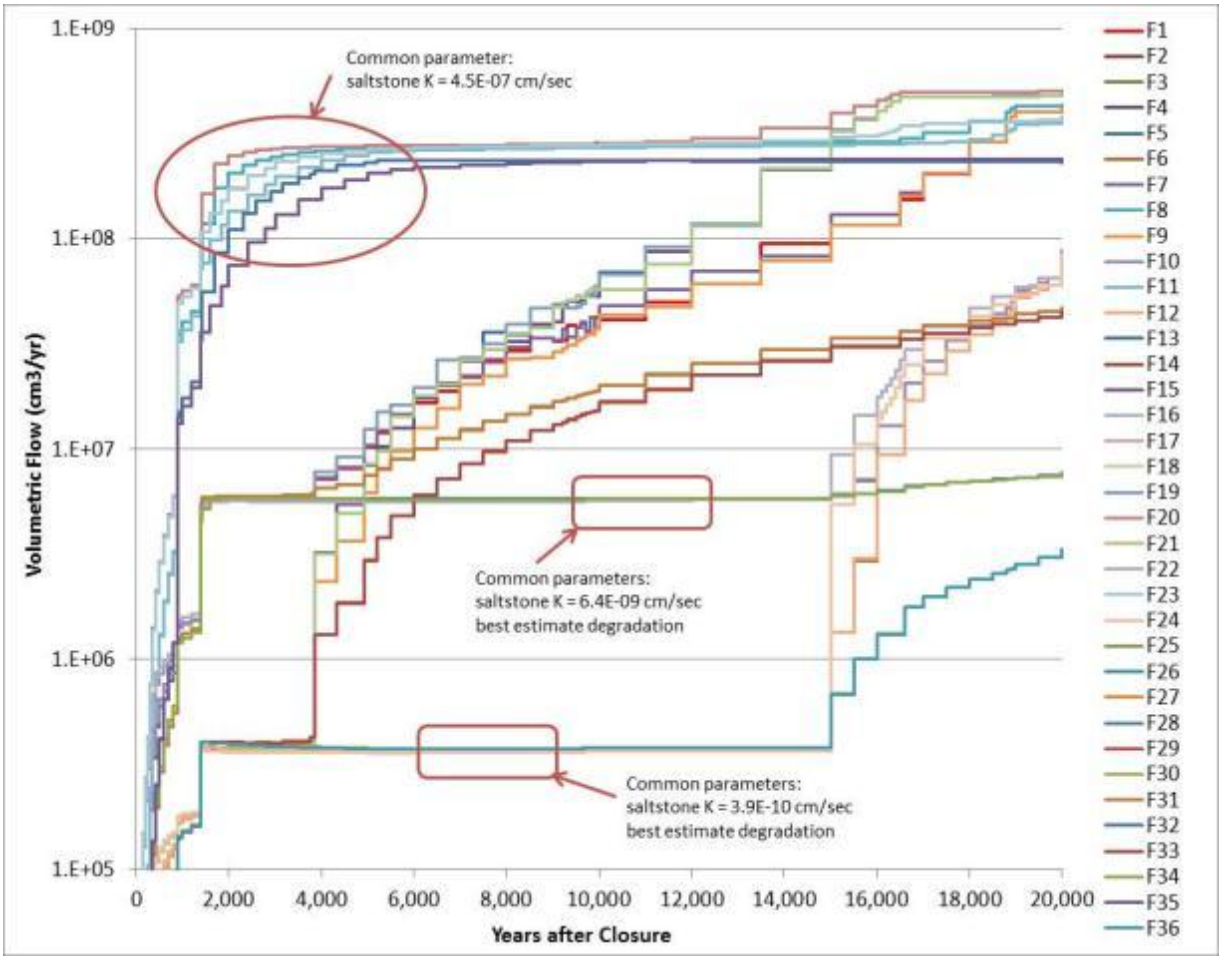

Out to 20,000 years, eight additional cases join the initial 12 cases for saltstone having a volumetric flow rate of between 2.3E+08 cm^3/yr and 5.0E+08 cm^3/yr. These additional eight cases have the nominal degradation rate as a common parameter indicating that flow through saltstone is more sensitive to cementitious material degradation rate than the infiltration rate and that the choice of MCC behavior for the joint has no appreciable impact on the flow in saltstone.

Figure 4.4-16 presents the total flow in saltstone for the 20 cases just discussed (i.e., those 12 cases with the initial saltstone saturated hydraulic conductivity of 4.5E-07 cm/s and the eight additional cases with nominal degradation). The legend in Figure 4.4-16 lists the flow cases from the highest total flow at 20,000 years to the lowest total flow at 20,000 years for these 20 cases.

Figure 4.4-16: Total Volumetric Flow Rates through FDC Saltstone for Selected Cases

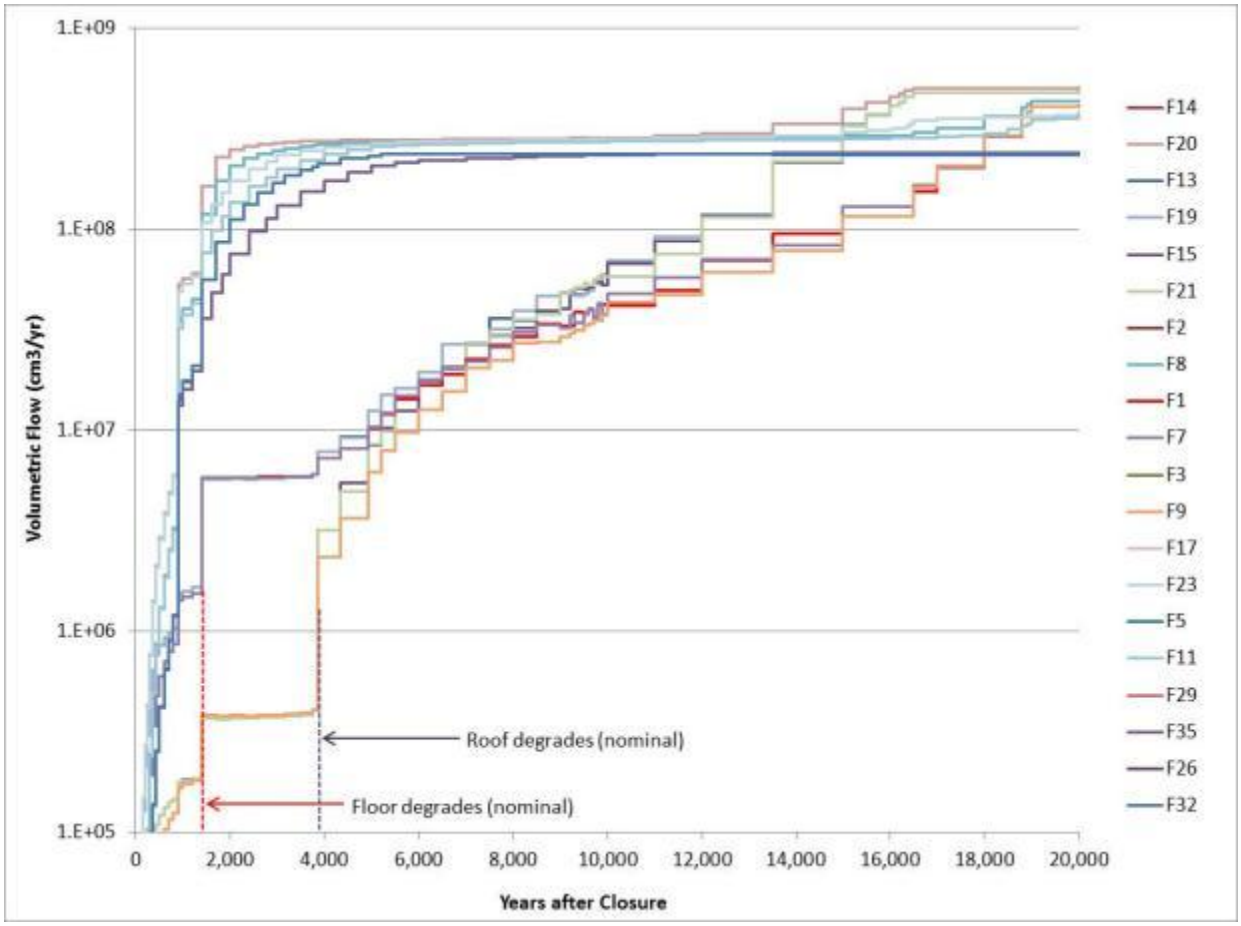

Figure 4.4-17 presents the same data as Figure 4.4-15, including all 36 flow cases, except each curve has been specifically colored based on (1) the initial hydraulic conductivity of saltstone (or K_{sat}) and (2) the cementitious degradation rate. Significant overlap within each group makes it difficult to distinguish all 36 flow curves, indicating that the hydraulic conductivity and the cementitious degradation rates have a much stronger influence over the flow behavior than infiltration or the MCCs of the joints.

Figure 4.4-17: Total Volumetric Flow Rates in FDC Saltstone (36 Cases, Grouped)

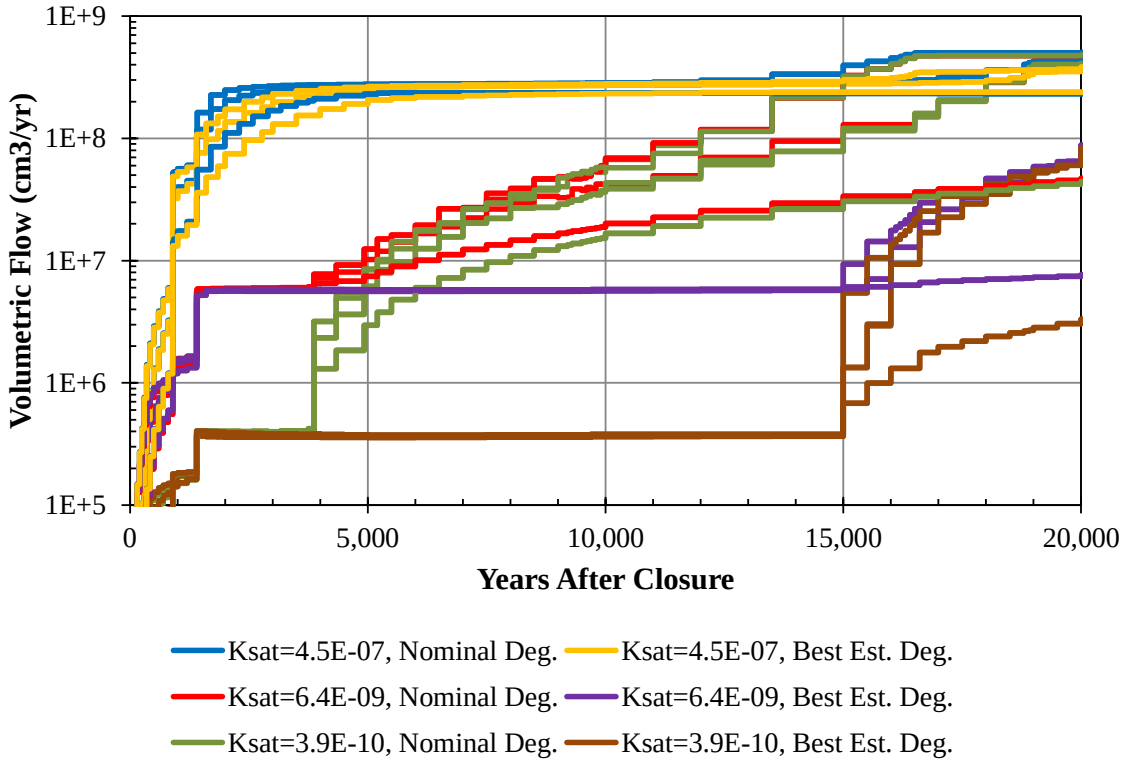

Figure 4.4-18 presents the total volumetric flow through the floor in FDCs for the 36 flow cases. This figure illustrates that the maximum flow through the floor between approximately 7,000 years and 12,000 years lies within a relatively narrow band between 2.4E+08 cm^3/yr and 3.0E+08 cm^3/yr. The common parameter among the 12 cases comprising this band is the initial saltstone saturated hydraulic conductivity of 4.5E-07 cm/s, regardless of the infiltration rate and the degradation rate of cementitious material and the choice of MCC for the joint. Thus, as in the case for flow through saltstone, the initial saltstone saturated hydraulic conductivity has much more impact on the volumetric flow rate through the floor within the first 12,000 years than the other flow parameters.

Figure 4.4-18: Total Volumetric Flow Rates through the FDC Floor (36 Cases)

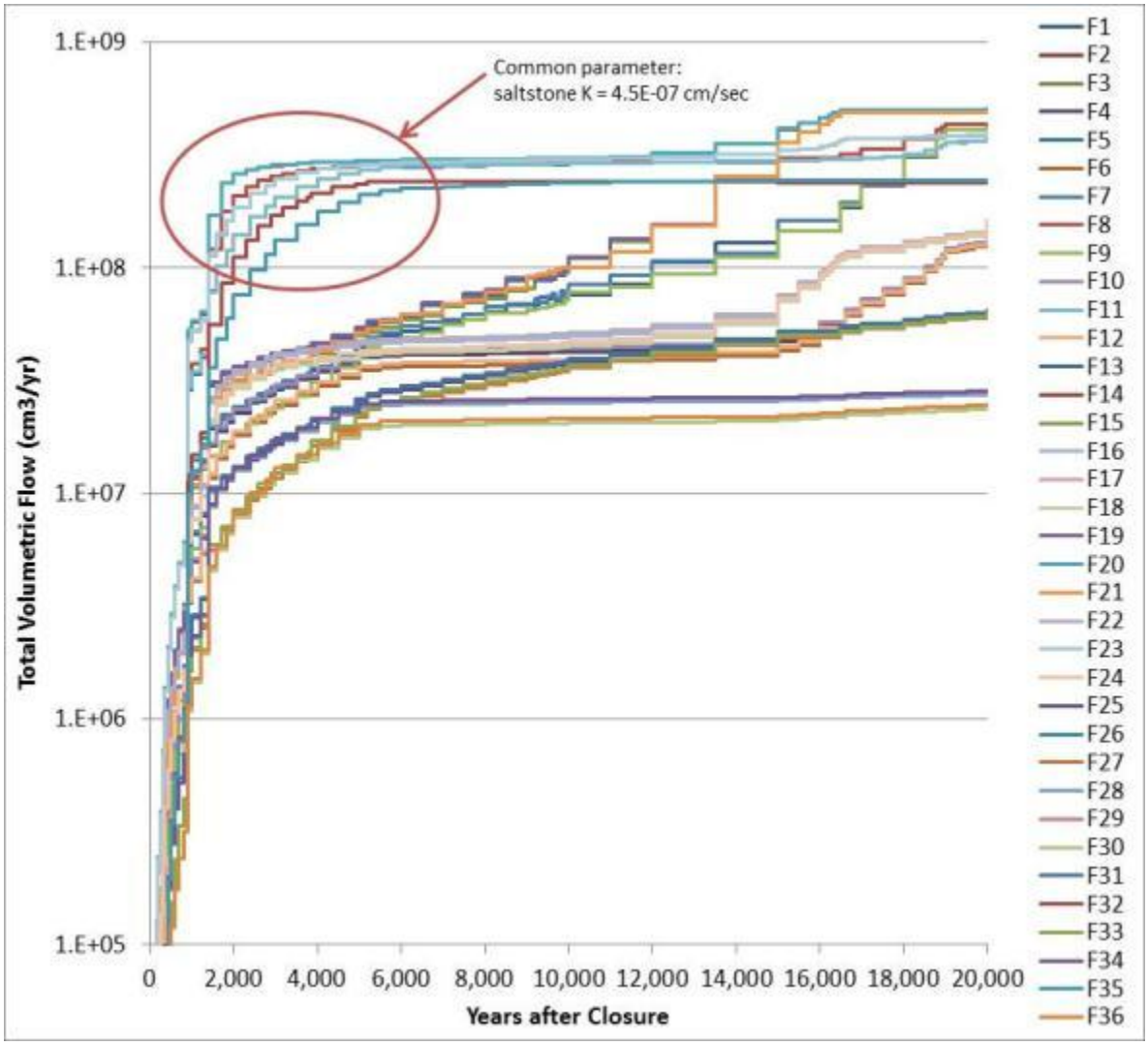

Figure 4.4-19 presents the total volumetric flow through the FDC wall for the 36 flow cases. The 12 flow cases with the higher volumetric flow rates through the wall at 1,000 years have as a common parameter, the initial saltstone hydraulic conductivity. Again, the saltstone hydraulic conductivity has the most impact on flow performance of the parameters included in this analysis. Toward the end of the 20,000-year period, the 12 cases that apply the best estimate cementitious material degradation rate show higher volumetric flow. Differences in relative flow between these 12 cases are due to the infiltration rate and the saltstone hydraulic conductivity.

Figure 4.4-19: Total Volumetric Flow Rates through FDC Wall (All Cases)

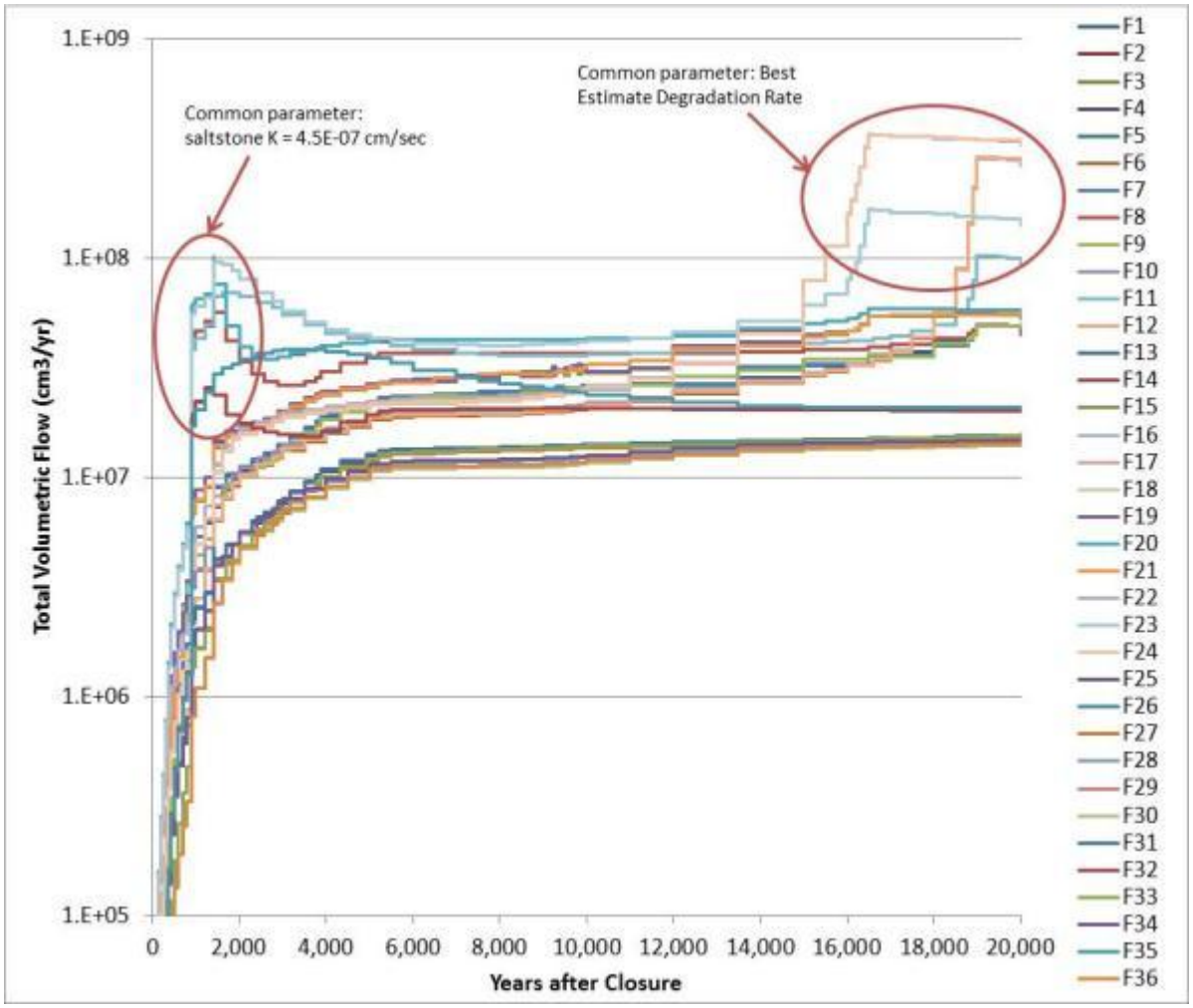

Of interest is the impact that the choice of MCC material may have on the flow through the joint. Comparison of flow results shows that the choice of MCC material chosen for the joints has no discernible impact on the flow through the joint. Table 4.4-5 presents the total flow for each case at 20,000 years after closure and the percentage increase between the flow cases with the same parameters except for the choice of joint MCC material. Table 4.4-5 indicates that the joint with gravel MCC, in most cases, has a lower volumetric flow rate than when that same case has a constant relative permeability of 1. The use of a constant relative permeability of 1 has no more than a 12 % increase in the flow through the joint when compared to the same case with a joint having an MCC of gravel. Note that the selection of an MCC in the joint is more significant to total volumetric flow though the joint for SDU 4 than for FDCs. This is attributed to the difference in joint lengths between the FDCs. SDU 4 has nearly 9,000 feet of joint length (Section 3.3.2) and FDCs each have less than 500 feet of joint length (Section 3.3.3).

Table 4.4-5: Comparison of Volumetric Flow Rate through FDC Joint at 20,000 Years

Gravel MCC		Relative Permeability = 1		Percent Difference from Gravel MCC
Flow Case	Flow at 20,000 Years (cm^3/yr)	Flow Case	Flow at 20,000 Years (cm^3/yr)	
F1	2.04E+07	F7	2.17E+07	6.4 %
F2	1.32E+07	F8	1.32E+07	0.0 %
F3	2.05E+07	F9	2.05E+07	0.0 %
F4	4.84E+07	F10	5.09E+07	5.1 %
F5	1.69E+07	F11	1.84E+07	9.1 %
F6	4.89E+07	F12	5.14E+07	5.1 %
F13	2.33E+07	F19	2.47E+07	6.3 %
F14	1.62E+07	F20	1.76E+07	8.6 %
F15	2.34E+07	F21	2.48E+07	6.2 %
F16	5.93E+07	F22	6.20E+07	4.6 %
F17	2.36E+07	F23	2.56E+07	8.2 %
F18	5.98E+07	F24	6.25E+07	4.6 %
F25	1.39E+07	F31	1.49E+07	7.7 %
F26	4.54E+06	F32	5.04E+06	11.0 %
F27	1.41E+07	F33	1.52E+07	7.4 %
F28	1.54E+07	F34	1.66E+07	7.5 %
F29	4.37E+06	F35	4.88E+06	11.8 %
F30	1.58E+07	F36	1.70E+07	7.4 %

4.4.4.3 Evaluation of FDC Roof Slope (2 Flow Cases)

Flow Cases 37 and 38 were developed to assess the potential impact on flow into FDCs for varying roof slopes. The other 36 flow cases assume that the roof on FDCs has a 2 % slope as is consistent with the SDF PA. Flow Case F37 considers the same parameters as Flow Case F1, except that the slope of the roof is modeled as 1.5 % rather than 2 %. Flow Case F38 also considers the same parameters as Flow Case F1, except that the slope of the roof is modeled as 2.5 % rather than 2 %.

Figure 4.4-20 presents the total volumetric flow rate through the saltstone monolith for Flow Cases F1 (2 % slope), F37 (1.5 % slope), and F38 (2.5 % slope). As shown in this figure, the roof slope of 2.5 % does not cause an increase to the flow through the saltstone monolith when compared to the 2 % roof slope case, and does not need to be further investigated. With a roof slope of 1.5 % the flow through the saltstone monolith causes an increase in the flow through the saltstone depending on the state of other FDC features. Prior to the complete degradation of the roof at 3,866 years, the flow through the saltstone is nearly identical, as indicated in Table 4.4-6, between the 1.5 % slope case and the 2 % slope case. After the roof degrades, the flow in saltstone can be as high as a 33 % increase from the 2 % roof slope within 10,000 years. The impact of this increase in the flow through saltstone is further investigated in Section 5.6.6.

Figure 4.4-20: Total Flow through FDC Saltstone for Various Roof Slopes

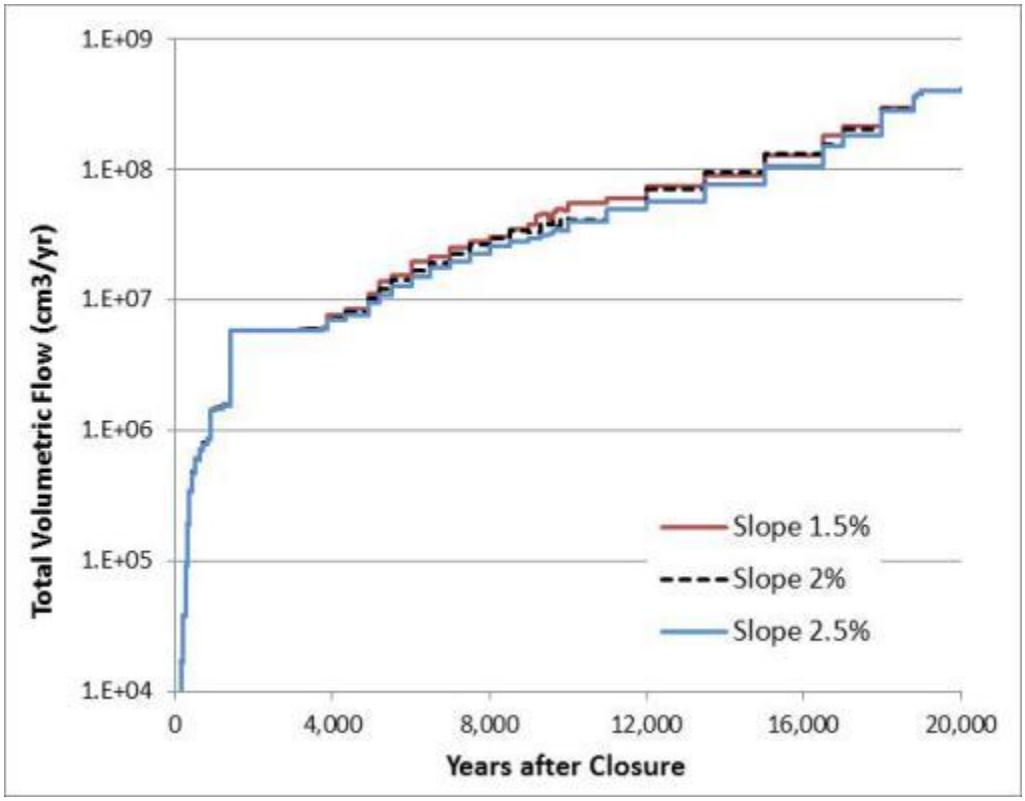

Table 4.4-6: Flow through FDC Saltstone for Roof Slope of 1.5 % and 2 %

Year after Closure	Flow (cm^3/yr)		Percent Difference from 2.0 % Roof Slope
	1.5 % Roof Slope	2.0 % Roof Slope	
1,000	1.50E+06	1.48E+06	1.1 %
2,300	5.84E+06	5.82E+06	0.4 %
3,500	5.93E+06	5.91E+06	0.3 %
3,866	6.08E+06	6.05E+06	0.5 %
4,338	7.64E+06	7.24E+06	5.6 %
6,500	1.96E+07	1.67E+07	17.4 %
7,000	2.16E+07	1.89E+07	14.1 %
9,200	4.39E+07	3.30E+07	32.9 %
9,500	4.60E+07	3.87E+07	18.9 %
10,000	5.49E+07	4.14E+07	32.5 %
12,000	5.97E+07	4.96E+07	20.4 %
17,000	1.82E+08	1.54E+08	18.4 %
18,900	3.61E+08	3.58E+08	0.7 %
20,000	4.05E+08	4.04E+08	0.2 %

4.5 Air and Radon Analysis

Section 4.5 of SDF PA contains a discussion of the airborne and radon analysis methodology. The information presented in the SDF PA, with respect to these analyses, is not affected by the revised modeling approach discussed within this SA.

4.6 Biotic Pathways

Section 4.6 of SDF PA documents the bioaccumulation factors and human health exposure parameters used in the SDF PA modeling effort. The bioaccumulation factors and human health exposure parameters presented in the SDF PA have been revised to reflect the most recent available data. For example, applicable input parameters were updated based on the U.S. Environmental Protection Agency's (EPA's) 2011 *Exposure Factors Handbook* (EPA-600-R-090-052F). A complete discussion of the revised biotic pathways and related inputs is provided in the report, *Dose Calculation Methodology for Liquid Waste Performance Assessments at the Savannah River Site* (SRR-CWDA-2013-00058). An analysis of the revised approach (in Appendix A of SRR-CWDA-2013-00058) indicated that these updates do not significantly alter the dose results, relative to the approach used in the SDF PA. [SRR-CWDA-2013-00058] Although a number of values changes within the dose calculations, the changes were generally small. Also, changes that did increase dose results were balanced by changes that caused decreases to the dose.

4.7 Dose Analysis

Section 4.7 of SDF PA contains a discussion of the dose analysis approach used and presents the set of dose conversion factors (DCFs) used in the dose calculations modeling effort methodology. This approach and the related DCFs have been revised to reflect the most recent available data. For example, applicable ingestion and inhalation DCFs were updated based on the DOE's 2011 *DOE Standard Derived Concentration Technical Standard* (DOE-STD-1196-2011). A complete discussion of the revised dose approach and related inputs is provided in the report *Dose Calculation Methodology for Liquid Waste Performance Assessments at the Savannah River Site* (SRR-CWDA-2013-00058). An analysis of this revised approach (in Appendix A of SRR-CWDA-2013-00058) indicated that these updates do not significantly alter the dose results, relative to the approach used in the SDF PA.

5.0 RESULTS OF ANALYSES

This section will evaluate the new information on SDUs and FDCs at the time of final facility closure of the SDF.

5.1 Source Term (Analysis Results) Assumptions

In this SA, as in the SDF PA, the release of radionuclides from the SDUs and FDCs was controlled, in most cases, by advective movement, which may vary with pH, and can vary with redox potential as well. The stabilized contaminant release rate is impacted by the water flow through the SDUs and FDCs and changes over time as the hydraulic properties of the saltstone and containment materials change. After a contaminant had left its applicable containment, concrete retardation and soil retardation impacted the contaminant's transport rate into the aquifers.

5.2 Environmental Transport of Radionuclides

As presented in Section 5.2 of the SDF PA, the groundwater concentrations for all of the radionuclides are discussed in the source term screening.

5.2.1 Key Radionuclide Determination

Section 5.2.2 of the SDF PA presents the methodology used in determining which radionuclides would be considered "key." The key radionuclides were determined based on the peak groundwater doses calculated using the 100-meter concentrations calculated in PORFLOW. The key radionuclide determination was conducted based on the peak groundwater doses within 20,000 years. Unlike the SDF PA, which used a threshold of 0.05 mrem/yr, this SA used a threshold of 0.25 mrem/yr to select key radionuclides in order to ensure that sensitivity studies placed greater emphasis on those radionuclides that have the greatest influence over peak doses. The 0.25 mrem/yr threshold was used as it represents 1/100th of the 25 mrem/yr requirement described in DOE M 435.1-1. This change to the methodology is consistent with other liquid waste PAs (e.g., HTF PA). [SRR-CWDA-2010-00128]

The screening conclusions are provided in Table 5.2-1. The resulting key radionuclides are I-129, Tc-99, and Cs-135.

Table 5.2-1: Determination for Key Radionuclides

Sector	Peak all-Pathways Dose Contribution in 20,000 Years (mrem/yr)				
	I-129	Tc-99	Cs-135	Ra-226	Pa-231
A	6.0	1.9	1.6	0.14	<0.05
B	7.2	2.3	1.6	0.18	<0.05
C	7.8	2.5	1.6	0.17	<0.05
D	6.8	2.1	1.4	<0.05	<0.05
E	5.7	1.8	1.3	<0.05	<0.05
F	4.1	1.3	1.3	<0.05	<0.05
G	9.8	2.7	1.3	<0.05	<0.05
H	10.1	2.8	1.3	<0.05	<0.05
I	11.3	3.1	1.3	<0.05	<0.05
J	9.9	2.6	1.3	<0.05	<0.05
K	10.4	2.9	1.3	<0.05	<0.05
L	8.4	2.3	1.3	<0.05	<0.05

For this SA, no new PORFLOW modeling was performed to determine seepline dose. Instead, the 35 % seepline dose factor described in Section 5.2.2 of the SDF PA was applied to the 100-meter concentrations to determine radionuclide dose at the seepline for all constituents. Currently, the seepline doses are developed for information only and are not used to assess potential future compliance with performance objectives. This seepline factor was also applied in the key radionuclide determination.

5.2.2 Groundwater Concentrations at 100 Meters

The radionuclide inventories used in this SA are presented in Table 3.4-1. The 100-meter groundwater concentrations for the SA were calculated using the SDF PORFLOW Model for the Evaluation Case, which divides the area around SDF into computational cells. The PORFLOW 100-meter concentrations are calculated for 12 sectors (Sectors A – L). The groundwater concentrations at 100 meters are presented in Table A-1 through A-3 (Appendix A). Results are presented for the maximum groundwater concentration in any of the three distinct aquifers modeled UTRA-UZ, Upper Three Runs Aquifer–Lower Zone (UTRA-LZ), and the Gordon Aquifer by sector within the 1,000-year compliance period.

The blue and green dots in Figure 5.2-1 show the 1-meter and 100-meter distances from SDF. The blue and green dots also indicate the "sector" used for compilation of results. Each sector has a companion 1-meter and 100-meter field.

Figure 5.2-1: SDF 1-Meter and 100-Meter Modeled Cells and Sectors

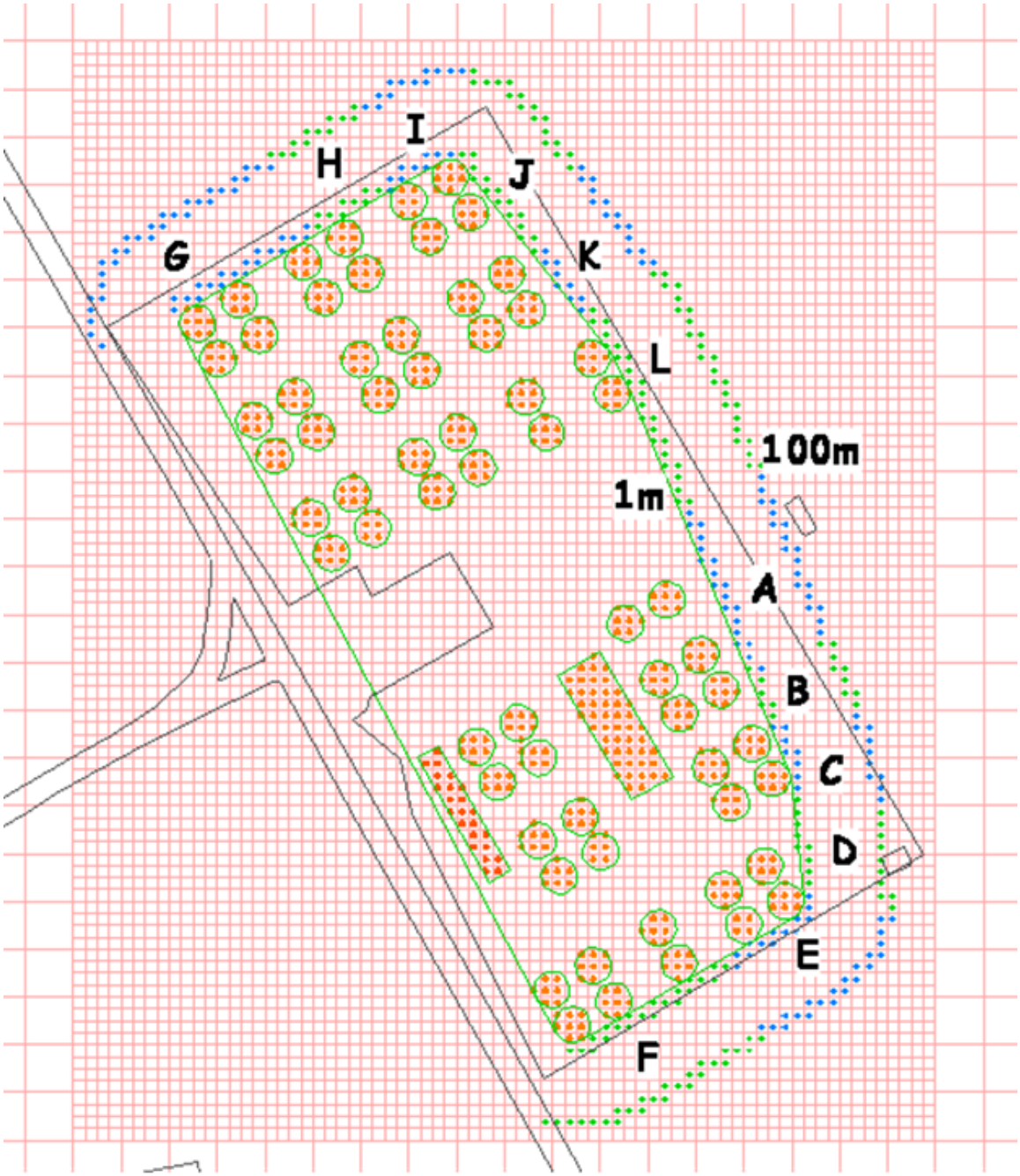

Inputs to calculation of the 100-meter groundwater concentrations using the SDF PORFLOW Model is discussed in more detail in Section 5.2.1 of the SDF PA.

Tables A-1 through A-3 (Appendix A) also list the Maximum Contaminant Level (MCL) for each constituent with the derived values for beta-gamma and photon emitters from Table II-3 of FR-00-9654. The MCLs provided in the reference are based on a beta-gamma dose of 4 mrem/yr. The peak concentration of each beta-gamma emitter in 1,000 years is compared

to a specific MCL to determine their fraction. To determine if the 4 mrem/yr beta-gamma limit is met, the sum of the fractions must be less than 1.0. The total alpha MCL includes Ra-226, but does not include radon or uranium. The radium MCL includes both Ra-226 and Ra-228. [SCDHEC R.61-58]

5.2.3 Groundwater Concentrations at the Seeplines

For this SA, no new PORFLOW calculations were performed to determine the seepline groundwater concentrations. Instead, the 35 % seepline dose factor described in Section 5.2.2 of the SDF PA was applied to the 100-meter concentrations for determining radionuclide doses at the seepline for all constituents.

5.3 Air Pathways and Radon Analysis

Section 5.3 of SDF PA describes the methodology and approach for determining the results of the airborne and radon analyses. The information presented in the SDF PA, with respect to these analyses, is not affected by the revised modeling approach discussed within this SA.

5.4 Biotic Pathways

Section 5.4 of SDF PA describes how the biotic pathways doses to the MOP are calculated for the receptor with 100-meter well water as a primary water source and for the receptor with groundwater from a stream as a primary water source. As mentioned in Section 4.6, this has been revised to reflect the most recent available data. A complete discussion of the revised biotic pathways and related methodology is provided in *Dose Calculation Methodology for Liquid Waste Performance Assessments at the Savannah River Site* (SRR-CWDA-2013-00058). An analysis of the revised approach (in Appendix A of SRR-CWDA-2013-00058) indicated that these updates do not alter the dose results, relative to the approach used in the SDF PA.

5.5 Dose Analysis of MOP Exposure

Section 5.5 (Dose Analysis) of the SDF PA contains calculations of the peak total doses to the MOP at the 100-meter well for the Base Case (Case A). A peak dose is identified for the 10,000-year performance period. In order to provide additional insight into the modeling, a peak dose is also identified for a 20,000-year period after SDF closure. Finally, a peak dose associated with a subset of the full suite of radionuclides for 100,000 years after facility closure is provided. The peak doses have been recalculated using the peak groundwater concentrations presented in this SA (i.e., the groundwater concentrations at 100 meters and at the seepline) for this Evaluation Case. The doses were recalculated using the SDF PORFLOW Model described in Section 4.4.1 and the Evaluation Case described in Section 4.4.3, using the revised SDF inventories presented in Section 3.4 and the dose methodology presented in Sections 4.6, 4.7, and 5.4.

5.5.1 Member of the Public at 100-Meter Groundwater Pathways Dose Results

The groundwater pathways peak doses for the 12, 100-meter sectors (A through L) are calculated using the peak concentration for each radionuclide in the sector (a discussion of how peak concentrations are determined by sector is provided in SDF PA Section 5.2).

These groundwater pathways peak doses are the total dose associated with all the individual 100-meter well pathways identified in Section 5.4.

5.5.1.1 Member of the Public 100-Meter Peak Annual Groundwater Pathways Dose

Table 5.5-1 shows a comparison of the 100-meter peak groundwater pathways doses for the 12 different 100-meter sectors within the first 1,000-year compliance period, the first 10,000 years, and within the time period bounded by 10,000 years and 20,000 years. For the Evaluation Case, the peak dose within the first 20,000 years is also the peak dose within 10,000 years. In calculating the peak groundwater pathways dose, the highest radionuclide concentration within the vertical computational meshes is used from each of the three distinct aquifers modeled (UTRA-UZ, UTRA-LZ, and the Gordon Aquifer).

As presented in Table 5.5-1, during the 1,000-year compliance period, the peak groundwater pathways dose to the MOP is 0.04 mrem/yr at the year 1,000, in Sector B. As shown in Figure 5.5-1, the higher doses to the MOP occur in Sectors B and C, followed by Sectors A and D. The peak dose is dominated by the release of I-129 and Tc-99 from the walls of SDU 4. Nearly 90 % of the peak dose is from the water ingestion pathway.

Table 5.5-1: 100-Meter MOP Peak Groundwater Pathways Dose by Sector

Sector	Peak Dose in 1,000 Years	Peak Dose in 10,000 Years	Peak Dose between 10,000 Years and 20,000 Years
A	0.032 mrem/yr (year 1,000)	6.8 mrem/yr (year 7,680)	2.0 mrem/yr (year 19,956)
B	0.039 mrem/yr (year 1,000)	8.1 mrem/yr (year 7,682)	2.5 mrem/yr (year 19,956)
C	0.038 mrem/yr (year 1,000)	8.6 mrem/yr (year 7,676)	2.8 mrem/yr (year 19,950)
D	0.021 mrem/yr (year 1,000)	7.1 mrem/yr (year 7,676)	2.2 mrem/yr (year 19,950)
E	0.0089 mrem/yr (year 1,000)	5.9 mrem/yr (year 7,676)	1.8 mrem/yr (year 19,950)
F	0.0056 mrem/yr (year 1,000)	4.2 mrem/yr (year 7,678)	1.3 mrem/yr (year 19,954)
G	0.0010 mrem/yr (year 1,000)	10 mrem/yr (year 7,688)	2.7 mrem/yr (year 19,960)
H	0.0010 mrem/yr (year 1,000)	10 mrem/yr (year 7,688)	2.8 mrem/yr (year 19,960)
I	0.0010 mrem/yr (year 1,000)	12 mrem/yr (year 7,700)	3.1 mrem/yr (year 19,972)
J	0.0080 mrem/yr (year 1,000)	10 mrem/yr (year 7,702)	2.7 mrem/yr (year 10,000)
K	0.0095 mrem/yr (year 1,000)	11 mrem/yr (year 7,702)	2.9 mrem/yr (year 19,972)
L	0.0092 mrem/yr (year 1,000)	8.6 mrem/yr (year 7,692)	2.3 mrem/yr (year 19,956)

Note: Sectors illustrated in Figure 5.2-1

Figure 5.5-1: 100-Meter MOP Peak Groundwater Pathways Dose within 1,000 Years, Sectors A through L

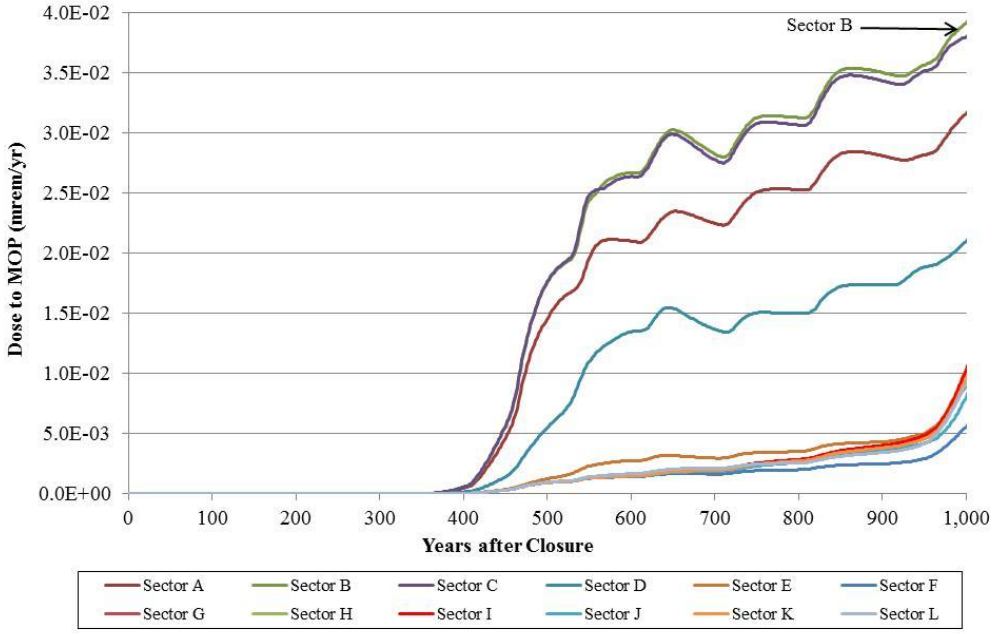

The highest overall peak groundwater pathways dose in the 10,000-year performance period is associated with Sector I. The Sector I 10,000-year dose is dominated by the I-129 release from the FDCs. Figure 5.5-2 shows the peak doses to a 100-meter MOP receptor over time during the performance period (10,000 years) for the 12, 100-meter sectors.

Figure 5.5-2: 100-Meter MOP Peak Groundwater Pathways Dose within 10,000 Years, Sectors A through L

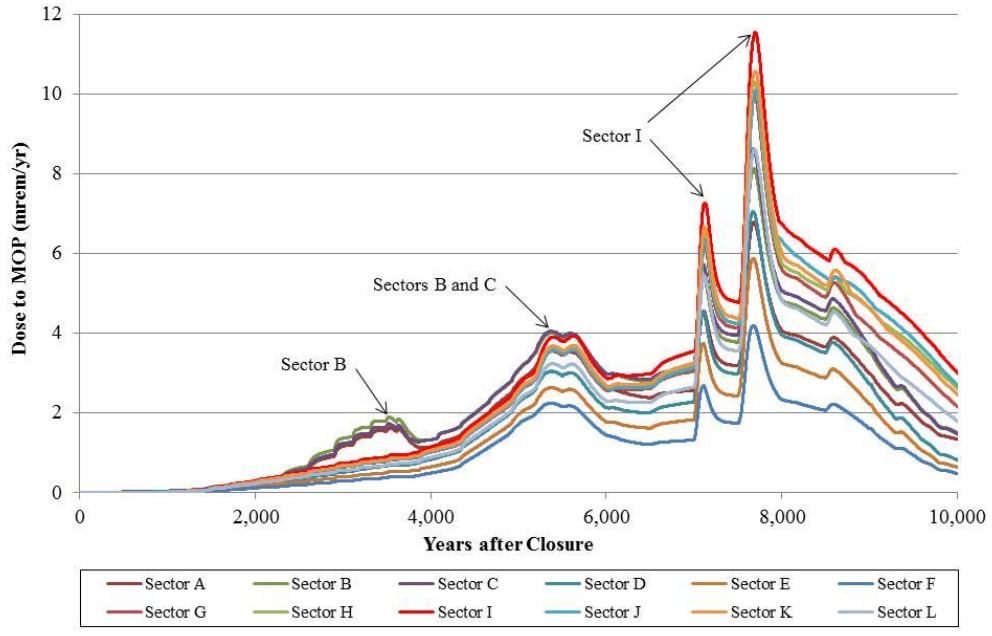

As shown in Figure 5.5-2, the initial peak occurs in Sector B at approximately 3,500 years and is dominated by the release of I-129 from SDU 4. SDU 4 was modeled to experience more rapid degradation of the cementitious barriers than the FDCs and thus the contaminants are released relatively earlier than from the FDCs. The double hump peak at approximately 5,300 years is equally shared by Sectors B and C. This dump hump peak results from the release of Cs-135 and Tc-99 from SDU 4 and the initial release of I-129 from the FDCs. The first peak dose in Sector I, occurring at approximately 7,100 years, is attributed to the release of I-129 from the FDCs shortly after the lower mud mat transitions to Oxidized Region III. The second peak dose in Sector I, occurring at approximately 7,700 years, is attributed to the release from the FDCs shortly after the floor transitions to Oxidized Region III. The slight bump, occurring at approximately 8,600 years, is attributed to the release from the FDCs shortly after the wall transitions to Oxidized Region III. The release of I-129, Cs-135, and Tc-99 from SDU 4 and from an FDC are shown in Figures 5.5-3 and 5.5.4, respectively.

Figure 5.5-3: Radionuclide Release through SDU 4 Floor

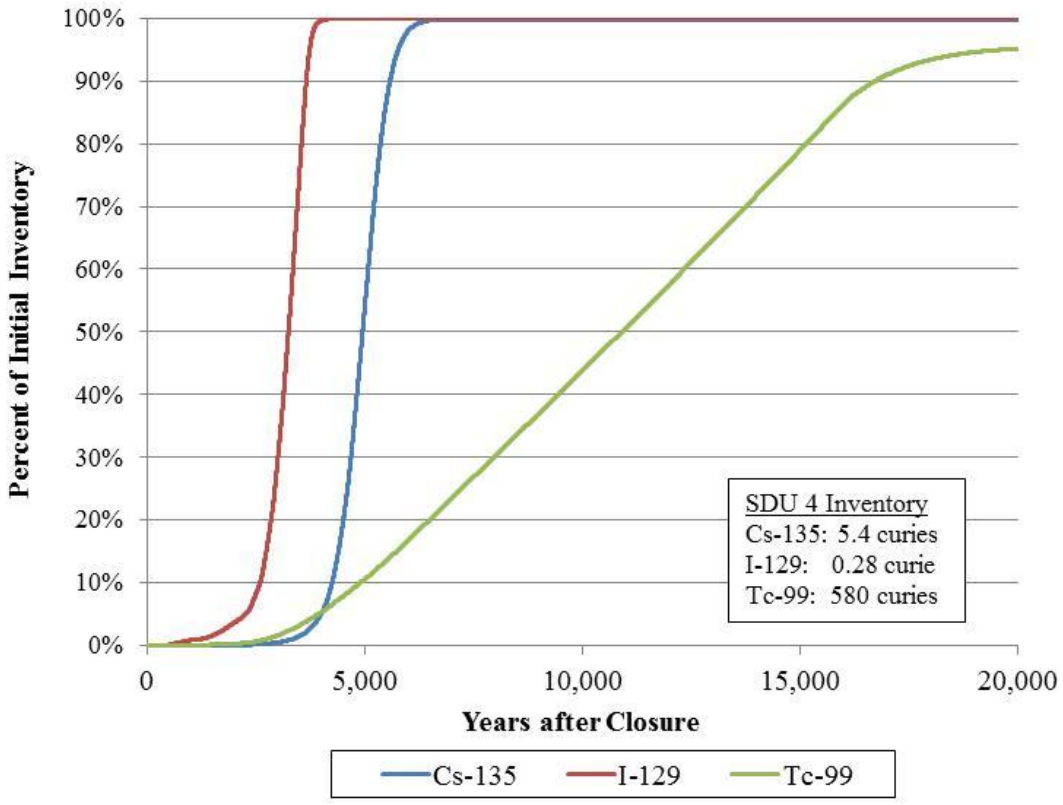

Figure 5.5-4: Radionuclide Release through FDC Floor

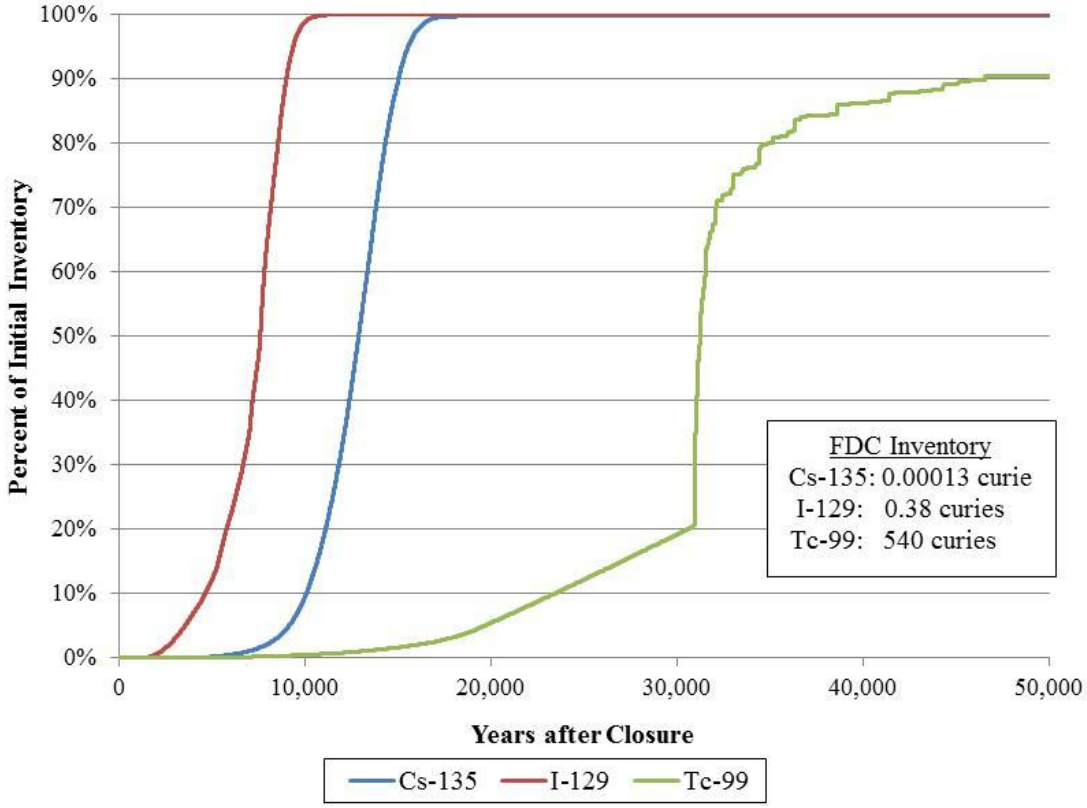

Figure 5.5-5 presents the dose to the MOP within 20,000 years. The dose to the MOP early in the time period from 10,000 years until approximately 11,000 years is highest in Sector I until the I-129 release from the FDCs is exhausted. From 11,000 years to approximately 17,000 years, Sectors A, B, and C have the highest dose caused by the release of Tc-99 from SDU 4. After 17,000 years, Sector I has the highest dose when the dose from Tc-99 begins to be dominated by the Tc-99 release from the FDCs.

Figure 5.5-5: 100-Meter MOP Peak Groundwater Pathways Dose within 20,000 Years, Sectors A through L

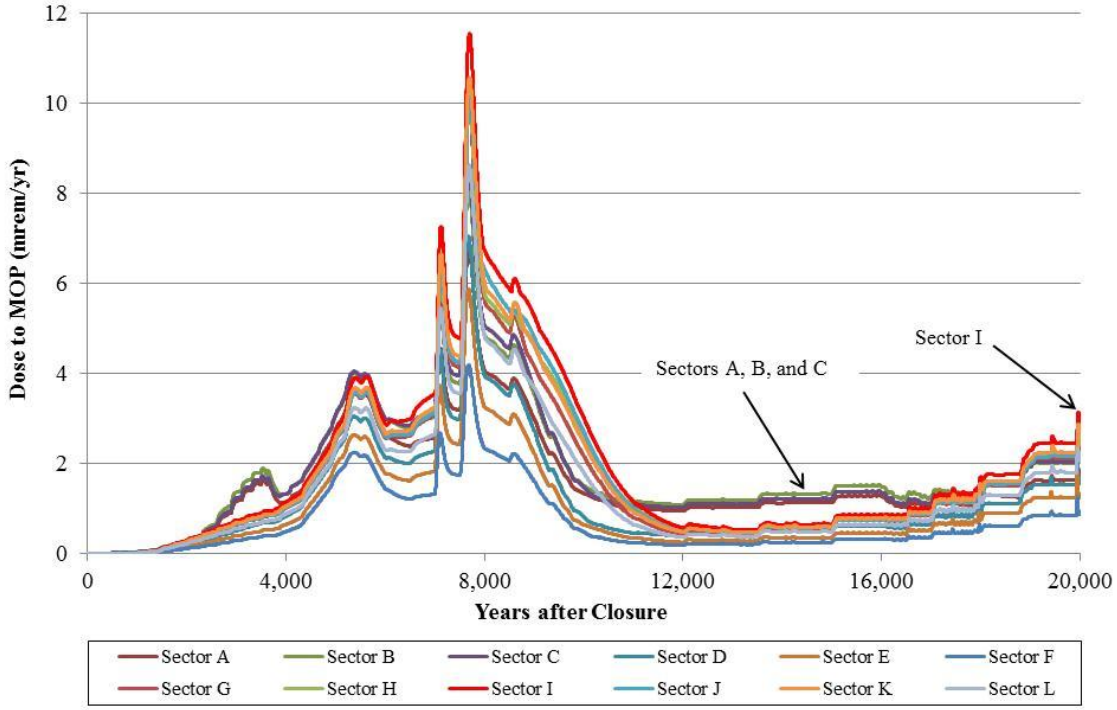

5.5.1.2 Individual Radionuclide Contributions to the MOP 100-Meter Peak Annual Groundwater Pathways Dose

Table 5.5-2 shows the relative contribution from the key radionuclides to the Sector I 100-meter peak groundwater pathways dose over 10,000 years. Figure 5.5-6 shows the relative contribution from the key radionuclides to the < 12-mrem/yr Sector I peak groundwater pathways dose. The peak groundwater pathways dose to a MOP at 100 meters during the 10,000-year performance period is primarily associated with I-129 (98 %) and Tc-99 (1.8 %). Figure 5.5-7 shows the relative contribution from the key radionuclides to the 3-mrem/yr Sector I peak groundwater pathways dose during the 10,000-year to 20,000-year time period. Figure 5.5-7 and Table 5.5-3 display the relative contributions from the key radionuclides to the Sector I 100-meter groundwater pathways dose during the 10,000-year to 20,000-year time period.

Table 5.5-2: Sector I 100-Meter MOP Peak Groundwater Pathways Dose in 10,000 Years

Radionuclide	Contribution to Sector I Peak dose at Year 7,700 (mrem/yr)	Percentage of Total Peak Dose
I-129	11	98 %
Tc-99	0.21	1.8 %
Cs-135	0.025	0.2 %
Others	< 0.01	< 0.1 %
Total	**< 12**	**100 %**

Figure 5.5-6: Contributors to the Sector I 100-Meter Peak Groundwater Pathways Dose, 10,000 Years

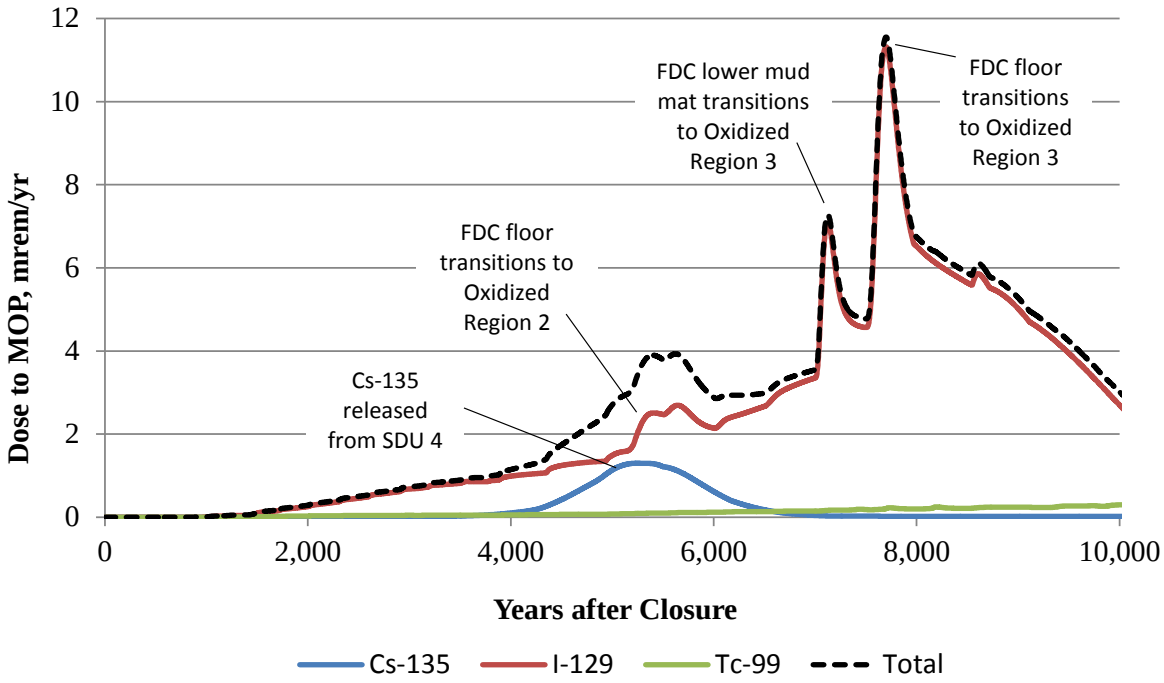

Figure 5.5-7: Contributors to the Sector I 100-Meter Peak Groundwater Pathways Dose, 10,000 Years - 20,000 Years

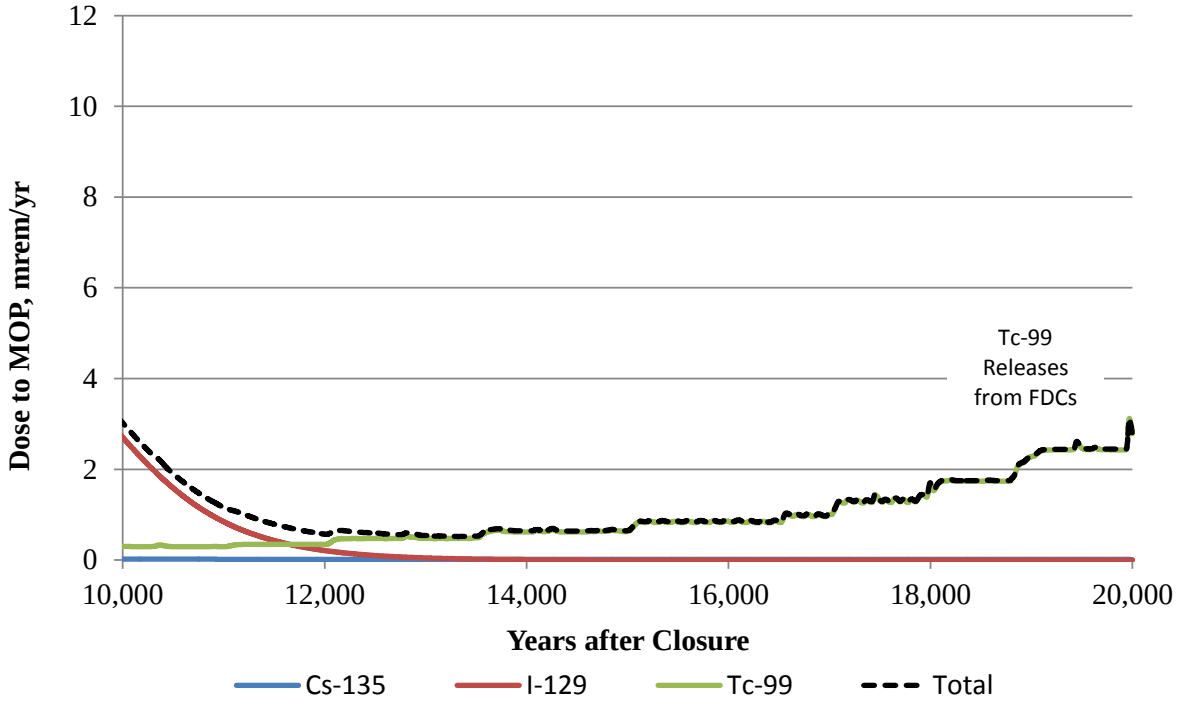

Table 5.5-3: Sector I 100-Meter MOP Peak Groundwater Pathways Dose in 10,000-Year to 20,000-Year Time Period

Radionuclide	Contribution to Sector I Peak Dose at Year 19,972 (mrem/yr)	Percentage of Total Peak Dose
Tc-99	3.1	99 %
Cs-135	0.011	0.3 %
Others	< 0.01	< 0.1 %
Total	**3.1**	**100 %**

Sector I has the highest dose within 10,000 years because of the contribution of I-129. Figure 5.5-6 shows three uplifts during the 10,000-year timeframe associated with I-129 and Cs-135. The first uplift of dose occurs at approximately 5,400 years and is due to the release of Cs-135 from SDU 4, which controls the fish ingestion dose pathway and the release of I-129 from FDCs when the floor of FDC transitions at 5,540 years from reduced to oxidized conditions. The second uplift of dose occurs at approximately 7,100 years. It is attributed to the increase of I-129 release from FDCs when the lower mud mat transitions from Oxidized Region II to Oxidized Region III at approximately 7,000 years. The third uplift of dose at approximately 7,700 years is attributed to the increase of I-129 release from FDCs when the floor of FDC transitions to Oxidized Region III at approximately 7,500 years, The 10,000-year to 20,000-year dose results for Sector I at 100 meters are influenced by Tc-99 with a total peak dose at 19,972 years.

5.5.1.3 Individual Pathways Contributions to a MOP 100-Meter Peak Annual Groundwater Pathways Dose

As stated previously, the total peak groundwater pathways dose results are the summation of the doses associated with all the individual 100-meter well pathways identified in Section 5.4. Table 5.5-4 shows the relative contributions from the individual groundwater pathways to the Sector I 100-meter MOP receptor dose at 7,700 years (the year of the peak dose). The primary contributors are water ingestion (88 % of peak dose) and fish ingestion (6 % of peak dose).

Table 5.5-4: 100-Meter MOP Peak Dose Groundwater Pathways Contributions in Sector I for 10,000 Years after Closure

Pathway	Associated Contribution to Sector I peak at year 7,700 (mrem/yr)	Percentage of Sector I Total Peak Dose
Water Ingestion	10	88 %
Fish Ingestion	0.64	5.6 %
Vegetable Ingestion	0.34	3.0 %
Milk Ingestion	0.17	1.5 %
Meat Ingestion	0.14	1.2 %
Egg Ingestion	0.039	0.34 %
All Other Pathways	< 0.015	< 0.1 %
Total	**< 12**	**100 %**

Because of the timing of the individual radionuclide dose peaks, the peak dose at 7,700 years in Sector I is dominated by I-129 as shown in Table 5.5-2. Figures 5.5-8, 5.5-9, and 5.5-10 present the radionuclide contributions from the key radionuclides (Cs-135, I-129, and Tc-99) for the three principal dose pathways of water ingestion, fish ingestion, and vegetable ingestion, respectively.

Figure 5.5-8: Radionuclide Contribution to the Water Ingestion Pathway in Sector I

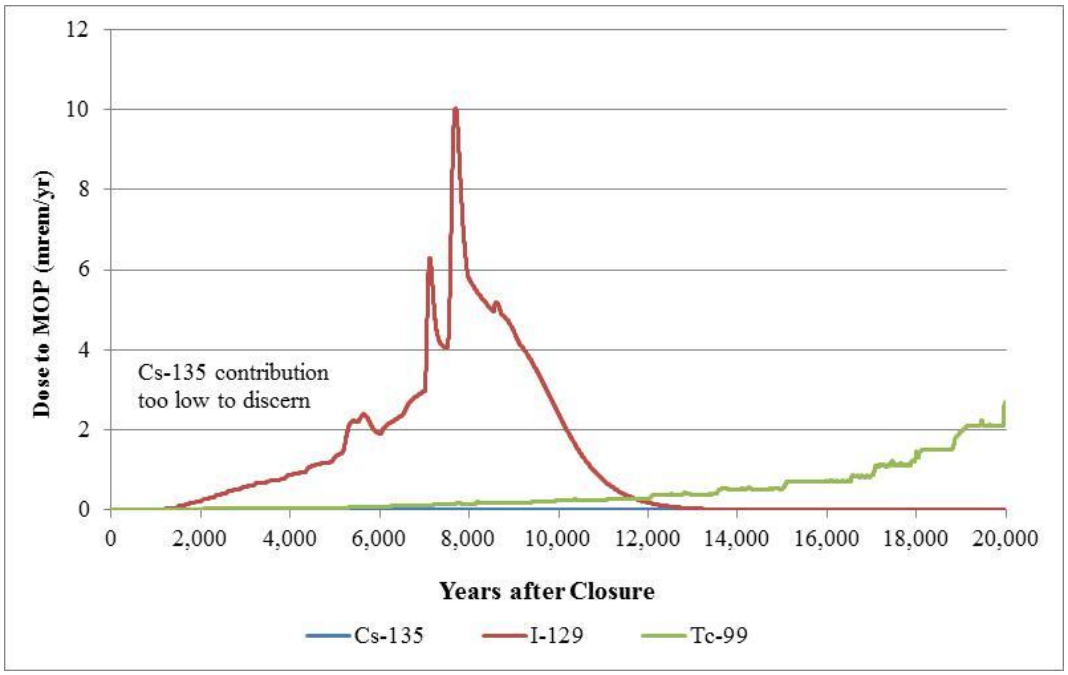

Figure 5.5-9: Radionuclide Contribution to the Fish Ingestion Pathway in Sector I

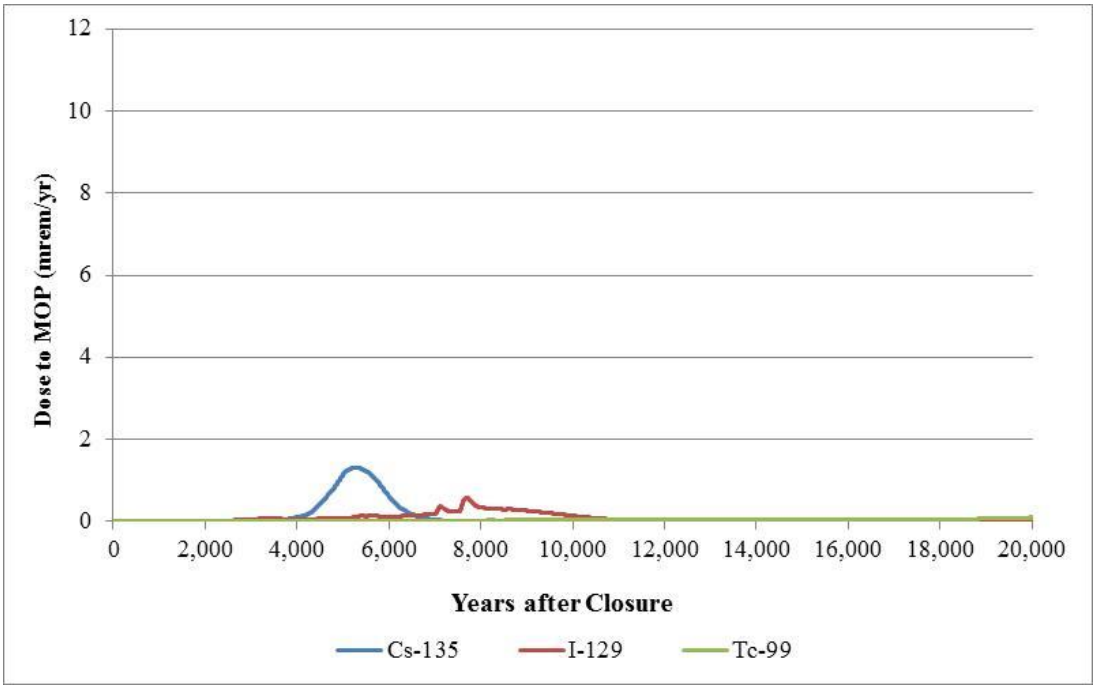

Figure 5.5-10: Radionuclide Contribution to the Vegetable Ingestion Pathway in Sector I

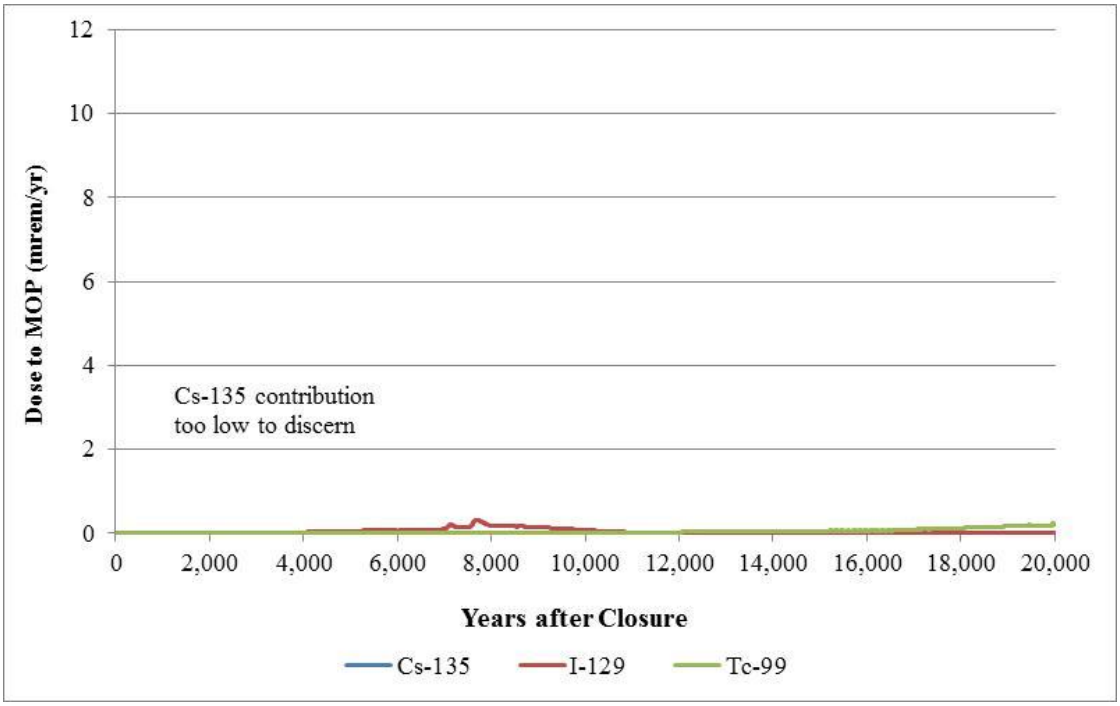

Table 5.5-5 shows the relative contributions from the individual groundwater pathways to the Sector I 100-meter MOP receptor dose at 19,972 years (the year of the peak dose for the time period between 10,000 years and 20,000 years). The primary contributors are water ingestion (86 % of peak dose) and vegetable ingestion (7.6 % of peak dose). Figures 5.5-8, 5.5-9, and 5.5-10 present the radionuclide contributions from the key radionuclides (Cs-135, I-129, and Tc-99) for the three principal dose pathways of water ingestion, fish ingestion, and vegetable ingestion, respectively.

Table 5.5-5: 100-Meter MOP Peak Dose Groundwater Pathways Contributions in Sector I for the Time Period at 19,972 Years

Pathway	Associated Contribution to Sector I peak at year 19,972 (mrem/yr)	Percentage of Sector I Total Peak Dose
Water Ingestion	2.7	86 %
Vegetable Ingestion	0.24	7.6 %
Fish Ingestion	0.12	3.8 %
Meat Ingestion	0.049	1.6 %
Milk Ingestion	0.020	0.63 %
Egg Ingestion	0.015	0.47 %
All Other Pathways	< 0.01	< 0.1 %
Total	**~ 3**	**100 %**

5.5.1.4 Member of the Public 100-Meter Peak Annual Groundwater Pathways Dose Results for 100,000 years

The peak groundwater pathways dose is estimated for the key radionuclides and others for 100,000 years in order that the dose behavior well past the 1,000-year compliance period can be evaluated. These groundwater pathways doses are the total doses associated with the individual MOP 100-meter pathways identified in Section 5.4. In addition to the key radionuclides identified in Section 5.2.1 (Cs-135, I-129, and Tc-99), the following radionuclides (and their progenies) have been included in this evaluation, Ra-226, Pb-210, and Pa-231. Ra-226, Pb-210, and Pa-231 were included based on the dose results from the 20,000-year run, which indicated that only these radionuclides have a contribution to the peak dose to the MOP that exceed 0.25 mrem/yr.

Figure 5.5-11 shows the peak 100-meter groundwater pathways doses over time for 100,000 years for Sectors B and I. The dose to the MOP peaks at approximately 400 mrem/yr in Sector I at 31,000 years after closure. This peak dose is from the significant initial release of Tc-99 that occurs when the FDC floor experiences break-through as the floor becomes oxidized. The subsequent spikes out to about 47,000 years after closure are from Tc-99 being released until the slag in the FDC concrete floor has been completely consumed by oxygen. After about 50,000 years, the higher doses to the MOP are in Sector B, which are mostly from Ra-226.

Figure 5.5-11: 100-Meter MOP Peak Groundwater Pathways Dose within 100,000 Years, Sectors B and I

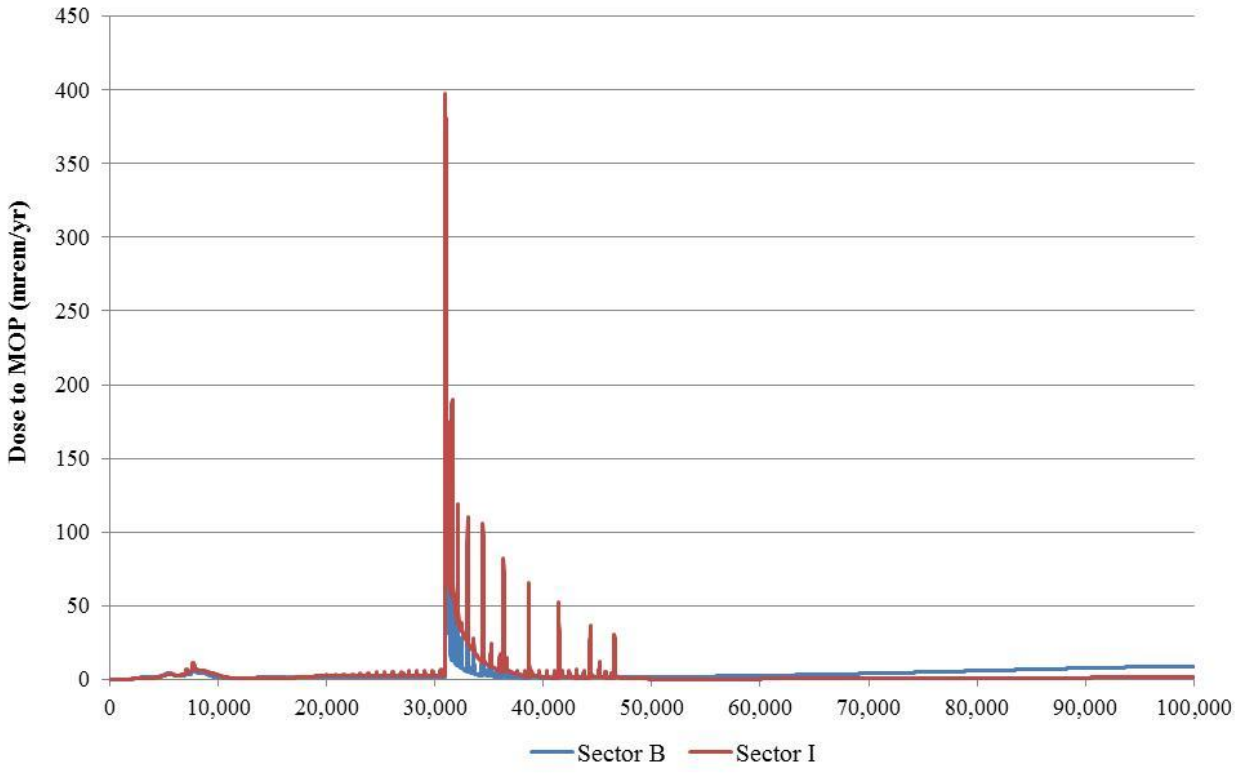

Movement and magnitude of the peak, approximately 400 mrem/yr at 31,000 years, to within the 10,000-year time frame was considered unlikely due to several factors. The first would require the combination of multiple releases. A modeling simplification of allowing all events associated with the FDCs to occur simultaneously produces spikes in the dose results. Although this condition is understood to be unrealistic, it manufactures conservative results. This peak is due to Tc-99 release from the FDCs. Tc-99 release is due to oxidation of the saltstone material and the rate of the movement affects the release timing. This oxygen movement oxidizes the slag contained within the saltstone and changes the Tc-99 release mechanism. The oxidation movement is primarily a function of the saltstone reduction capacity and oxygen flow, which is affected by the infiltration rate, hydraulic conductivity, and dissolved oxygen contained in the infiltrating liquid.

5.6 Uncertainty and Sensitivity Analyses

Section 5.6 of the SDF PA considers the effects of uncertainties in the conceptual models used and sensitivities in the parameters used in the mathematical models. The uncertainty analyses and sensitivity analyses were primarily performed using a probabilistic model (i.e., the SDF GoldSim Model), but some additional single parameter sensitivity analyses were performed through deterministic modeling using both the PORFLOW and GoldSim models.

The probabilistic model varies multiple parameters simultaneously, so concurrent effects of changes in the model can be analyzed, and the potential impact of changes can be assessed. This assessment allows for identification of parameters that are only of significance when varied simultaneously with another parameter. The deterministic model single parameter analysis provides a method to evaluate parametric effects in isolation, so the importance of the uncertainty around a parameter of concern can be more effectively evaluated. Using both probabilistic and deterministic models for sensitivity analysis versus a single approach provides additional information concerning which parameters are of most importance to the SDF PA modeling.

5.6.1 Uncertainty and Sensitivity Analyses using Probabilistic Modeling

The objective of these analyses was to investigate uncertainties that are inherent in conceptual models, mathematical models, and related data and assumptions to provide reasonable expectation/assurance that performance objectives will be met and ensure any future work focuses on issues of importance.

5.6.1.1 SDF GoldSim Model

In order to address uncertainty and sensitivity for the modeling of the SDF, a probabilistic model was constructed. This model is simpler in design than the PORFLOW groundwater model in its environmental transport calculations, but includes additional calculations that cannot be performed in PORFLOW, such as dose calculations. The SDF GoldSim Model is described in detail in Section 4.4.2.

The probabilistic model, developed using GoldSim software, accepts uncertainty and variability in the input parameters, the values of which can be defined using probability distributions. If a given model input (e.g., the K_d of saltstone) is given a distribution, or range of values, then this distribution is sampled in the collection of Monte Carlo runs that

constitutes a probabilistic analysis. The collective uncertainty of all stochastic (probabilistic) inputs is reflected in the range and distribution of modeled results, such as water concentrations or dose to hypothetical future human receptors. If a given input parameter is given no range of input values, that is, if it is defined deterministically, then it contributes nothing to the overall uncertainty in the results. In reality, few parameters have zero uncertainty. An example of a parameter without a defined range is the half-life of radionuclides.

The probabilistic model allows evaluation of the uncertainty in the PA. The results of the uncertainty analysis of this model are discussed in Section 5.6.4. Adopting a probabilistic approach also allows analysts to determine which model input parameters are the most significant to the results. This is done through sensitivity analysis, which identifies covariance between model inputs and results. Section 5.6.5 discusses the sensitivity analysis performed for the SDF model.

A benchmarking of the environmental transport calculations within a deterministic version of the SDF GoldSim Model and those performed by the PORFLOW model is discussed in Section 5.6.2.

5.6.2 GoldSim Benchmarking

5.6.2.1 Benchmarking Between the GoldSim and PORFLOW Models

The SDF GoldSim Model is a probabilistic model designed to perform parameter uncertainty and parameter sensitivity analyses used to help evaluate the potential for radionuclide migration from the SDUs and FDCs to the accessible environment, as described in *Updates to the Saltstone Disposal Facility Fate and Transport Model* (SRR-CWDA-2013-00073). The probabilistic model used for this SA was constructed using the GoldSim systems analysis software and represents an enhancement to previous versions. A description of the probabilistic model and the enhancements provided for this SA is presented in Section 4.4.2. The probabilistic model uses an abstraction of the SDF PORFLOW Model to perform radionuclide transport simulations. Dose calculations are performed using the same dose calculations that were used to determine the PORFLOW dose results.

Use of the abstraction model reduces the analysis time needed for multi-realization processes, such as Monte Carlo sampling or Latin Hypercube Sampling (LHS). In order for the probabilistic model abstraction to be used in lieu of the SDF PORFLOW Model, its validity must be tested by comparing the abstraction model results with SDF PORFLOW Model results for the Evaluation Case. A reasonable degree of agreement between the two models is necessary to give confidence that the trends produced in the probabilistic analysis reflect the trends that would occur if the SDF PORFLOW Model is run repeatedly in a probabilistic mode.

Because of the simplifications associated with the abstraction presented in Section 4.4.2 (i.e., reduction in dimensionality, coarser spatial and temporal discretization, etc.), a perfect match between GoldSim and PORFLOW results is not expected, but basic features of breakthrough curves reflecting processes such as material degradation and changes in chemical environments should be similar.

The following sections describe the approach used to benchmark the SDF GoldSim Model to the SDF PORFLOW Model and the results of that benchmarking.

5.6.2.2 Saltstone Disposal Facility SA Benchmarking Activities

The benchmarking analysis was comprised of four phases. The first phase focused on how well the abstraction model (i.e., the SDF GoldSim Model) can approximate the PORFLOW-generated radionuclide releases from the SDUs and FDCs. Radionuclide releases to the saturated zone from the two models were compared. The second phase focused on how well the abstraction model approximates the radionuclide transport behavior in the saturated zone. PORFLOW-to-GoldSim model comparisons of radionuclide concentrations within specified sectors along the 100-meter boundary (Figure 5.2-1) form the basis of how well the abstraction model approximates in the dilution/attenuation processes in the saturated zone. Breakthrough curves representing the radionuclide concentrations over time for each of the several sectors form the basis of this comparison.

5.6.2.3 Benchmarking Results

The SA Evaluation Case, which is used in the benchmarking process, represents an alternate scenario for the time-based degradation of the SDU and FDC components, including the grout, wall, floor and mud mats (for the FDCs only), simulated to help answer specific questions asked by the NRC.

The species evaluated during the benchmarking represent the most important dose contributors noted in the PORFLOW simulations: I-129, Cs-135, Tc-99, and Ra-226. An additional species of less importance to dose results, Np-237, is also included to evaluate the ability of the model to handle extremely sorbent species. Because the "shrinking core" release model for Tc-99 (as utilized in PORFLOW and described in SDF PA Section 4.2.3.2.4) is not part of the abstraction model, the SDF GoldSim Model samples Tc-99 mass fluxes from a set of breakthrough curves from PORFLOW and applies the mass fluxes as a boundary condition to the saturated zone as modeled in GoldSim (Section 4.4.2.3).

5.6.2.3.1 Mass Releases to the Saturated Zone

For all SDU and FDC types, I-129, Ra-226, and Np-237 mass flux breakthrough curves at the water table from the GoldSim and PORFLOW models are compared during the benchmarking process. Cs-135 results are not presented for SDU 1 because the inventory of Cs-135 in SDU 1 is considered to be negligible. Also, note that Tc-99 comparisons are not presented in this section because the releases are directly sampled from PORFLOW model outputs. Tc-99 concentration and dose level time-history comparisons are presented in later sections as indicators of how well the GoldSim saturated zone transport and dose models represent the PORFLOW saturated zone transport and dose models. The breakthrough curves presented here represent the total mass fluxes released at the bottom of the unsaturated zone.

SDU 1

A comparison of the SDF PORFLOW Model and SDF GoldSim Model mass releases of I-129 presented in Figure 5.6-1 indicate that the GoldSim model can produce a good approximation of the spike-type releases of I-129 from SDU 1 generated by the PORFLOW model. The GoldSim model produces a peak release that is slightly (3.7 %) higher than the PORFLOW results (see Table 5.6-1). The GoldSim model Ra-226 release, presented in Figure 5.6-2, also closely resembles the PORFLOW model releases when breakthrough starts to occur at 20,000 years. The GoldSim Model peak at 20,000 years is 4.0 % higher than the PORFLOW model peak. A comparison of Np-237 releases at the water table from the two models presented in Figure 5.6-3 shows a similar release pattern. Relative to results for the other two species, a greater difference in the breakthrough curves is seen with the peaks differing by 40 % and the PORFLOW generated breakthrough curve lower than the GoldSim curve. The difference between the curves is reflective of the differences in the dimensionality of the flow field conceptualizations (vertically downward in the GoldSim model and fully 2-D in the PORFLOW model as described in Section 4.4.2). The models also differ in the degree of refinement (the PORFLOW model is more finely discretized), the GoldSim model uses zone-averaged flow rates based on the PORFLOW results, and floor joints are modeled as a single series of mixing cells in the GoldSim model. These differences are accentuated by radionuclide retardation associated with the extremely high K_ds of neptunium (5,000 mL/g to 10,000 mL/g) in cementitious materials. Figure 5.6-4 depicts the two breakthrough curves in semi-log form showing that the general trends of the two models are similar with the PORFLOW release breakthrough curve showing a more dispersed form.

Table 5.6-1: SDF GoldSim and PORFLOW Model Peak Unsaturated Zone Release Comparisons for SDU 1

Radionuclide	PORFLOW Peak Release (g/yr)	PORFLOW Time of Peak Release (yr)	GoldSim Peak Release (g/yr)	GoldSim Time of Peak Release (yr)	Percent Difference
I-129	4.54E-04	5,580	4.71E-04	5,580	4 %
Cs-135	N/A	N/A	N/A	N/A	N/A
Ra-226	4.20E-06	20,000	4.37E-06	20,000	4 %
Np-237	2.36E-06	20,000	3.21E-06	20,000	40 %

Figure 5.6-1: SDU 1 I-129 Release to the Saturated Zone

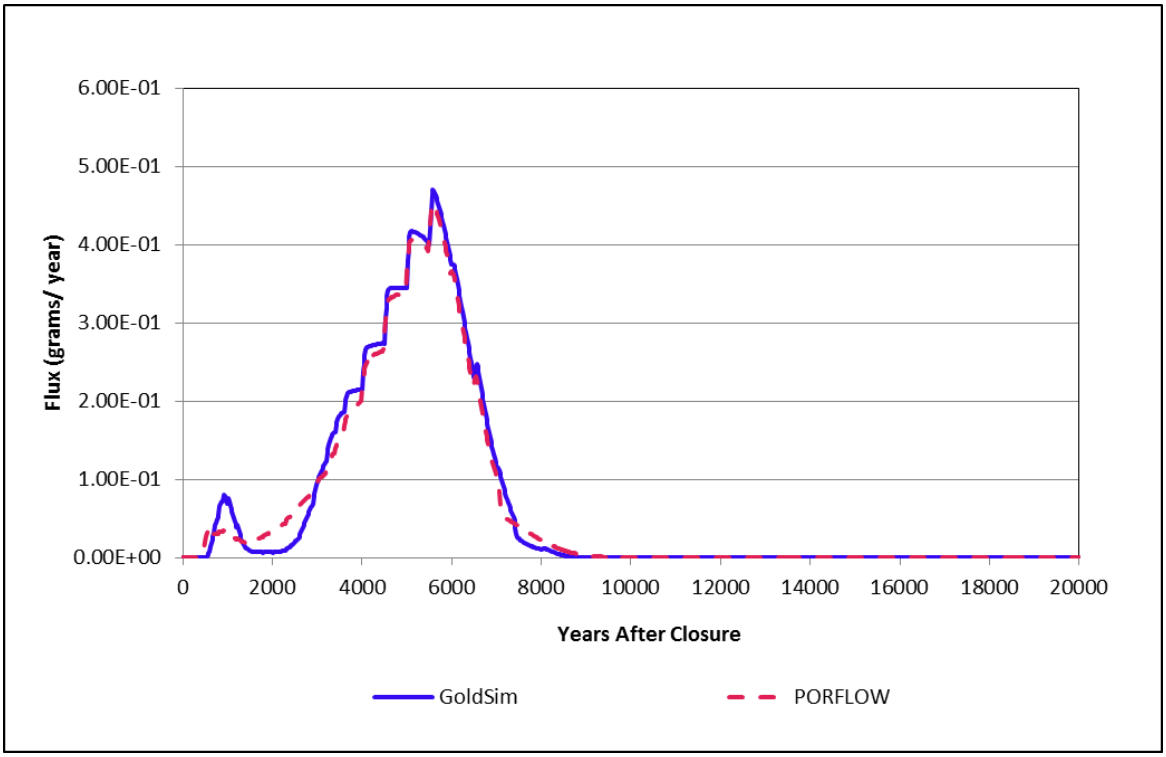

Figure 5.6-2: SDU 1 Ra-226 Release to the Saturated Zone

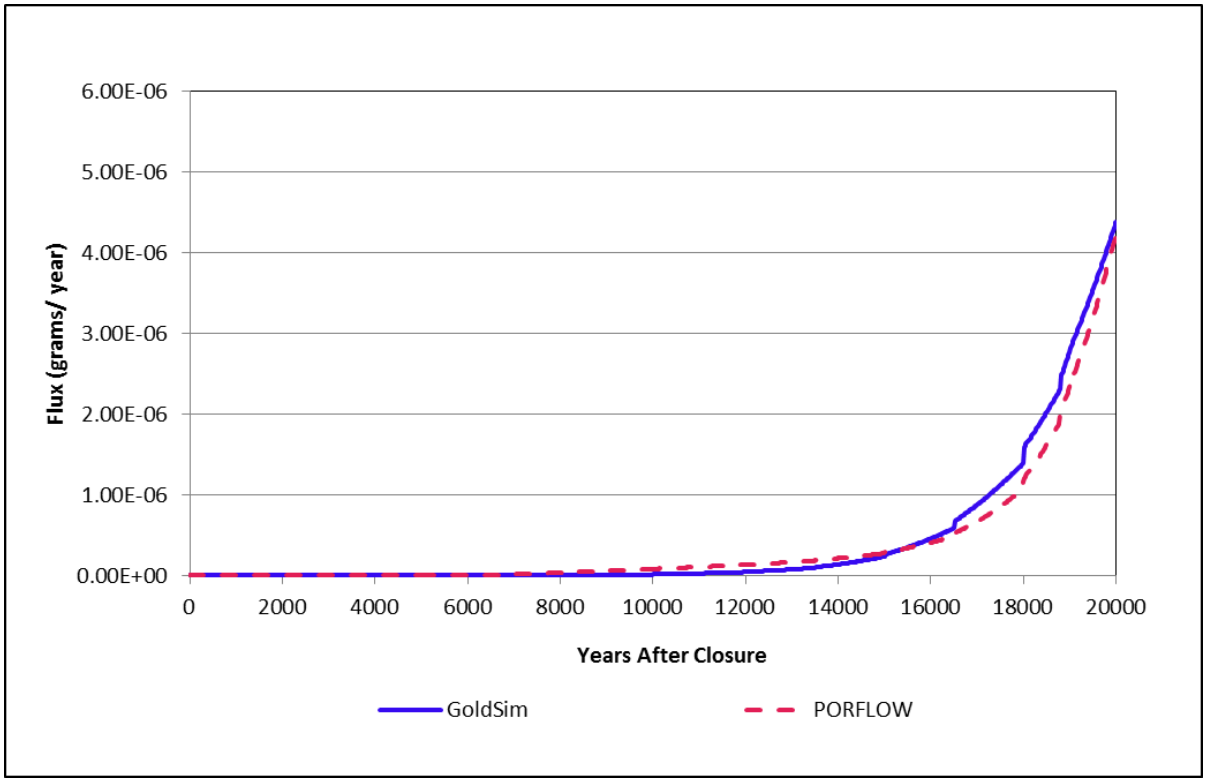

Figure 5.6-3: SDU 1 Np-237 Release to the Saturated Zone

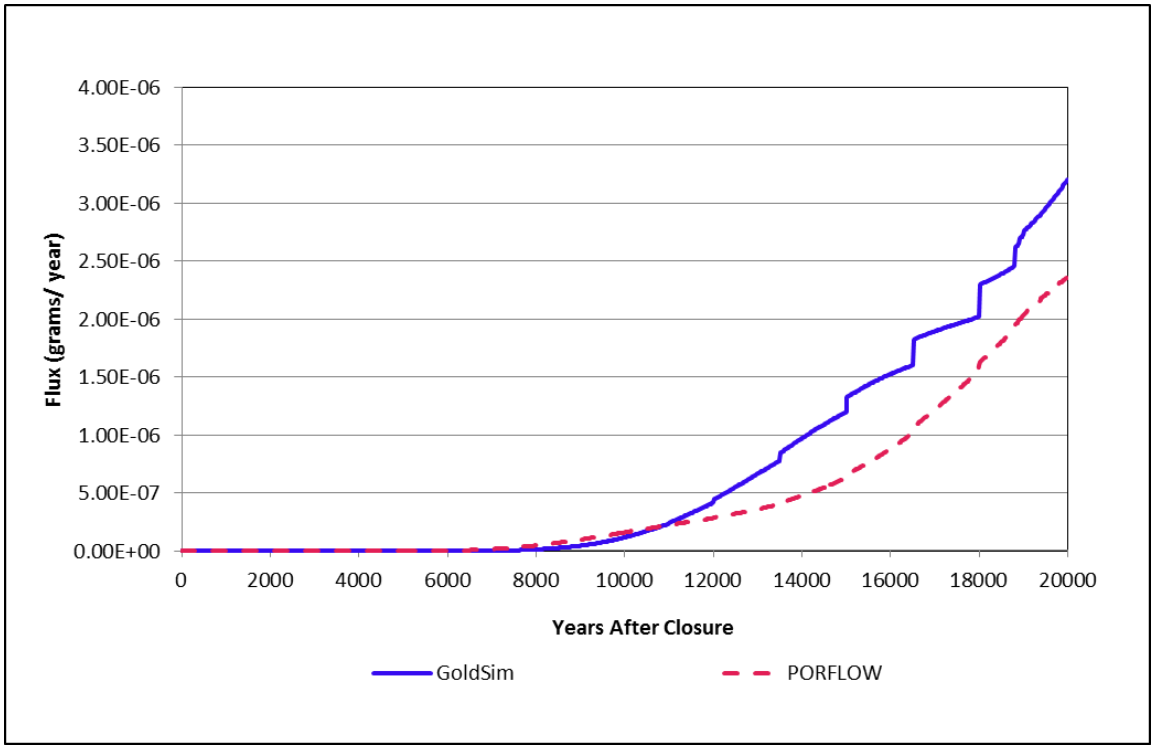

Figure 5.6-4: Semi-Log Plot of SDU 1 Np-237 Release to the Saturated Zone

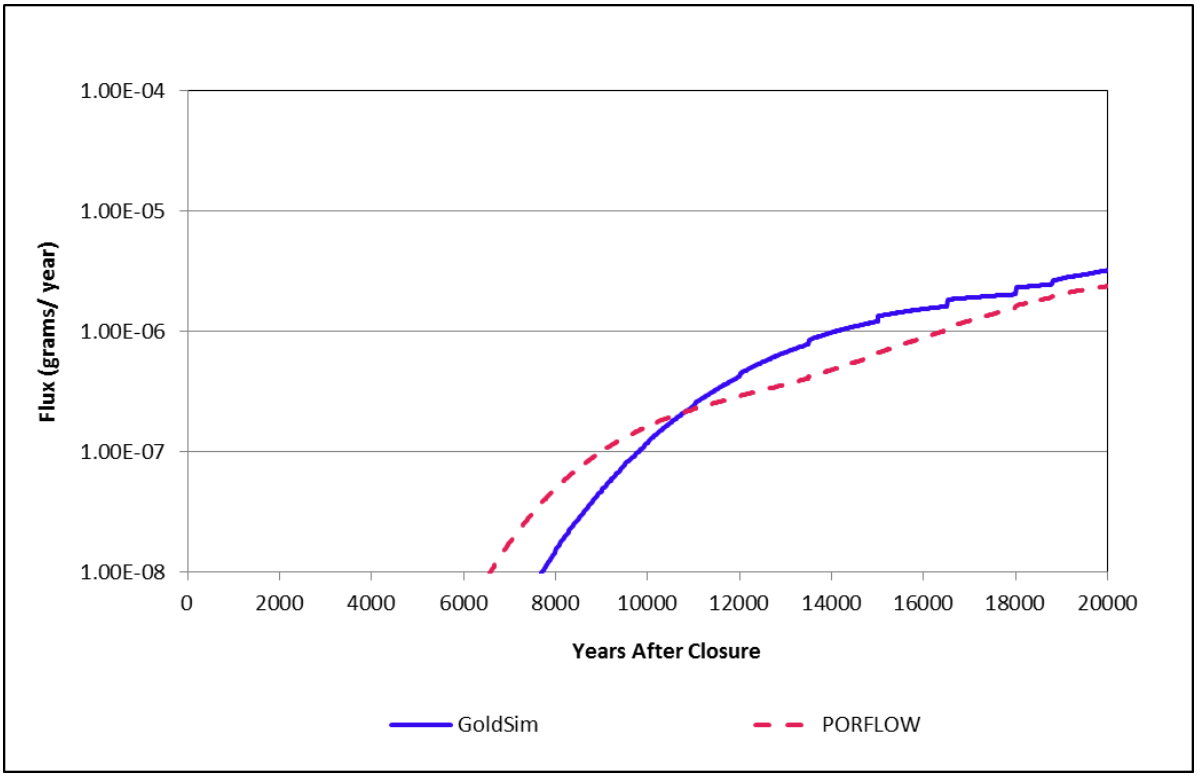

SDU 4

Similar to results for SDU 1, the SDU 4 SDF PORFLOW Model and SDF GoldSim Model I-129 mass releases presented in Figure 5.6-5 indicate that the GoldSim model can produce a good approximation of the I-129 releases from SDU 4 generated by the PORFLOW model. The GoldSim model produces a peak release that is approximately 10 % lower than the PORFLOW results (see Table 5.6-2).

Table 5.6-2: SDF GoldSim and PORFLOW Model Peak Unsaturated Zone Release Comparisons for SDU 4

Radionuclide	PORFLOW Peak Release (g/yr)	PORFLOW Time of Peak Release (yr)	GoldSim Peak Release (g/yr)	GoldSim Time of Peak Release (yr)	Percent Difference
I-129	1.67E+00	3,480	1.51E+00	3,620	-10 %
Cs-135	3.72E+00	5,120	3.95E+00	5,120	6 %
Ra-226	3.80E-05	20,000	3.11E-05	20,000	-18 %
Np-237	3.62E-04	20,000	3.32E-04	12,200	-8 %

Figure 5.6-5: SDU 4 I-129 Release to the Saturated Zone

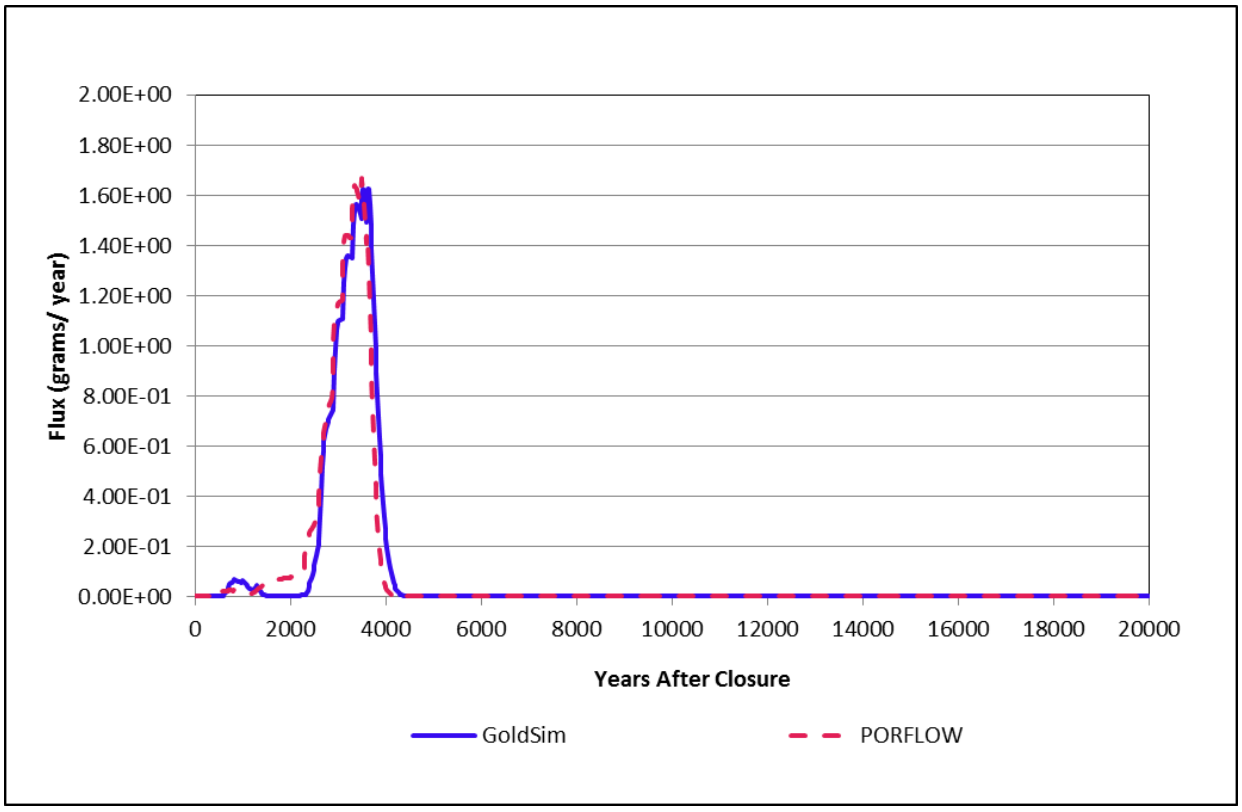

The GoldSim model Cs-135 release presented in Figure 5.6-6, also closely resembles the PORFLOW model releases with peak releases occurring at 5,120 years. The GoldSim Model peak, also at 5,120 years, is 6.2 % higher than the PORFLOW model peak.

Figure 5.6-6: SDU 4 Cs-135 Release to the Saturated Zone

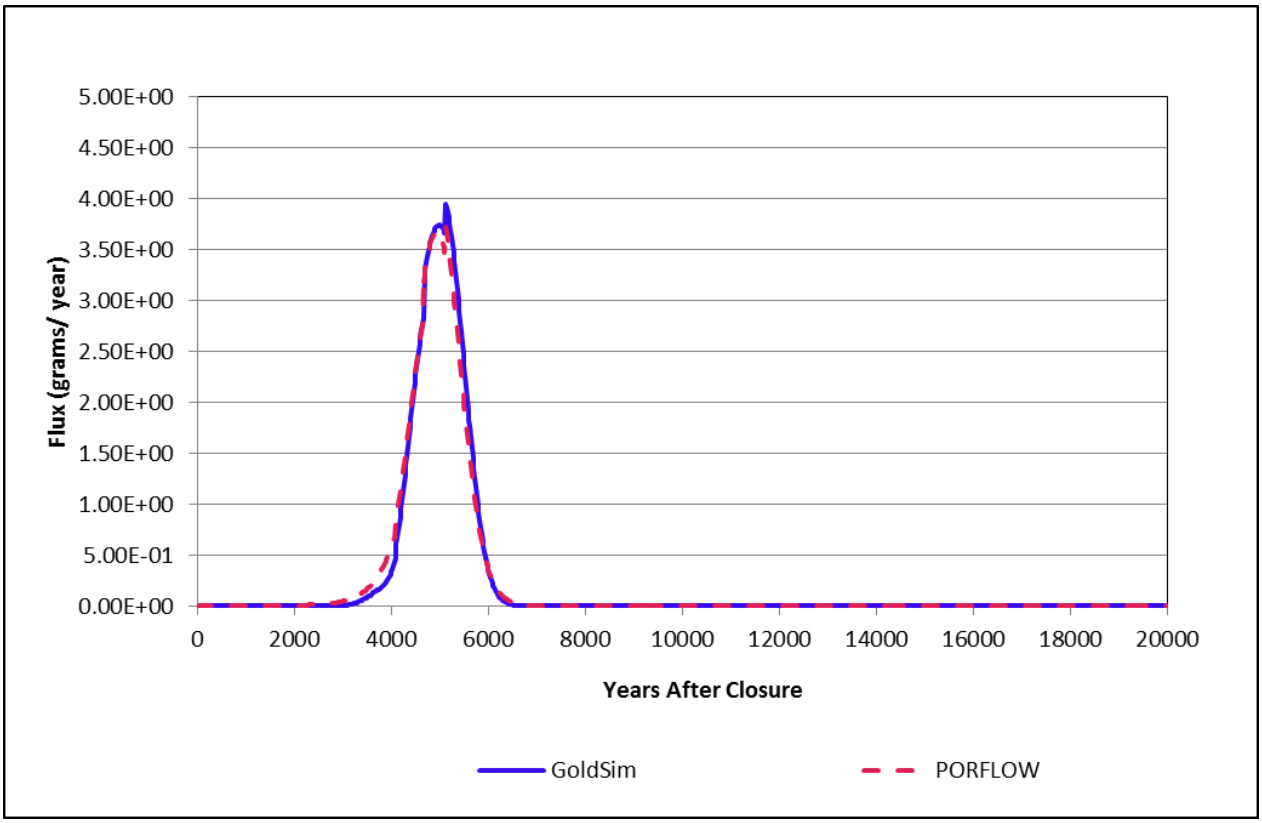

The GoldSim model Ra-226 release presented in Figure 5.6-7 also resembles the PORFLOW model releases with the GoldSim Model peak at 20,000 years being 18.2 % lower than the PORFLOW model peak at the same time. The Ra-226 curves do not match quite as well as in the SDU 1 comparison, but when viewed in a semi-log plot the similarity of the trends of the curves is readily seen (Figure 5.6-8).

Figure 5.6-7: SDU 4 Ra-226 Release to the Saturated Zone

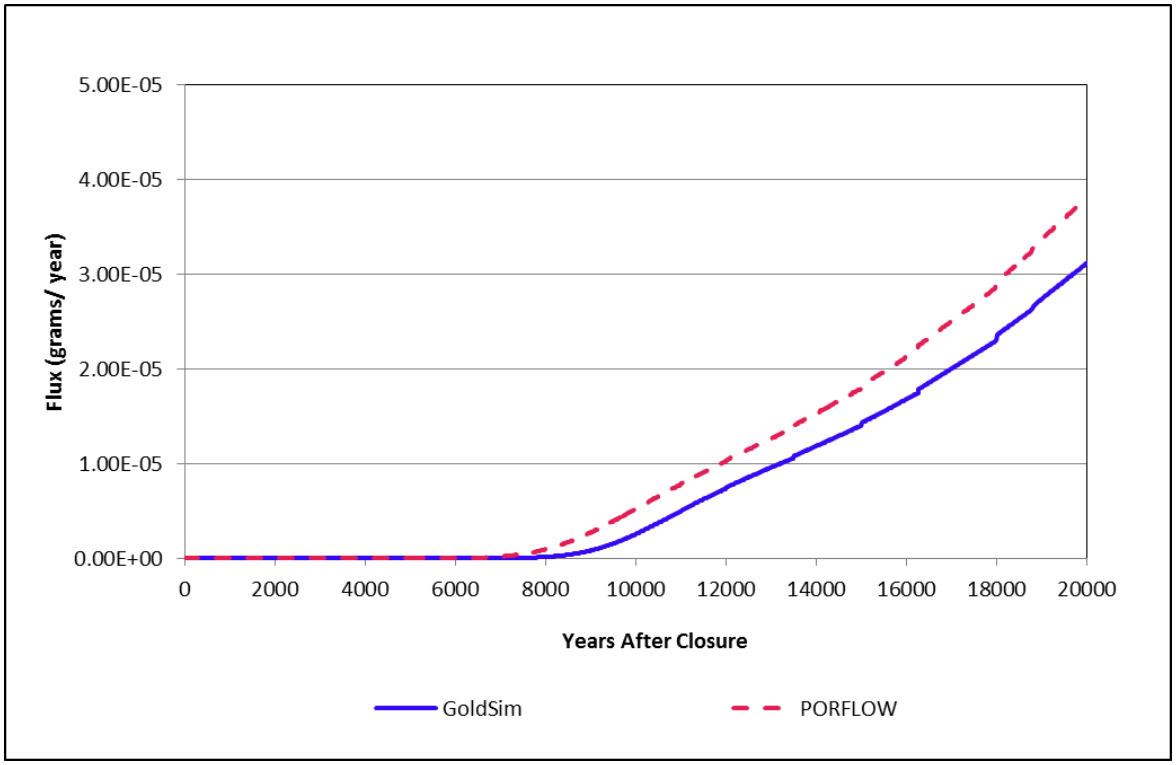

Figure 5.6-8: Semi-Log Plot of SDU 4 Ra-226 Release to the Saturated Zone

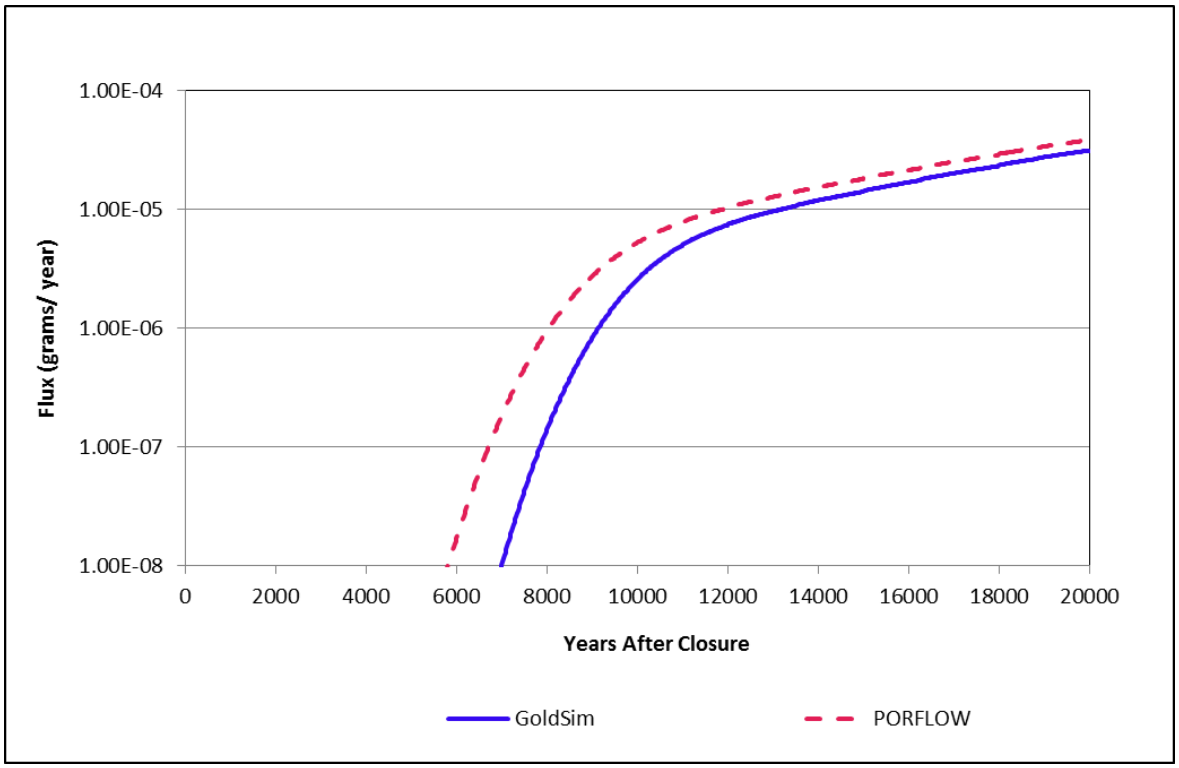

A comparison of Np-237 releases at the water table from the two models presented in Figure 5.6-9 differ, but when looked at on a semi-log scale (Figure 5.6-10) the breakthrough curves have the same basic trend, with the PORFLOW curve being more dispersed. The difference in Np-237 peaks for the two models is only 8 % (Table 5.6-2), but the time of the peak values differs by 7,800 years. The difference between the curves can be partially attributed to differences in the dimensionality of the flow-field conceptualizations (vertically downward in the GoldSim model and fully 2-D in the PORFLOW model as described in Section 4.4.2).

Figure 5.6-9: SDU 4 Np-237 Release to the Saturated Zone

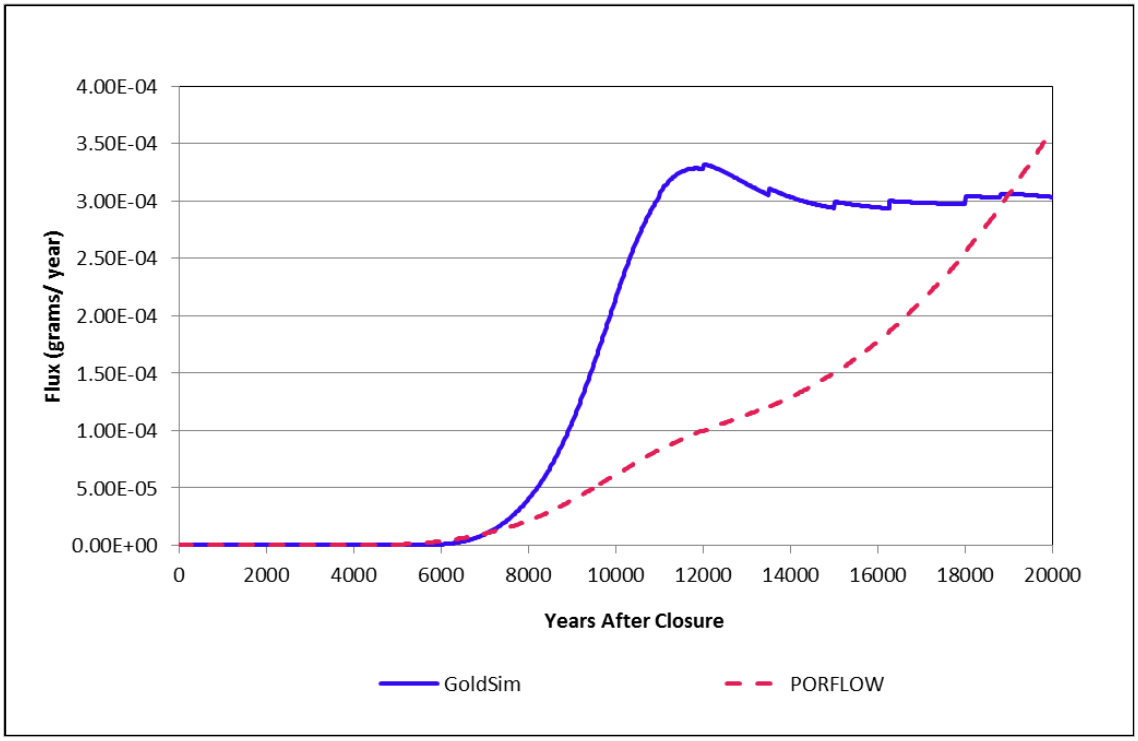

Figure 5.6-10: Semi-Log Plot of SDU 4 Np-237 Release to the Saturated Zone

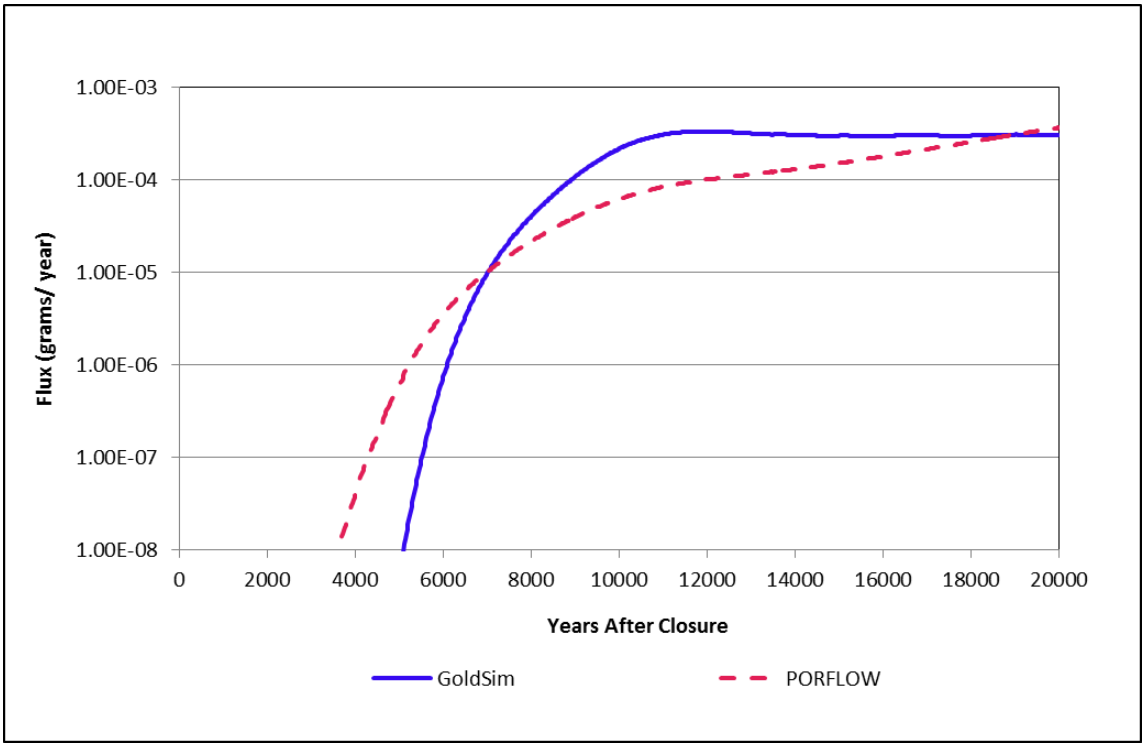

These differences are accentuated by radionuclide retardation associated with the extremely high K_ds of neptunium (5,000 mL/g to 10,000 mL/g) in cementitious materials. In addition to controlling the main release of Np-237, the high cementitious K_ds of neptunium play an important role on the localized effects in the model, accentuating the differences between the two models. Because of the high K_ds, the dominant source of release for the first 20,000 years in SDU 4 is in the area of thee walls. In the wall area, horizontal flow from the backfill into the wall and floor occurs, a process not considered in the abstraction model. The limitation in the model is not considered important because it only influences a small percentage of the Np-237 in SDU 4. Figure 5.6-10 depicts the two breakthrough curves in semi-log form showing that the general trends of the two models are similar with the PORFLOW release exhibiting a greater degree of dispersion.

FDCs

In the FDCs, SDF PORFLOW Model and SDF GoldSim Model I-129 mass releases presented in Figure 5.6-11 indicate that the GoldSim model can produce a good approximation of the I-129 releases and trends generated by the PORFLOW model. The GoldSim model produces a peak release that is (13 %) higher than the PORFLOW results (see Table 5.6-3).

Table 5.6-3: SDF GoldSim and PORFLOW Model Peak Unsaturated Zone Release Comparisons for FDCs

Radionuclide	PORFLOW Peak Release (g/yr)	PORFLOW Time of Peak Release (yr)	GoldSim Peak Release (g/yr)	GoldSim Time of Peak Release (yr)	Percent Difference
I-129	1.11E+00	7,660	1.25E+00	7,580	13 %
Cs-135	2.57E-05	13,520	2.10E+00	12,020	-18 %
Ra-226	5.44E-08	20,000	7.47E-08	20,000	18 %
Np-237	2.91E-09	20,000	3.03E-09	20,000	4 %

Figure 5.6-11: FDC I-129 Release to the Saturated Zone

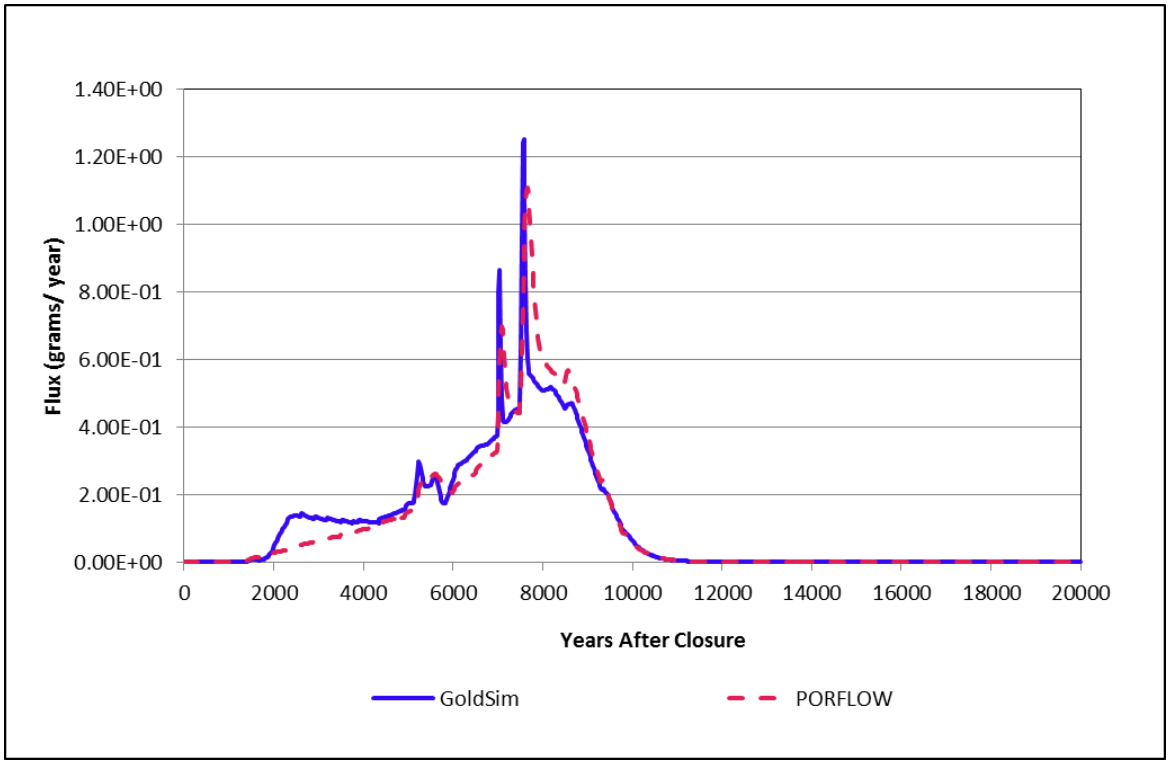

The GoldSim model Cs-135 release presented in Figure 5.6-12, closely replicates the PORFLOW model release in shape but the GoldSim breakthrough curve does arrive sooner (the peak is at 12,020 years as opposed to 13,520 years) and is slightly more dispersed with a peak value that is 18 % lower than the PORFLOW peak. The difference in peak arrival time between the two models can be attributed to the dimensional aspects of the two models. The vertical flow rate in the UTRA-UZ below the outer area of the SDU is much greater (approximately 5 to 10 times) than under the center of the SDU. This, combined with the flow towards the center of the model, creates a situation where the mass in the outer portions of the saltstone reaches the saturated zone sooner in the GoldSim model, where only vertical flow is imposed. I-129 has the same tendency for early arrival in the GoldSim model (Table 5.6-3), but the trend is more obvious for Cs-135 than I-129 because of the higher K_d of cesium (10 cc/g versus 0.3 cc/g). The

release in the GoldSim model would also spread the release of the mass over time leading to a more dispersed (over time) nature to the breakthrough curve. Note that the spatial differentiation in the flow fields dissipates at later times. Also, note that this difference in breakthrough timing does not occur in the SDU 4 results (see Figure 5.6-6) where the unsaturated zone flow is more dominantly vertical and the vertical component of flow does not vary as much from the SDU centerline outward. The trends in the release curves are still adequately similar.

Figure 5.6-12: FDC Cs-135 Release to the Saturated Zone

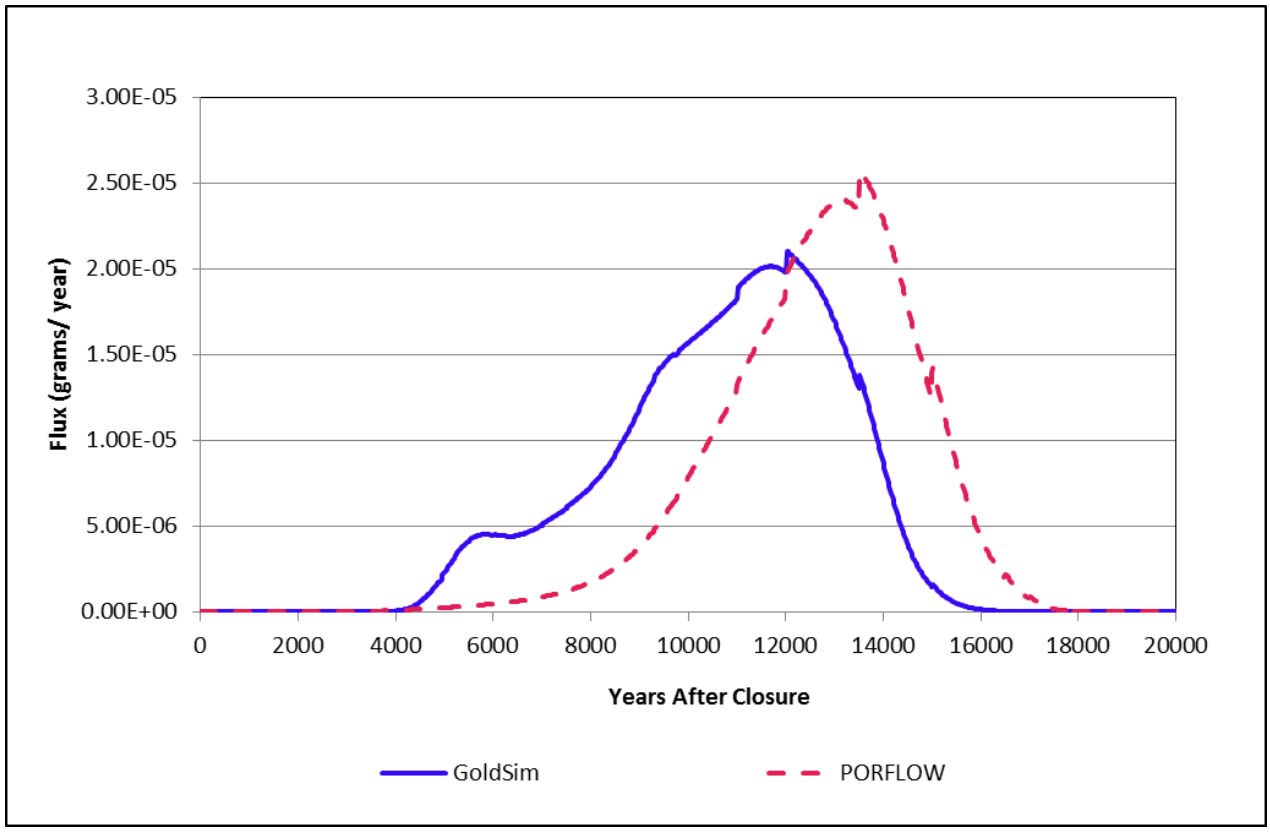

The GoldSim model Ra-226 release presented in Figure 5.6-13 also resembles the PORFLOW model releases with the GoldSim Model peak at 20,000 years being 18 % higher than the PORFLOW model peak at the same time. A comparison of Np-237 releases at the water table, generated by the two models presented in Figure 5.6-14 shows quite similar releases with the difference in peak values being only 4 % (Table 5.6-3).

Figure 5.6-13: FDC Ra-226 Release to the Saturated Zone

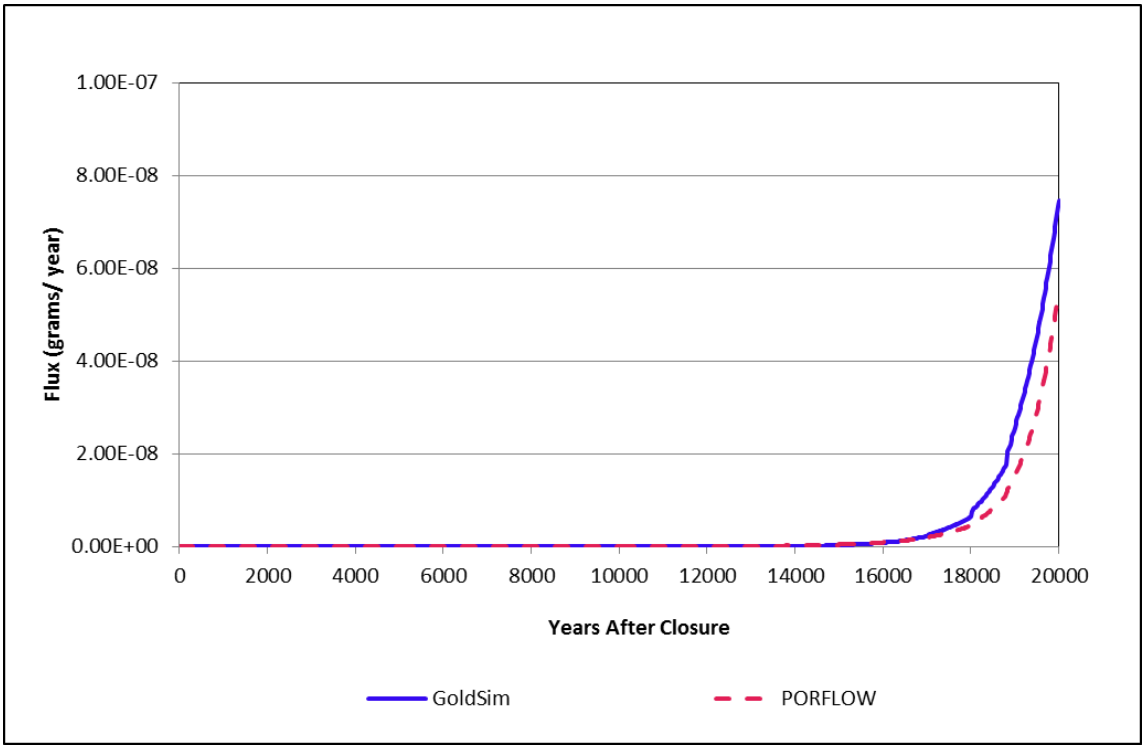

Figure 5.6-14: FDC Np-237 Release to the Saturated Zone

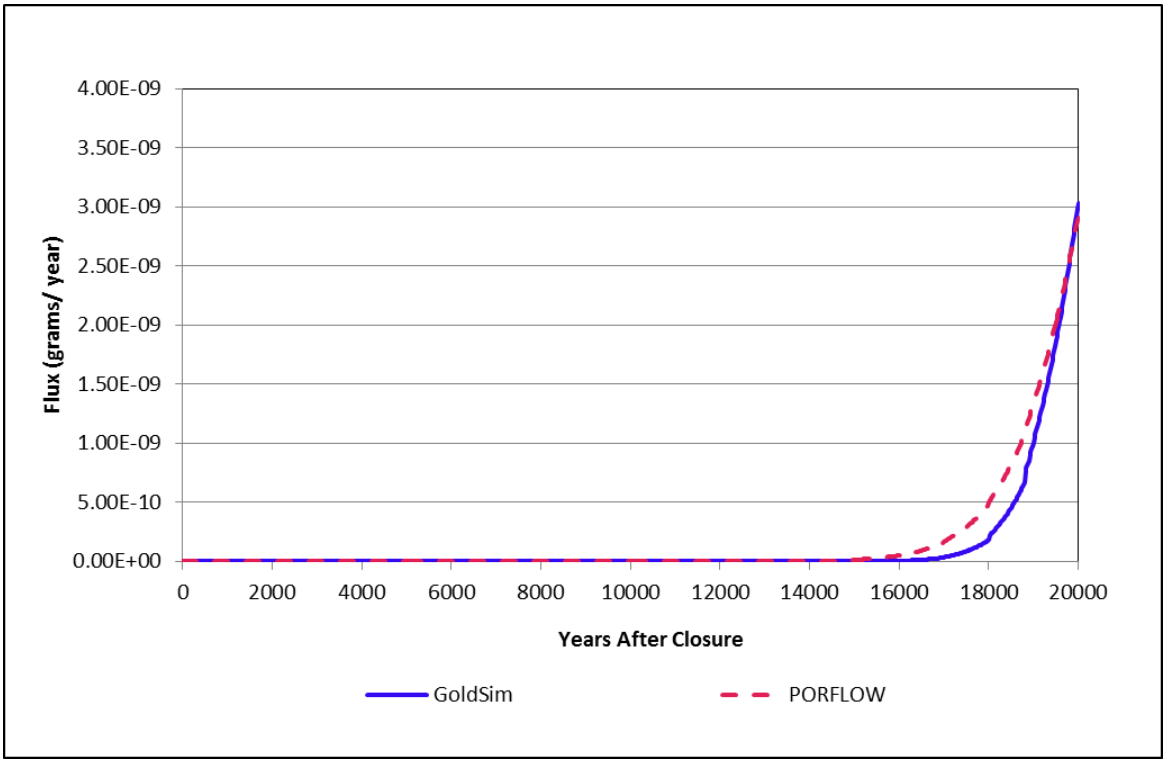

5.6.2.4 Radionuclide Concentrations at the 100-Meter Boundary

The second phase of the benchmarking process focuses on examining how well the abstracted model approximates the radionuclide transport behavior in the saturated zone. Radionuclide concentrations (in picocuries per liter) in four sectors (B, G, H, and I) were examined for this task (See Figure 5.2-1). Sector B was selected for this analysis because it contains the highest PORFLOW and GoldSim model concentrations of the southern sectors. Sector G was chosen because it contains the peak GoldSim model concentration for the northern locations and Sector I was chosen because it contains the peak PORFLOW model concentration for the northern locations. Sector H was in turn selected due to its proximity to Sector I, and the similarity between PORFLOW Sector H and I results. Concentration comparisons between PORFLOW and GoldSim model results showed less consistency in Sector I, which is located above a groundwater divide, than for Sector H. For this exercise, breakthrough curves of PORFLOW and GoldSim model results for the five species (I-129, Cs-135, Ra-226, Tc-99, and Np-237) were examined.

5.6.2.4.1 Sector B

An examination of PORFLOW and GoldSim-generated radionuclide concentrations presented in Figure 5.6-15 indicates that the SDF GoldSim Model can provide a computationally efficient approximation of 100-meter boundary radionuclide concentrations in Sector B. There is a good consistency in the trends observed in the two sets of model results throughout the 20,000-year simulation. The basic dilution/attenuation processes in the saturated zone are captured by the abstraction. Note that there are also differences but they will have little impact on the utility of the abstraction model to evaluate peak doses.

Figure 5.6-15: Maximum Radionuclide Concentrations at 100-Meter Boundary for Sector B

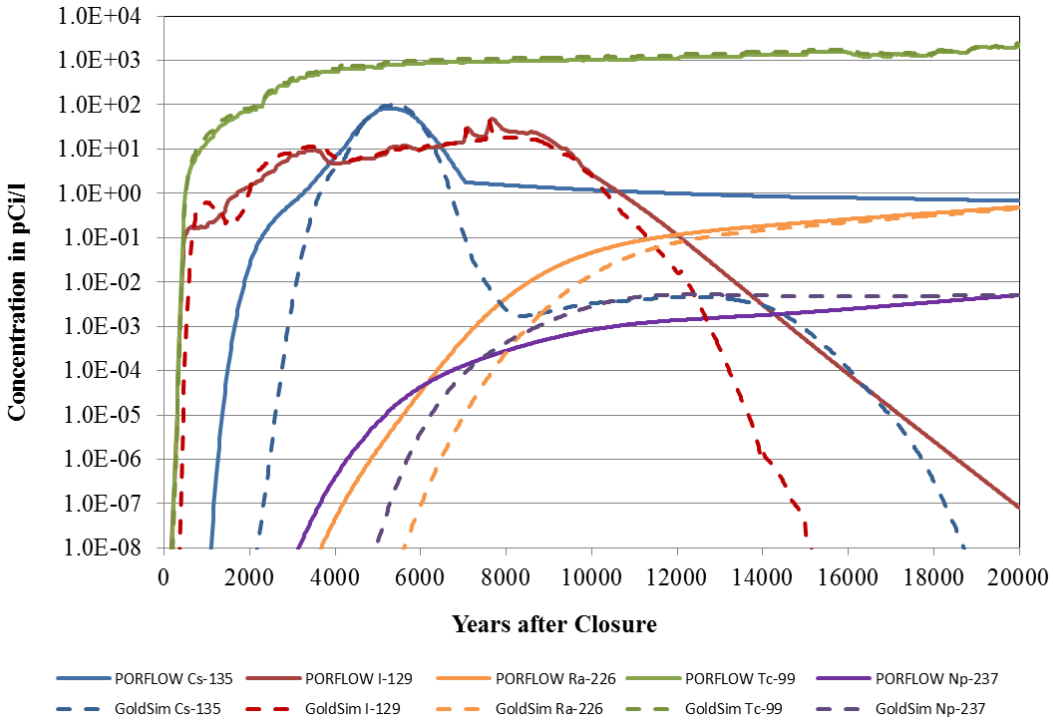

As noted above, Tc-99 in the saturated zone, as modeled in GoldSim, uses sampled mass-release time histories from a set of PORFLOW simulations as a boundary condition. Comparing the PORFLOW-generated and GoldSim-generated Tc-99 concentration breakthrough curves for Sector B it can be seen that the saturated zone as modeled in GoldSim closely approximates the saturated zone as modeled in PORFLOW.

A comparison of the Cs-135 breakthrough curves in Figure 5.6-15 shows that the peak of the PORFLOW concentration breakthrough curve is accurately reproduced, but at lower concentrations the breakthrough curve appears to be broader. This difference in breakthrough curves is consistent with the SDU 4 mass flux release curve when shown in semi-log presented in Figure 5.6-16. Therefore, the modeled results from the saturated zone abstraction are consistent with the PORFLOW model results. It should be noted that after 6,500 years, the GoldSim concentrations decrease at a faster rate than the PORFLOW concentrations. This difference in the curves is associated with the occurrence of the "green clay" layer (i.e., the Gordon confining unit), which is modeled explicitly in the PORFLOW model, but not in the GoldSim model. The "green clay" layer provides a storage zone for more sorptive elements such as cesium, from which the radionuclides, like Cs-135, are more slowly released. Since the breakthrough curves differ at well below peak levels, the simplification in the GoldSim model is not important in dose calculations.

Figure 5.6-16: Semi-Log Plot of the SDU 4 Cs-135 Release to the Saturated Zone

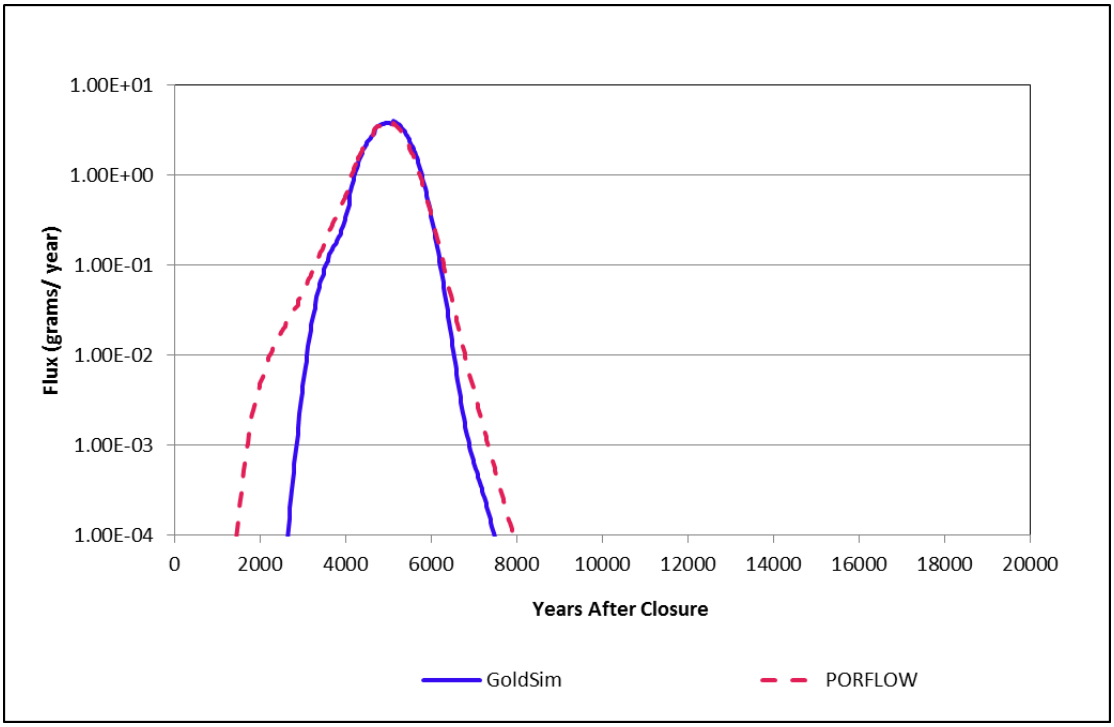

A comparison of the I-129 breakthrough curves in Figure 5.6-15 also shows that the PORFLOW concentration breakthrough curve is accurately represented. As with Cs-135, the influence of the "green clay" layer at lower concentrations can be seen. Note that the difference, between the I-129 and Cs-135 PORFLOW model breakthrough curve slopes (at low concentrations) is reflective of the lower I-129 K_d value. Comparing the PORFLOW- and GoldSim-generated Ra-226 and Np-237 breakthrough curves presented Figure 5.6-15 with the mass flux release curves presented in Figures 5.6-8 and 5.6-10, respectively, it can also be seen that the saturated zone as modeled in GoldSim performs well (i.e., consistent with the PORFLOW representation).

5.6.2.4.2 Sector G

An examination of PORFLOW and GoldSim-generated radionuclide concentrations presented in Figure 5.6-17 indicates that the SDF GoldSim Model can also provide a computationally efficient approximation of 100-meter boundary radionuclide concentrations in northern sectors such as Sector G. There is a consistency in the trends observed in the two sets of model results throughout the 20,000-year simulation. The basic dilution/attenuation processes in the saturated zone are captured by the abstraction, but again there are also differences that will have little impact on the utility of the abstraction model to evaluate peak doses.

Figure 5.6-17: Maximum Radionuclide Concentrations at 100-Meter Boundary for Sector G

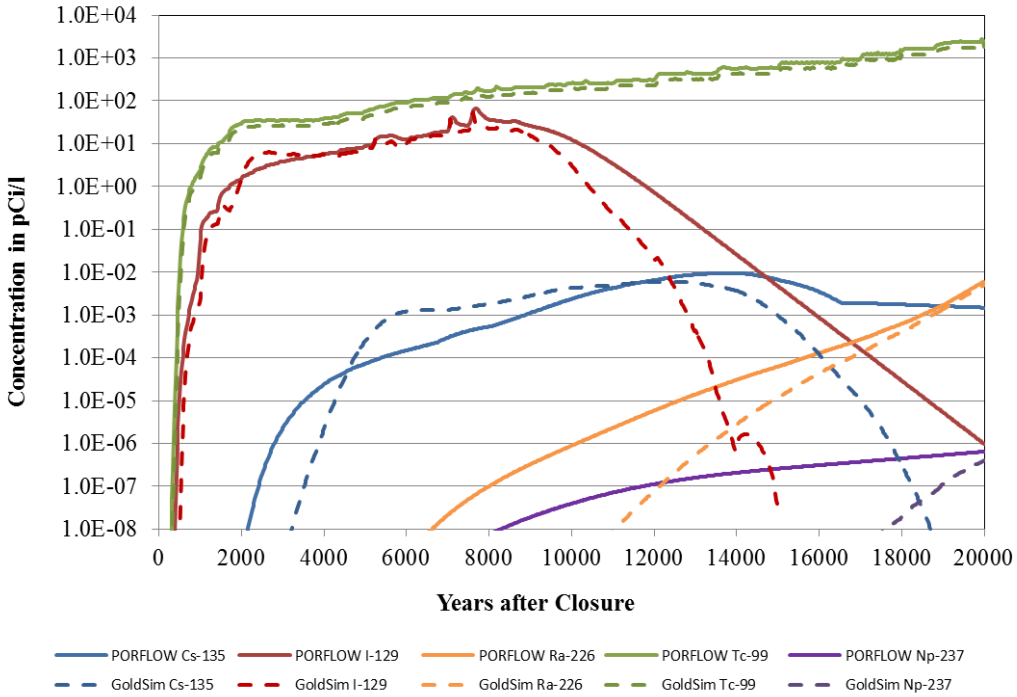

As discussed in more detail in Section 5.6.2.4.1, comparing the PORFLOW-generated and GoldSim-generated Tc-99 concentration breakthrough curves for Sector G, shows that the saturated zone as modeled in GoldSim closely approximates the results of the more rigorous PORFLOW saturated zone transport simulations. A comparison of the Cs-135 breakthrough curves in Figure 5.6.2-17 shows differences that reflect the temporal differences in the peaks of the PORFLOW and GoldSim model mass flux release curves discussed in in Section 5.6.2.3. Again, the tail of the PORFLOW Cs-135 breakthrough curve shows the influence of the "green clay" layer at lower concentrations.

A comparison of the I-129 breakthrough curves presented in Figure 5.6-17 also shows that the PORFLOW concentration breakthrough curve is accurately represented by the GoldSim model results. As with the Cs-135 breakthrough curve, the influence of the "green clay" layer at lower concentrations can be seen. Note that at very low concentrations the GoldSim-generated I-129 breakthrough curve behaves strangely. This seems to reflect a breakdown of the analytic solution used in the GoldSim pipe model, which may be associated with the numerical inversion of the LaPlace domain solution in the model. This is only occurs at very low concentrations and does not affect the results.

When comparing the PORFLOW-generated and GoldSim-generated Ra-226 breakthrough curves presented Figure 5.6-17 with Figure 5.6-18 below which is a semi-log plot of the FDC Ra-226 release curve, it can be seen that the saturated zone as modeled in GoldSim closely approximates the results generated by the saturated zone as modeled in PORFLOW. Note that the mass-flux release curves differ mainly at very low concentrations.

Figure 5.6-18: Semi-Log Plot of an FDC Ra-226 Release to the Saturated Zone

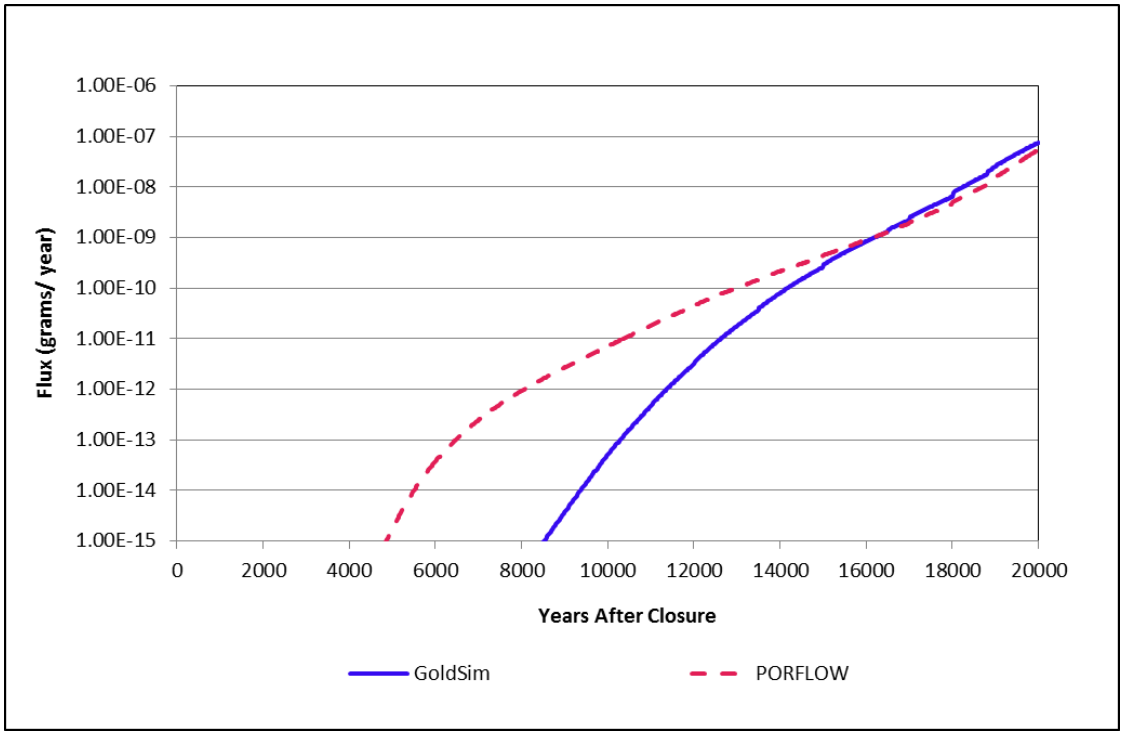

Comparing the PORFLOW- and GoldSim-generated Np-237 breakthrough curves presented Figure 5.6-17 a major difference is seen between the two models. The PORFLOW-generated Np-237 breakthrough occurs well before the GoldSim model breakthrough. This difference is associated with another simplification used in the GoldSim abstraction. The GoldSim abstraction does not explicitly model the Gordon Aquifer in the radionuclide transport analysis. The early-time segment of the Np-237 breakthrough curve seen in the PORFLOW results presented in Figure 5.6-17 reflects transport through the Gordon Aquifer of a portion of the SDU 4 Np-237 mass release presented in Figure 5.6-10. The omission is acceptable because PORFLOW simulations indicate that the concentrations in the Gordon Aquifer tend to be much lower than in the UTRA-UZ and UTRA-LZ and would therefore not be important in peak dose analyses.

5.6.2.4.3 Sector H

Radionuclide concentrations at the 100-meter boundary are presented here for Sector H because the concentrations in Sectors H and I are very similar in the PORFLOW runs. This is not true for the GoldSim runs because the simpler analytical solutions used in the GoldSim model do not fully capture the influence of the groundwater divide on the 100-meter boundary concentrations in Sector I.

An examination of PORFLOW and GoldSim-generated radionuclide concentrations presented in Figure 5.6-19 indicates that the SDF GoldSim Model can also provide a computationally efficient approximation of 100-meter boundary radionuclide concentrations in northern sectors such as Sector H. This is important because of the model differences for Sector I. Similar to the Sector G comparison, there is a good

consistency in the trends observed in the two sets of model results throughout the 20,000-year simulation. The basic dilution/attenuation processes in the saturated zone are similarly captured by the abstraction, but again there are also differences that have little impact on the utility of the abstraction model to evaluate peak doses.

Figure 5.6-19: Maximum Radionuclide Concentrations for at 100-Meter Boundary for Sector H

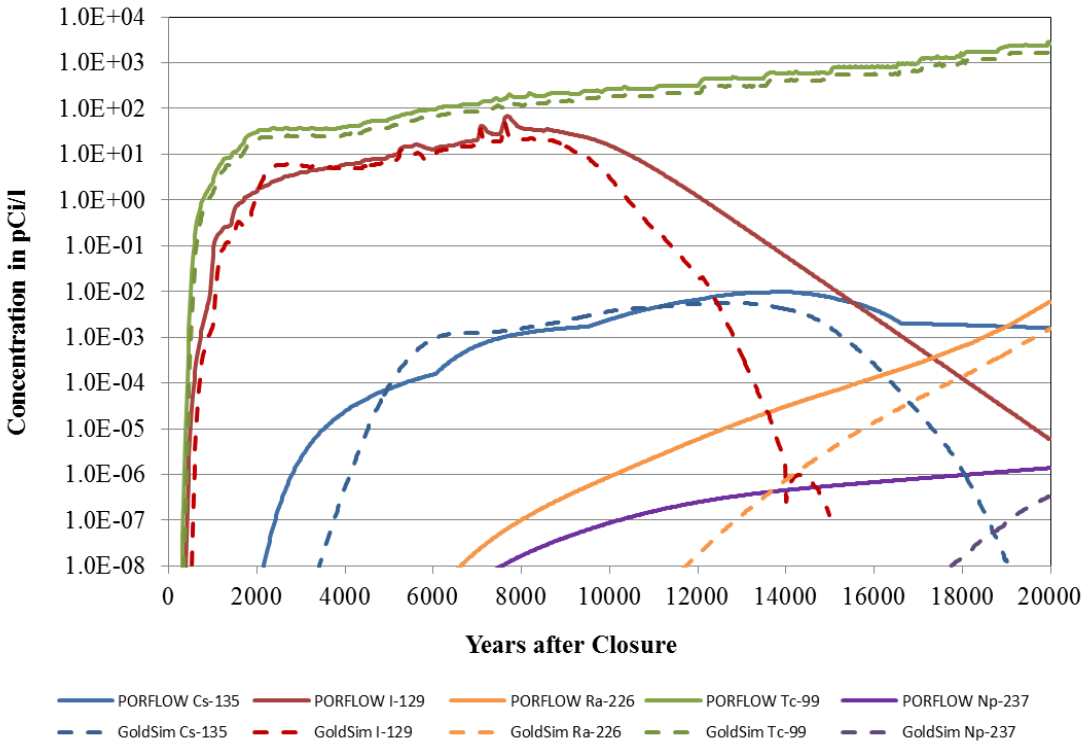

For Tc-99, I-129, Cs-135, and Np-237, a comparison between the PORFLOW-generated and GoldSim-generated concentration breakthrough curves for Sector H is consistent with the comparison for Sector G such that the similar aspects will not be discussed here. The major difference between the Sector G and Sector H results can be seen by comparing Ra-226 curves. As can be seen in the Sector G plot (Figure 5.6-17) the GoldSim model concentrations approach the PORFLOW model concentrations at later times (higher concentrations). This is not true for Sector H where the influence of the ground water divide increases the Ra-226 concentrations enough that the differences are perceptible and the PORFLOW breakthrough curve is seen to be higher.

5.6.2.4.4 Sector I

Radionuclide concentrations at the 100-meter boundary are presented here for Sector I because the concentrations in Sector I are generally the highest in the PORFLOW runs. This is not true for the GoldSim runs because the simpler analytical solutions used in the GoldSim model do not fully capture the influence of the groundwater divide (as reflected in the streamlines presented in Figure 5.2-1) on the 100-meter boundary concentrations in

Sector I. Figure 5.6-20 presents the concentrations from the SDF PORFLOW Model and the SDF GoldSim Model at the 100-meter boundary for all the examined species. Note that despite underestimating the concentrations, the basic trends indicative of flow field and chemistry changes are captured by the GoldSim model.

Figure 5.6-20: Maximum Radionuclide Concentrations at 100-Meter Boundary for Sector I

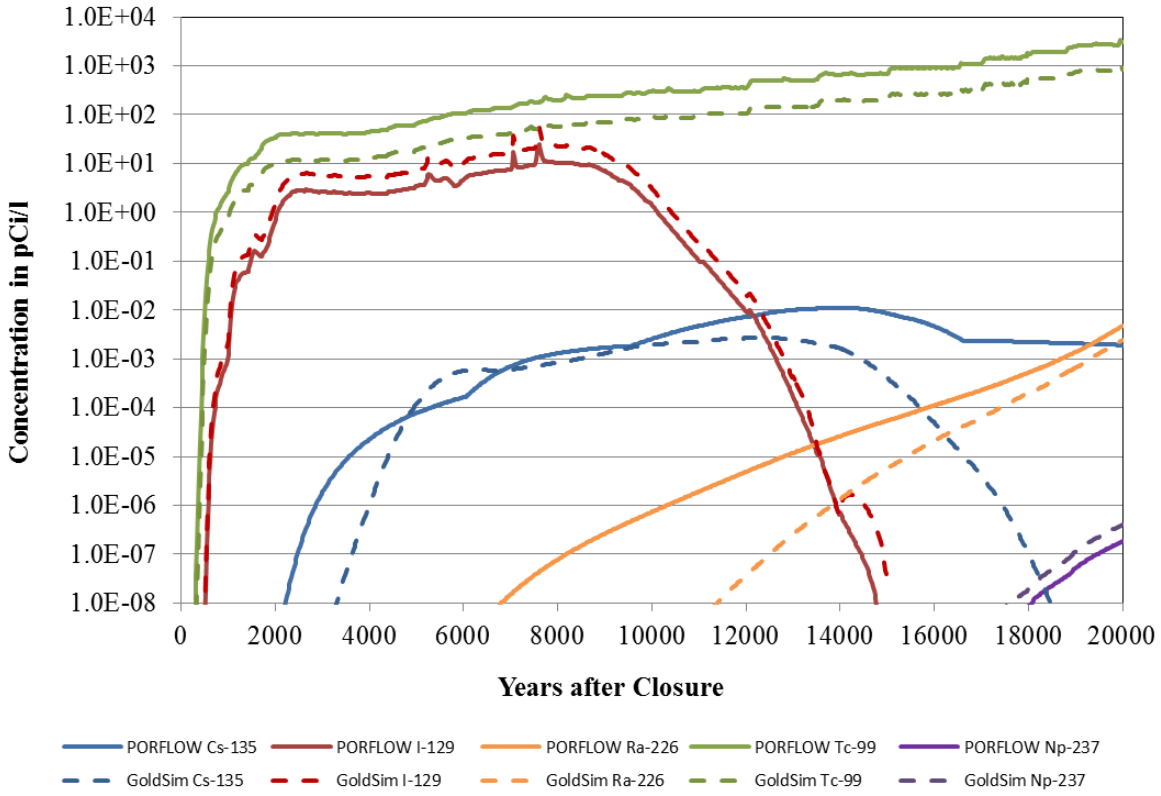

5.6.2.5 MOP Dose Time Histories

The third phase of the benchmarking process focuses on examining how well the abstracted model approximates the MOP dose results. Comparisons of the maximum total MOP dose levels (in millirem per year) generated by the two models form the basis of the benchmarking effort along with a comparison of dose contributions from the major contributing radionuclides.

5.6.2.5.1 Total MOP Dose Time Histories

An important check on the appropriateness of the SDF GoldSim Model as a surrogate for the SDF PORFLOW Model is a comparison between the maximum total doses generated by the two models. The Evaluation Case maximum dose and sector specific dose time histories for the first 10,000 years from the GoldSim model are presented in Figure 5.6-21. The maximum dose and sector specific dose time histories from the GoldSim model over 20,000 years are in turn depicted in Figure 5.6-22.

Figure 5.6-21: GoldSim Total Maximum MOP Dose Evaluation Case Results by Sector over 10,000 Years

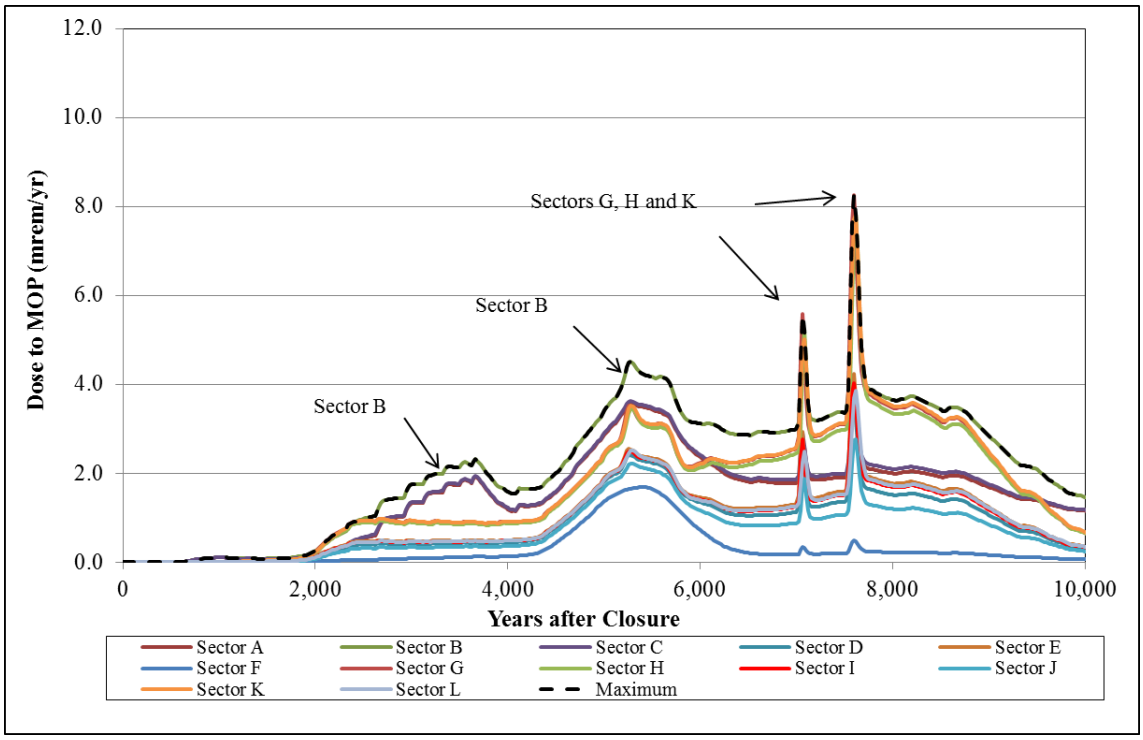

Figure 5.6-22: GoldSim Total Maximum MOP Dose Evaluation Case Results by Sector over 20,000 Years

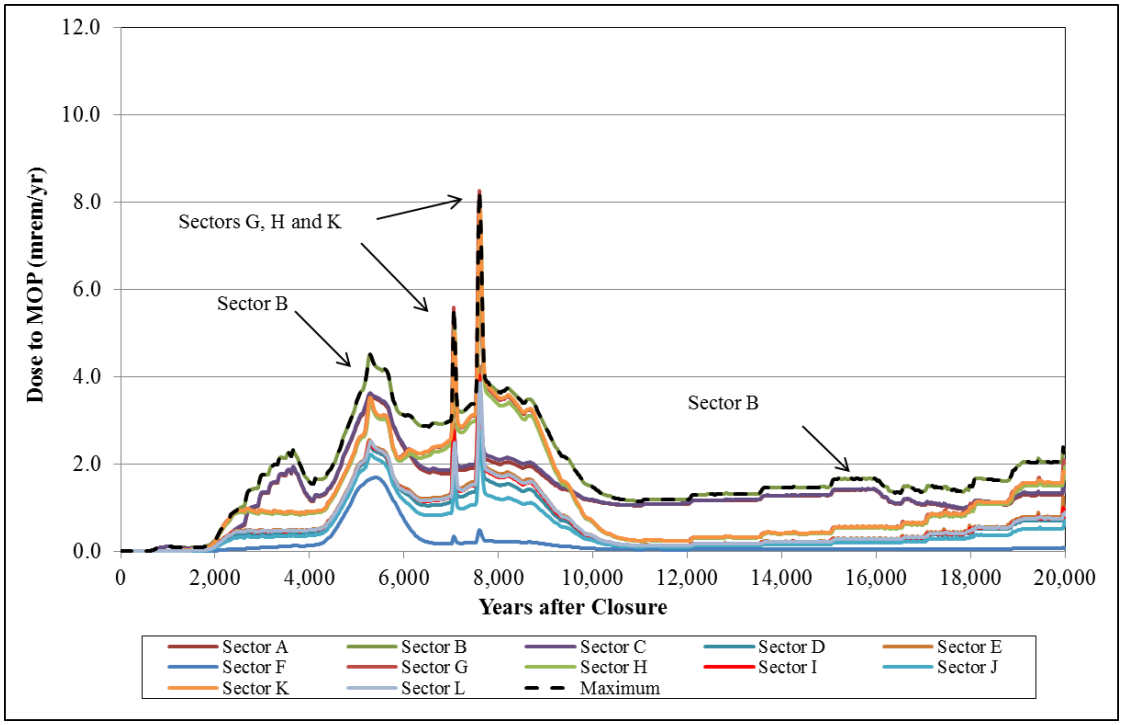

A comparison between Figure 5.6-21 and the equivalent data from the PORFLOW model simulations presented in Figure 5.5-2 shows that the GoldSim model closely approximates the maximum dose calculations generated by the PORFLOW model and the trends in dose for most sectors. Similarly over 20,000 years, a comparison between Figure 5.6-22 and the equivalent data from the PORFLOW model simulations presented in Figure 5.5-3 shows that the GoldSim model closely approximates the maximum doses generated using the PORFLOW model and the trends in dose for most sectors. The 20,000-year maximum doses curve plotted in Figure 5.6-22 is also presented in Figure 5.6-23 along with the PORFLOW generated maximum dose curve.

Figure 5.6-23: GoldSim Maximum MOP Dose Evaluation Case Results over 20,000 Years

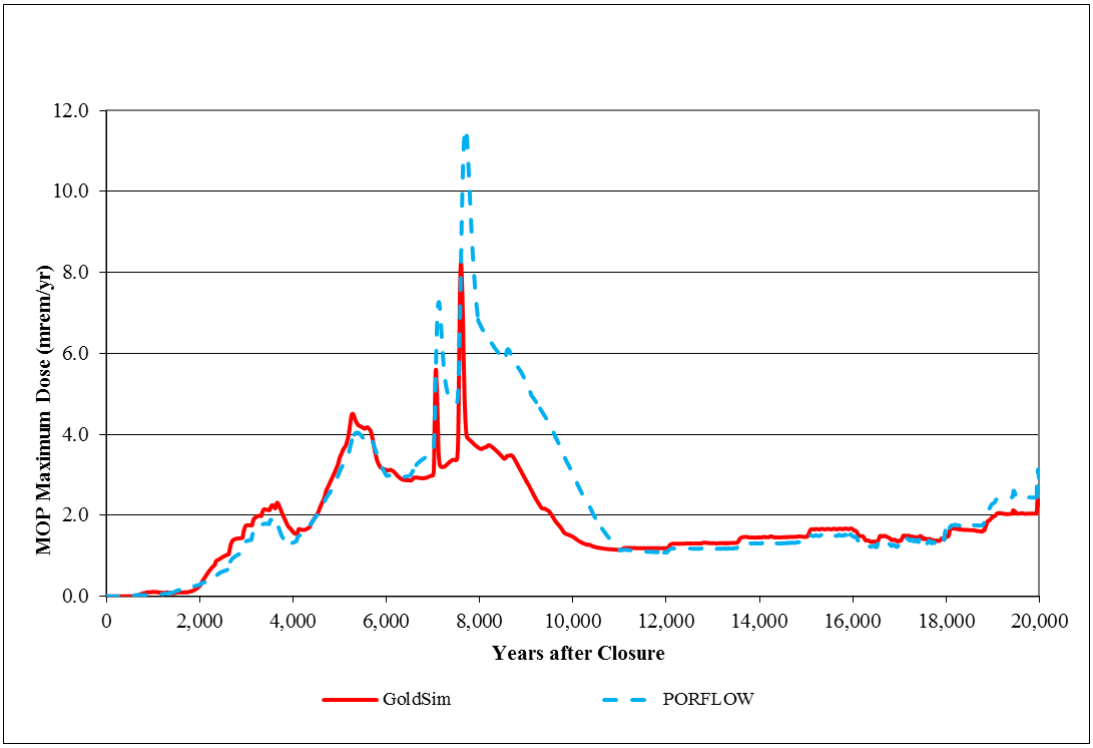

Differences do arise due to the influence of the groundwater divide as discussed in Section 5.6.2.4. For the PORFLOW model, the Evaluation Case has a peak dose of 12 mrem/yr, occurring in Sector I at 7,700 years. For the GoldSim model, the Evaluation Case has a peak dose of 8 mrem/yr, occurring in Sector G at 7,600 years. In addition to the influence of the groundwater divide, other simplifications in the GoldSim model that influence how well individual sector results from both models match include the nature of the spatial and temporal discretization of the models. Because the PORFLOW results are generated at each node in a finely discretized grid, for a given time, sector results are based upon the maximum concentration of any node within the sector, including nodes from the UTRA-UZ, the UTRA-LZ, or the Gordon Aquifer. In contrast, the GoldSim model results are based on the concentrations generated at the center of each sector resulting from the superposition of plume concentrations from the various SDU and FDC releases. This center-point analysis may potentially underestimate the GoldSim peak

doses relative to the PORFLOW results. The PORFLOW maximum point analysis will add a degree of numerical dispersion to the PORFLOW breakthrough curves since the point of analysis can shift in time.

The one sector that shows a large degree of variance between the two models due to the center-point analysis is Sector F. This difference is associated with the GoldSim model evaluating the results at the center of the sector and PORFLOW consistently choosing the results near the contact between Sectors E and F, picking up more of the mass from SDU 4. Since the GoldSim model also bases maximum dose results for the southern sectors on Sectors A through E, the model differences in Sector F calculations are unimportant.

In addition, the GoldSim simulations use larger time steps (20 years versus 2 years) to reduce the simulation run times. This will also slightly underestimate the maximum dose results for spike-type releases. Despite the GoldSim model simplifications, the similarity between GoldSim model results and PORFLOW model results justifies the use of the GoldSim model for evaluating parameter sensitivity and the influence of parameter uncertainty on the system to support DOE decision making related to reasonable expectation/assurance that performance objectives will be met for the SDF.

5.6.2.5.2 Radionuclide Contributions to Total MOP Dose Time Histories

This section presents a comparison of the SDF GoldSim and SDF PORFLOW Model dose breakthrough curves for the major contributing species to MOP dose: I-129, Cs-135, Tc-99, and Ra-226. The MOP dose breakthrough curves are presented for Sectors B, G, and H.

Sector B

As can be seen by comparing the GoldSim model generated species dose contributions presented in Figure 5.6-24 to the comparable results from PORFLOW presented in Figure 5.6-25, the GoldSim model closely approximates the PORFLOW generated results for Sector B for all species. The peak dose from the GoldSim model over the 20,000-year analysis period is 7 mrem/yr, occurring at 7,600 years. For the PORFLOW model the peak dose over the same period is 8 mrem/yr, occurring at 7,682 years. The GoldSim generated Sector B peak dose is therefore 9 % lower. As can be readily seen, the release of I-129 dominates the peak dose results over the 20,000-year period.

Figure 5.6-24: Individual Radionuclide Contributions to GoldSim Sector B 100-Meter Peak Groundwater Pathway Dose Results at 20,000 Years

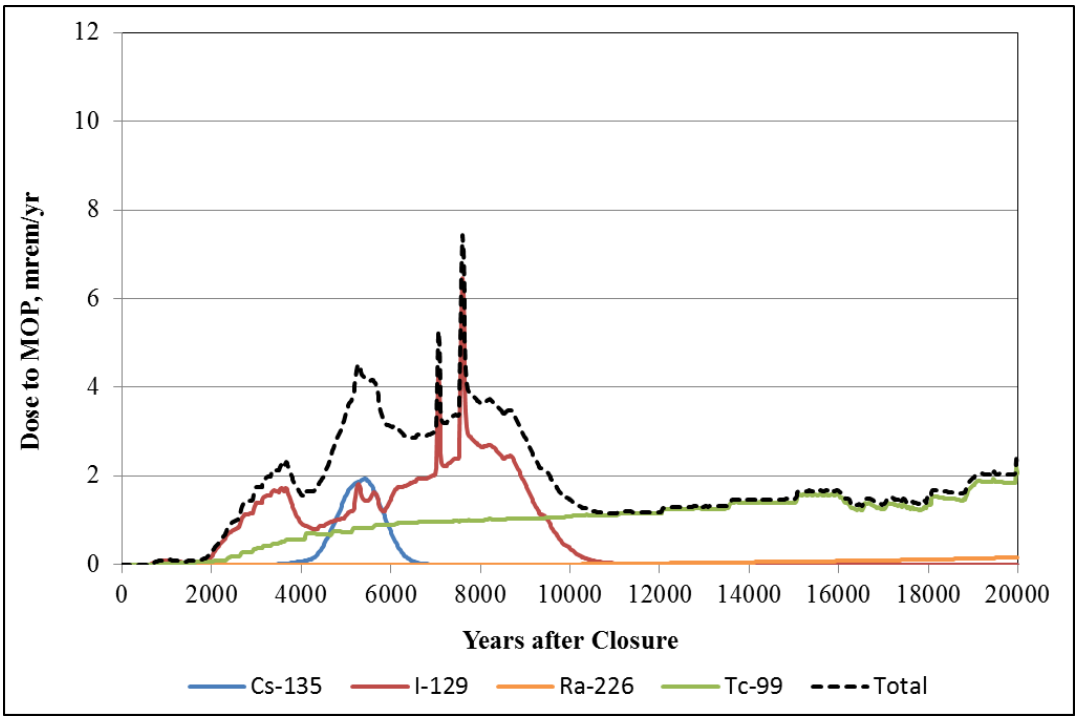

Figure 5.6-25: Individual Radionuclide Contributions to PORFLOW Sector B 100-Meter Peak Groundwater Pathway Dose Results at 20,000 Years

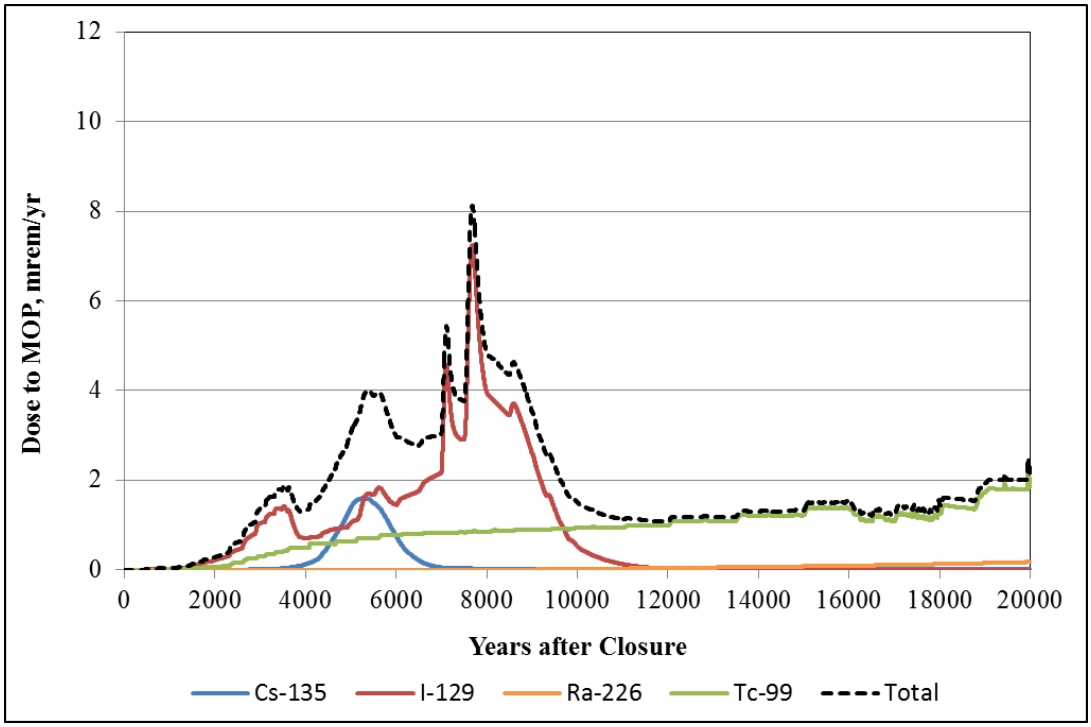

Sector G

By comparing the GoldSim model generated species dose contributions presented in Figure 5.6-26 to the comparable results from PORFLOW presented in Figure 5.6-27, it can be seen the SDF GoldSim Model closely approximates the PORFLOW generated results in Sector G for all species, although not quite as good as in Sector B. The peak dose for Sector G, from the GoldSim model over the 20,000-year analysis period is 8.3 mrem/yr, occurring at 7,600 years. For the PORFLOW model, the peak dose over the same period is 10.0 mrem/yr, occurring at 7,688 years. The GoldSim generated Sector G peak dose is therefore 17 % lower. As with Sector B, the release of I-129 dominates the peak dose results in Sector G over the 20,000-year period.

Figure 5.6-26: Individual Radionuclide Contributions to GoldSim Sector G 100-Meter Peak Groundwater Pathway Dose Results at 20,000 Years

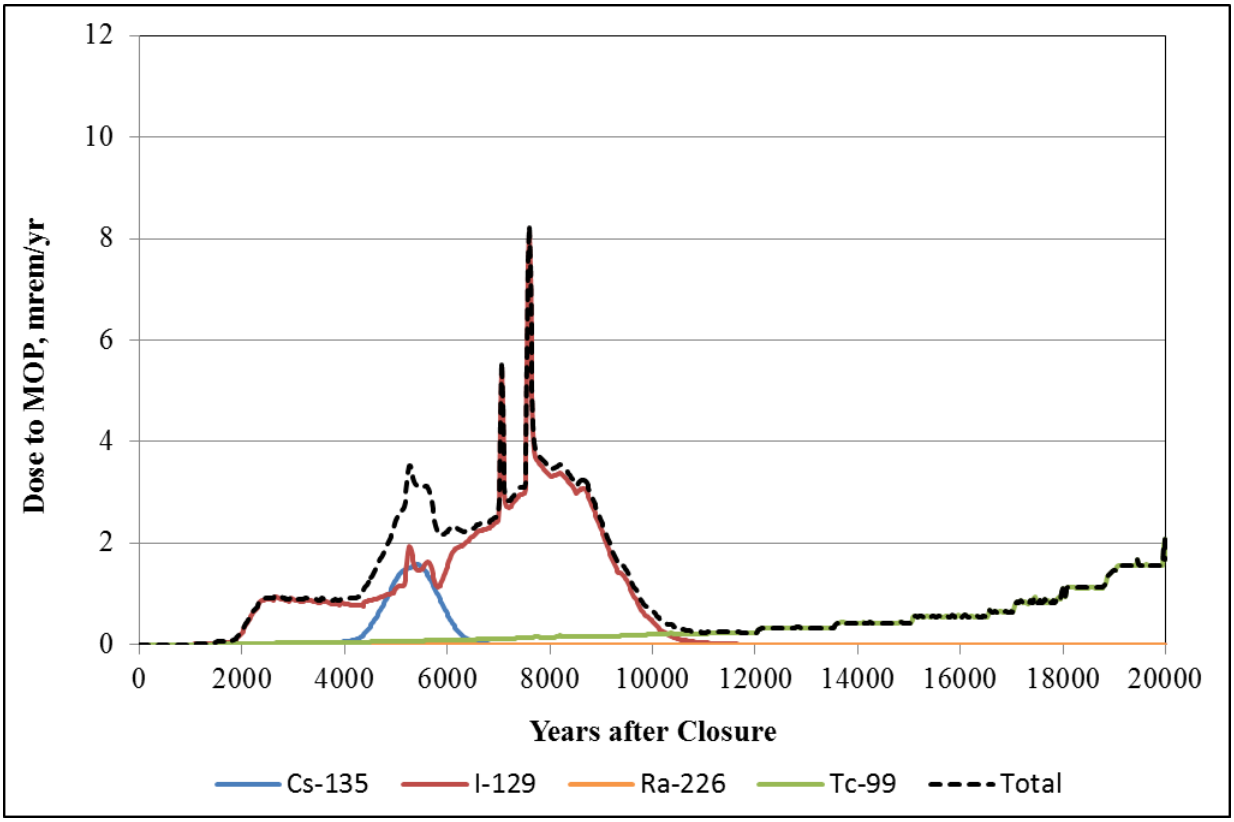

Figure 5.6-27: Individual Radionuclide Contributions to PORFLOW Sector G 100-Meter Peak Groundwater Pathway Dose Results at 20,000 Years

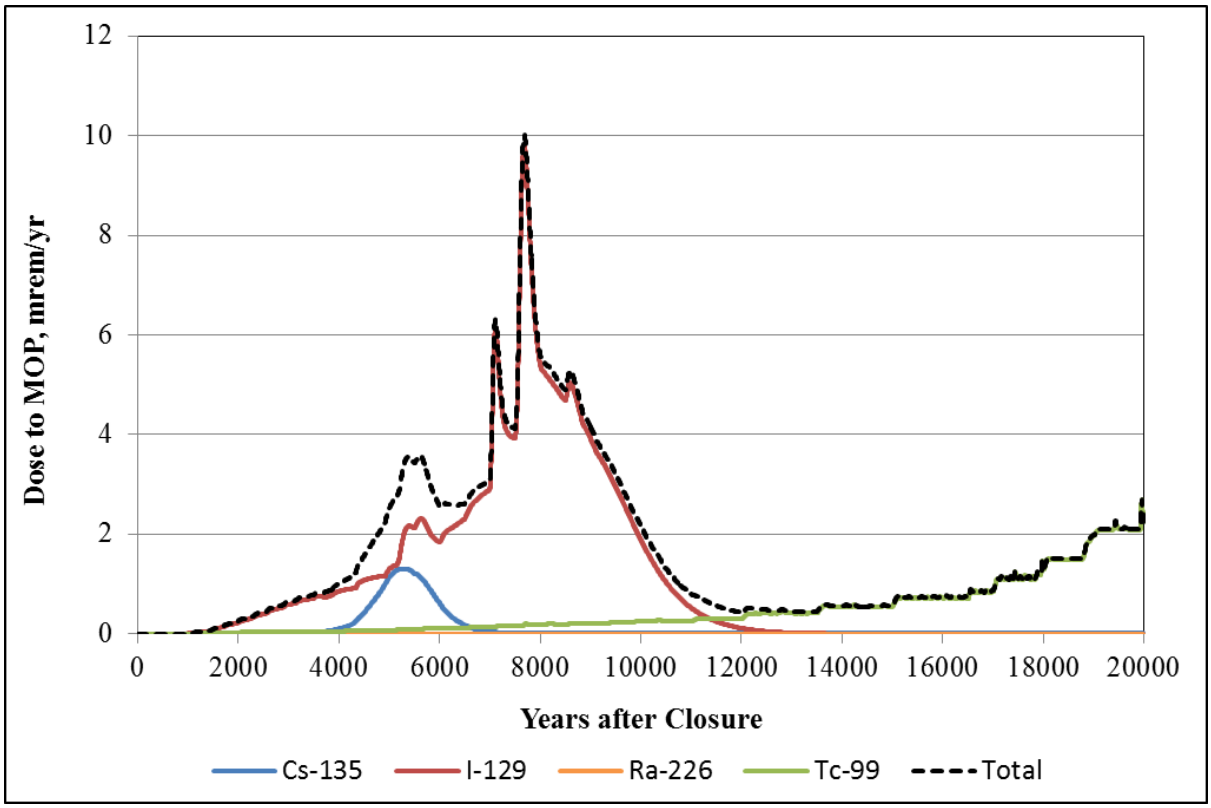

Sector H

By comparing the GoldSim model generated species dose contributions presented in Figure 5.6-28 to the comparable results from PORFLOW as presented in Figure 5.6-29, it can be seen the GoldSim model closely approximates the PORFLOW generated results for Sector H for all species, but again not quite as good as in Sector B. The peak total dose for Sector H, from the GoldSim model over the 20,000-year analysis period is 7.8 mrem/yr, occurring at 7,620 years. For the PORFLOW model, the peak dose over the same period is 10.3 mrem/yr, occurring at 7,688 years. The GoldSim generated Sector H peak dose is therefore 24 % lower. As with Sectors B and G, the release of I-129 dominates the peak dose results in Sector H over the 20,000-year period.

Figure 5.6-28: Individual Radionuclide Contributions to GoldSim Sector H 100-Meter Peak Groundwater Pathway Dose Results at 20,000 Years

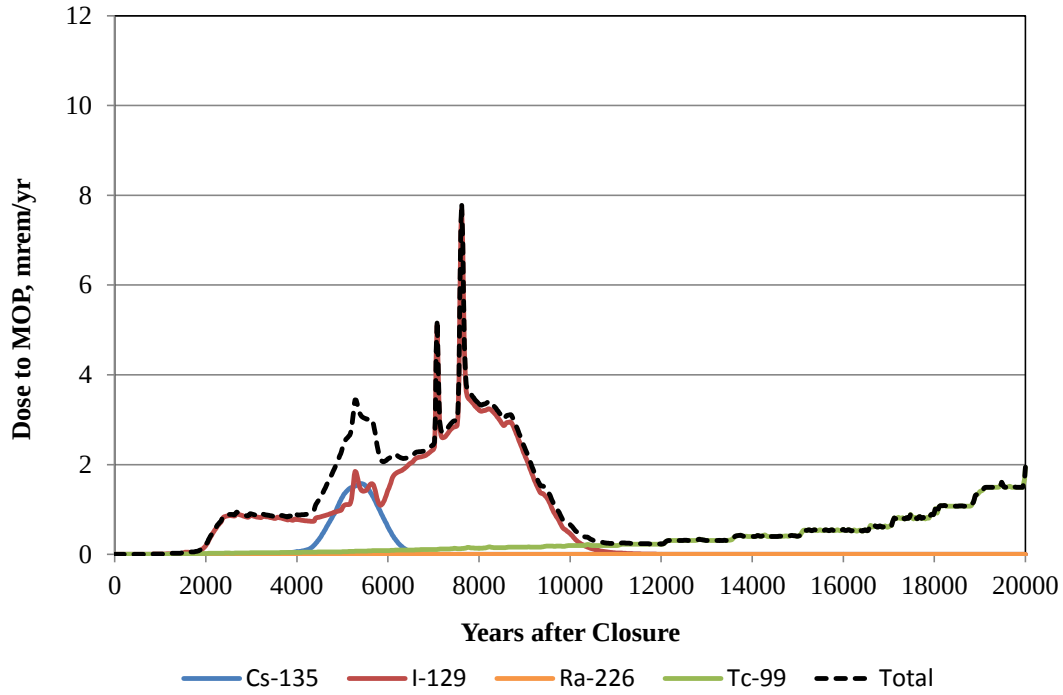

Figure 5.6-29: Individual Radionuclide Contributions to PORFLOW Sector H 100-Meter Peak Groundwater Pathway Dose Results at 20,000 Years

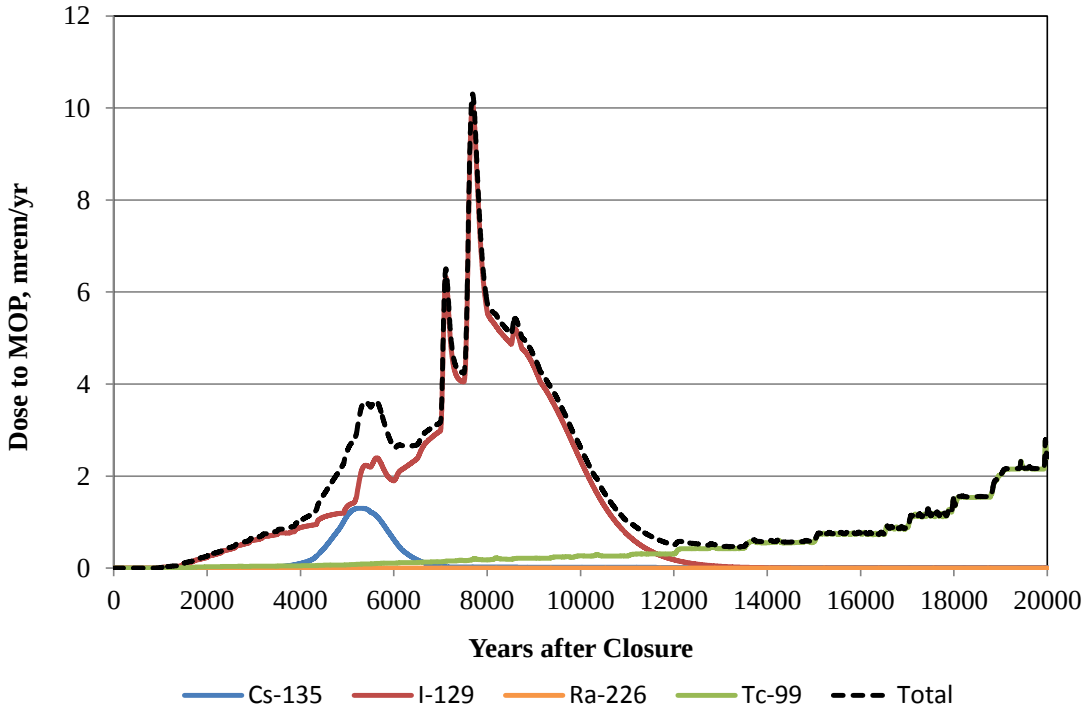

5.6.2.6 IHI Well Dose Time Histories

The fourth phase of the benchmarking process focuses on examining how well the abstracted model approximates the IHI dose results at the seven wells analyzed in the GoldSim and PORFLOW Models. Comparisons of the maximum total dose results (in millirem per year) and individual well dose levels generated by the two models for the IHI are the basis for the fourth phase.

5.6.2.6.1 Total IHI Dose Time Histories

In this section, the IHI analysis for the SDF PORFLOW and SDF GoldSim Models are compared to demonstrate how closely the GoldSim model approximates the PORFLOW IHI dose time histories. The results are presented in the form of dose time histories for the seven wells (Well #1 through Well #7) whose locations are shown in Figure 4.4-2. An additional time history representing the maximum value from all wells for each time step is also presented.

The results of the IHI dose history analyses for the two models are presented in Figures 5.6-30 (for the GoldSim model) and 5.6-31 (for the PORFLOW model). As a group, it can be seen that the trends predicted by the GoldSim model are quite similar to the trends predicted by the PORFLOW model. For the GoldSim model, the maximum peak value for all wells is 36 mrem/yr and occurs at 7,600 years. For the PORFLOW model, the maximum peak value for all wells generated by the PORFLOW model is 32 mrem/yr and occurs at 7,668 years. A closer look at the curves shows that though trends are always similar, there are differences with respect to which of the individual wells has the higher peak value and differences in the peak values.

Figure 5.6-30: GoldSim Model IHI Well Dose Time Histories

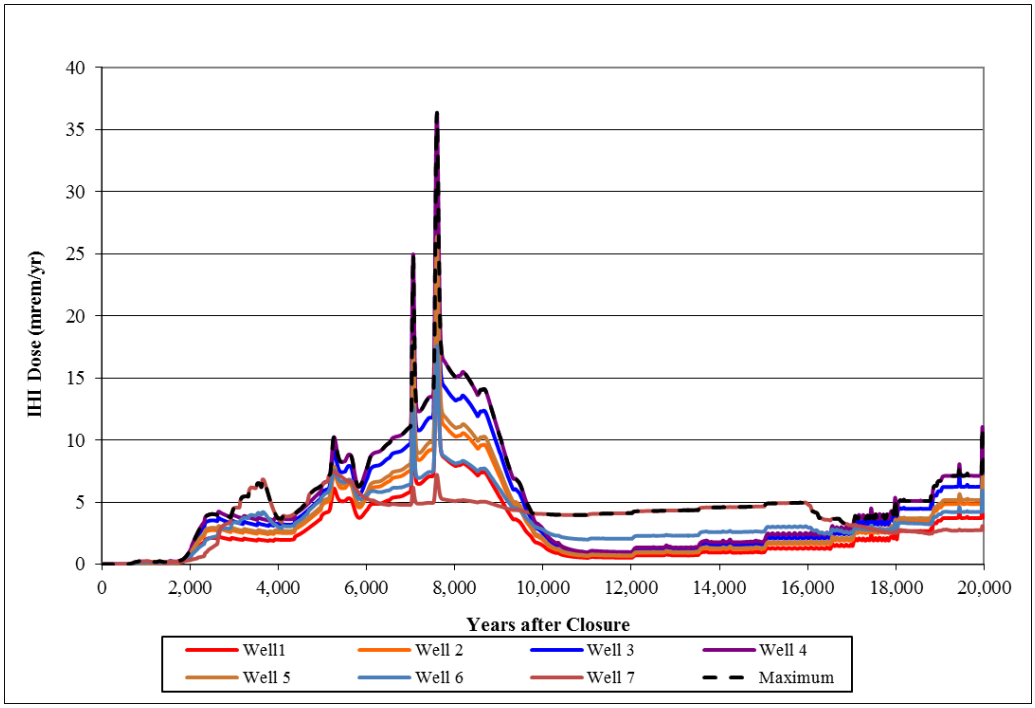

Figure 5.6-31: PORFLOW Model IHI Well Dose Time Histories

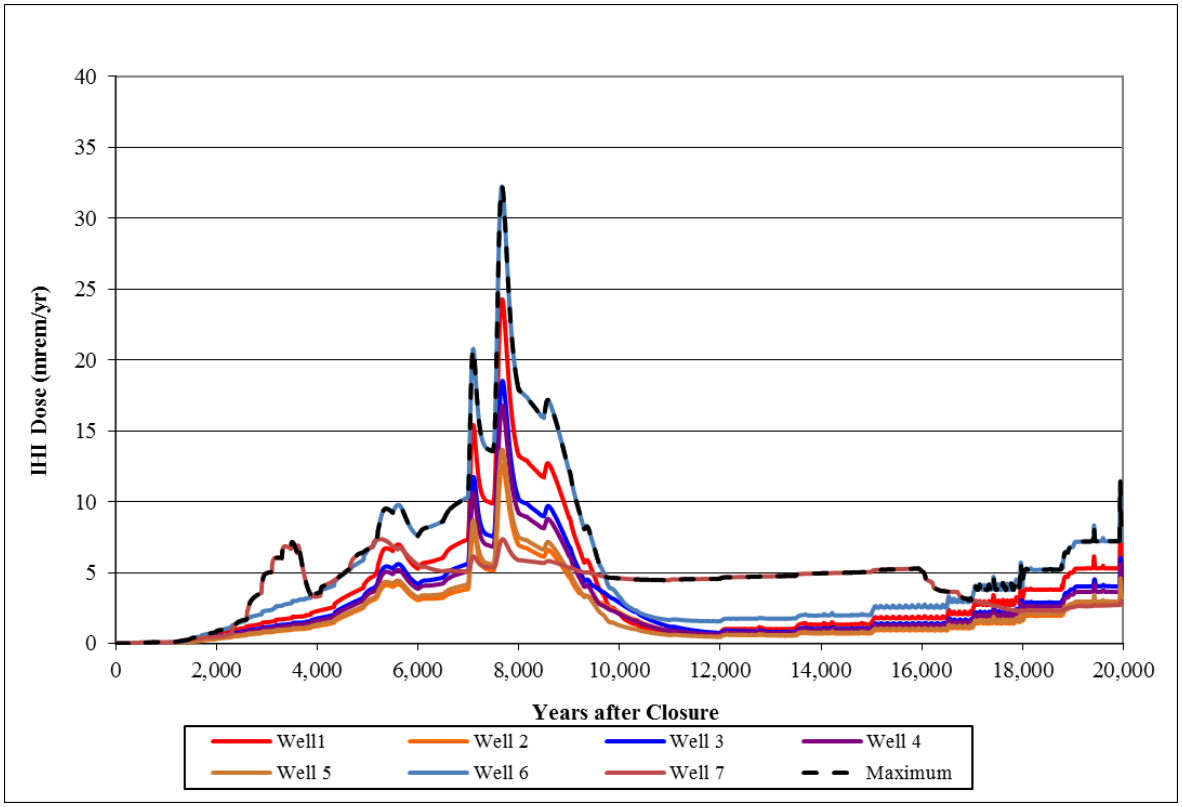

Figures 5.6-32 (for the GoldSim model) and 5.6-33 (for the PORFLOW model) show the dose time histories for the northern wells. The peak values tend to be around twice as high for the GoldSim results, although, the GoldSim and PORFLOW model results are similar for Well #1. The peak exposure levels for Well #1 are 19 mrem/yr for the GoldSim results and 24.3 mrem/yr for the PORFLOW results, a difference of 21 %. Figure 5.6-34 (for the GoldSim model) and Figure 5.6-35 (for the PORFLOW model) show the dose time histories for the southern wells (#6 and #7). Although showing similar trends, the peak values for Well #6 are 18 mrem/yr and 32 mrem/yr for the GoldSim and PORFLOW simulations, respectively. Note that the peak exposure levels for Well #7 are quite close, 7.5 mrem/yr and 7.4 mrem/yr for the GoldSim and PORFLOW simulations, respectively.

Figure 5.6-32: GoldSim Model IHI Well Dose Time Histories for Northern Wells

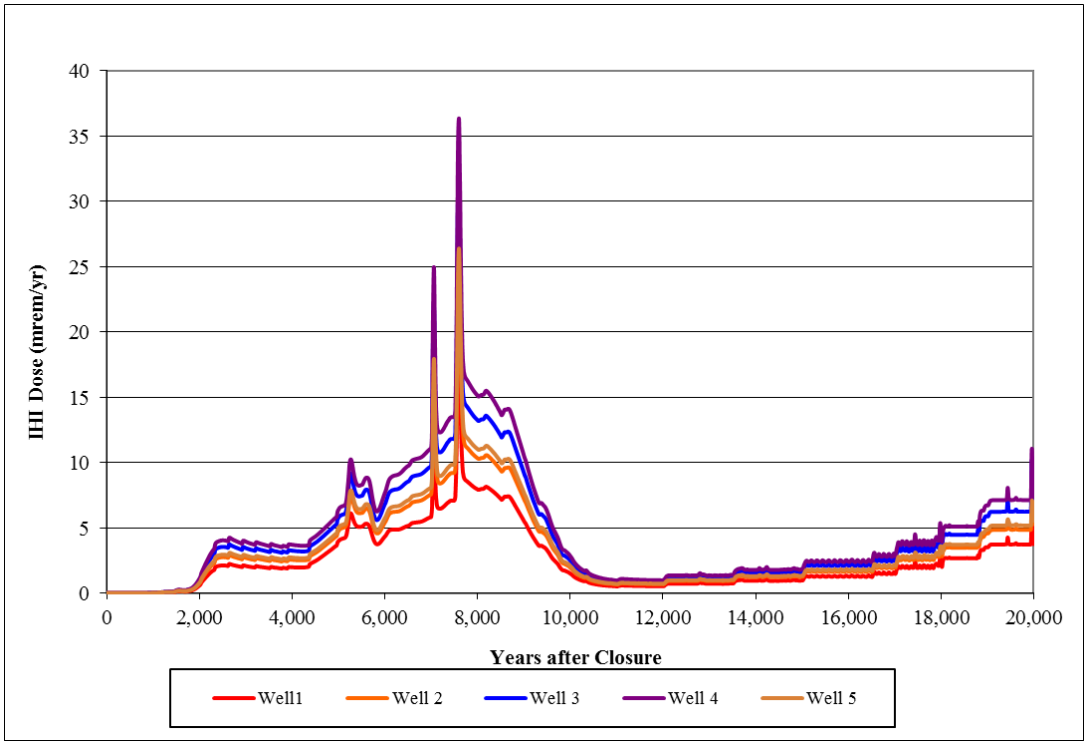

Figure 5.6-33: PORFLOW Model IHI Well Dose Time Histories for Northern Wells

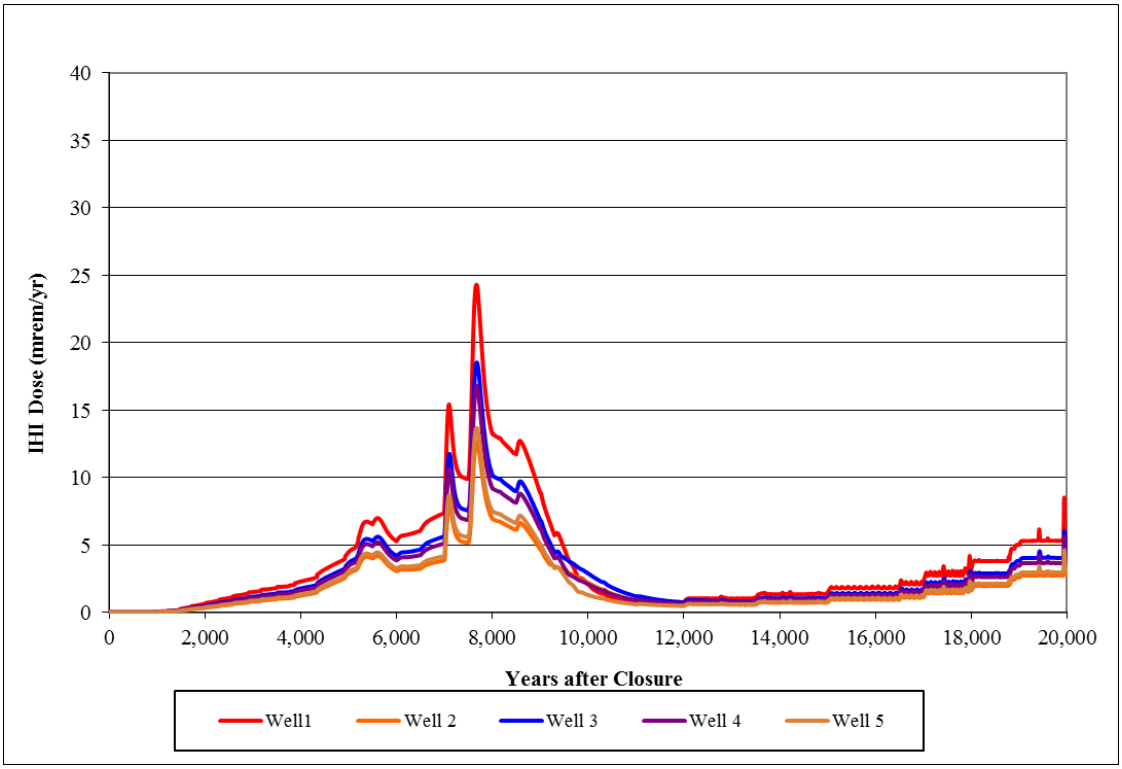

Figure 5.6-34: GoldSim Model IHI Well Dose Time Histories for Southern Wells

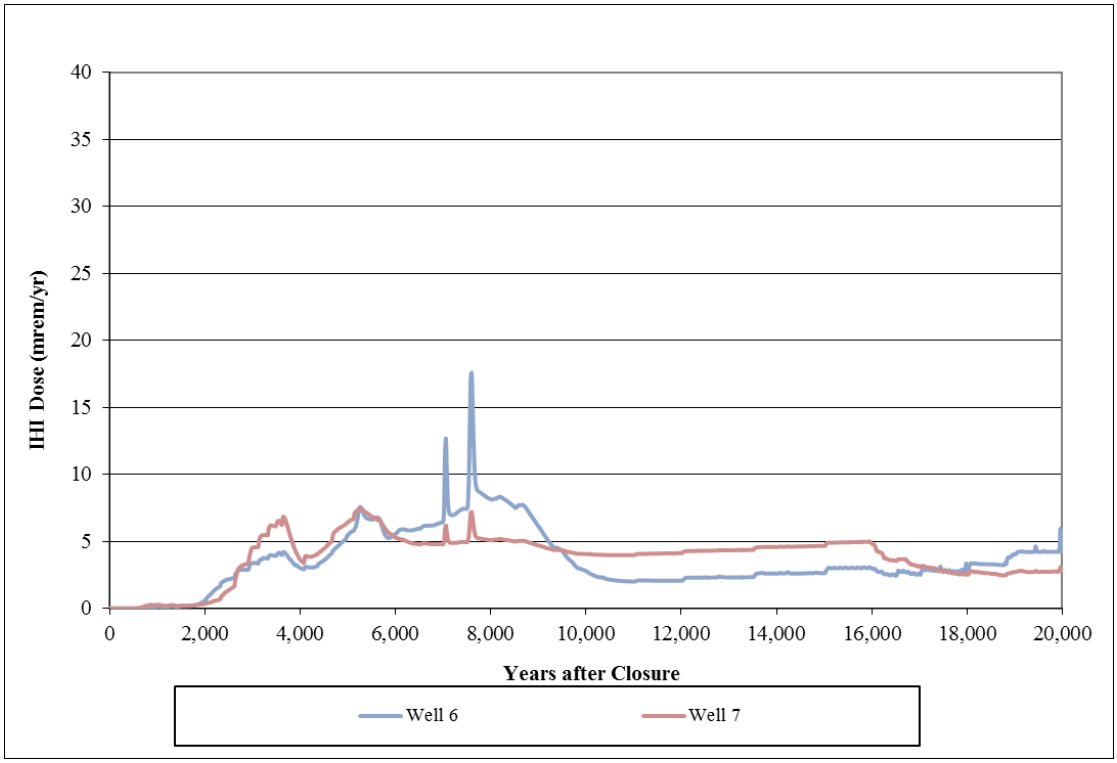

Figure 5.6-35: PORFLOW Model IHI Well Dose Time Histories for Southern Wells

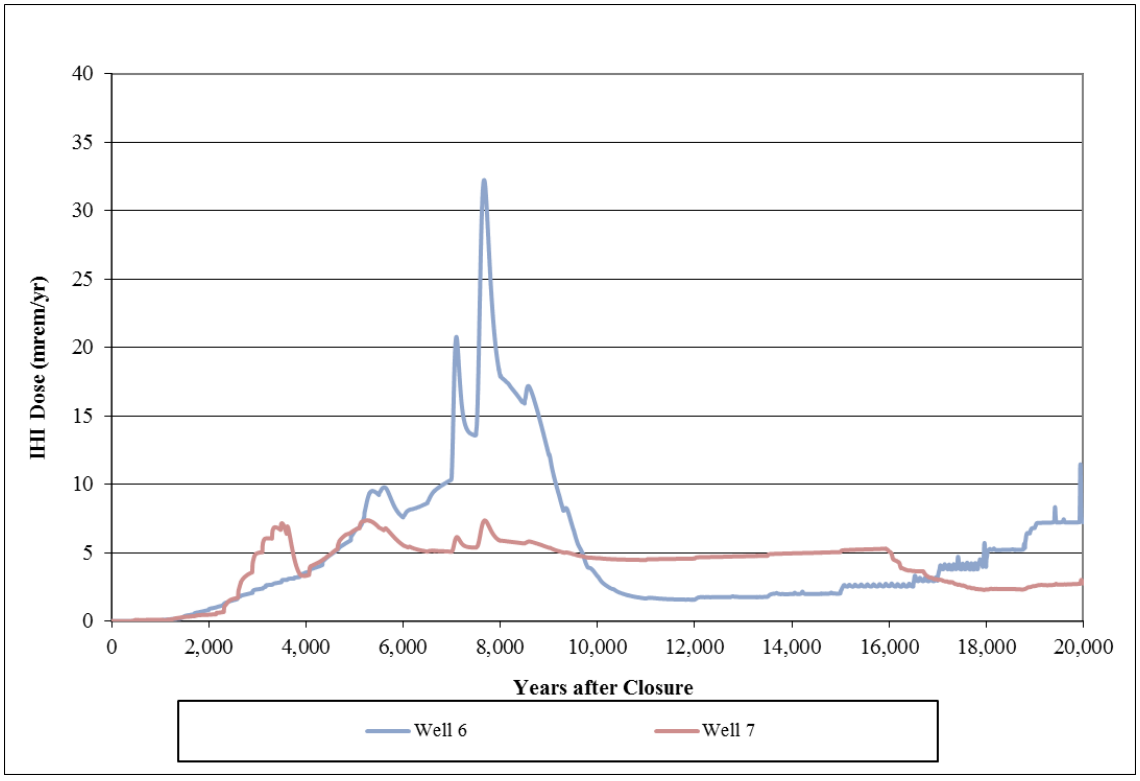

The differences between the individual well results are not surprising because of the proximity of the wells to the SDUs and FDCs and differences in the effects on dispersion over short distances. As discussed in Section 4.4.2, the GoldSim concentrations are taken at the centerline of the source as opposed to over an element thickness, which may explain the generally higher GoldSim results. On the other hand, when taking into account the maximum exposure levels from all wells as depicted in Figure 5.6-36, the two models generate quite similar results.

Figure 5.6-36: GoldSim and PORFLOW Model Maximum IHI Well Dose Time Histories

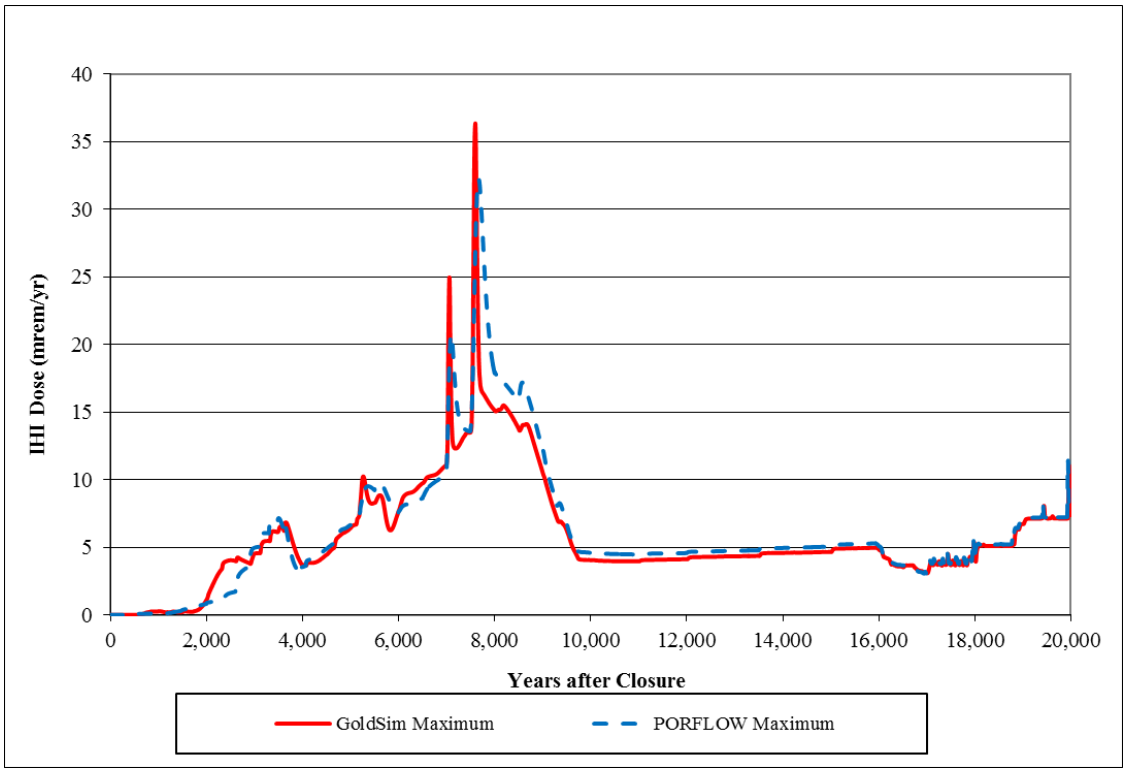

5.6.3 Parameters Evaluated in the SDF Probabilistic Model

Section 5.6.3 of the SDF PA describes various parameters selected for evaluation in the stochastic analyses based on modeling experience informed by the basis for the selected values and available generic and site-specific data. Except for a few parameters, discussed below, the information presented in the SDF PA with respect to probabilistic parameters is not affected by the revised modeling approach discussed within this SA.

Those parameters that have changed are as follows:

- This SA introduces flow cases developed from parametric modeling runs performed with the SDF PORFLOW Model. These flow cases were based on parameters that influence flow conditions, including the infiltration rate, cementitious degradation rate, moisture characteristic curves for disposal unit joints, and the initial hydraulic conductivity of saltstone. In the SDF PA flow conditions were modeled using static parameters (i.e., there was no probabilistic modeling of various flow conditions). Initially, 36 parametric flow cases were developed; however, analysis of the flow

fields indicated that there were significant similarities among many of the sets of flow fields, such that sampling all 36 flow cases would create a sampling bias preferential to similar flow fields. Given the uncertainty inherent in the flows, it was determined that 12 of the 36 flow cases provide a representative distribution that could be equally sampled from to ensure sufficient propagation of flow variability throughout the uncertainty sampling. The development of these flow fields and the revised sampling is discussed in greater detail in Sections 4.4.2.3 and 4.4.3.

- To facilitate the effects of the dynamic flow conditions relative to the shrinking core model used for Tc-99 release, the initial inventory of Tc-99 is no longer probabilistically sampled. In other words, every modeled realization of the SDF SA applies the same initial Tc-99 inventories as is used in the deterministic model. This is appropriate as the sampling distribution recommended for the Tc-99 inventory (as defined in Section 5.6.3.2 of the SDF PA) is less variable than the distribution sampled for the solubility controls as described in Section 4.4.2.3, and is evaluated deterministically in Section 5.6.6.5.
- Modeling of the saturated zone thickness was revised based on the observation of cross sections of PORFLOW-generated plumes as described in Section 4.4.2.1 of the *Saltstone Disposal Facility Stochastic Fate and Transport Model* (SRR-CWDA-2011-00178). Specifically, the mean of the sampled saturated zone thickness was increased (relative to the SDF PA) from 12 meters to 20 meters, the minimum increased from 5 meters to 12 meters, and the maximum increased from 19 meters to 28 meters.
- Finally, the parameters associated with the dose calculations were revised to reflect current information from the EPA and other appropriate sources, as described in *Dose Calculation Methodology for Liquid Waste Performance Assessments at the Savannah River Site* (SRR-CWDA-2013-00058). For example, Section 7.2.1 of SRR-CWDA-2013-00058 recommends a mean water consumption rate of 377 L/yr (or 1,033 mL/day). The SDF PA used a mean value of 337 L/yr (or about 923 mL/day). This increase was based on new information as published in the EPA's 2011 *Exposure Factors Handbook* (EPA-600-R-090-052F).

5.6.4 Uncertainty/Sensitivity Analysis using the SDF Probabilistic Model

The model for performing the uncertainty and sensitivity analyses were developed using the GoldSim systems analysis software. This model is not intended to predict future potential doses for comparison to performance objectives, as the SDF PORFLOW Model has been used for assessment of peak doses versus performance objectives. Rather, the goal of this probabilistic SDF modeling is to characterize the context of uncertainty and sensitivity surrounding the PA calculations involving doses to MOP exposed via groundwater for better-informed decision-making. The air and radon pathways results in Section 5.3 of the SDF PA are such a small fraction of the performance measure that no uncertainty and sensitivity analyses were performed.

The GoldSim model was run multiple times, using 20-year time steps, to develop results to support the probabilistic uncertainty and sensitivity analyses. These modeling runs use the

Monte Carlo method to sample uncertain parameters. Each run performed multiple realizations, where each realization represents a unique possible future outcome. The Monte-Carlo method samples values from each of the uncertain parameters during each realization using LHS. The results of the independent realizations are assembled into probability distributions of possible outcomes.

The uncertainty analyses are concerned with how the uncertainty in model input parameters is propagated through the model to the selected model results, or endpoints. For the purpose of this SA, these model endpoints are potential radiological doses to hypothetical human receptors (i.e., MOP). In contrast, the sensitivity analyses, discussed in Section 5.6.5 (and in 6.5 for the IHI), are focused on determining which of the many input parameters are most responsible for influencing the endpoint values.

SRS Saltstone v4.101.gsm, as described in *Updates to the Saltstone Disposal Facility Fate and Transport Model* (SRR-CWDA-2013-00073) was the model file used for these uncertainty and sensitivity analyses. This file evaluates the system for the 12 flow cases identified in Section 4.4.2.3, with an equal weighting assigned to each of the 12 selected flow cases. The selection of the 12 specific flow cases is described in Section 5.6.6. This approach is likely to sample flows that are faster than those of expected conditions for increasing understanding of how flow variability will influence the release and transport of contaminants.

Two modeling runs were performed each using 1,000 probabilistic realizations and a different sampling seed for each set. The green and blue lines in Figure 5.6-37 show the 95th percentile and mean dose curves, respectively, from the first model file (*SRS Saltstone v4.101_20yr_RS01.gsm* or "TcRS1"), which used a random seed of 1 for sampling. Similarly, the red and gold lines show the 95th percentile and mean dose curves, respectively, from the second model file (*SRS Saltstone v4.101_20yr_RS02.gsm* or "TcRS2"), which used a random seed of 2 for sampling. A third set of 1,000 realizations was performed, using a separate sampling seed, to increase confidence in that an appropriate number of realizations was performed to support uncertainty analyses. The black dotted line and dashed lines show the 95th percentile and the mean dose curves from incorporating dose results from all 3,000 modeled realizations. The peak of the mean doses from each of these sets was 8 mrem/yr. The similarity between these curves demonstrates good convergence of mean and 95th percentile results when using 1,000 realizations.

Figure 5.6-37: Mean Dose Results Comparison 1,000-Realizations (*SRS Saltstone v4.101)*

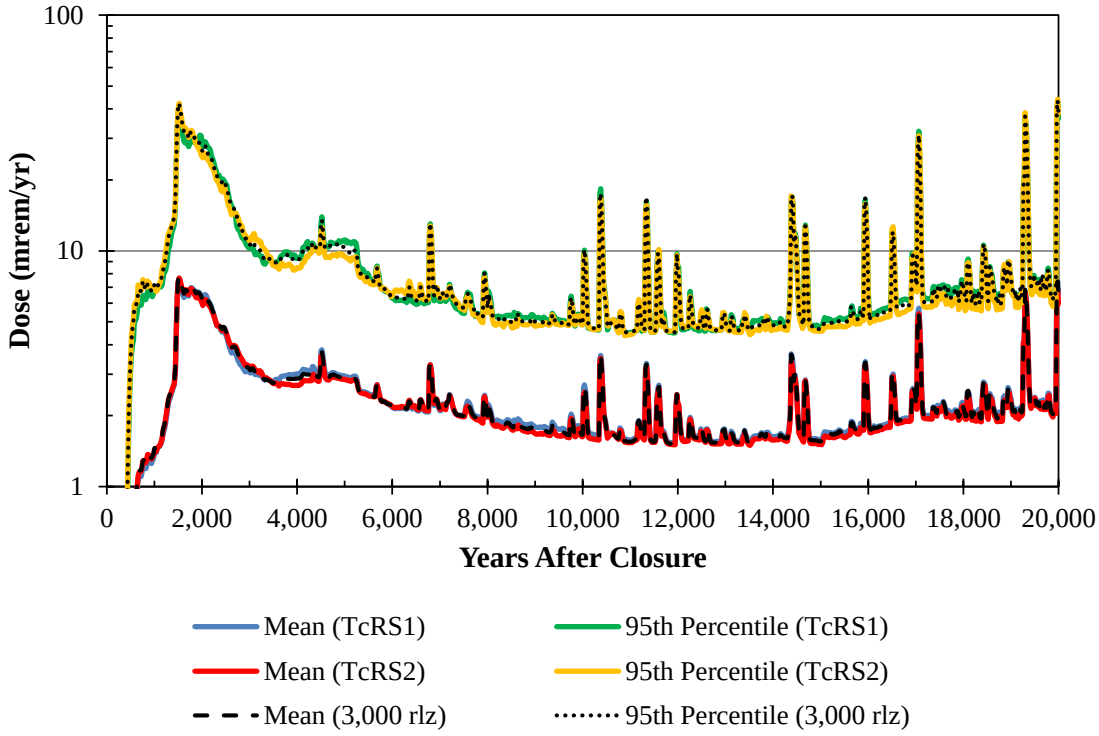

The names of the GoldSim model files used in the probabilistic uncertainty and sensitivity analyses are listed in Table 5.6-4. The second column (Model ID) provides an abbreviated name that is used within the SA text when referring to these model files.

Table 5.6-4: GoldSim Model Files Used in Probabilistic Analyses

GoldSim Model Files	Model ID	Sampling Seed	Duration of Model (years)	Number of Realizations
SRS Saltstone v4.101_20yr_RS01.gsm	TcRS1	1	20,000	1,000
SRS Saltstone v4.101_20yr_RS02.gsm	TcRS2	2	20,000	1,000
SRS Saltstone v4.101_20yr_RS11.gsm	N/A[a]	11	20,000	1,000

Note: (a) The model using a sampling seed value of 11 was only used to demonstrate confidence that 1,000 realizations is an appropriate number of realizations for conducting uncertainty and sensitivity analyses (i.e., increasing the number of realizations does not significantly change the results). This model is not discussed further within this report.

When reviewing results from the probabilistic uncertainty and sensitivity analyses, it should be noted that model variability is limited by which model parameters are defined as uncertain variables (which are sampled during each realization) as opposed to those parameters defined as known quantities (i.e., input parameters that remain unchanged regardless of sampling). From the model's perspective, the definition of an input variable as a single value implies that the value is known. Uncertainty shown in the results does not take into account any

contributions from these static (or deterministic) inputs, thereby potentially understating system uncertainty.

5.6.4.1 Uncertainty Analysis: Statistics of the Peaks

The most direct way to communicate the uncertain nature of the model results is to show graphs of certain key model endpoints. Statistics for peak values (e.g., mean of the peaks) are summarized in Table 5.6-5 for any time step within 20,000 years. The table focuses on peak doses to the MOP at the 100-meter boundary of the SDF because this is a relevant performance metric that was analyzed in the SDF PA. [SRR-CWDA-2009-00017]

Table 5.6-5: Statistics of the Peak MOP Endpoints within Any Time Step

Endpoint Evaluated	Model IDs Used [a]	Mean of the Peaks	Median of the Peaks (50th Percentile)	95th Percentile of the Peaks
All Sectors: MOP dose from Evaluation Case within 10,000 years (mrem/yr)	TcRS1 and TcRS2	15	8	50
All Sectors: MOP dose from Evaluation Case within 20,000 years (mrem/yr)	TcRS1 and TcRS2	23	11	83
Sector B: MOP dose from Evaluation Case within 10,000 years (mrem/yr)	TcRS1 and TcRS2	12	7	41
Sector G: MOP dose from Evaluation Case within 10,000 years (mrem/yr)	TcRS1 and TcRS2	12	6	45
Sector B: Tc-99 Concentration from Evaluation Case within 20,000 years (pCi/L)	TcRS1 and TcRS2	12,100	4,460	41,400
Sector G: Tc-99 Concentration from Evaluation Case within 20,000 years (pCi/L)	TcRS1 and TcRS2	15,800	2,690	57,900
Sector B: I-129 Concentration from Evaluation Case within 20,000 years (pCi/L)	TcRS1 and TcRS2	52	25	183
Sector G: I-129 Concentration from Evaluation Case within 20,000 years (pCi/L)	TcRS1 and TcRS2	63	30	219

a See Table 5.6-4.

The values presented in Table 5.6-5 do not reflect the same statistical data as the statistical values and time histories shown in the following table and figures, although these are complementary of one another. The difference between information presented in the table above and information below is important to understand. The previous table shows summary statistics for peaks of the MOP doses achieved at any time within the given time frames (e.g., 0 years to 10,000 years after closure). These are "statistics of the peak values" (e.g., mean of the peaks), regardless of when the peaks were achieved within the specific time frames. Alternatively, the information provided below examines statistics relative to each time step and offers "peak values of the statistics" (e.g., peak of mean). Figure 5.6-38 illustrates the difference between the mean of the peaks and the peak of the mean. This figure also demonstrates that the mean of the peaks can exceed the peak of the mean, as reflected in these uncertainty results.

Figure 5.6-38: Difference between the Mean of Peaks and the Peak of Mean

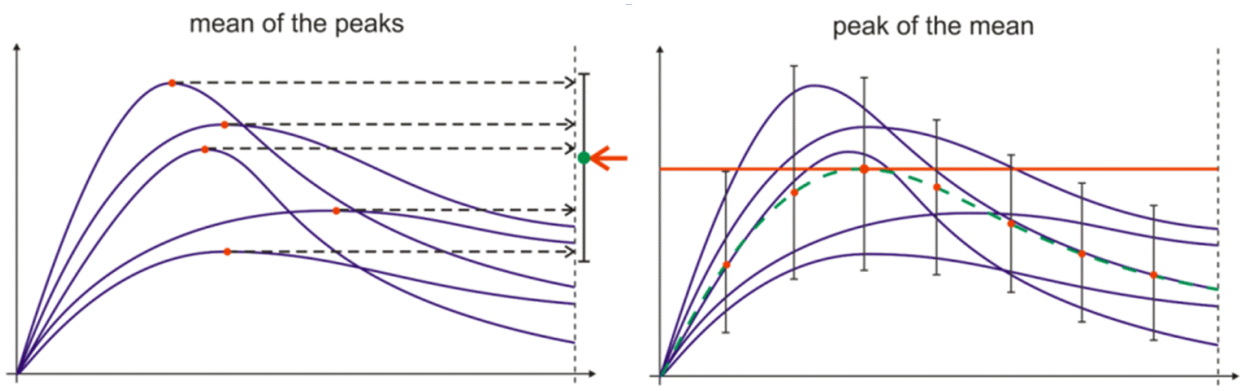

As an example, Figure 5.6-39 shows the peak MOP doses (for all sectors) within 10,000 years for all modeled realizations. The information presented in Table 5.6-5 gives no credit to the time of occurrence for each of these points, presenting statistics only on the dose values.

Figure 5.6-39: Peak MOP Doses within 10,000 Years from SDF Uncertainty Analysis GoldSim Files (*SRS Saltstone v4.101)*

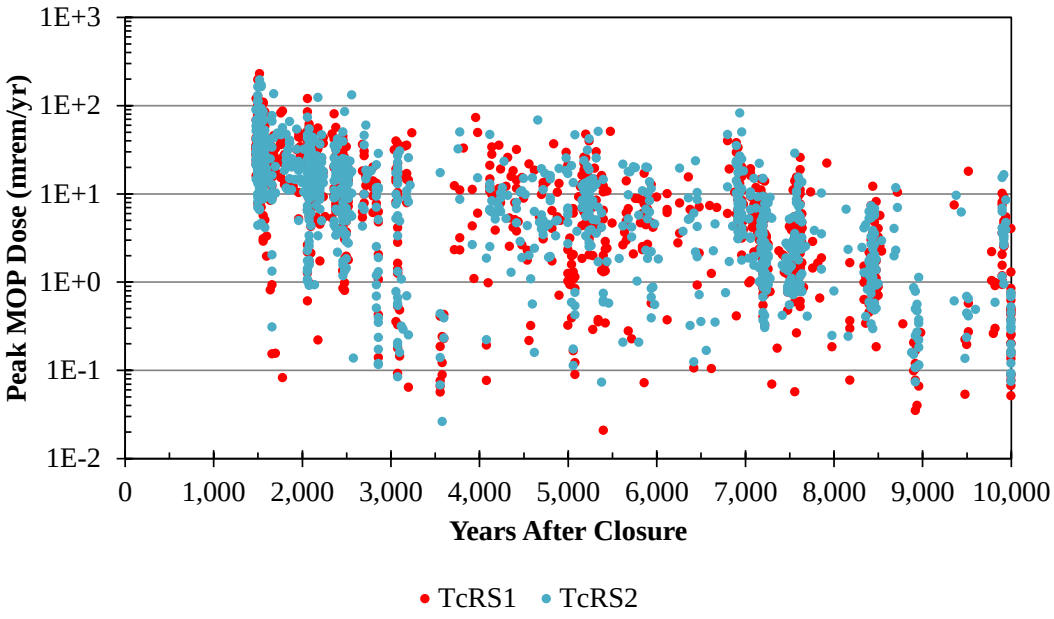

5.6.4.2 Uncertainty Analysis: Peaks of the Statistics

Where Table 5.6-5 showed the statistics of the peaks of the endpoints, regardless of timing, Table 5.6-6 shows the peaks of the statistics and identifies the timing of such peaks. Figures following this table illustrate these.

Table 5.6-6: Peaks of the Endpoint Statistics in 10,000 Years

Endpoint Evaluated	Model IDs Used [a]	Peak of the Means		Peak of the Medians (50th Percentile)		Peak of the 95th Percentiles	
		Peak	Time (yrs)	Peak	Time (yrs)	Peak	Time (yrs)
All Sectors: Total MOP dose (mrem/yr)	TcRS1 and TcRS2	8	1,520	2.0	4,500	40	1.520
Sector B: MOP dose (mrem/yr)	TcRS1 and TcRS2	6	1,520	1.8	4,500	32	1,520
Sector G: MOP dose (mrem/yr)	TcRS1 and TcRS2	6	1,520	1.4	4,500	32	1,520
Sector B: Tc-99 MOP dose (mrem/yr)	TcRS1 and TcRS2	2	4,500	0.7	8,020	8	6,780
Sector G: Tc-99 MOP dose (mrem/yr)	TcRS1 and TcRS2	2	6,800	0.3	9,980	10	6,800
Sector G: I-129 MOP dose (mrem/yr)	TcRS1 and TcRS2	5	1,520	0.6	2,220	30	1,500
Sector B: I-129 MOP dose (mrem/yr)	TcRS1 and TcRS2	5	1,520	0.5	1,940	26	1,520

a See Table 5.6-4.

Note that the timing of the peak of the means and the peak 95th percentile are generally similar, whereas the peak of the median has a different time of occurrence. This indicates that the distributions may skew results, toward the high end, as discussed below.

Figure 5.6-40 shows the statistical time histories of the total dose at any sector for the MOP at the 100-meter boundary. This figure incorporates data from all realizations that were executed (TcRS1, and TcRS2).

Figure 5.6-40: Total MOP Dose Statistical Time Histories Any Sector at 100-Meter Boundary (*SRS Saltstone v4.101)*

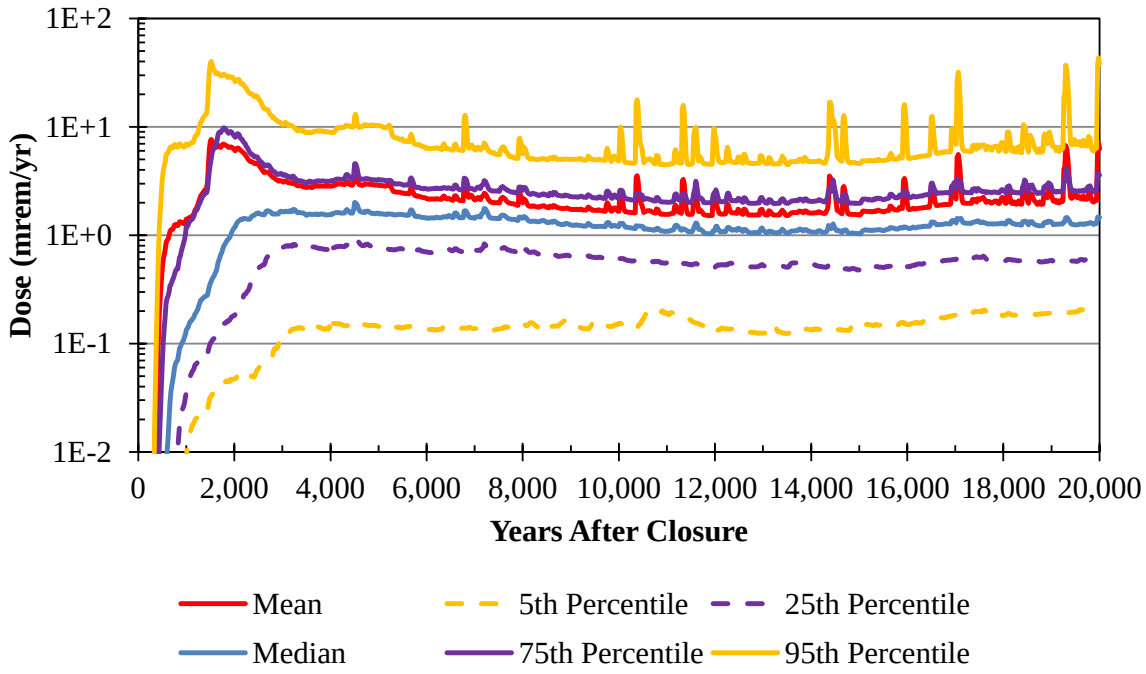

The 5th and 95th percentiles are significantly below and above the median value, respectively. The mean values are driven higher by the uncertainty distributions of the modeled parameters, approaching (and sometimes exceeding) the 75th percentile. This indicates that the model applies distributions with long tails (e.g., lognormal distributions) or extreme values are inherent in these distributions. It is expected that the mean value is higher than the median because many of the dominant distributions were established to be reasonably conservative, resulting in the distributions being skewed to the high end. This approach inflates the variance in the uncertainty analyses, resulting in a few realizations dominating the uncertainty analysis results. The intent of Section 5.6.4.3 is to investigate outlier realizations to determine which parameters are having the most impact on this aspect of the uncertainty analysis.

Figure 5.6-41 shows the mean values from the total (or maximum) dose to the MOP along with the mean of the dose contributions from I-129, Cs-135, Ra-226, and Tc-99 from the two sets of probabilistic modeling runs. These figures illustrate that at the time of the peak doses (between approximately 1,500 and 2,500 years after closure), and the most significant radionuclide dose contributors are only I-129, Tc-99, and Cs-135.

Figure 5.6-41: Mean Doses to a MOP, Major Radionuclide Contributors within 20,000 Years (*SRS Saltstone v4.101)*

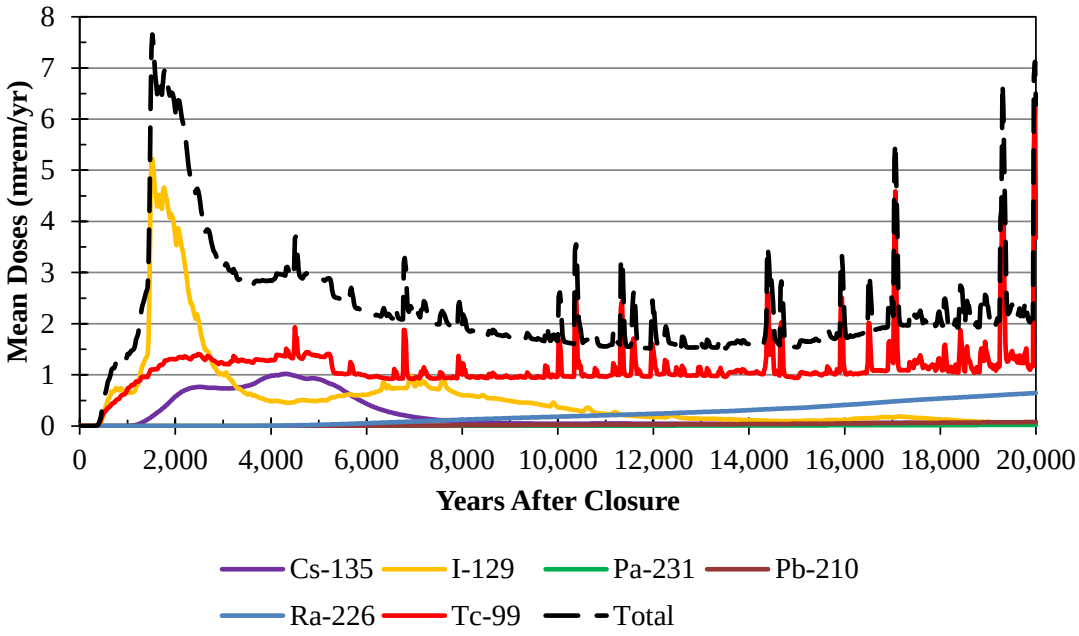

Figure 5.6-42 shows the mean dose to a MOP located within each of the defined PORFLOW sectors (Sectors A through L), at any point in time, for 20,000 years from the two set of modeling runs.

Figure 5.6-42: Mean MOP Doses, Each Sector within 20,000 Years (*SRS Saltstone v4.101)*

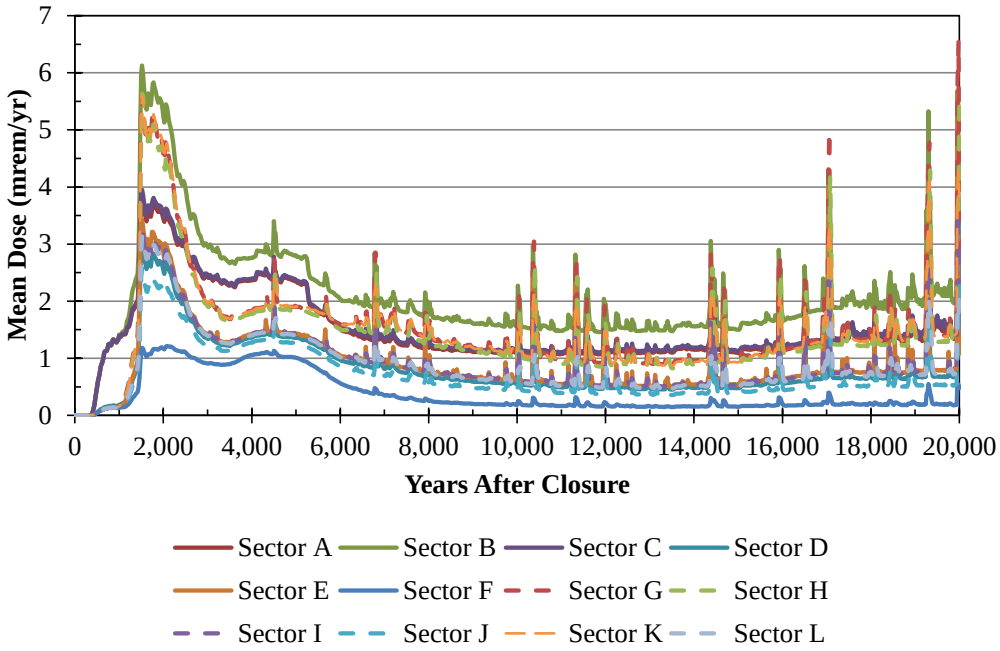

Note that for *SRS Saltstone v4.101*, the mean of the maximum MOP dose (Figure 5.6-41) is 1 to 2 mrem/yr more than the mean of the individual wells (Figure 5.6-42). The mean of the maximum MOP dose reflects the dose from the highest sector at any given time during each realization, regardless of which well is driving the mean dose. As such, the maximum MOP dose is pulled up, relative to the mean dose from each individual sector, by the effects of higher doses from the other sector locations. For example, in some realizations, Sector G has a higher dose than Sector B, such that the maximum MOP dose uses the Sector G data to compute the mean value instead of the Sector B dose from those realizations. Selecting the highest dose from each of the 12 sectors provides a comprehensive and conservative approach for considering the impacts of uncertainty on dose. However, as the MOP receptor is not omnipresent (i.e., at all locations at all times), this approach is not the most effective for analyzing results; rather, it makes sense to select the highest individual sector for further analysis.

Close review of the sector-specific dose results from the probabilistic modeling shows that Sector B yields the highest mean dose among the southern sectors and Sector G yields the highest mean dose among the northern sectors. To communicate uncertainty effectively, Sectors B and G are examined individually, below.

Similar to Figure 5.6-40, Figures 5.6-43 and 5.6-44 show the statistical results of the peak doses from Sector B and Sector G, respectively. Again, these figures incorporate data from all the realizations that were executed (TcRS1 and TcRS2).

Figure 5.6-43: Statistic Results for Peak Doses at Sector B for MOP at 100-Meter Boundary (*SRS Saltstone v4.101)*

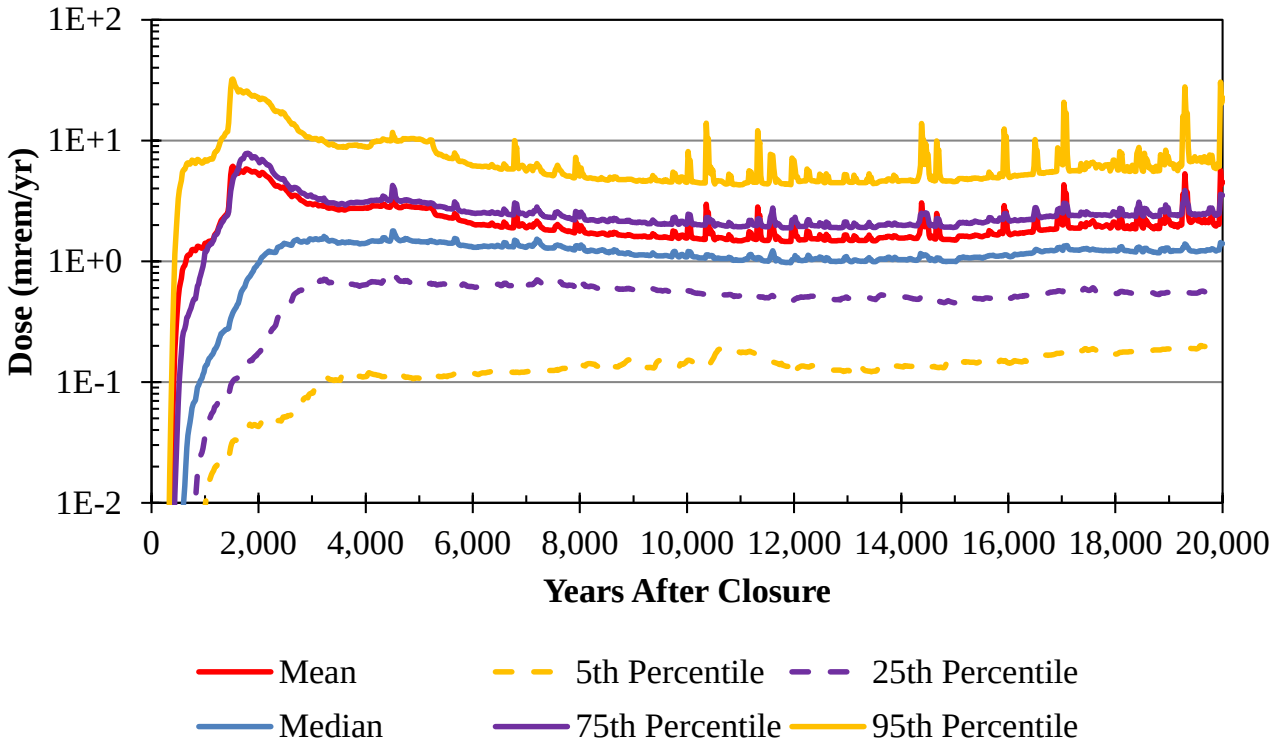

Figure 5.6-44: Statistic Results for Peak Doses at Sector G for MOP at 100-Meter Boundary (*SRS Saltstone v4.101)*

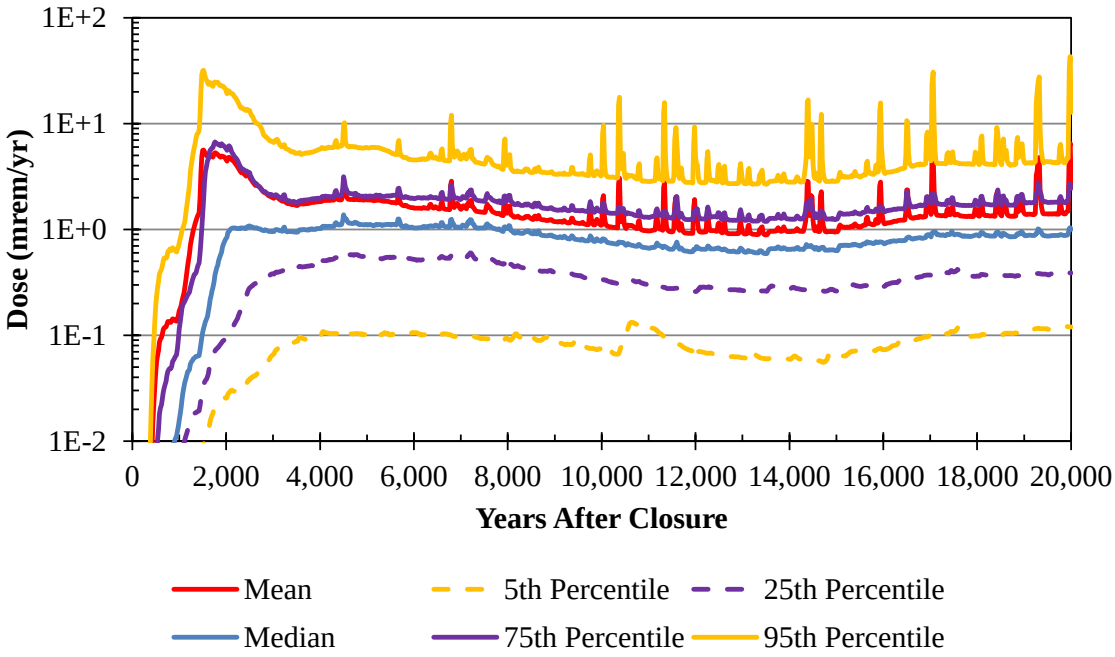

5.6.4.3 Uncertainty Analysis Realizations of Interest

This section identifies outlier realizations (i.e., those with dose results that significantly exceed expectations) to determine which sampled parameters drive the unexpected behavior. Demonstrating that these high-dose realizations result from the extreme sampling of a small number of key parameters provides confidence that such outcomes are improbable (or completely unrealistic). In addition, these outlier realizations influence the mean dose results; therefore, studying these realizations provides insights as to which parameters have the most influence on the statistical behavior of the modeled results and whether the controlling parameters are valid or a product of the distribution sampled (i.e., unrealistic bounds on the distributions). The five realizations with the highest peak doses from the *SRS Saltstone v4.101* uncertainty analysis models (i.e., TcRS1 and TcRS2), as identified in Table 5.6-4, were selected for evaluation.

All of the realizations from TcRS1 and TcRS2 (see Table 5.6-4) were used here to identify those realizations with the highest peak doses within 10,000 years of closure. The results of this review are shown in Table 5.6-7. The Evaluation Case peak dose from the deterministic PORFLOW model is also included for comparison.

Table 5.6-7: Five Highest MOP Dose Results from Probabilistic Realizations in 10,000 Years

Realization	Peak Dose (mrem/yr)	Time of Peak Dose (yr)	Sector of Peak Dose	Major Pathway Contributors at Peak Time	Major Radionuclide Contributors at Peak Time
Deterministic Case[a]	12	7,700	I	Water Ingestion (88 %) Fish Ingestion (6 %)	I-129 (98 %)
TcRS1-670[b]	229	1,520	K	Water Ingestion (93 %) Plant Ingestion (3 %)	I-129 (99 %)
TcRS1-487[b]	197	1,500	B	Water Ingestion (95 %) Fish Ingestion (4 %)	I-129 (78 %) Tc-99 (21 %)
TcRS2-101[c]	195	1,520	K	Fish Ingestion (67 %) Water Ingestion (29 %)	I-129 (97 %)
TcRS2-813[c]	171	1,520	H	Water Ingestion (59 %) Fish Ingestion (39 %)	I-129 (95 %)
TcRS2-292[c]	163	1,520	G	Water Ingestion (94 %) Fish Ingestion (5 %)	I-129 (99 %)

a From GoldSim model file: SDF_PORFLOW_Concentration-SA1-1SL_20130411.gsm
b From GoldSim model file: SRS Saltstone v4.101_20yr_RS01.gsm
c From GoldSim model file: SRS Saltstone v4.101_20yr_RS02.gsm

Inspection of Table 5.6-7 indicates that even though the peak dose from the individual realizations are significantly higher than the deterministic case, the location (i.e., northern sectors), the identification of the major radionuclide contributor to the dose (I-129), and the major pathway contributors are not significantly different from the deterministic case. The individual realizations are analyzed below by identifying those uncertainty parameters that have a direct impact on the magnitude or timing of the peak dose.

All five of these realizations sampled an initial hydraulic conductivity in saltstone of 4.5E-07 cm/s (nearly two orders of magnitude greater than the Evaluation Case, which applies a value of 6.4E-09 cm/s). Because this value is the same in all five realizations discussed below, the value is not repeated. Figure 5.6-45 illustrates the significance of sampling of the initial hydraulic conductivity of saltstone with respect to the peak MOP doses for the sampled realizations, where initial conductivity sampled three discrete values (3.9E-10 cm/s, 6.4E-09 cm/s, and 4.5E-07 cm/s).

Figure 5.6-45: Peak MOP Doses within 10,000 years, Sorted by Initial Hydraulic Conductivity in Saltstone (*SRS Saltstone v4.101)*

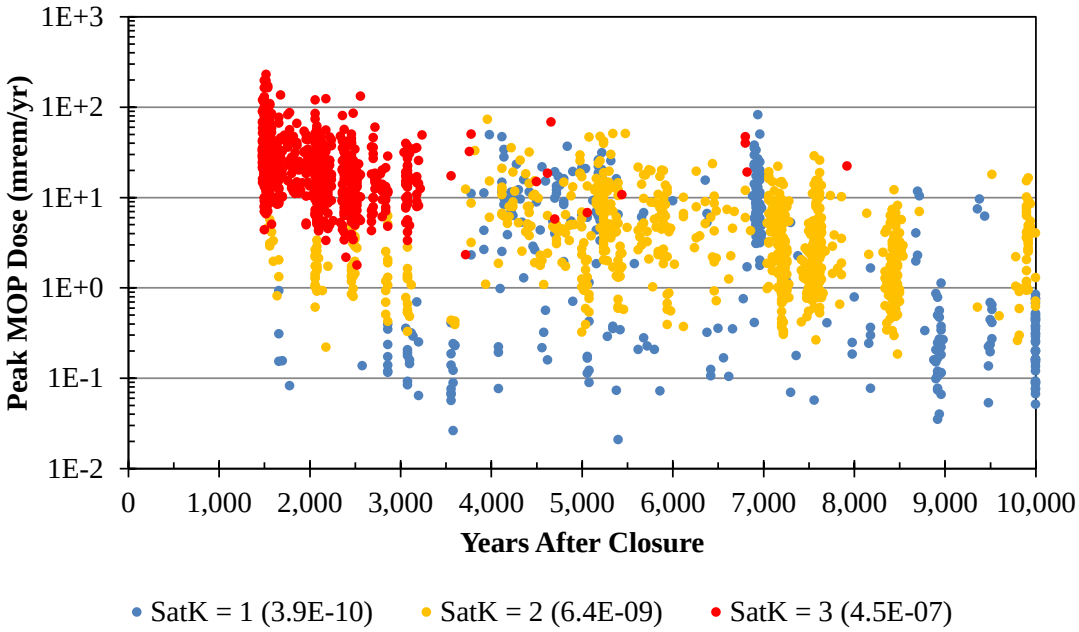

In general, the detailed descriptions of the highest realizations (below) show that the high peak doses are the result of a confluence of multiple variables being sampled such that conditions expedite the release and transport of contaminants through the system or decrease the degree of dilution due to vertical mixing. This includes the high initial value for saturated hydraulic conductivity in saltstone, higher infiltration rates, less thickness in the unsaturated and saturated zones, and decreased Darcy velocity. This is coupled with lower K_d values for iodine in cementitious materials and higher initial inventories of I-129 in FDCs that are near the 100-meter boundary. Finally, high consumption rate parameters from the dose calculation results in increased doses.

Realization TcRS1-670

As indicated in Table 5.6-7, the major radionuclide contributor to the peak MOP dose, at Sector K, is I-129 (99 %) with the major pathway contributor being water ingestion (93 %). Uncertainty parameters influencing the physical conditions affecting the release and transport of contaminants with respect to the sampled values are identified below, along with their respective values from the deterministic model. The deterministic value is presented within parentheses.

Infiltration rate distribution = steady state at 12.45 in/yr (steady state at 10.61 in/yr)
Unsaturated zone thickness under FDCs = 14.3 meter (12.8 meter)
Saturated zone thickness = 17.7 meter (20 meter)
Saturated zone Darcy velocity multiplier (unitless) = 1.09 (1)

Parameters that are specific to the transport of I-129 are:

Iodine K_d in Reduced Region II cement = 2.6 mL/g (9 mL/g)
Iodine K_d in Oxidized Region II cement = 20.4 mL/g (15 mL/g)
I-129 inventory in select saltstone disposal units:
FDC 10 (A,B,C,D) = 0.46 curies (0.38 curies)

Parameters affecting the estimate of the dose by pathway are identified below. The deterministic value is presented within parentheses.

Consumption of water = 1,194 L/yr (377 L/yr)
Fraction of drinking water from a contaminated source (unitless) = 0.84 (0.87)

Realization TcRS1-487

As indicated in Table 5.6-7, the major radionuclide contributors to the peak MOP dose, at Sector B, are I-129 (78 %) and Tc-99 (21 %) with the major pathway contributor being water ingestion (95 %). Uncertainty parameters influencing the physical conditions affecting the release and transport of contaminants with respect to the sampled values are identified below, along with their respective values from the deterministic model. The deterministic value is presented within parentheses.

Infiltration rate distribution = steady state at 12.45 in/yr (steady state at 10.61 in/yr)
Unsaturated zone thickness under FDCs = 14.5 meter (12.8 meter)
Saturated zone thickness = 19.4 meter (20 meter)
Saturated zone Darcy velocity multiplier (unitless) = 0.94 (1)

Parameters that are specific to the transport of I-129 are

Iodine K_d in Reduced Region II cement = 5.3 mL/g (9 mL/g)
Iodine K_d in Oxidized Region II cement = 12.3 mL/g (15 mL/g)
I-129 inventory in select saltstone disposal units:
- FDC 15 (A,B,C,D) = 0.53 curie (0.38 curie)

Parameters that are specific to the transport of Tc-99 are

Technetium solubility = 1E-07 mol/L

Parameters affecting the estimate of the dose by pathway are identified below. The deterministic value is presented within parentheses.

Consumption of water = 1,521 L/yr (377 L/yr)
Fraction of drinking water from a contaminated source (unitless) = 0.91 (0.87)

Realization TcRS2-101

As indicated in Table 5.6-7, the major radionuclide contributor to the peak MOP dose, at Sector K, is I-129 (97 %) with the major pathway contributors being fish ingestion (67 %) and water ingestion (29 %). Uncertainty parameters influencing the physical conditions affecting the release and transport of contaminants with respect to the sampled values are identified below, along with their respective values from the deterministic model. The deterministic value is presented within parentheses.

Infiltration rate distribution = steady state at 12.45 in/yr (steady state at 10.61 in/yr)
Unsaturated zone thickness under FDCs = 15.1 meter (12.8 meter)
Saturated zone thickness = 13.2 meter (20 meter)
Saturated zone Darcy velocity multiplier (unitless) = 0.75 (1)

Parameters that are specific to the transport of I-129 are

Iodine K_d in Reduced Region II cement = 4.8 mL/g (9 mL/g)
Iodine K_d in Oxidized Region II cement = 5.3 mL/g (15 mL/g)
I-129 inventory in select saltstone disposal units:
- FDC 9 (A,B,C,D) = 0.40 curie (0.38 curie)

Parameters affecting the estimate of the dose by pathway are identified below. The deterministic value is presented within parentheses.

Consumption of water = 235 L/yr (377 L/yr)
Fraction of drinking water from a contaminated source (unitless) = 0.86 (0.87)
Consumption of fish = 8.35 kg/yr (5.62 kg/yr)
Biotic accumulation multiplier factor for fish (unitless) = 11.8 (1)
Fraction of MOP that fish (unitless) = 0.45 (0.325)

Realization TcRS2-813

As indicated in Table 5.6-7, the major radionuclide contributor to the peak MOP dose, at Sector H, is I-129 (95 %) with the major pathway contributors being water ingestion (59 %) and fish ingestion (39 %). Uncertainty parameters influencing the physical conditions affecting the release and transport of contaminants with respect to the sampled values are identified below, along with their respective values from the deterministic model. The deterministic value is presented within parentheses.

Infiltration rate distribution = steady state at 10.61 in/yr (steady state at 10.61 in/yr)
Unsaturated zone thickness under FDCs = 9.2 meter (12.8 meter)
Saturated zone thickness = 17.4 meter (20 meter)
Saturated zone Darcy velocity multiplier (unitless) = 0.90 (1)

Parameters that are specific to the transport of I-129 are

Iodine K_d in Reduced Region II cement = 2.4 mL/g (9 mL/g)
Iodine K_d in Oxidized Region II cement = 8.4 mL/g (15 mL/g)
I-129 inventory in select FDCs:
- FDC 8 (A,B,C,D) = 0.35 curie (0.38 curie)

Parameters affecting the estimate of the dose by pathway are identified below. The deterministic value is presented within parentheses.

Consumption of water = 721 L/yr (377 L/yr)
Fraction of drinking water from a contaminated source (unitless) = 0.93 (0.87)
Consumption of fish = 15.2 kg/yr (5.62 kg/yr)
Biotic accumulation multiplier factor for fish (unitless) = 6.31 (1)
Fraction of MOP that fish (unitless) = 0.40 (0.325)

Realization TcRS2-292

As indicated in Table 5.6-7, the major radionuclide contributor to the peak MOP dose, at Sector G, is I-129 (99 %) with the major pathway contributors being water ingestion (94 %) and fish ingestion (5 %). Uncertainty parameters influencing the physical conditions affecting the release and transport of contaminants with respect to the sampled values are identified below, along with their respective values from the deterministic model. The deterministic value is presented within parentheses.

Infiltration rate distribution = steady state at 12.45 in/yr (steady state at 10.61 in/yr)
Unsaturated zone thickness under FDCs = 10.7 m (12.8 m)
Saturated zone thickness = 21.3 m (20 m)
Saturated zone Darcy velocity multiplier (unitless) = 1.04 (1)

Parameters that are specific to the transport of I-129 are

Iodine K_d in Reduced Region II cement = 2.4 mL/g (9 mL/g)
Iodine K_d in Oxidized Region II cement = 23.9 mL/g (15 mL/g)
I-129 inventory in select saltstone disposal units:
- FDC 5 (A,B,C,D) = 0.38 curie (0.38 curie)
- FDC 8 (A,B,C,D) = 0.42 curie (0.38 curie)

Parameters affecting the estimate of the dose by pathway are identified below. The deterministic value is presented within parentheses.

Consumption of water = 1,361 L/yr (377 L/yr)
Fraction of drinking water from a contaminated source (unitless) = 0.82 (0.87)
Consumption of fish = 12.9 kg/yr (5.62 kg/yr)
Biotic accumulation multiplier factor for fish (unitless) = 1.64 (1)
Fraction of MOP that fish (unitless) = 0.27 (0.325)

5.6.5 Sensitivity Analysis using the SDF Probabilistic Model

Given the uncertainties presented in Section 5.6.4, the next step was to identify those input parameters and other stochastic entities in the model that led to those uncertainties. Even in complex models, the results are often strongly dependent on only a handful of parameters. What is important for one result (e.g., the I-129 concentration) may be insignificant for another, such as the maximum dose achieved within 20,000 years. In fact, the dose to the MOP will have different sensitivities at different times, since it is driven by the presence of different radionuclides. For example, a MOP dose may be dominated by I-129 at one time and by Cs-135 or Tc-99 at another time, and these doses will be determined by different aspects of the model (different K_ds, dose conversion factors, etc.). Extracting the important model inputs for results of interest is the subject of the sensitivity analysis.

5.6.5.1 Introduction to SDF Probabilistic Model Sensitivity Analysis

Complex modeling, such as the probabilistic modeling of the SDF, is needed to explore dynamics of systems where multiple variables interact in a nonlinear manner. The probabilistic simulation approach used in the GoldSim model propagates uncertainty regarding the independent variables (e.g., inputs such as physical soil properties or inventory) through the model to the dependent variable or predicted response (e.g., dose or concentration). One of the goals of sensitivity analysis is to identify which independent variables have distributions that exert the greatest influence on the response.

The primary sensitivity analysis procedures in use involve the determination and presentation of partially ranked correlation coefficients (PRCCs) and stepwise rank regression analyses.

5.6.5.2 Partially Ranked Correlation Coefficients

PRCCs provide a measure of the strength of the monotonic relationships between an independent variable and a specific model result after a correction has been made to remove the monotonic effects of the other independent variables in the analysis (i.e., one independent variable is analyzed at a time by isolating and ignoring the combined effects of the other independent variables). Many of the independent variables have varying effects on the results as a function of time. For such variables, the presentation of PRCCs as functions of time provides an informative display of sensitivity analysis results.

As indicated by the name, PRCCs involve the analysis of rank-transformed data. With this approach, the values for variables are replaced with their ranks and then the PRCCs are calculated with these ranks rather than with the original values for the variables. Specifically, the smallest value of a variable is given a rank of 1, the next largest value is given a rank of 2, equal observations are assigned the average of what their ranks would have been if they had not been equal, and so on up to the largest value, which is given a rank equal to the number of sample elements in use. The effect of the rank transformation is to transform monotonic relationships into linear relationships. Further, the rank transform tends to reduce the skewing effects of outliers, which permits the regression analysis to represent the general relationships between the inputs and the specific result. Although no variable transformation is universally successful in improving the resolution of a sensitivity analysis in the presence of nonlinear relationships, the rank transformation has been found to be a

broadly effective and useful means of enhancing the insights in sensitivity analyses based on partial correlation and in sensitivity analyses based on stepwise regression.

The figures in Section 5.6.5.4 show the PRCCs over time, as determined using the sampling results from sets of 1,000 realizations (see Table 5.6-4). Thus, at each modeled time step there are 1,000 values for each result, for which a PRCC is calculated.

Note that due to the large number of variables in the SDF GoldSim Model and computational limitations of analyzing such large datasets, these PRCC calculations were performed using a sub-set of the variables. For example, variables related to Eu-154, which has very little influence over dose results, were screened out, while variables that were specific to I-129 and Cs-135 were explicitly screened in for these analyses.

For the analysis of the *SRS Saltstone v4.101* model results (TcRS1 and TcRS2) only used about 250 of the nearly 4,400 variables were used as inputs in this analysis. The exclusion of low-impact variables reduces the occurrence of spurious correlations in the PRCC calculation results. Also, the computational demands of this type of analysis limited the analysis to 1,000 realizations at a time.

To limit the number of time-dependent PRCC curves in a given plot frame, the analysis only examined variables whose PRCCs exceed 0.25 in absolute value at some point in time. Further, the PRCC plots only show PRCC curves for the eight variables with the PRCCs that had the largest absolute value over the time interval under consideration. Variables with PRCCs with a smaller absolute value than 0.25 have only a limited monotonic effect on the results under consideration. In the legend of a figure showing PRCCs, the variables are listed in decreasing order of PRCC (i.e., the variable having the largest PRCC in absolute value is listed first).

Values of PRCCs fall in the interval [−1, 1], where:

- positive PRCCs indicate that two variables tend to increase and decrease together (i.e., the independent variable has a positive effect on the dependent variable),
- negative PRCCs indicate that two variables tend to move in opposite directions (i.e., the independent variable has a negative effect on the dependent variable), and
- the absolute value of a PRCC indicate the strength of the relationship between two variables (i.e., a PRCC close to 1 in absolute value indicates a strong monotonic relationship between two variables after the removal of the monotonic effects associated with the other independent variables under consideration).

5.6.5.3 Stepwise Rank Regression

An alternative to the use of PRCCs is to carry out stepwise rank regressions to determine the effects of uncertain inputs on analysis results of interest. In analyses of this type, the regressions are carried out with rank transformed variables as previously discussed rather than with the original values.

In a stepwise rank regression, the single independent variable that makes the largest contribution to the uncertainty in the dependent variable (result) is selected in the first step. Then, at the second step, the single independent variable that, in conjunction with the first variable, makes the largest contribution to the uncertainty in the dependent variable is

selected. This process then continues until no additional variables are found that make identifiable (i.e., significant) contributions to the uncertainty in the dependent variable; at this point, the stepwise selection process terminates. For these analyses, a significance level of $\alpha_{in} = 0.15$ is used as the criterion for entering variables into the stepwise regression and $\alpha_{out} = 0.20$ was used for dropping variables from the stepwise regression analysis. Selection of these significance levels was based on preliminary sensitivity analyses, in which it was observed that a greater value tended to introduce obviously spurious variables into the regression models. In the context of stepwise regression analysis, variable importance is indicated by (1) the order of selection in the stepwise selection process, (2) incremental changes in R^2 values with the successive entry of individual variables into the regression model, and (3) the sign and size of the standardized regression coefficients in the final regression model. Because rank transformed values were used, the standardized regression coefficients are more correctly identified as standardized rank regression coefficients (SRRCs) in the tables below.

The R^2 value corresponds to the fraction of the uncertainty in the dependent variable that is accounted for by a regression model. Thus, R^2 values monotonically increase as additional variables are added to the regression model and, for a very successful regression analysis, approach 1 as additional variables are added to the model. The SRRCs provide a measure of the fractional contribution of individual independent variables to the uncertainty in the dependent variable under consideration. Further, like PRCCs, a positive SRRC indicates that the independent variable and dependent variable tend to increase and decrease together, and a negative SRRC indicates that the independent variable and dependent variable tend to move in opposite directions.

As discussed above, the PRCCs are computed as a function of time. In contrast, SRRCs are computed at fixed times (i.e., for each dependent variable, the time of the peak of the mean is used). These times for SRRC computation were chosen to illustrate the changes in importance of uncertain parameters over time. The same analysis times are generally used for analysis of all SDF model output variables to facilitate comparisons between the sensitivity analysis results across output variables.

Related, but not identical, information is provided by PRCCs and SRRCs. Specifically, PRCCs measure the strength of the monotonic relationship between an independent variable and a dependent variable after correcting for the effects of other independent variables, and SRRCs provide a measure of the fractional contribution of an individual independent variable to the uncertainty in the dependent variable under consideration. Except in rare situations involving SRRCs from a regression model involving multiple correlated variables, PRCCs and SRRCs have the same sign, which indicates either a positive or a negative correlation between an input variable and an output variable. Because PRCCs are selected for display based on the maximum absolute value over time, and SRRCs are computed at specific times, the selection and order of important variables indicated by PRCCs and SRRCs may be different between the two analyses.

As described in the PRCC analysis discussion above, subsets of the nearly 4,400 variables were used as inputs in these analyses. Low-impact variables were excluded from these

analyses in response to computational limitation and to reduce the occurrence of spurious correlations in the PRCC calculation results.

5.6.5.4 Sensitivity Analysis Results

This section presents sensitivity analysis results for the following endpoints, (1) total dose to the MOP at any sector, (2) maximum total dose to the MOP at Sector B, (3) maximum total dose to the MOP at Sector G, (4) I-129 dose to the MOP at any various sectors, (5) Tc-99 dose to the MOP at any various sectors, and (6) Cs-135 dose to the MOP at various sectors. Sectors B and G were selected because the peak of the mean doses from each of these sectors represent the highest southern sector mean and northern sector mean, respectively (see Figures 5.6-45 and 5.6-46). The dose results from I-129, Tc-99, and Cs-135 were chosen because they are the three most dominant dose contributors.

Sensitivity Analysis of the Total Dose to the MOP at Any Sector

The PRCCs for total dose to the MOP at any sector are depicted in the following Figures 5.6-46 and 5.6-47. As shown in Section 5.6.4, peak doses occurred between 1,000 and 10,000 years after closure; therefore, the analysis of PRCCs only depict the results within this applicable timeframe. These figures show PRCC results from two separate GoldSim runs (TcRS1 and TcRS2). The order (and therefore the colors) assigned to each variable within these figures is based on the magnitude of the peak absolute value of the PRCC value expressed in each analysis. Although the order of the variables shown in these figures of the TcRS1 and TcRS2 results may vary, the overall results are generally similar.

Figure 5.6-46: Total Dose to MOP PRCCs Any Sector, 1,000 Realizations (Model TcRS1)

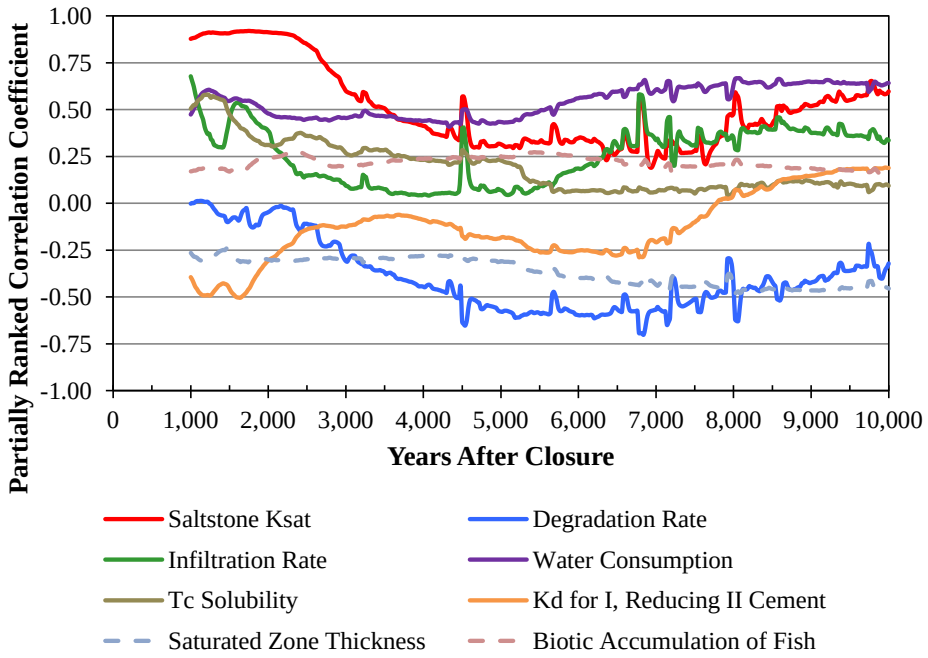

Figure 5.6-47: Total Dose to MOP PRCCs Any Sector, 1,000 Realizations (Model TcRS2)

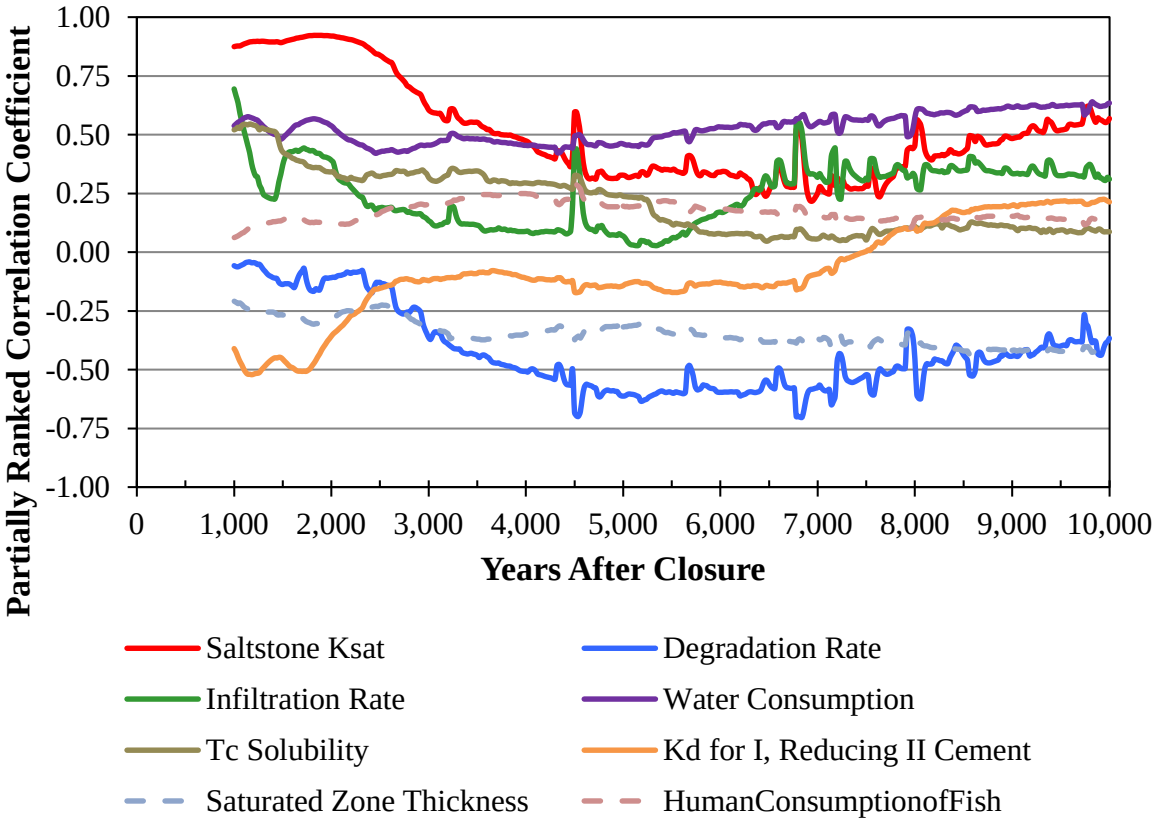

The key variables selected closely reflect those identified as important in the single-realization analyses discussed in Section 5.6.4.3.

Table 5.6-8 shows the results from the stepwise regression analysis. Again, results from two 1,000-realization models (TcRS1 and TcRS2) are depicted. The table only shows the first six variables from each model as the importance of each variable quickly diminishes with each successive analysis step. In this analysis, the first four or five variables effectively dominate any influence over the dependent variable at the time of the peak of the mean.

Table 5.6-8: MOP Total Dose Top Six SRRC Results, Any Sector at Time of Peak of the Mean Value

SRRCs Using 1,000 Realizations from Model TcRS1, t = 1,520 years, R^2 = 0.89			SRRCs Using 1,000 Realizations from Model TcRS2, t = 1,520 years, R^2 = 0.86		
Variable	**Cumulative R^2**	**SRRC**	**Variable**	**Cumulative R^2**	**SRRC**
Saltstone K_{sat}	0.67	0.80	Saltstone K_{sat}	0.65	0.82
Water Consumption	0.72	0.23	Water Consumption	0.70	0.24
Infiltration Rate	0.77	0.21	K_d for Iodine, Reduced Region II Cement	0.74	-0.21
K_d for Iodine, Reduced Region II Cement	0.81	-0.19	Technetium Solubility	0.78	0.19
Technetium Solubility	0.84	0.18	Infiltration Rate	0.80	0.18
Saturated Zone Thickness	0.85	-0.10	Saturated Zone Thickness	0.82	-0.11

Both sets of realizations yield the same variables as the top three and both with similar values for the cumulative R^2 and SRRC values. This provides confidence in the identification of these three variables as important.

Specifically, "Saltstone K_{sat}" (i.e., the variable that selects the initial value for the saturated hydraulic conductivity in saltstone), "K_d for Iodine, Reduced Region II Cement" (i.e., the K_d value for iodine in Reduced Region II cementitious materials), and "Water Consumption" (the rate at which the MOP consumes water) are the dominant variables. Note that the R^2 values for "Saltstone K_{sat}" under represent the effect of this variable because of the nonlinear relationship between this variable and total dose to the MOP. Figure 5.6-48 illustrates the nonlinearity in the sampling of the initial hydraulic conductivity of saltstone with respect to the peak MOP doses for the sampled realizations, where initial conductivity sampled three discrete values (3.9E-10 cm/s, 6.4E-09 cm/s, and 4.5E-07 cm/s).

Figure 5.6-48: Peak MOP Doses within 10,000 Years vs. Sampling of Initial Hydraulic Conductivity in Saltstone

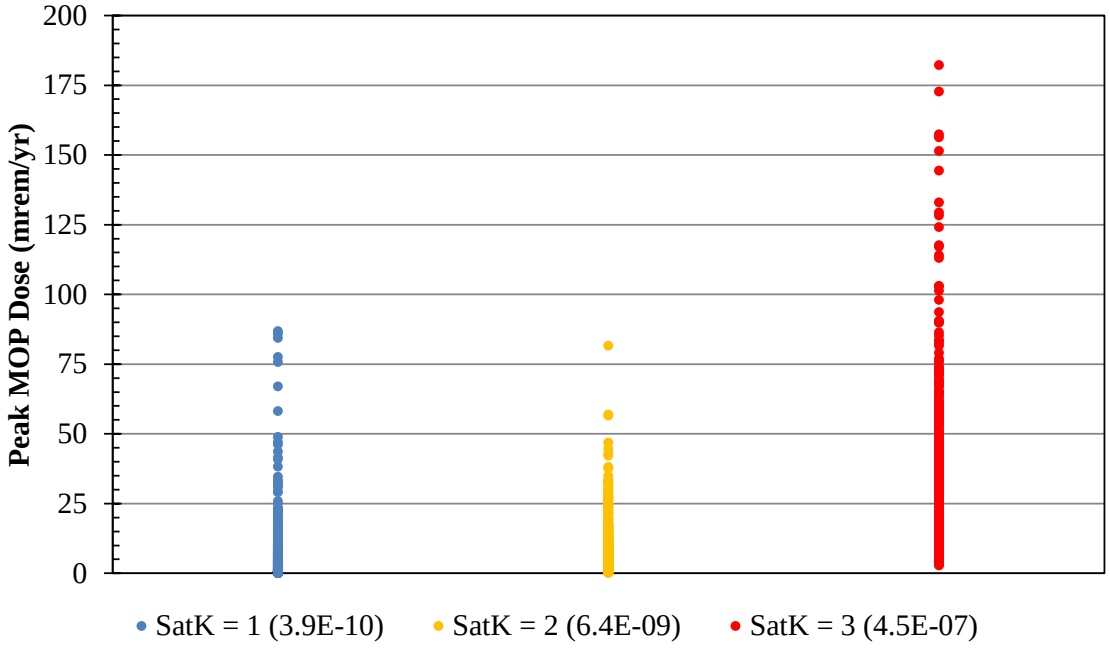

Sensitivity Analysis of the Total Dose to the MOP at Sector B

The PRCCs for total dose to the MOP at Sector B are shown in the following Figures 5.6-49 and 5.6-50.

Figure 5.6-49: PRCCs of MOP Total Dose, Sector B, 1,000 Realizations (Model TcRS1)

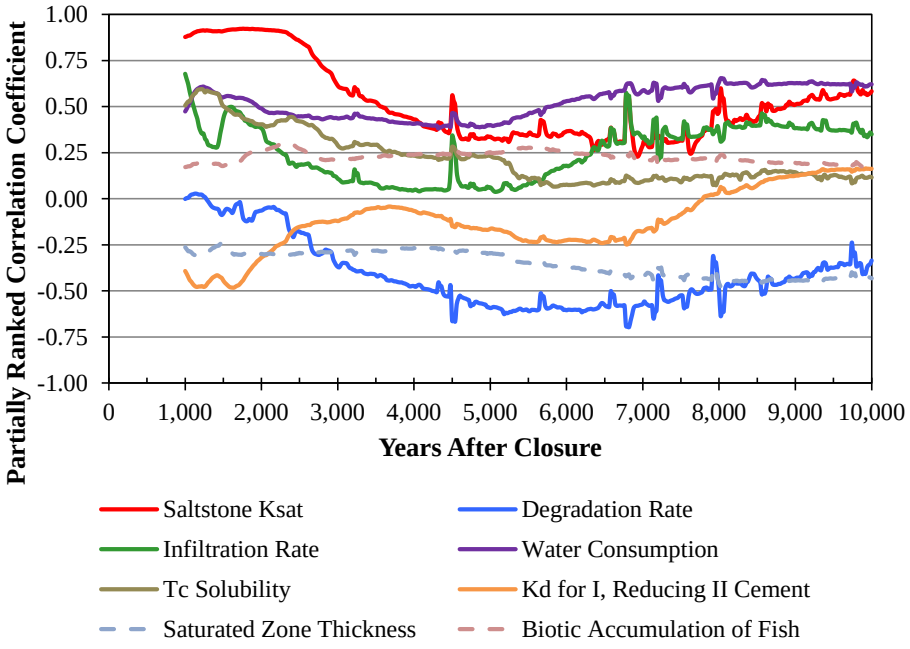

Figure 5.6-50: PRCCs of MOP Total Dose, Sector B, 1,000 Realizations (Model TcRS2)

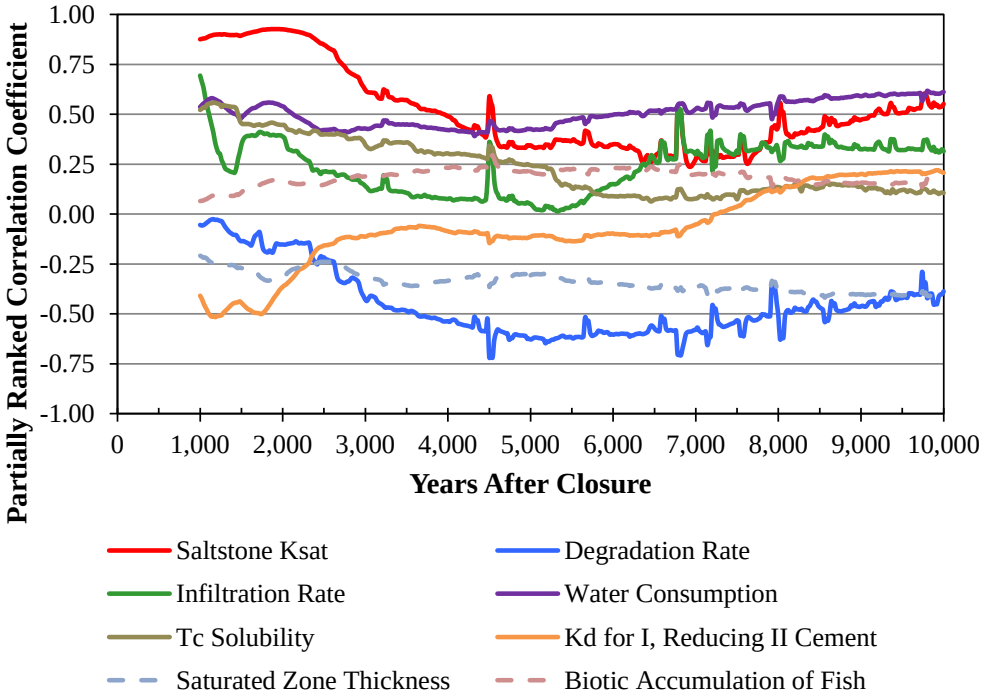

Table 5.6-9 shows the results from the stepwise regression analysis. Again, results from two 1,000-realization models (TcRS1 and TcRS2) are depicted.

Table 5.6-9: MOP Total Dose Top Six SRRC Results, Sector B at Time of Peak of the Mean Value

SRRCs Using 1,000 Realizations from Model TcRS1, t = 1,520 years, R^2 = 0.89			SRRCs Using 1,000 Realizations from Model TcRS2, t = 1,520 years, R^2 = 0.87		
Variable	**Cumulative R^2**	**SRRC**	**Variable**	**Cumulative R^2**	**SRRC**
Saltstone K_{sat}	0.67	0.80	Saltstone K_{sat}	0.65	0.82
Water Consumption	0.73	0.23	Water Consumption	0.70	0.23
Technetium Solubility	0.77	0.20	Technetium Solubility	0.74	0.20
Infiltration Rate	0.81	0.20	K_d for Iodine, Reduced Region II Cement	0.78	-0.20
K_d for Iodine, Reduced Region II Cement	0.84	-0.18	Infiltration Rate	0.80	0.17
Saturated Zone Thickness	0.85	-0.10	Saturated Zone Thickness	0.82	-0.11

Sensitivity Analysis of the Total Dose to the MOP at Sector G

The PRCCs for total dose to the MOP at Sector G are depicted in the following Figures5.6-51 and 5.6-52.

Figure 5.6-51: PRCCs of MOP Total Dose, Sector G, 1,000 Realizations (Model TcRS1)

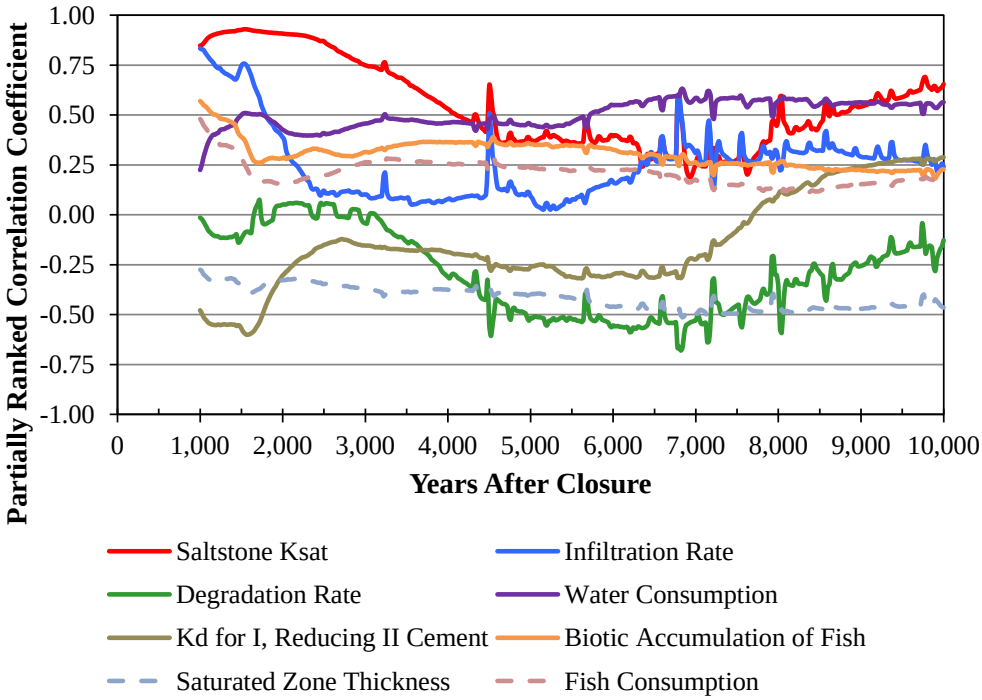

Figure 5.6-52: PRCCs of MOP Total Dose, Sector G, 1,000 Realizations (Model TcRS2)

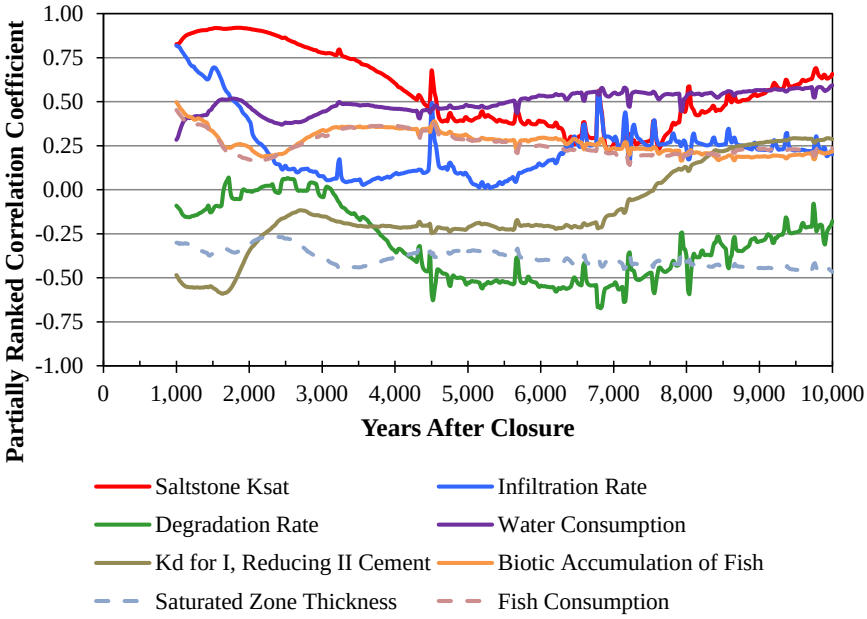

Table 5.6-10 shows the results from the stepwise regression analysis. Again, results from two 1,000-realization models (TcRS1 and TcRS2) are depicted.

Table 5.6-10: MOP Total Dose Top Six SRRC Results, Sector G at Time of Peak of the Mean Value

SRRCs Using 1,000 Realizations from Model TcRS1, t = 1,520 years, R^2 = 0.92			SRRCs Using 1,000 Realizations from Model TcRS2, t = 1,520 years, R^2 = 0.90		
Variable	**Cumulative R^2**	**SRRC**	**Variable**	**Cumulative R^2**	**SRRC**
Saltstone K_{sat}	0.64	0.77	Saltstone K_{sat}	0.63	0.80
Infiltration Rate	0.76	0.36	Infiltration Rate	0.73	0.34
K_d for Iodine, Reduced Region II Cement	0.81	-0.22	K_d for Iodine, Reduced Region II Cement	0.78	-0.24
Water Consumption	0.85	0.18	Water Consumption	0.82	0.19
Biotic Accumulation of Fish	0.86	0.12	Saturated Zone Thickness	0.84	-0.13
Saturated Zone Thickness	0.88	-0.13	Biotic Accumulation of Fish	0.85	0.12

Sensitivity Analysis of the I-129 Dose to the MOP

The PRCCs and SRRCs for maximum I-129 dose to the MOP at various sectors (B and G) are depicted in Figures 5.6-53 through 5.6-56 and summarized in the Table 5.6-11, below.

Figure 5.6-53: PRCCs of MOP Max I-129 Dose, Sector B, 1,000 Realizations (Model TcRS1)

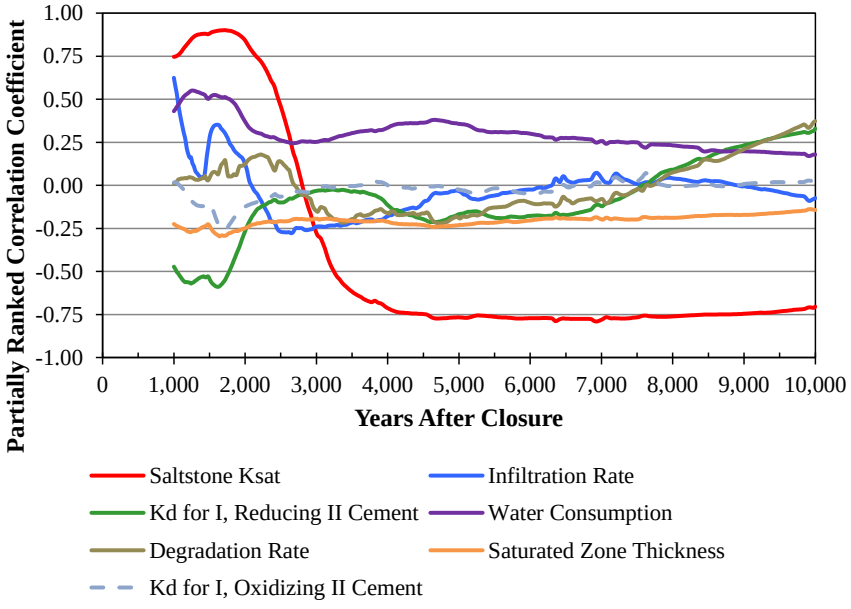

Figure 5.6-54: PRCCs of MOP Max I-129 Dose, Sector G, 1,000 Realizations (Model TcRS1)

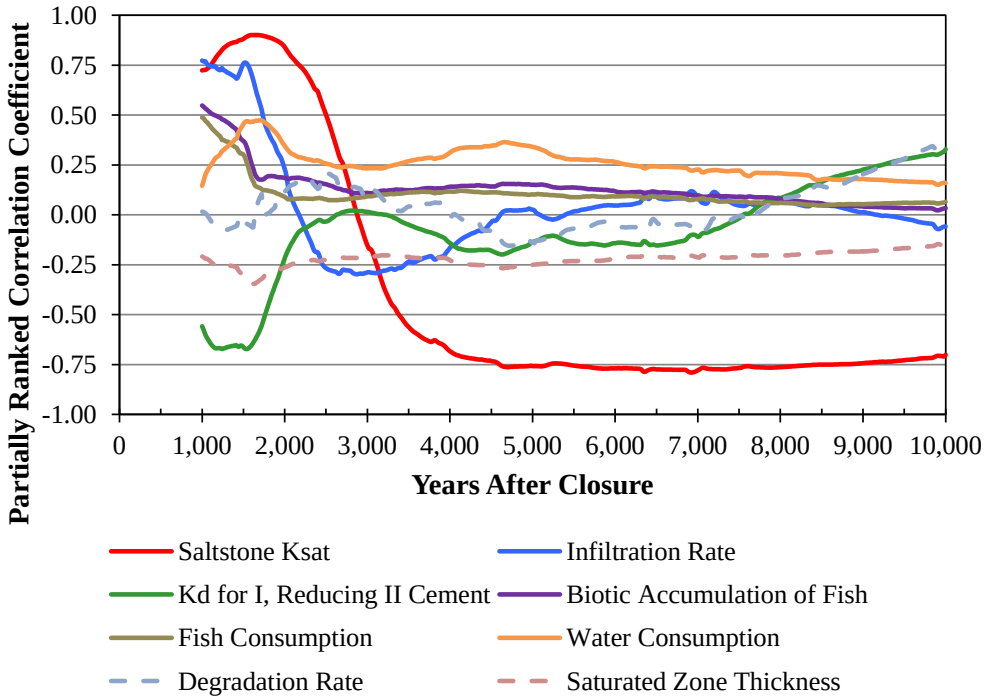

Figure 5.6-55: PRCCs of MOP Max I-129 Dose, Sector B, 1,000 Realizations (Model TcRS2)

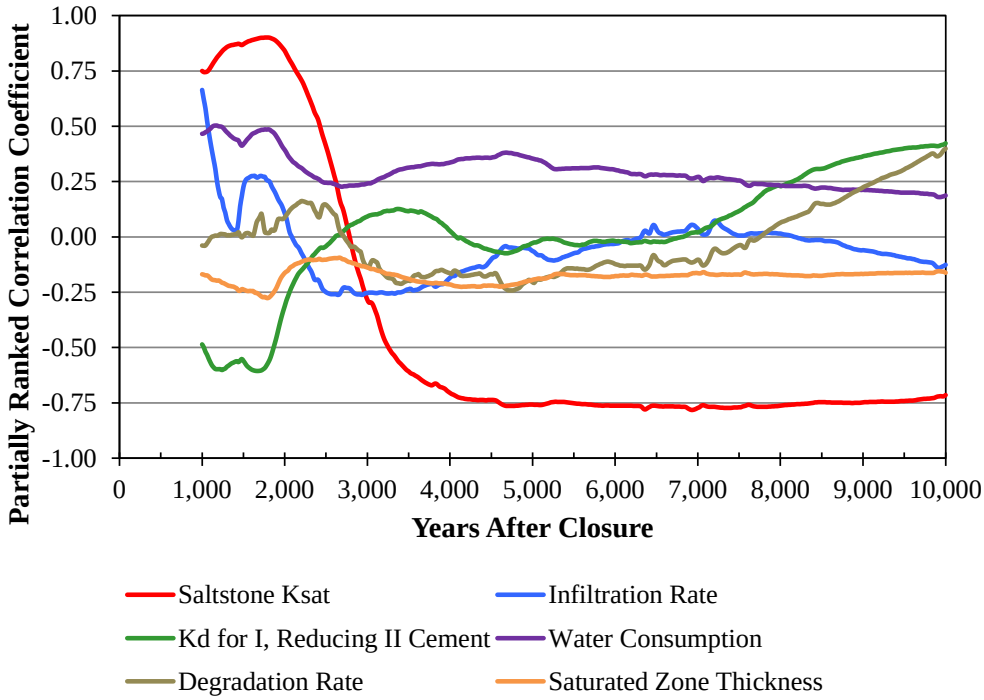

Figure 5.6-56: PRCCs of MOP Max I-129 Dose, Sector G, 1,000 Realizations (Model TcRS2)

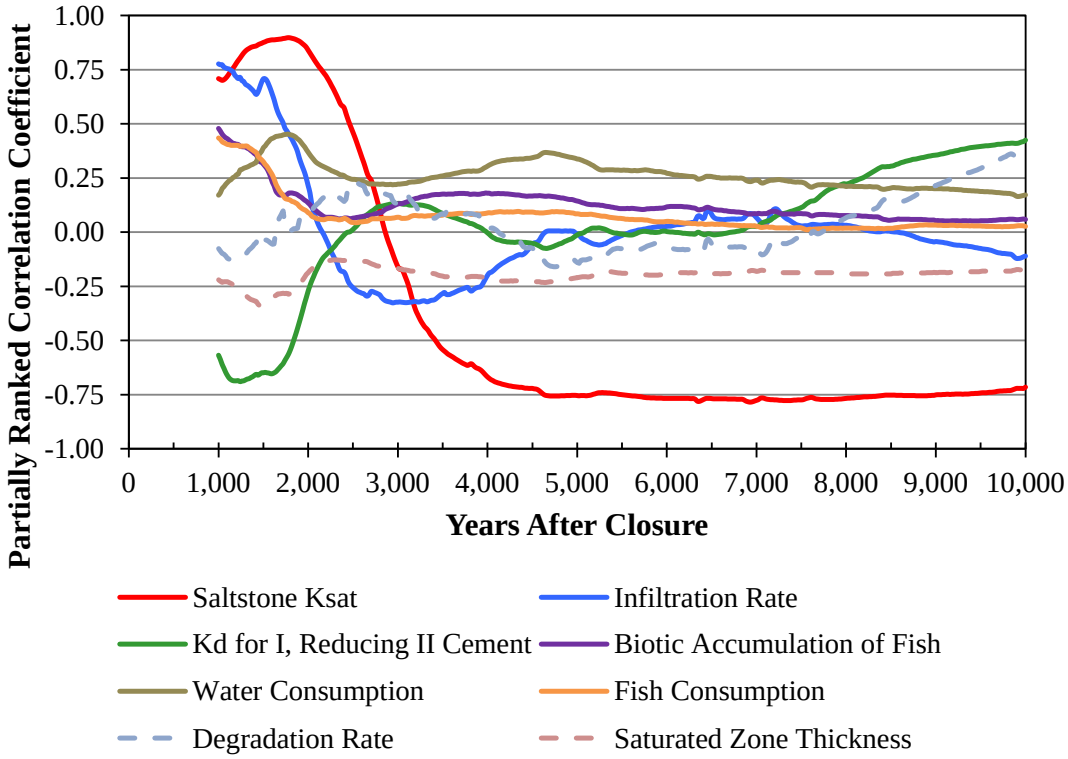

Table 5.6-11: MOP Max I-129 Dose Top Six SRRC Results at Time of Peak of the Mean Value (*SRS Saltstone v4.101*)

SRRCs Using 1,000 Realizations from Model TcRS1 (Sector B), t = 1,520 years, R^2 = 0.87			SRRCs Using 1,000 Realizations from Model TcRS2 (Sector B), t = 1,520 years, R^2 = 0.84		
Variable	**Cumulative R^2**	**SRRC**	**Variable**	**Cumulative R^2**	**SRRC**
Saltstone K_{sat}	0.66	0.78	Saltstone K_{sat}	0.63	0.80
K_d for Iodine, Reduced Region II Cement	0.73	-0.27	K_d for Iodine, Reduced Region II Cement	0.71	-0.31
Water Consumption	0.79	0.24	Water Consumption	0.77	0.22
Infiltration Rate	0.81	0.14	Saturated Zone Thickness	0.78	-0.11
Saturated Zone Thickness	0.82	-0.11	Infiltration Rate	0.79	0.12
Biotic Accumulation of Fish	0.82	0.06	Fish Consumption	0.79	0.08

Table 5.6-11: MOP Max I-129 Dose Top Six SRRC Results at Time of Peak of the Mean Value (*SRS Saltstone v4.101*) (Continued)

SRRCs Using 1,000 Realizations from Model TcRS1 (Sector G), t = 1,520 years, R^2 = 0.89			SRRCs Using 1,000 Realizations from Model TcRS2 (Sector G), t = 1,520 years, R^2 = 0.87		
Variable	**Cumulative R^2**	**SRRC**	**Variable**	**Cumulative R^2**	**SRRC**
Saltstone K_{sat}	0.53	0.69	Saltstone K_{sat}	0.51	0.73
Infiltration Rate	0.69	0.42	Infiltration Rate	0.65	0.39
K_d for Iodine, Reduced Region II Cement	0.78	-0.30	K_d for Iodine, Reduced Region II Cement	0.75	-0.33
Water Consumption	0.82	0.19	Water Consumption	0.79	0.18
Biotic Accumulation of Fish	0.84	0.13	Saturated Zone Thickness	0.80	-0.13
Saturated Zone Thickness	0.85	-0.12	Biotic Accumulation of Fish	0.82	0.12

Sensitivity Analysis of the Tc-99 Dose to the MOP

The PRCCs and SRRCs for maximum Tc-99 dose to the MOP at Sectors B and G are depicted in Figures 5.6-57 through 5.6-60 and summarized in Table 5.6-12. As with the analysis of I-129 doses above, the following analysis of Tc-99 doses uses the TcRS1 and TcRS2 model data and focuses on Sectors B and G.

Figure 5.6-57: PRCCs of MOP Max Tc-99 Dose, Sector B, 1,000 Realizations (Model TcRS1)

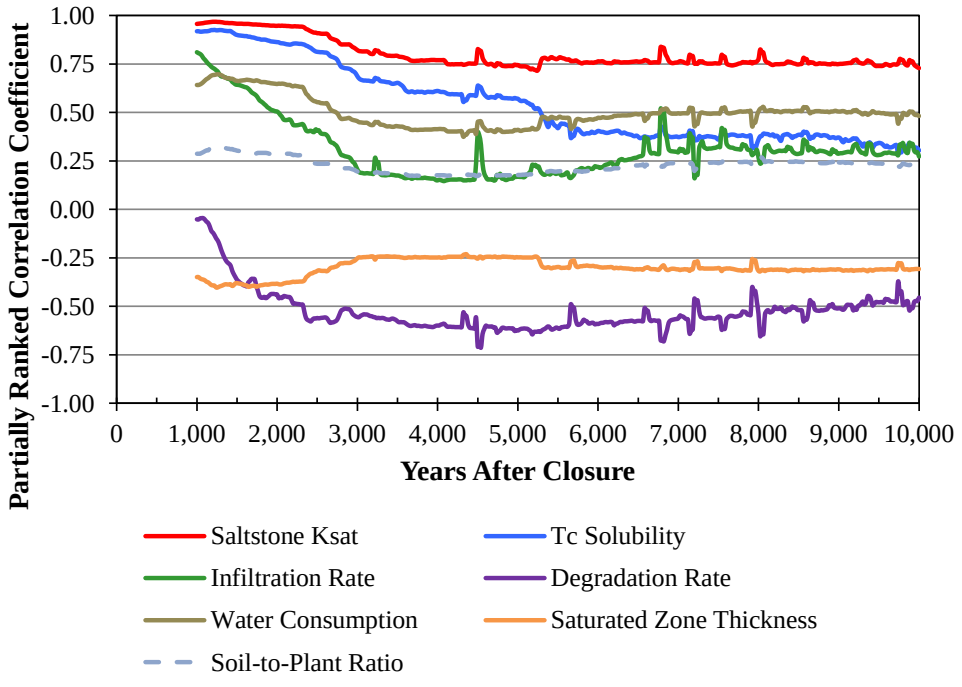

Figure 5.6-58: PRCCs of MOP Max Tc-99 Dose, Sector G, 1,000 Realizations (Model TcRS1)

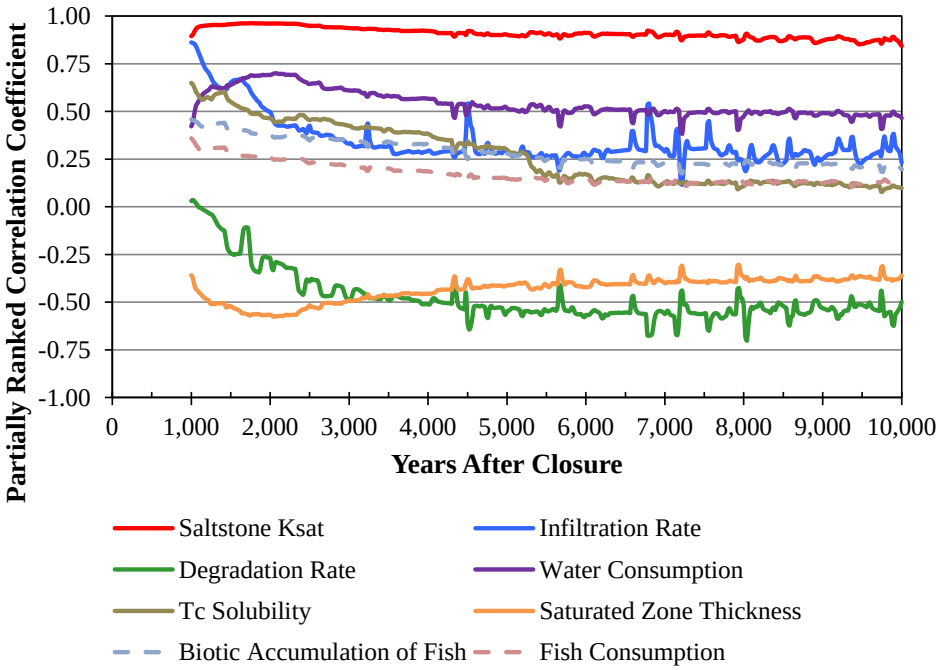

Figure 5.6-59: PRCCs of MOP Max Tc-99 Dose, Sector B, 1,000 Realizations (Model TcRS2)

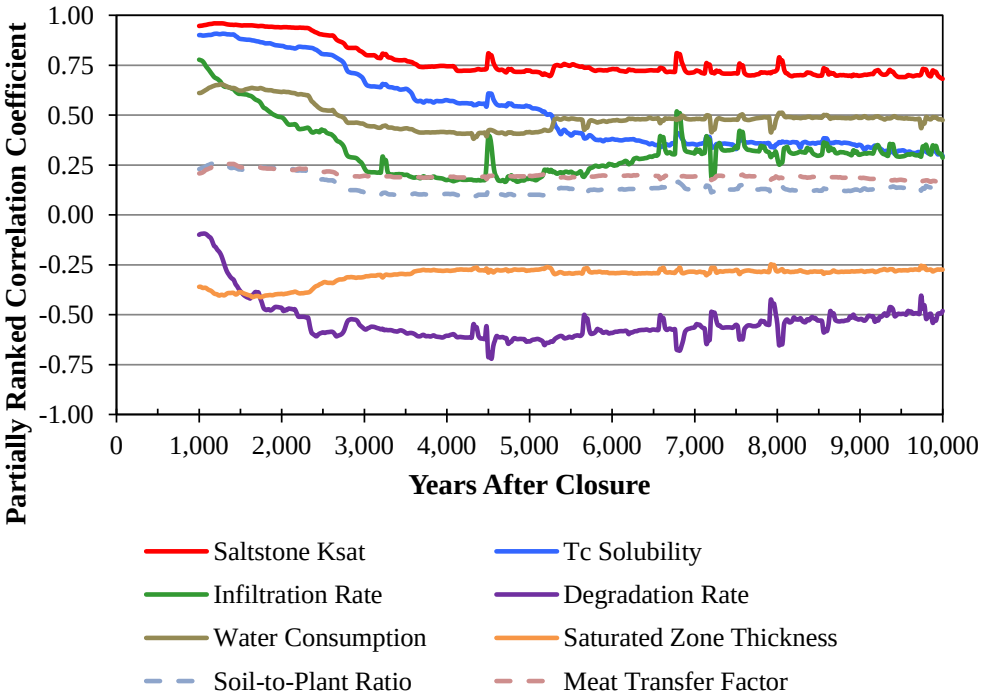

Figure 5.6-60: PRCCs of MOP Max Tc-99 Dose, Sector G, 1,000 Realizations (Model TcRS2)

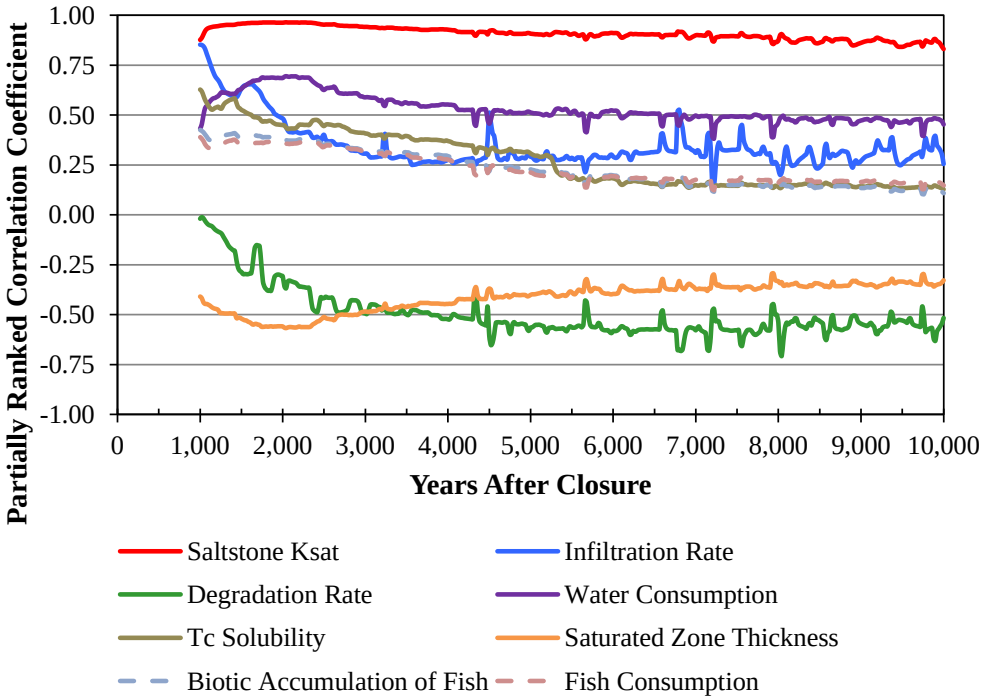

Table 5.6-12: MOP Max Tc-99 Dose Top Six SRRC Results at Time of Peak of the Mean Value (*SRS Saltstone v4.101*)

SRRCs Using 1,000 Realizations from Model TcRS1 (Sector B), t = 1,520 years, R^2 = 0.95			SRRCs Using 1,000 Realizations from Model TcRS2 (Sector B), t = 1,520 years, R^2 = 0.94		
Variable	**Cumulative R^2**	**SRRC**	**Variable**	**Cumulative R^2**	**SRRC**
Saltstone K_{sat}	0.58	0.78	Saltstone K_{sat}	0.58	0.77
Technetium Solubility	0.82	0.47	Technetium Solubility	0.82	0.48
Water Consumption	0.87	0.20	Water Consumption	0.86	0.21
Infiltration Rate	0.91	0.20	Infiltration Rate	0.90	0.20
Saturated Zone Thickness	0.92	-0.10	Saturated Zone Thickness	0.91	-0.11
Degradation Rate	0.93	-0.10	Degradation Rate	0.92	-0.11

Table 5.6-12: MOP Max Tc-99 Dose Top Six SRRC Results at Time of Peak of the Mean Value (*SRS Saltstone v4.101*) (Continued)

SRRCs Using 1,000 Realizations from Model TcRS1 (Sector G), t = 1,520 years, R^2 = 0.94			SRRCs Using 1,000 Realizations from Model TcRS2 (Sector G), t = 1,520 years, R^2 = 0.94		
Variable	**Cumulative R^2**	**SRRC**	**Variable**	**Cumulative R^2**	**SRRC**
Saltstone K_{sat}	0.73	0.85	Saltstone K_{sat}	0.74	0.88
Infiltration Rate	0.79	0.23	Water Consumption	0.79	0.22
Water Consumption	0.85	0.21	Infiltration Rate	0.83	0.22
Saturated Zone Thickness	0.87	-0.16	Saturated Zone Thickness	0.86	-0.16
Technetium Solubility	0.90	0.16	Technetium Solubility	0.89	0.16
Biotic Accumulation of Fish	0.91	0.11	Biotic Accumulation of Fish	0.90	0.12

Sensitivity Analysis of the Cs-135 Dose to the MOP

The dose contributions from Cs-135 are driven by seepline concentrations that are converted into doses via the fish ingestion pathway. Because seepline concentrations are determined as a fraction of the maximum 100-meter concentration, regardless of sector, there is less variability in the Cs-135 doses. For simplicity, the following analysis only examined only Sector B (for both TcRS1 and TcRS2) (Figures 5.6-61 and 5.6-62).

Figure 5.6-61: PRCCs of MOP Max Cs-135 Dose, Sector B, 1,000 Realizations (Model TcRS1)

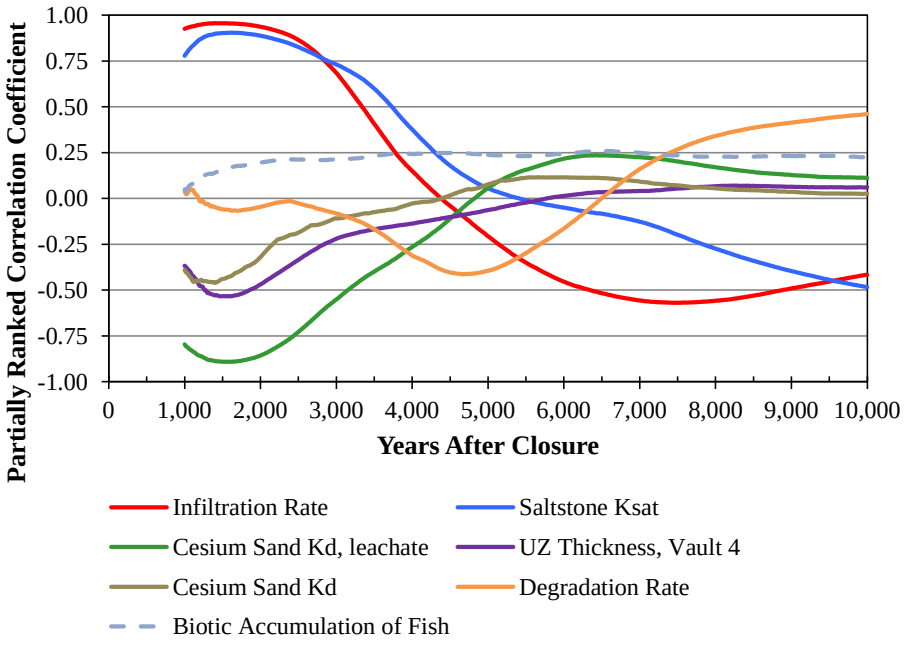

Figure 5.6-62: PRCCs of MOP Max Cs-135 Dose, Sector B, 1,000 Realizations (Model TcRS2)

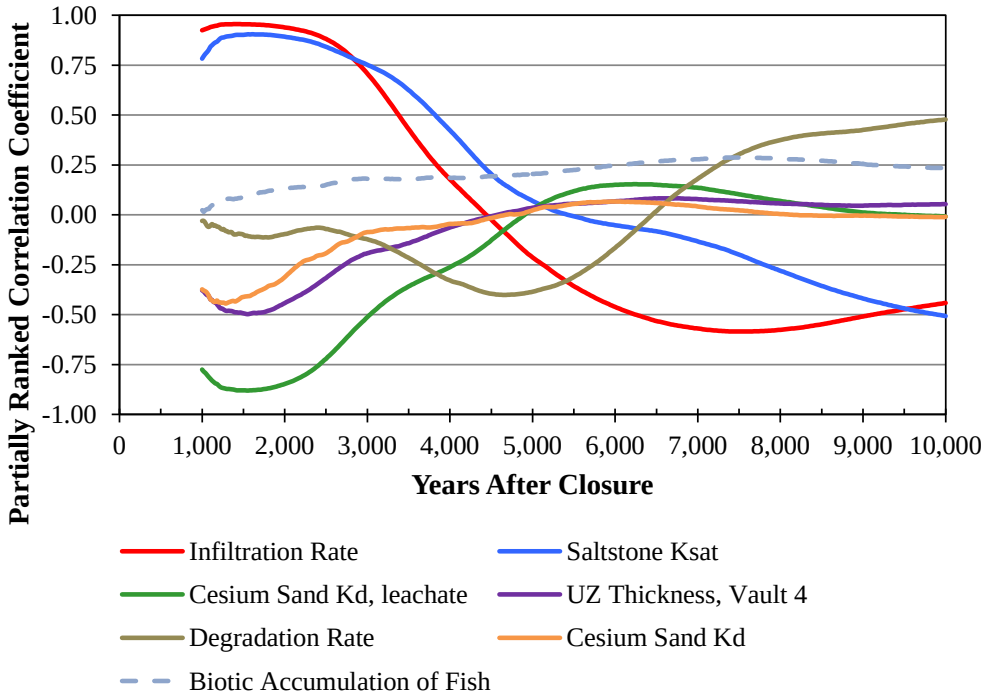

Table 5.6-13 shows the results from the stepwise rank regression analysis. Again, only results from Sector B (for TcRS1 and TcRS2) are depicted.

Table 5.6-13: MOP Max Cs-135 Dose Top Six SRRC Results at Select Locations at Time of Peak of the Mean Value

SRRCs Using 1,000 Realizations from Model TcRS1 (Sector B), t = 1,520 years, R^2 = 0.96			**SRRCs Using 1,000 Realizations from Model TcRS2 (Sector B), t = 1,520 years, R^2 = 0.96**		
Variable	**Cumulative R^2**	**SRRC**	**Variable**	**Cumulative R^2**	**SRRC**
Infiltration Rate	0.58	0.70	Infiltration Rate	0.55	0.74
Saltstone K_{sat}	0.76	0.44	Saltstone K_{sat}	0.76	0.46
Cesium Sand K_d, leachate	0.92	-0.41	Cesium Sand K_d, leachate	0.92	-0.41
Unsaturated Zone Thickness, SDU 4	0.94	-0.13	Unsaturated Zone Thickness, SDU 4	0.94	-0.13
Cesium Sand K_d	0.95	-0.10	Cesium Sand K_d	0.95	-0.10
Biotic Accumulation of Fish	0.95	0.04	K_d for Cesium, Reduced Region II Cement	0.95	-0.04

5.6.5.5 Summary of the SDF Probabilistic Model Sensitivity Analysis

The purpose of this section is to present general conclusions that can be made regarding the SDF GoldSim Model sensitivity analyses presented in Sections 5.6.5.2 through 5.6.5.4. The following recurring themes appeared in these sensitivity analyses:

- The primary dose contributors to the MOP dose within the first 10,000 years after closure are I-129, Tc-99, and Cs-135.
- The magnitude and timing of dose is most strongly influenced by the initial saturated hydraulic conductivity of saltstone, wherein the more conductive the saltstone, the greater and earlier the peak dose.
- Aside from the initial saturated hydraulic conductivity of saltstone, iodine transport is most strongly influenced by its K_d in Reduced Region II concrete and moderately influenced by its K_d in Oxidized Region II concrete.
- The magnitude of the peak dose is strongly impacted by the amount of water consumed by the MOP.
- Technetium solubility has more control over Tc-99 doses in Sector B (where SDU 4 has a large Tc-99 inventory) than in Sector G, where the Tc-99 inventory is more distributed.
- Dose contributions from Cs-135 are influenced by the infiltration rate and dose parameters related to the fish ingestion dose pathway.

5.6.6 Sensitivity Analyses Using PORFLOW

The purpose of this section is to consider the impact varying certain parameters might have on the SDF deterministic model, so that the sensitivity of the models to changes in select parameters expected to be of concern might be discovered.

5.6.6.1 Flow Cases of Interest (F10 and F20) Analyzed in PORFLOW

Section 4.4.3 presents the development of the various flow cases with Table 4.4-3 identifying the 38 flow cases being considered. Flow Cases F37 and F38 were specifically developed to evaluate the sensitivity that the roof slope on the FDC would have on potential releases from FDCs. Flow Cases F37 and F38 are analyzed in Section 5.6.6.2.

Two flow cases, F10 and F20 were selected to investigate the impact of flow variability on the potential groundwater dose to the MOP at 100 meters. Flow Case F10 was chosen to determine the potential dose to the MOP using flow parameters that could be considered as expected; that is, the best estimate degradation rate of cementitious material, the average infiltration rate and the average, or nominal, initial saturated hydraulic conductivity of 6.4E-09 cm/s for saltstone. Flow Case F20 was selected to investigate the most pessimistic flow conditions; that is, the nominal degradation rate of cementitious material, the maximum infiltration rate, and the very large initial saturated hydraulic conductivity of 4.5E-07 cm/s for saltstone. Flow Cases F10 and F20 assume that the joint zones have a relative permeability of one at any suction level, rather than an MCC associated with gravel, as an additional potential level of conservatism. The potential groundwater dose to the MOP for these two flow cases are evaluated using PORFLOW concentrations for the key

radionuclides discussed in Section 5.2.2. The key radionuclides are Cs-135, I-129, and Tc-99.

Figure 5.6-63 presents the total volumetric flow through saltstone in SDU 4 for the Evaluation Case and Flow Cases F10 and F20. As shown in this figure, the large initial saturated hydraulic conductivity of saltstone in Flow Case F20 causes a rapid rise in the flow through saltstone. However, the rapid degradation of the top portion of saltstone, caused by carbonation, after the roof has degraded, causes the flow through the remaining portion of saltstone to increase rapidly in the Evaluation Case. For Flow Case F10, the top portion of saltstone starts to degrade after the roof has degraded, at approximately 7,400 years, and the remaining portion of saltstone does not start degrading until after 19,000 years. Prior to the start of roof degradation, the flow through saltstone is driven by the increasing infiltration rate from the closure cap and the degradation of the sand drainage layer.

Figure 5.6-64 presents the total volumetric flow through saltstone in an FDC for the Evaluation Case and Flow Cases F10 and F20. As shown in this figure, similar to Figure 5.6-63, the large initial saturated hydraulic conductivity of saltstone in Flow Case F20 causes a rapid rise in flow through saltstone. Unlike SDU 4, the degradation of saltstone in an FDC is not impacted by carbonation and the increasing flow rate, for the Evaluation Case, starts to climb, after the roof has degraded, at a rate corresponding to the saltstone degradation rate. For Flow Case F10, saltstone starts to degrade after the roof has degraded, at approximately 15,000 years. Prior to the start of roof degradation, the flow through saltstone is driven by the increasing infiltration rate from the closure cap, the degradation of the sand drainage layer, and the performance of the HDPE-GCL until it is degraded in 1,400 years.

Figure 5.6-63: Flow Rates through Saltstone in SDU 4 for Flow Variability Cases

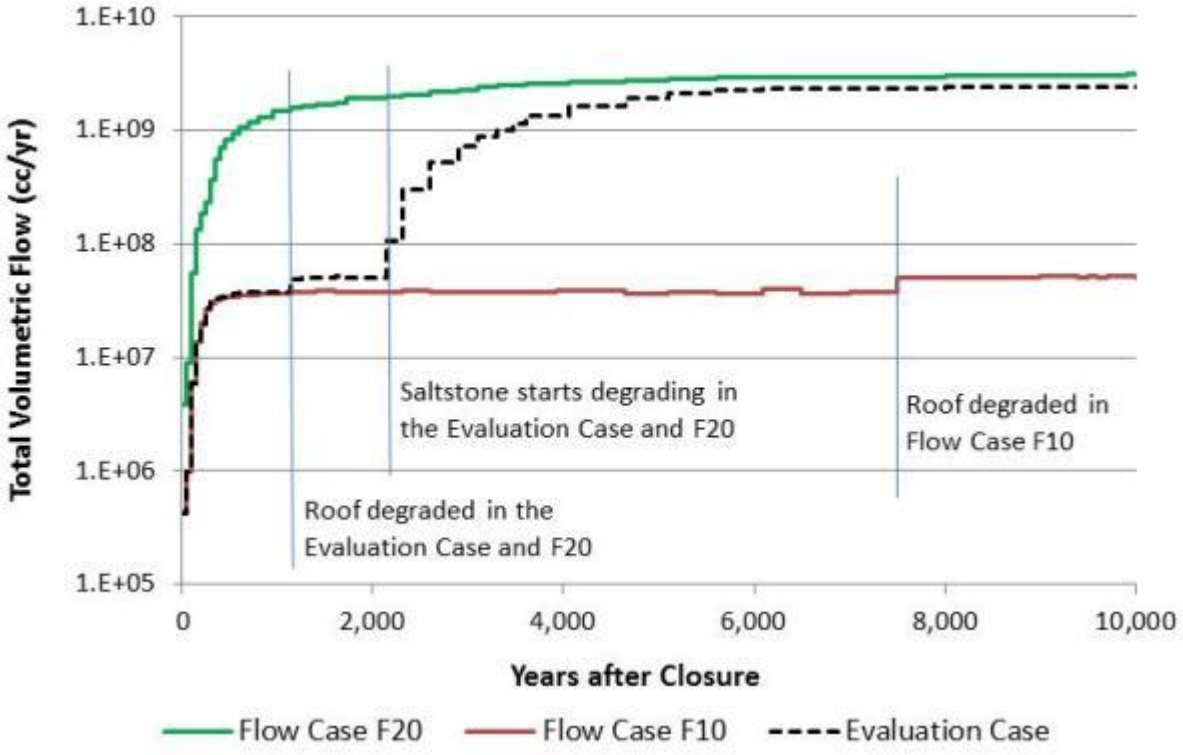

Figure 5.6-64: Flow Rates through Saltstone in an FDC for Flow Variability Cases

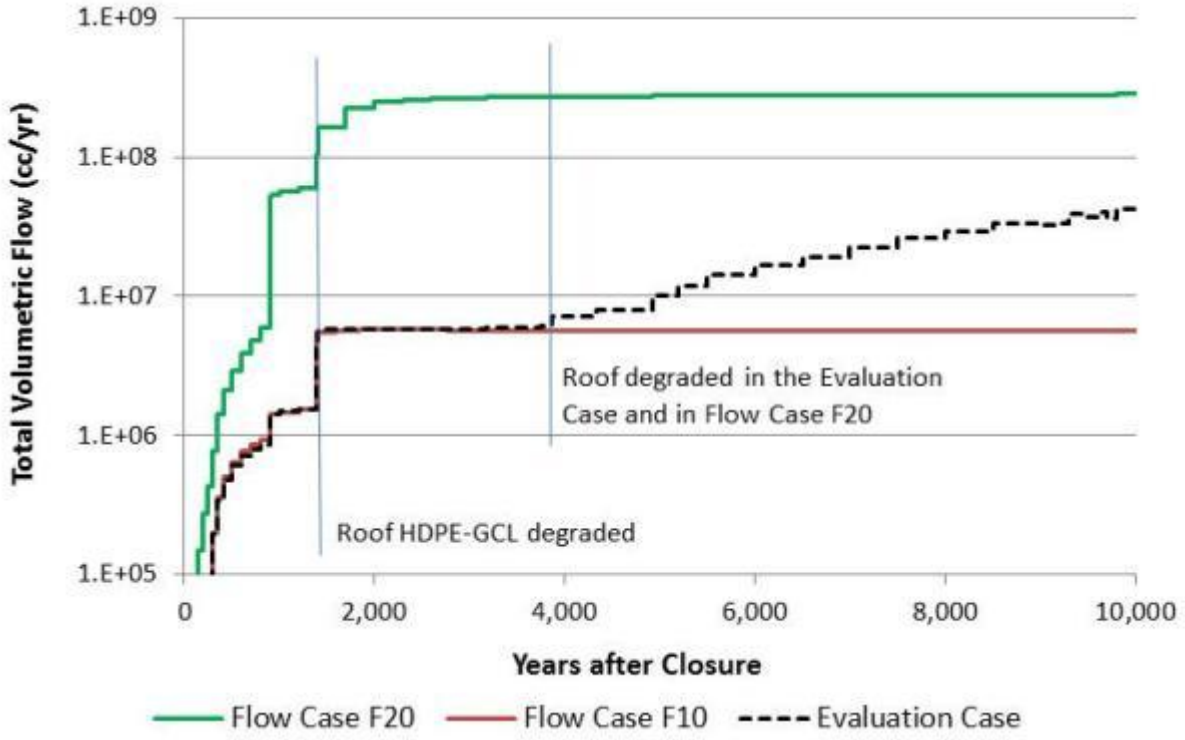

Flow Case F10

Figure 5.6-65 presents the dose to the MOP for Sectors B, C, and I for Flow Case F10, out to 20,000 years after closure. These sectors were chosen based on the dose results presented in Section 5.5.1, which indicated that these sectors would have the highest dose to the MOP at some time during the 20,000-year period. Sectors B and C have the highest dose to the MOP early in the evaluation period, caused by the initial release of I-129 from SDU 4. After about 1,500 years, Sector I has the controlling dose caused by the release of I-129 from the FDCs. I-129 is the controlling dose contributor for this flow case. Because of the best estimate degradation rate for cementitious materials assumed for this flow case, the degradation of saltstone is significantly delayed as compared to the Evaluation Case. Figure 5.6-66 presents the dose profile to the MOP in the maximum sector for the Evaluation Case and Flow Case F10, out to 20,000 years. For this flow case, saltstone begins degrading in approximately 15,000 years as compared to approximately 4,000 years in the Evaluation Case. The release of I-129 and Cs-135 from SDU 4 occurs late in the 20,000-year period and their dose contributions are over shadowed by the release of I-129 from the FDCs. Table 5.6-14 presents the peak dose comparisons between the Evaluation Case and Flow Case F10.

Table 5.6-14: Peak Groundwater Dose Comparison to the MOP within 20,000 Years for the Evaluation Case and Flow Case F10

Peak Groundwater Dose	Evaluation Case	Flow Case F10
Peak Dose in 10,000 Years	12 mrem/yr	2.4 mrem/yr
Contribution from I-129	98 %	98.4 %
Contribution from Tc-99	1.8 %	1.4 %
Contribution from Cs-135	0.2 %	0.2 %
Time of Peak Dose	7,700 Years	8,508 Years
Peak Dose between 10,000 Years and 20,000 Years	3.1 mrem/yr	3.9 mrem/yr
Contribution from I-129	0 %	95.3 %
Contribution from Tc-99	99 %	4 %
Contribution from Cs-135	0.3 %	0.7 %
Time of Peak Dose	19,972 Years	17,138 Years

Figure 5.6-65: MOP Dose Profile for Flow Case F10 for 20,000 Years

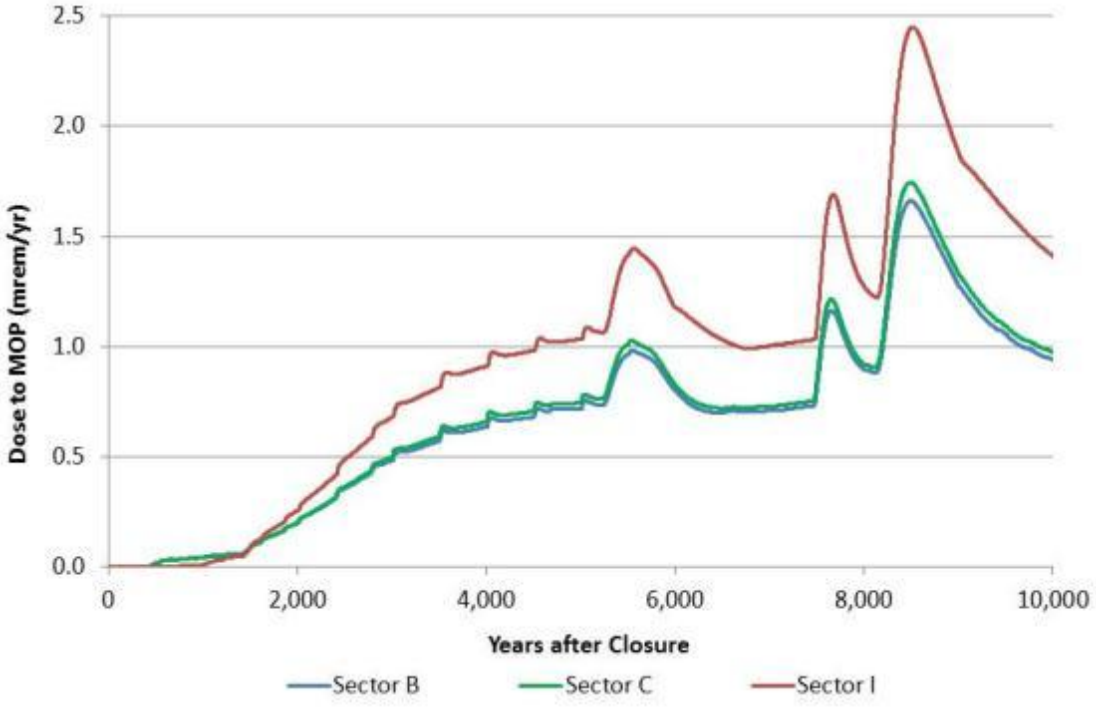

Figure 5.6-66: MOP Dose Profile in the Maximum Sector for the Evaluation Case and Flow Case F10

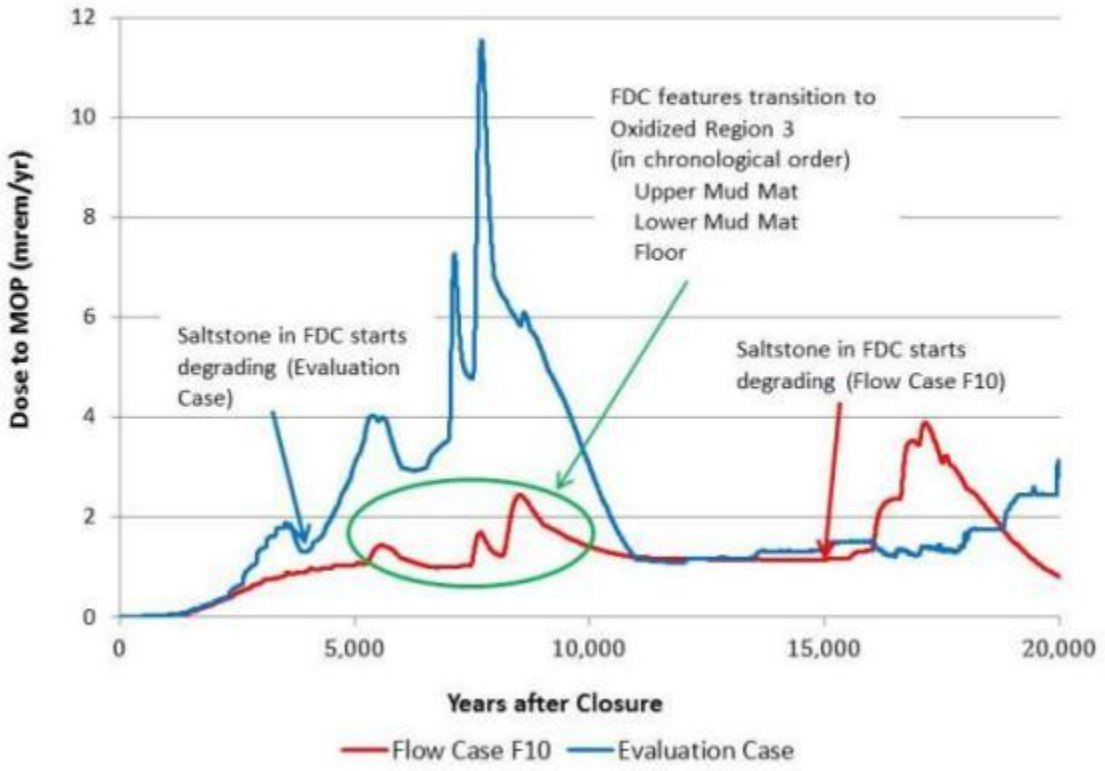

Flow Case F20

Figure 5.6-67 presents the dose to the MOP for Sectors B, C, and I for Flow Case F20, out to 20,000 years after closure. The peak dose to the MOP arrives early in the 10,000 year time period because of the significant flow through saltstone afforded by this flow case, as compared to the Evaluation Case. Figure 5.6-68 presents the dose profile to the MOP in the maximum sector for the Evaluation Case and Flow Case F10, out to 20,000 years. Initially, the dose to the MOP is dominated by I-129 from SDU 4 when the peak release rate occurs at less than 1,000 years and the SDU 4 I-129 inventory is exhausted in approximately 1,400 years. When the HDPE-GCL, covering the roof of an FDC, is degraded at 1,400 years, the release of I-129 from an FDC greatly increases. The peak release rate of I-129 from an FDC occurs at approximately 1,950 years and the inventory of I-129 in an FDC is exhausted at approximately 2,200 years. The release rate of Cs-135 from SDU 4 peaks at approximately 2,300 years, but its contribution to the peak dose within 10,000 years is not significant. Tc-99 begins to dominate the dose to the MOP at approximately 4,000 years, with the peak dose occurring near the end of the 20,000 year period, associated with a spike release from the FDCs. Table 5.6-15 presents the peak dose comparisons between the Evaluation Case and Flow Case F20.

Figure 5.6-67: MOP Dose Profile for Flow Case F20 in 20,000 Years

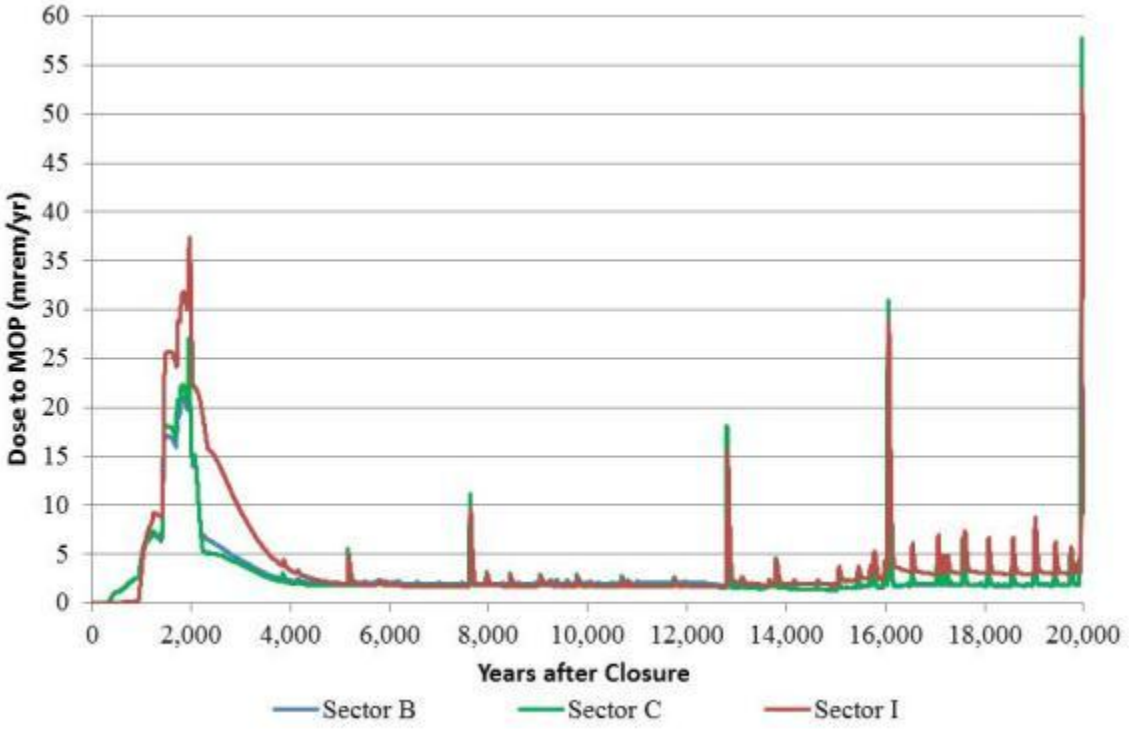

Table 5.6-15: Peak Groundwater Dose Comparison to the MOP within 20,000 Years for the Evaluation Case and Flow Case F20

Peak Groundwater Dose	Evaluation Case	Flow Case F20
Peak Dose in 10,000 Years	12 mrem/yr	37 mrem/yr
Contribution from I-129	98 %	95 %
Contribution from Tc-99	1.8 %	4 %
Contribution from Cs-135	0.2 %	1 %
Time of Peak Dose	7,700 Years	1,966 Years
Peak Dose between 10,000 Years and 20,000 Years	3.1 mrem/yr	58 mrem/yr
Contribution from I-129	0 %	0 %
Contribution from Tc-99	99 %	100 %
Contribution from Cs-135	0.3 %	0 %
Time of Peak Dose	19,972 Years	19,956 Years

Figure 5.6-68: MOP Dose Profile in the Maximum Sector for the Evaluation Case and Flow Case F20

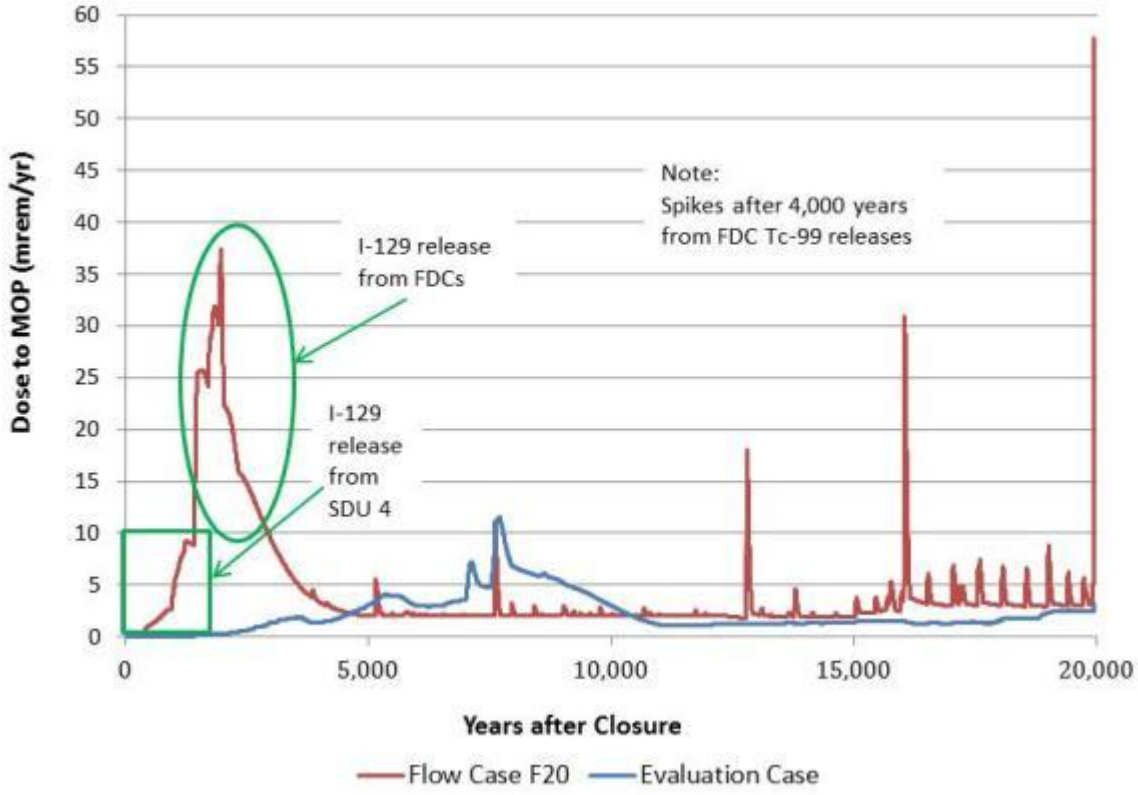

The flow variability cases discussed in this section provide insights on the behavior of the Tc-99 release from SDU 4 and an FDC. Figure 5.6-69 illustrates the release of Tc-99 from SDU 4 for the Evaluation Case and Flow Cases F10 and F20. The release of Tc-99 from SDU 4 is void of any spike releases because of the solubility of Tc-99 and flows through SDU 4 allow the release of Tc-99 at the solubility limit without any discrete "packets" of released Tc-99. Figure 5.6-70 illustrates the release of Tc-99 from an FDC for the Evaluation Case and Flow Cases F10 and F20. The release spikes shown for Flow Case F20, in Figure 5.6-70, are attributed to the release of Tc-99 as discrete nodes of saltstone and concrete become oxidized in the FDC via the shrinking core model and the Tc-99 mass is flushed from the FDC.

Figure 5.6-69: Tc-99 Release Rate from SDU 4

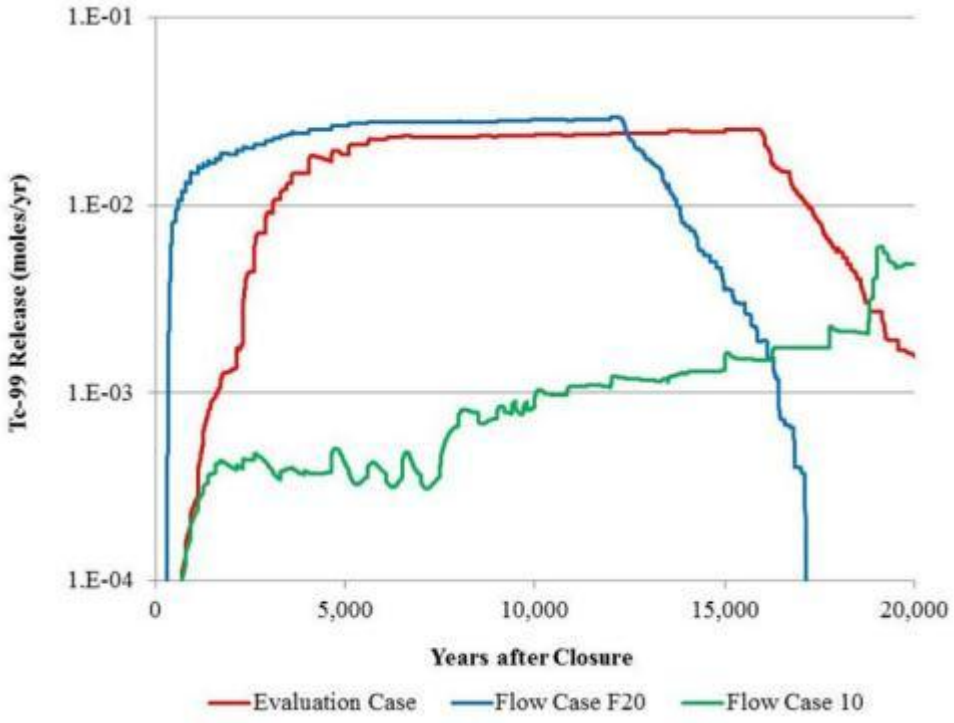

Figure 5.6-70: Tc-99 Release Rate from FDCs

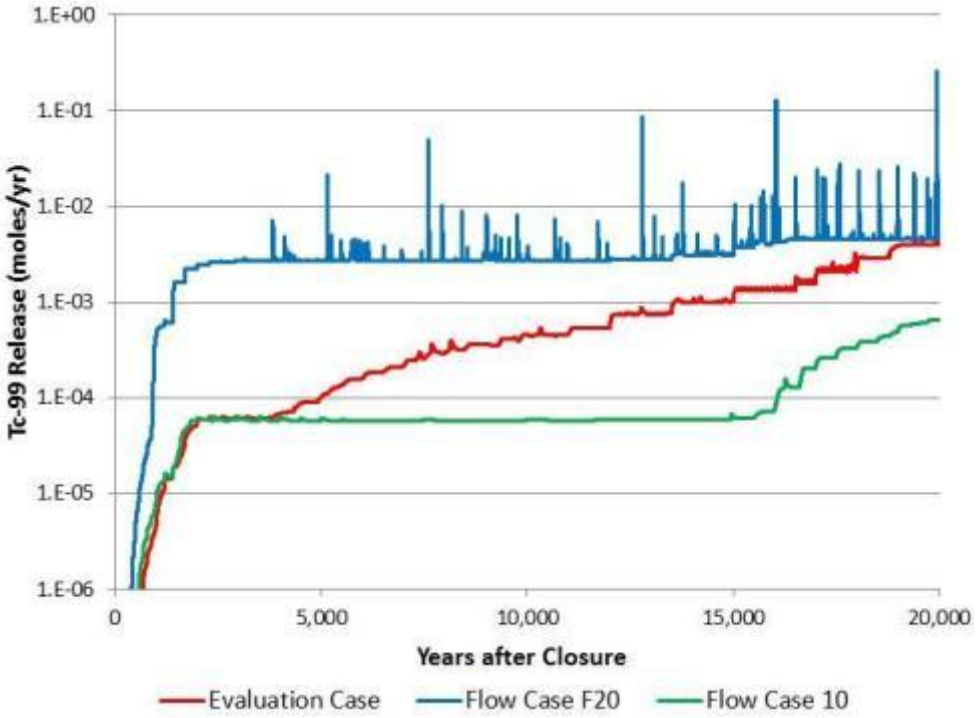

In summary, the release of the key radionuclides is highly dependent on the flow through the disposal units. The very pessimistic flow case F20, assumes an initial saturated hydraulic conductivity for saltstone that is 7,000% greater than for the Evaluation Case; yet the peak dose to the MOP, within 10,000 years, is only 50% greater than the performance objective of 25 mrem/yr.

5.6.6.2 FDC Roof Slope Sensitivity

Section 4.4.4.3 analyzed the volumetric flow through saltstone for the nominal roof slope of 2 % and for roof slopes of 1.5 % and 2.5 %. The roof slope of 2.5 % caused a slight decease in the flow through saltstone as compared to the nominal case; thus further evaluation of this roof slope is not warranted. However, for a roof slope of 1.5 % the flow through saltstone increased by nearly 33 % from the nominal case at 10,000 years as shown in Table 4.4-6. Thus, further evaluation is warranted for the 1.5 % slope.

As indicated in Sections 5.2.2 and 5.5.1, the key radionuclides are Cs-135, I-129, and Tc-99. As shown in Figure 5.5-5, the most significant contributor to the dose to the MOP within 10,000 years is I-129. As shown in Figure 5.5-6, the most significant contributor to the dose to the MOP in the 10,000-year to 20,000-year period is Tc-99, which occurs after about year 12,000. To ascertain the potential impact on the release of I-129 and Tc-99 from FDCs, the release rates to the water table of I-129 and Tc-99 are shown in Figures 5.6-71 and 5.6-72, respectively. As shown in Figure 5.6-71, I-129 has a slightly higher release rate at earlier times for the 1.5 % roof slope case, as compared to the nominal roof slope case. This earlier release would not have a significant impact on the dose from I-129 to the MOP. In fact, because there is a higher release rate earlier, the peak dose from I-129 would be expected to be less for the 1.5 % roof slope case, compared to the nominal roof slope case. Figure 5.6-72 illustrates the release of Tc-99 to the water table from an FDC with a roof slope of 2 % or 1.5 %. As shown in Figure 5.6-72, the release rate of Tc-99 is not appreciably different between the two cases for the first 10,000 years and the magnitude of the release rate is small; thus, the dose to the MOP would not be significantly different between the two cases.

Figure 5.6-71: I-129 Release Rate to the Water Table from FDCs

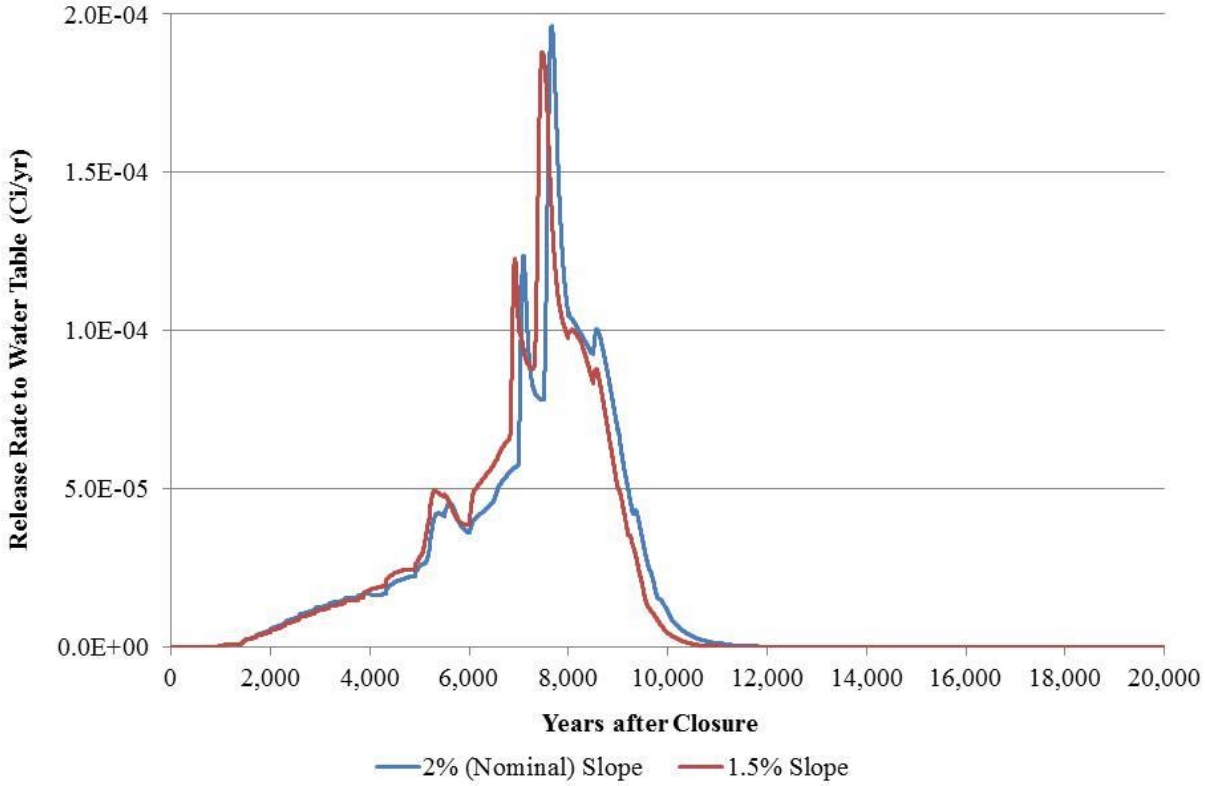

Figure 5.6-72: Tc-99 Release Rate to the Water Table from FDCs

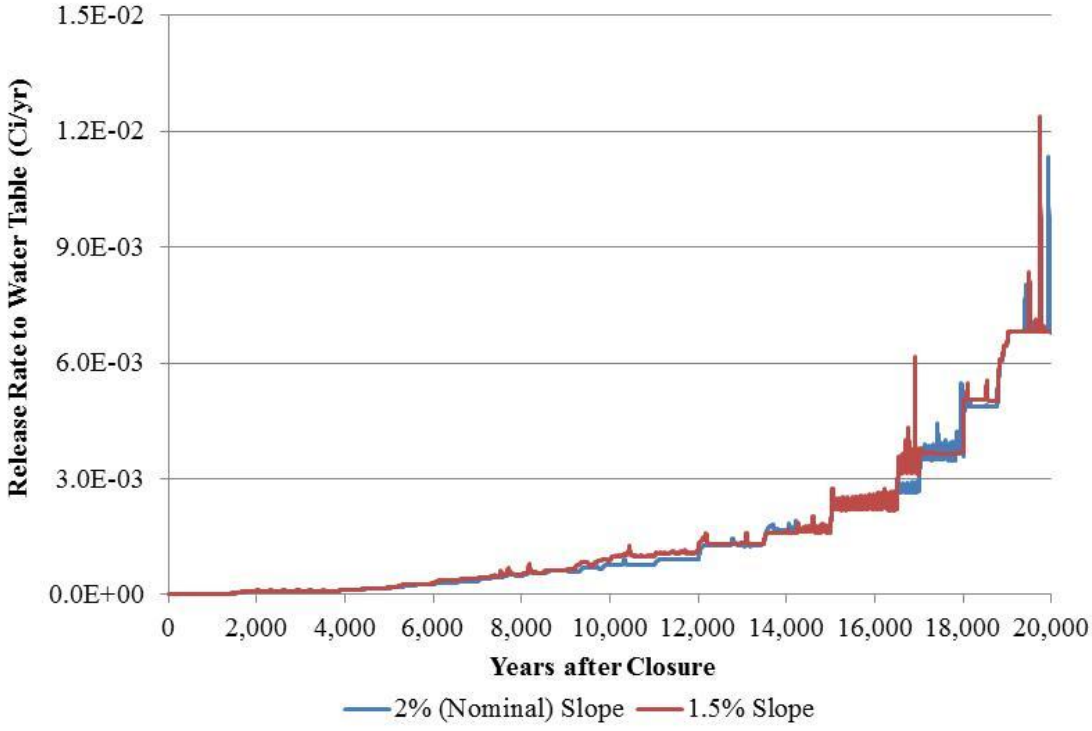

Based on this release rate analysis, the increase in the release rate of the significant dose contributing radionuclides would not have a significant impact on the dose results to the MOP. Thus, the results and conclusions of this SA would not be adversely impacted by a roof slope of 1.5 %.

5.6.6.3 Joint Zone MCC Sensitivity

Of the 36 flow cases developed in Section 4.4.3, one-half of these flow cases are dependent on the selection of the moisture retention capability, characterized by the MCC, of the joint zone. The joint zone is assumed to have an MCC attributed to gravel for one-half of the flow cases and, for the other one-half of the flow cases, the MCC is considered to be one at all suction levels. Figure 5.6-73 illustrates the difference between these two conditions of relative permeability.

Figure 5.6-73: Relative Permeability of Joint Zones in the Flow Cases

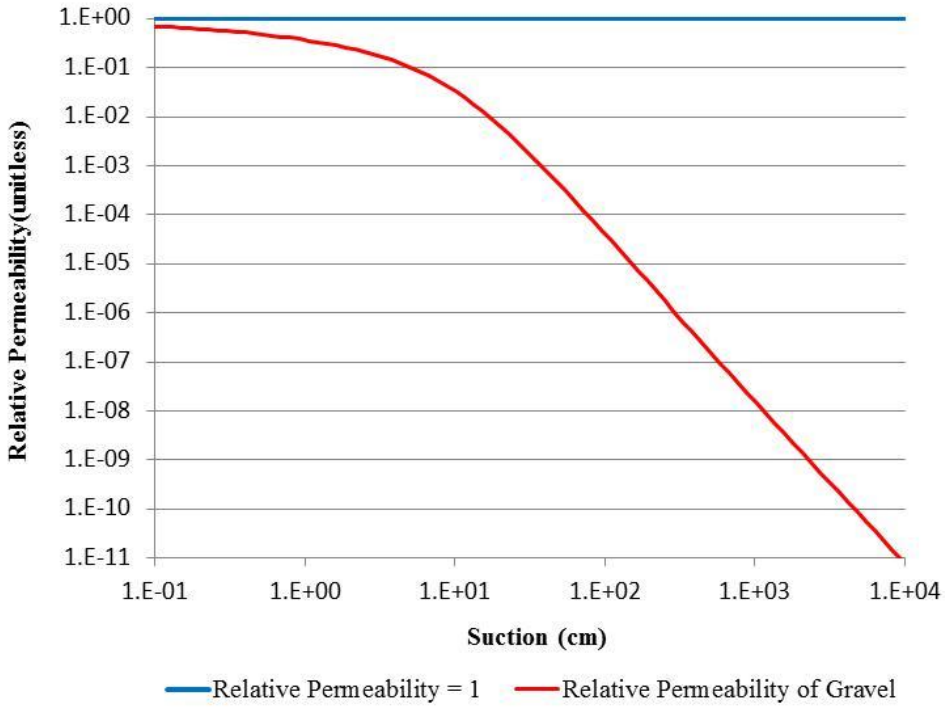

As discussed in Section 4.4.4.1, the selection of the MCC has a significant impact on the flow though the joints in SDU 4; but not very significant for the flow through the joints in FDCs, discussed in Section 4.4.4.2. Of importance in these flow cases is the estimated release of contaminants from the saltstone into the environment. To ascertain the importance of the selection of joint zone MCC to the performance of the SDUs, the Tc-99 releases from SDU 4 and FDCs are compared to various flow cases that differ only by the selection of the joint zone MCC. Section 5.6.6.1 evaluated Flow Cases F1 (Evaluation Case), F10 (an expected case), and F20 (a very pessimistic case). Flow Cases F10 and F20 assume that the joint zone has a relative permeability of one. The corresponding flow cases for F10 and F20 that would have gravel as the joint zone are Flow Cases F4 and F14. The Evaluation Case, Flow Case F1, has gravel as the joint zone and the corresponding flow case with the joint

zone having a relative permeability of one is Flow Case F7. Figures 5.6-74 and 5.6-75 present the Tc-99 release rates to the water table from SDU 4 and FDCs, respectively, for the flow cases described above. These figures indicate that the choice of MCC for the joint zones has no appreciable impact on the release rate of Tc-99 from the FDCs.

Figure 5.6-74: Tc-99 Release Rate to the Water Table from SDU 4

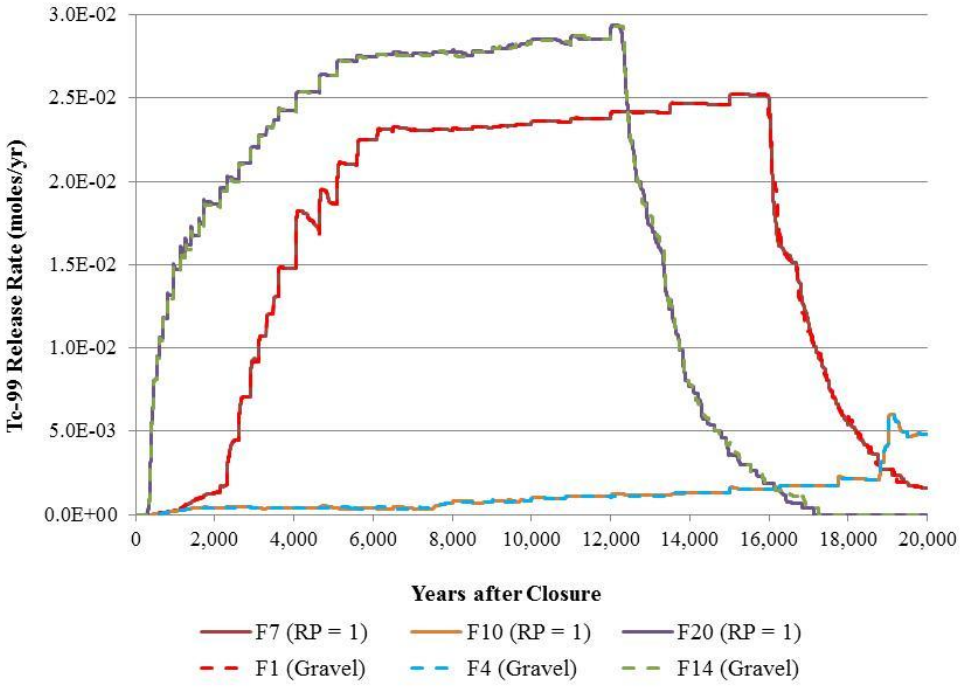

Figure 5.6-75: Tc-99 Release Rate to the Water Table from FDCs

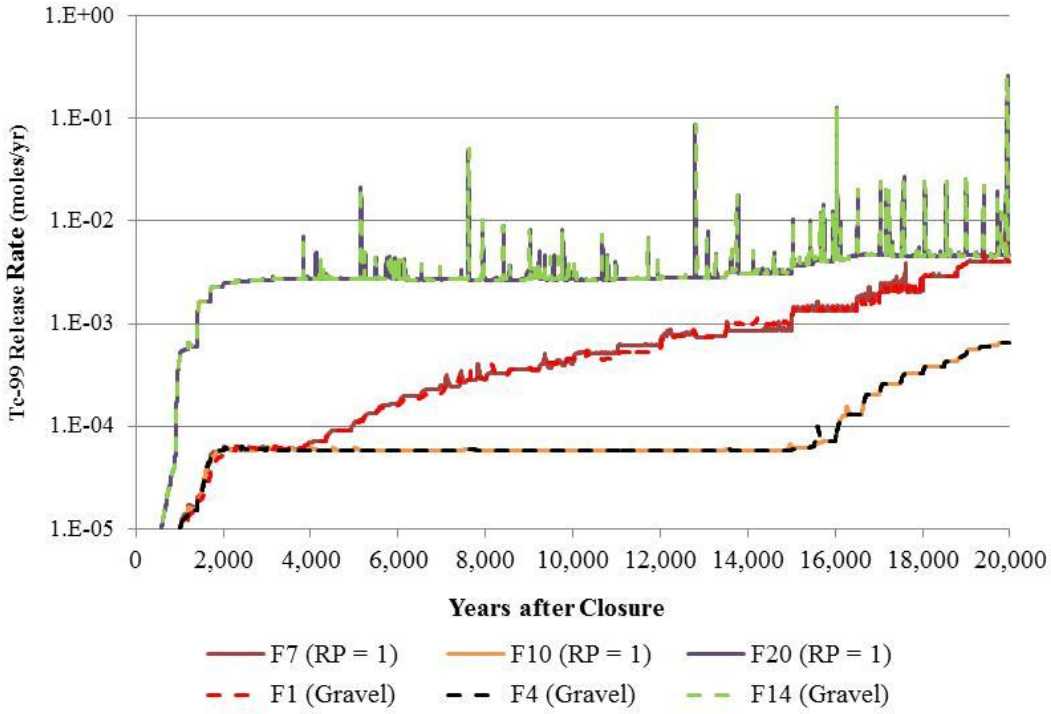

5.6.6.4 Tc-99 Release Sensitivity to Oxygen Sources Within Saltstone

This SA considers that the release of Tc-99 is contolled by solubility and that the expected Tc-99 solubility value is 1.0E-08 mol/L for saltstone and for concrete containing slag. As a sensitivity, regions of non-depleting sources of oxygen are assumed to exist initially within the saltstone monolith. Five cases were considered: 1 %, 2 %, 5 %, 10 %, and 20 % of the volume of the saltstone monolith is comprised of these oxygen containing blocks that would hasten the consumption of slag within the saltstone monolith and increase the rate of Tc-99 release. In this set of runs the concrete containing slag maintains its technetium solubility control of 1.0E-08 mol/L via the shrinking core model.

Figure 5.6-76 illustrates the total (integrated) release of Tc-99 to the water table from SDU 4 for these cases of oxygen sources within saltstone and the Evaluation Case. Table 5.6-16 provides the total integrated release of Tc-99 for these cases and the Evaluation Case and compares these releases to the Evaluation Case at 10,000 years and 20,000 years. As shown in Table 5.6-16, the release of Tc-99 is not significantly impacted within 10,000 years for oxygen regions present in 1 % and 2 % of the saltstone volume. When the sources of oxygen are present in 5 %, 10 % and 20 % of the saltstone volume, the total release of Tc-99 increases by approximately 25 %, 60 % and 100 %, respectively, at 10,000 years. Because the total inventory of Tc-99 in SDU 4 is essentially released within 20,000 years for the Evaluation Case, these sensitivity cases have no significant impact on the total Tc-99 release in 20,000 years.

Figure 5.6-76: Integrated Tc-99 Release to the Water Table from SDU 4 for Oxygen Sources within Saltstone Sensitivity Cases

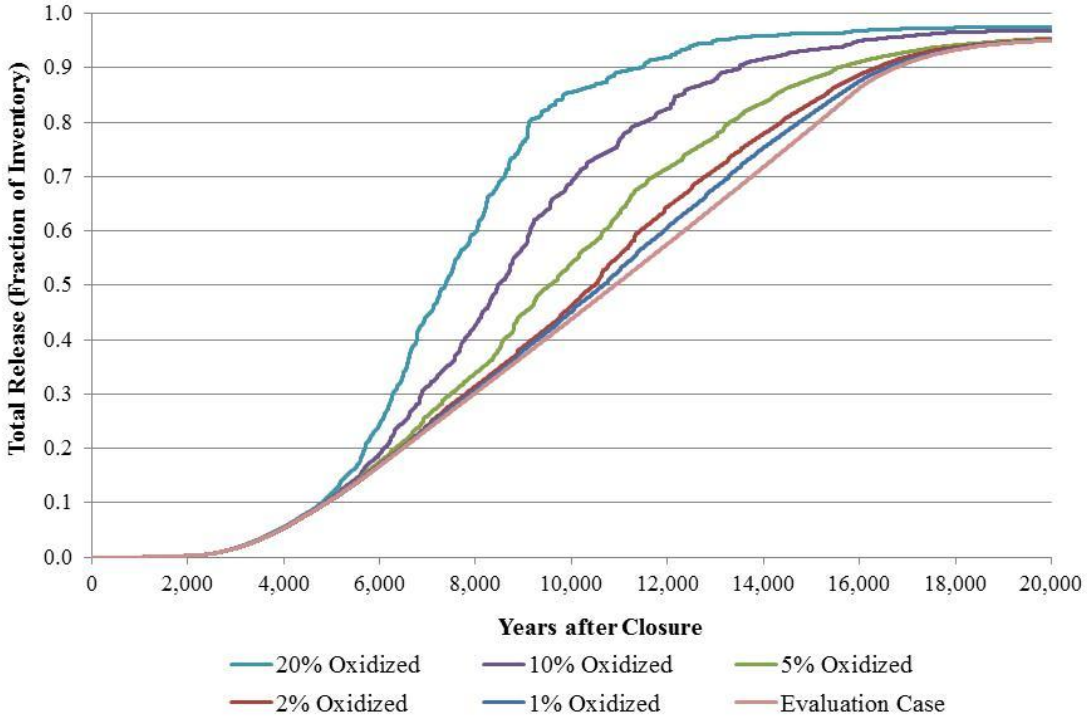

Table 5.6-16: Integrated Tc-99 Release from SDU 4 for Oxygen Sources within Saltstone Sensitivity Cases with Concrete Initially Reduced

Case Analyzed	Fraction Tc-99 Released at 10,000 years		Fraction Tc-99 Released at 20,000 years	
	Fraction of SDU 4 Inventory	Ratio to Evaluation Case	Fraction of SDU 4 Inventory	Ratio to Evaluation Case
Evaluation Case	4.4E-01	N A	9.5E-01	N A
Oxygen Sources at 1 % SaltstoneVolume	4.5E-01	1.03E+00	9.5E-01	1.00E+00
Oxygen Sources at 2 % SaltstoneVolume	4.6E-01	1.06E+00	9.5E-01	1.00E+00
Oxygen Sources at 5 % SaltstoneVolume	5.4E-01	1.24E+00	9.5E-01	1.00E+00
Oxygen Sources at 10 % Saltstone Volume	6.9E-01	1.57E+00	9.7E-01	1.02E+00
Oxygen Sources at 20 % Saltstone Volume	8.6E-01	1.95E+00	9.8E-01	1.03E+00

Figure 5.6-77 illustrates the total (integrated) release of Tc-99 to the water table from FDCs for these cases of oxygen sources within saltstone and the Evaluation Case. Table 5.6-17 provides the total integrated release of Tc-99 for these cases and the Evaluation Case and compares these releases to the Evaluation Case at 10,000 years and 20,000 years. As shown

in Table 5.6-17, the release of Tc-99 is not significantly impacted within 10,000 years for oxygen regions present in 1 % and 2 % of the saltstone volume. When the sources of oxygen are present in 5 %, 10 % and 20 % of saltstone volume, the total release of Tc-99 increases by approximately 20 %, 40 % and 110 %, respectively, at 10,000 years. At 20,000 years, the total release of Tc-99 from FDCs increases significantly for these sensitivity cases when compared to the Evaluation Case. As shown in Table 5.6-17, when saltstone is assumed to have oxygen sources comprising 20 % of the saltstone volume, the total Tc-99 release in 20,000 years is more than 10 times greater than the Evaluation Case. Section 5.6.6.6 provides the estimated dose impact to the MOP when the oxygen sources are present in 20 % of the saltstone volume.

Figure 5.6-77: Integrated Tc-99 Release to the Water Table from FDCs for Oxygen Sources within Saltstone Sensitivity Cases

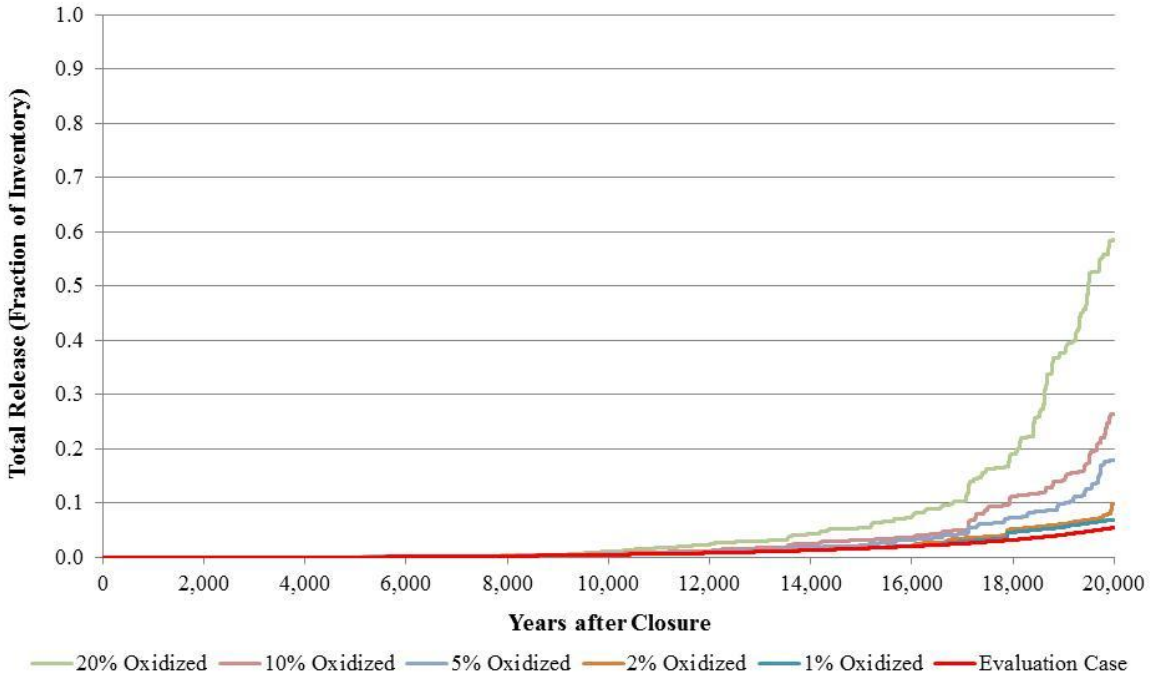

Table 5.6-17: Integrated Tc-99 Release from FDCs for Oxygen Sources within Saltstone Sensitivity Cases with Concrete Initially Reduced

Case Analyzed	Tc-99 Released at 10,000 years		Tc-99 Released at 20,000 years	
	Fraction of FDC Inventory	Ratio to Evaluation Case	Fraction of FDC Inventory	Ratio to Evaluation Case
Evaluation Case	4.96E-03	N/A	5.47E-02	N/A
Oxygen Sources at 1 % Saltstone Volume	5.00E-03	1.01E+00	6.97E-02	1.27E+00
Oxygen Sources at 2 % Saltstone Volume	5.10E-03	1.03E+00	9.88E-02	1.81E+00
Oxygen Sources at 5 % Saltstone Volume	5.94E-03	1.20E+00	1.80E-01	3.28E+00
Oxygen Sources at 10 % Saltstone Volume	6.85E-03	1.38E+00	2.64E-01	4.83E+00
Oxygen Sources at 20 % Saltstone Volume	1.06E-02	2.13E+00	5.85E-01	1.07E+01

5.6.6.5 Tc-99 Release Sensitivity to Technetium Solubility in Saltstone and Concrete

This section provides results of the sensitivity cases associated with changing the technetium solubility value in saltstone and concrete. Three runs were made to evaluate the impact of Tc-99 release from the FDCs with different solubility values in saltstone with the concrete maintaining the Evaluation Case solubility value of 1.0E-08 mol/L. Three solubility values were considered for saltstone, 1.0E-08 mol/L (Evaluation Case), 1.0E-09 mol/L (10 times less than the Evaluation Case), and 1E-07 mol/L (10 times more than the Evaluation Case). These cases illustrate that the release of Tc-99 is controlled by the technetium solubility value of saltstone, as shown in Figures 5.6-78 and 5.6-79 for SDU 4 and FDCs, respectively.

Figure 5.6-78: Integrated Tc-99 Release to the Water Table from SDU 4 for Saltstone Solubility Sensitivity Cases

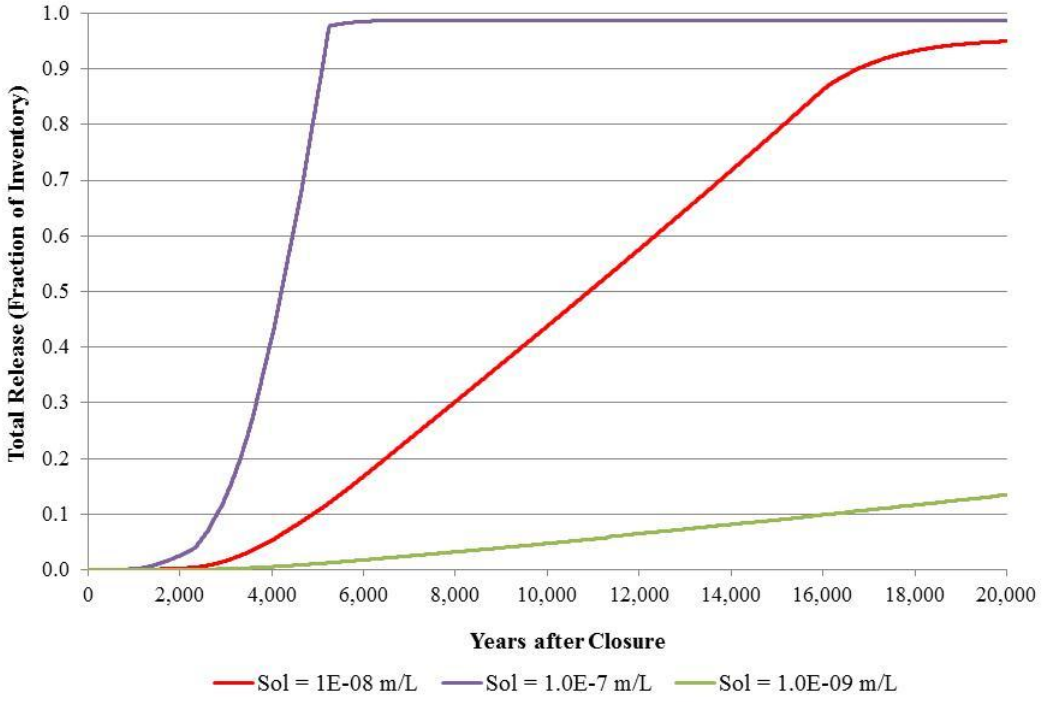

Figure 5.6-79: Integrated Tc-99 Release to the Water Table from FDCs for Saltstone Solubility Sensitivity Cases

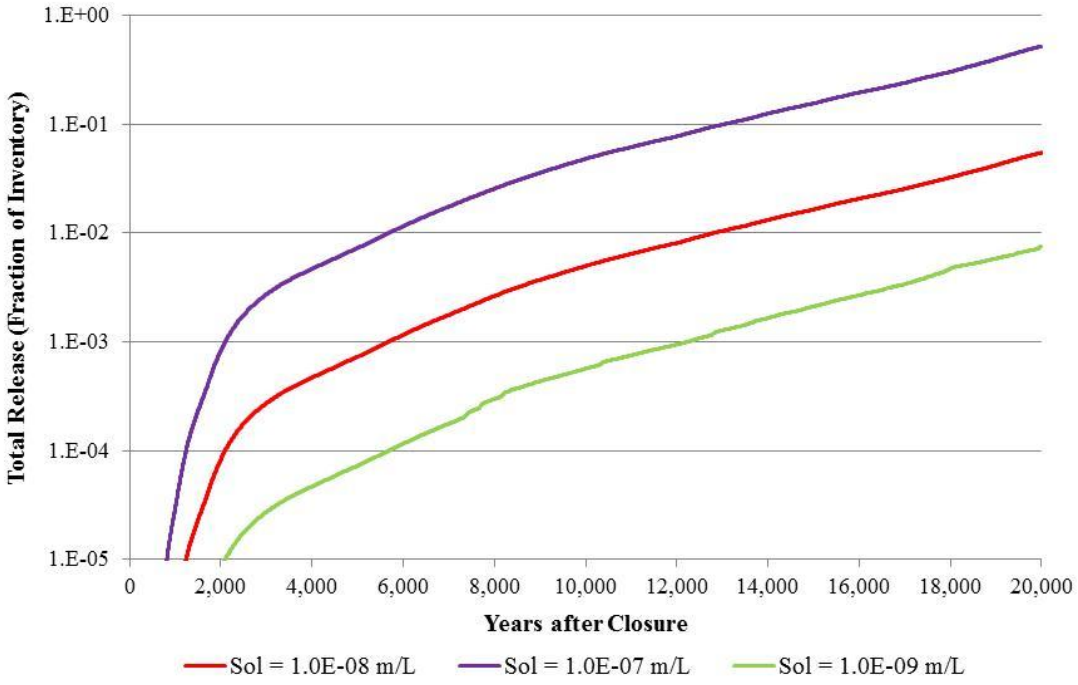

An additional analysis was conducted to evaluate the impact of having the concrete inially oxidized with a distribution coefficient (K_d value) of 0.5 mL/g for technetium. The previous cases of differing solubility values for saltstone were redone with the concrete initially oxidized. The results of these sensitivity cases are illustrated in Figures 5.6-80 and 5.6-81, for SDU 4 and FDCs, respectively. These figures also include the results from the previous cases when the concrete is initially reduced with a solubility of 1.0E-08 mol/L. The comparisons shown in Figures 5.6-80 and 5.6-81 indicate that the initial condition of the concrete has essentially no impact on the Tc-99 release from the FDCs when the Tc-99 release is controlled via solubility.

Figure 5.6-80: Comparison of Tc-99 Release to the Water Table from SDU 4 for Saltstone Solubility Sensitivity Cases with Concrete Reduced or Oxidized

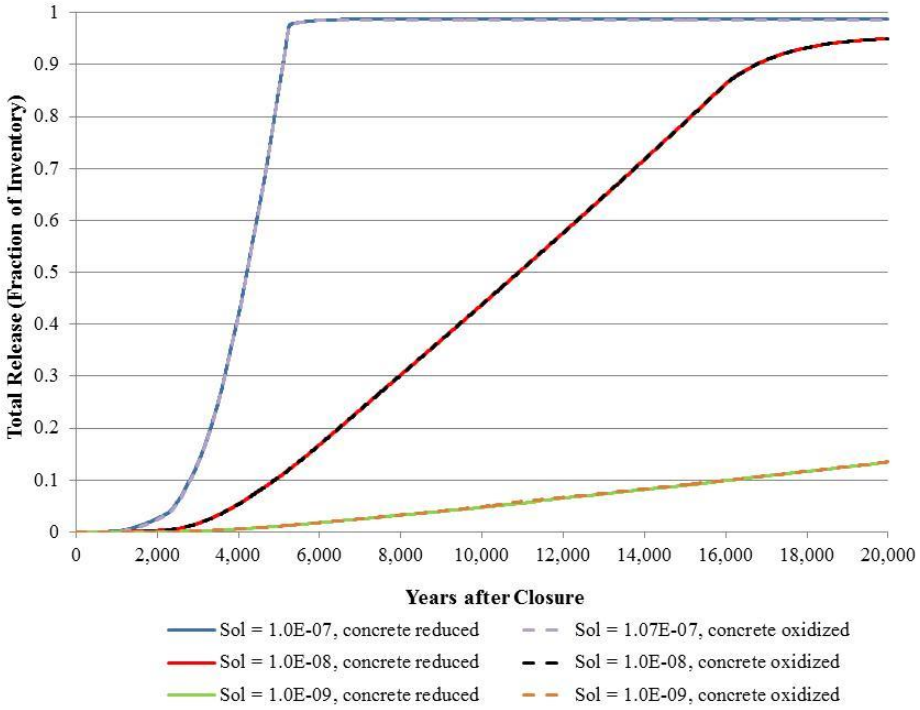

Figure 5.6-81: Comparison of Tc-99 Release to the Water Table from FDCs for Saltstone Solubility Sensitivity Cases with Concrete Reduced or Oxidized

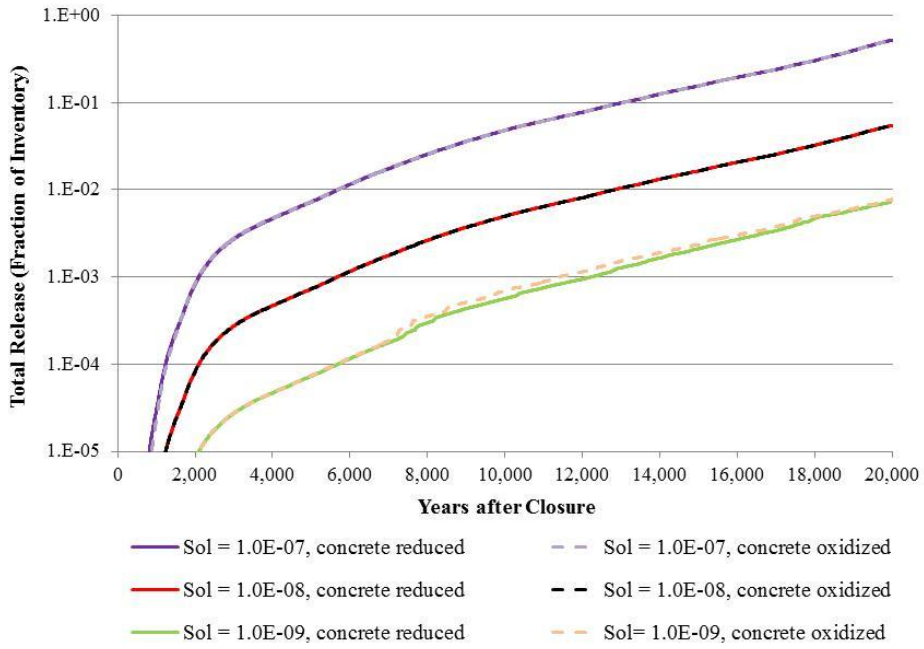

5.6.6.6 Tc-99 Release Sensitivity to Saltstone Oxygen Sources with Concrete Oxidized

Section 5.6.6.4 discusses the Tc-99 release sensitivity to oxygen sources within the saltstone monolith with the concrete initially reduced with a technetium solubility of 1.0E-08 mol/L. As a follow-up on the analysis presented in Section 5.6.6.5, the sensitivity analysis conducted in Section 5.6.6.4 is redone but with the concrete initially oxidized and a technetium K_d value of 0.5 mL/g. As discussed in Section 5.6.6.4, the release of Tc-99 is not significantly impacted when the oxygen sources within the saltstone monolith comprise 1 % or 2 % of the saltstone volume. However, at higher levels of oxygen sources that would comprise 5 %, 10 %, or 20 % of the saltstone volume the release of Tc-99 can be significantly impacted, especially in FDCs. Therefore, these additional runs of oxygen sources within saltstone, with concrete initially oxidized, are limited to the cases where the sources of oxygen are present in 5 %, 10 %, and 20 % of the saltstone volume.

The results of these sensitivty cases are illustrated in Figures 5.6-82 and 5.6-83, for SDU 4 and FDCs, respectively. These figures also include the results from the previous cases when the concrete is initially reduced with a solubility of 1.0E-08 mol/L. Also included in these figures are the results from Section 5.6.6.5 for the Evaluation Case and the 10 times greater solubility case when the concrete is initially reduced or oxidized. The comparisons shown in Figures 5.6-82 and 5.6-83 indicate that the initial condition of the concrete has an impact on the potential release of Tc-99 for the various volumes of oxygen sources within saltstone. However, these cases are bounded by the 10 times greater solubility case.

Figure 5.6-82: Comparison Tc-99 Release to Water Table from SDU 4 for Oxygen Sources within Saltstone and Solubility Sensitivity Cases with Concrete Reduced or Oxidized

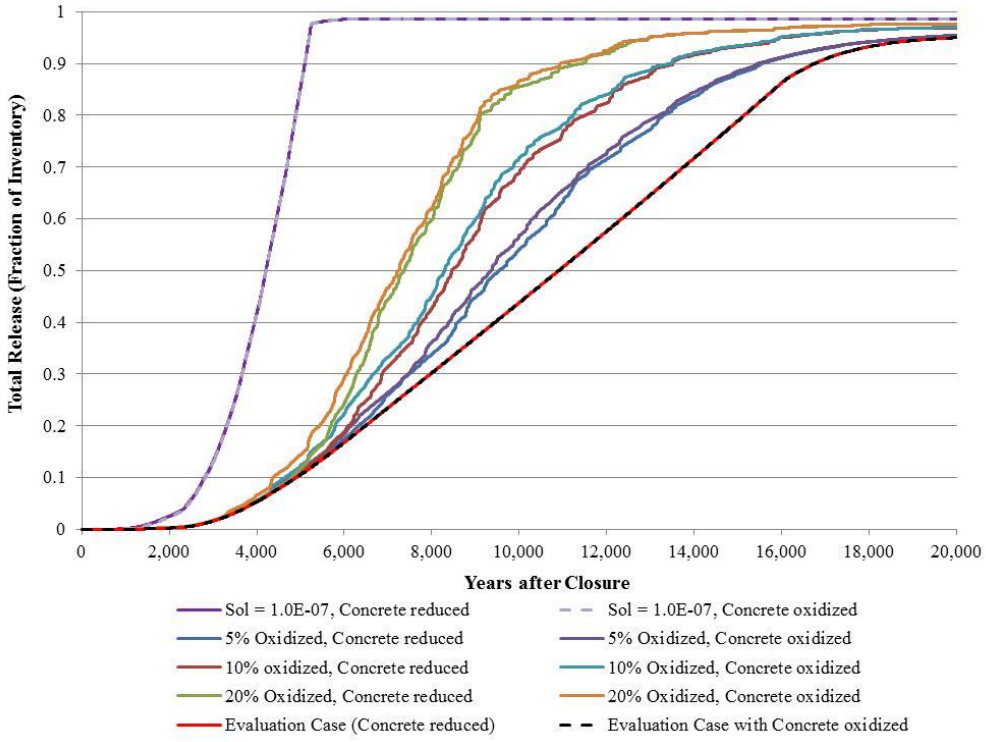

Figure 5.6-83: Comparison of Tc-99 Release to the Water Table from FDCs for Oxygen Sources within Saltstone and Solubility Sensitivity Cases with Concrete Reduced or Oxidized

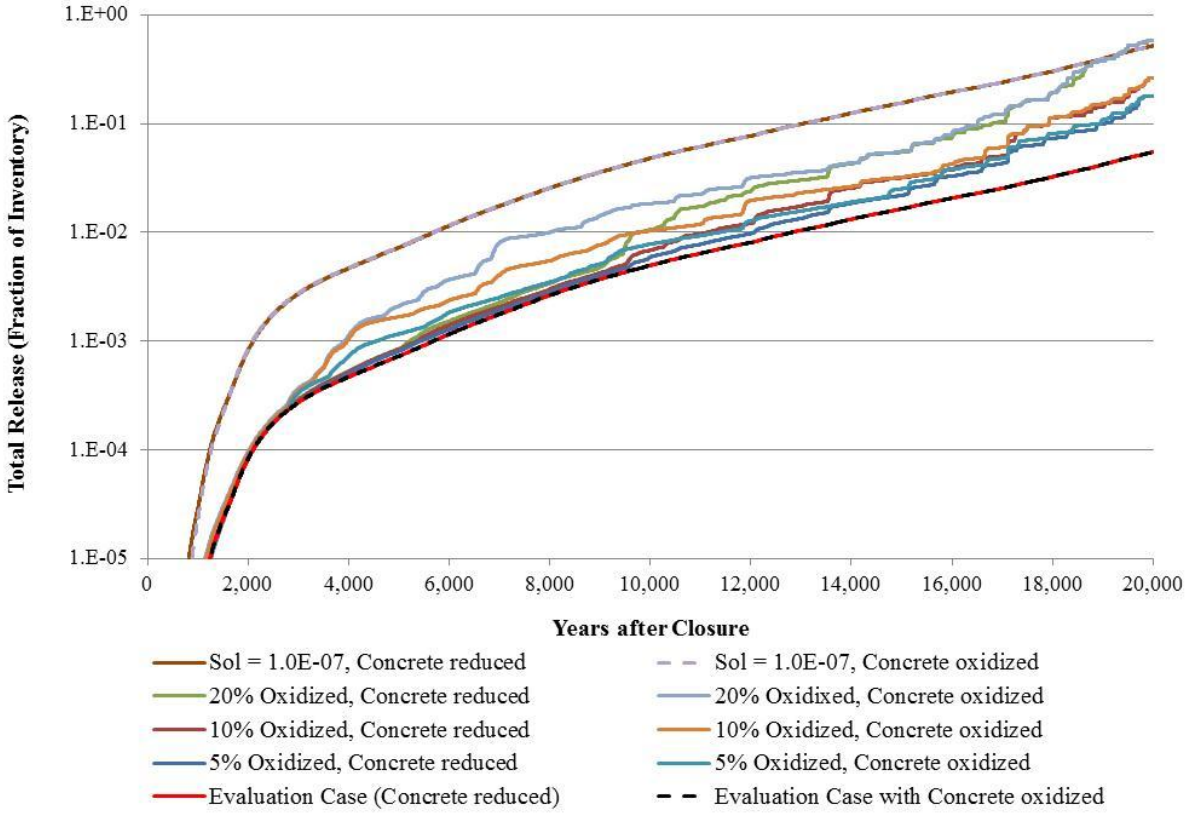

Even though the concrete is initially reduced, the sensitivity case of considering that the concrete is initially oxidized may serve as a case where fracturing within the concrete could result in faster oxidation of the concrete from environmental sources, and hasten the release of Tc-99 from the FDCs. To evaluate the impact to the potential dose to the MOP from the case of an elevated saltstone solubility value of 1.0E-07 mol/L and the case of oxygen sources within saltstone initially present in 20 % of the saltstone volume, the concrete is also assumed to be initially oxidized.

For the case of oxygen sources within saltstone present in 20 % of the saltstone volume and concrete initially oxidized, Figure 5.6-84 presents the dose to the MOP from Tc-99 out to 10,000 years after closure using the Evaluation Case flow parameters. Table 5.6-18 presents the estimated dose to the MOP for Sectors B, C, and I after adding the Cs-135 and I-129 contribution to the MOP dose for the Evaluation Case, presented in Section 5.5.1.

Figure 5.6-84: Dose to MOP from Tc-99 for Oxygen Sources within Saltstone at 20 % Saltstone Volume Sensitivity Case with Concrete Initially Oxidized

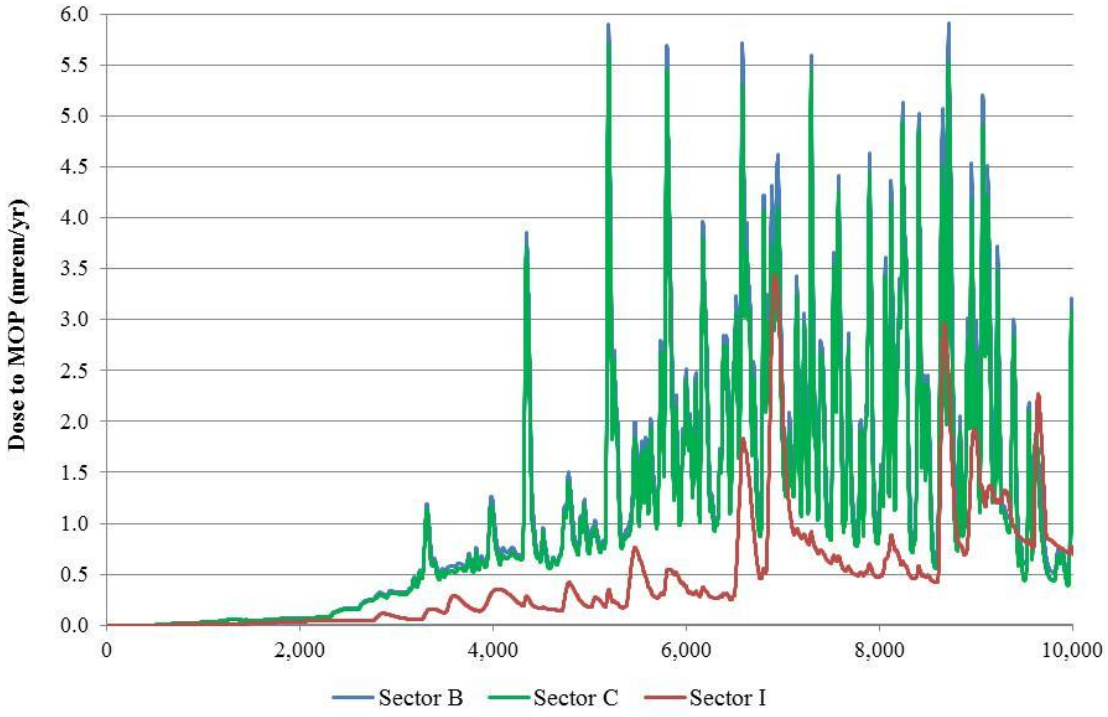

Table 5.6-18: Peak Dose to MOP within 10,000 Years in Sectors B, C, and I for Oxygen Sources within Saltstone at 20 % Saltstone Volume Sensitivity Case with Concrete Initially Oxidized, Compared to the Evaluation Case

Sector	Evaluation Case (Table 5.5-1)		Oxygen Sources in 20 % Saltstone Volume with Oxidized SDU Concrete	
	Peak Dose to MOP	Time of Peak Dose	Peak Dose to MOP	Time of Peak Dose
B	8.1 mrem/yr	7,682 years	10 mrem/yr	7,682 years
C	8.6 mrem/yr	7,676 years	11 mrem/yr	7,682 years
I	12 mrem/yr	7,700 years	12 mrem/yr	7,696 years

For the case of 10 times the nominal solubility value and concrete initially oxidized, Figure 5.6-85 presents the dose to the MOP from Tc-99 out to 10,000 years after closure using the Evaluation Case flow parameters. Table 5.6-19 presents the estimated dose to the MOP for Sectors B, C, and I after adding the Cs-135 and I-129 contribution to the MOP dose for the Evaluation Case, presented in Section 5.5.1.

Figure 5.6-85: Dose to MOP from Tc-99 for Ten Times Saltstone Solubility Value Sensitivity Case with Concrete Initially Oxidized

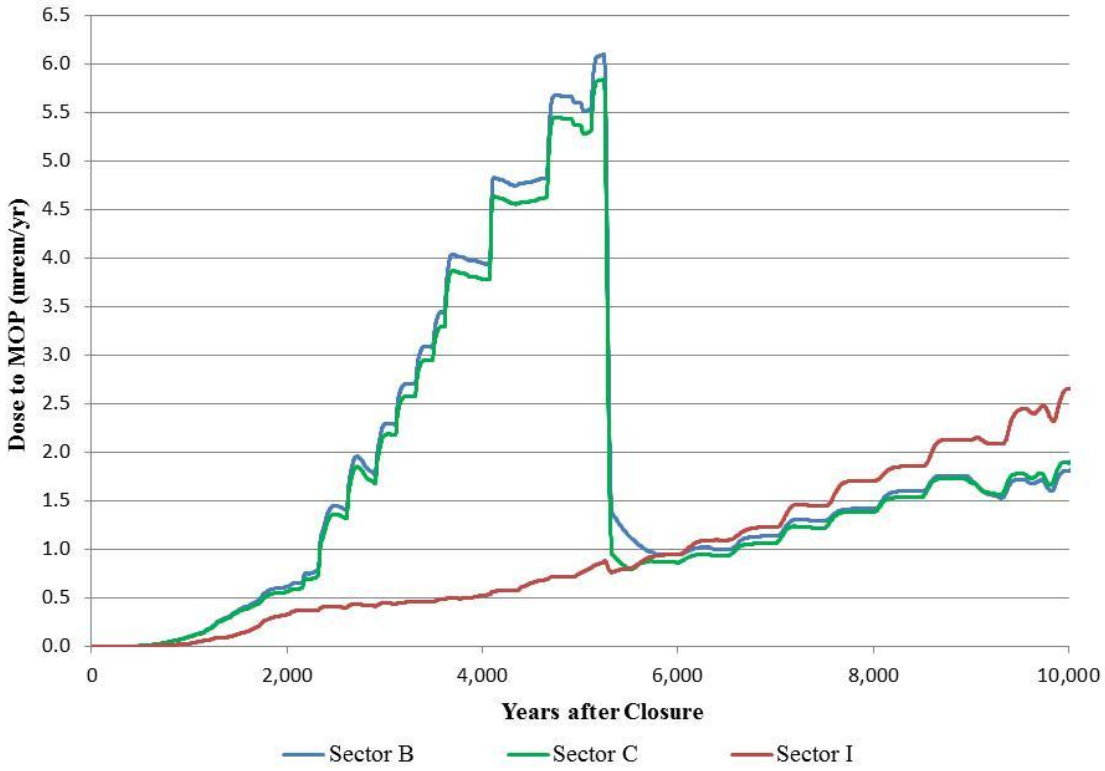

Table 5.6-19: Saltstone Solubility Value Sensitivity Case with Concrete Initially Oxidized, Compared to the Evaluation Case

Sector	Evaluation Case (Table 5.5-1)		10 Times Saltstone Nominal Technetium Solubility Value with Oxidized SDU Concrete	
	Peak Dose to MOP	Time of Peak Dose	Peak Dose to MOP	Time of Peak Dose
B	8.1 mrem/yr	7,682 years	9.1 mrem/yr	5,224 years
C	8.6 mrem/yr	7,676 years	9.2 mrem/yr	7,674 years
I	12 mrem/yr	7,700 years	13 mrem/yr	7,698 years

Comparison of Figures 5.6-84 and 5.6-85 and Tables 5.6-18 and 5.6-19 indicates that the sensitivity case of 10 times the nominal solubility value for saltstone, with initially oxidized concrete, would encompass the potential dose to the MOP for the sensitivity cases analyzed for oxygen sources within saltstone.

5.6.6.7 Selection of Flow Cases for Tc-99 Sensitivity and Uncertainty Analysis

Table 4.4-3 provides a summary of the 38 flow cases that are thoroughly discussed in Sections 4.4.3 and 4.4.4. Ignoring the two roof-slope sensitivity analyses, preliminary modeling results indicate that 12 of the 36 flow cases can be used to effectively simulate a

full range of flow fields. Specifically, flow cases F1, F4, F5, F14, F15, F16, F17, F25, F26, F28, F29, and F30 were selected as cases for further evaluations.

Of the 36 flow cases, 18 were screened out from further analysis based on the MCCs of the joints. The preliminary modeling results indicated that varying the MCCs of the joints provided a negligible impact with respect Tc-99 release, as discussed in Section 5.6.6.3. As such, the following flow cases were screened out, F7-F12, F19-F24, and F-31-F36.

Of the 18 remaining flow cases:

- F2 was screened out as being very similar to F5
- F3 was screened out as being very similar to F1
- F6 and F18 were screened out as both being very similar to F30 during the first 15,000 years and similar to F4 after 15,000 years
- F13 was screened out as being very similar to F15
- F27 was screened out as being very similar to F25

This screening leaves 12 flow cases for use in subsequent evaluations. Table 5.6-20 summarizes the remaining flow cases for subsequent evaluation. Figures 5.6-86 and 5.6-87 present the Tc-99 release from SDU 4 and FDCs, respectively, for the 12 flow cases based on the conditions described in Table 5.6-20 with the nominal saltstone solubility value of 1.0E-8 mol/L for technetium and with the concrete having the same technetium solubility value as saltstone. The legend in each figure is ranked from high to low based on the Tc-99 total release at 10,000 years.

Table 5.6-20: Summary of Evaluation Flow Cases

Case	Infiltration Rate (Figure 3.3-4)	Cementitious Degradation Rate (Section 4.2.2.5)	Initial Saltstone Saturated Hydraulic Conductivity (cm/s)
F1	Average	Nominal	6.4E-09
F4	Average	BE[a]	6.4E-09
F5	Average	BE[a]	4.5E-07
F14	Maximum	Nominal	4.5E-07
F15	Maximum	Nominal	3.9E-10
F16	Maximum	BE[a]	6.4E-09
F17	Maximum	BE[a]	4.5E-07
F25	Minimum	Nominal	6.4E-09
F26	Minimum	Nominal	4.5E-07
F28	Minimum	BE[a]	6.4E-09
F29	Minimum	BE[a]	4.5E-07
F30	Minimum	BE[a]	3.9E-10

[a] "BE" refers to best estimate values for cementitious material degradation

Figure 5.6-86: Tc-99 Total Release from SDU 4 for the 12 Flow Cases to be Analyzed

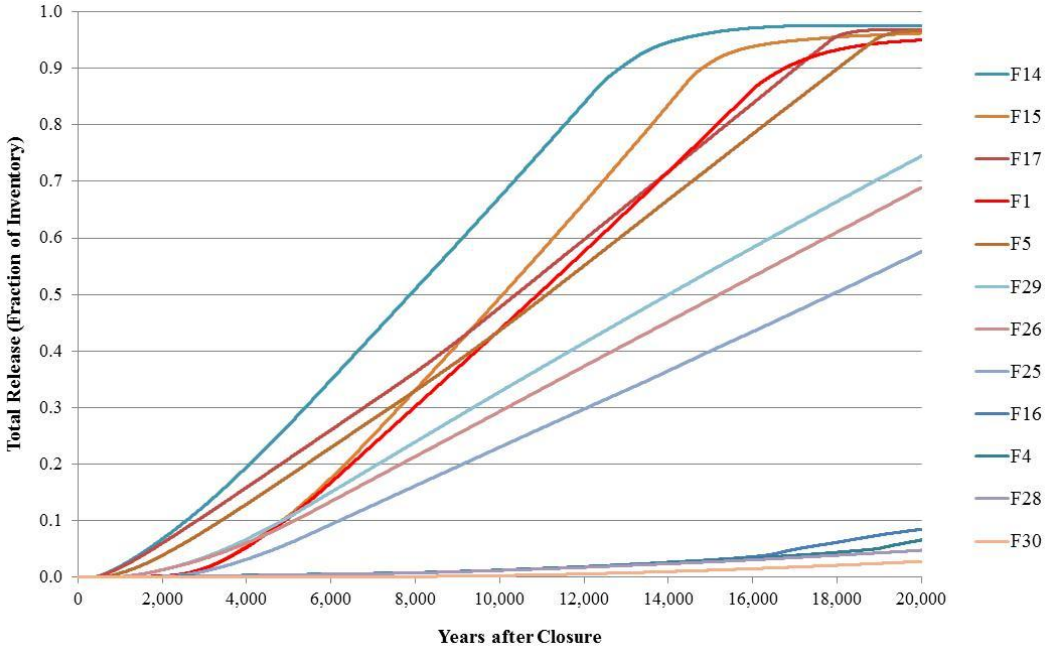

Technetium solubility value of 1.0E-08 mol/L for saltstone and SDU 4 concrete

Figure 5.6-87: Tc-99 Total Release from FDCs for the 12 Flow Cases to be Analyzed

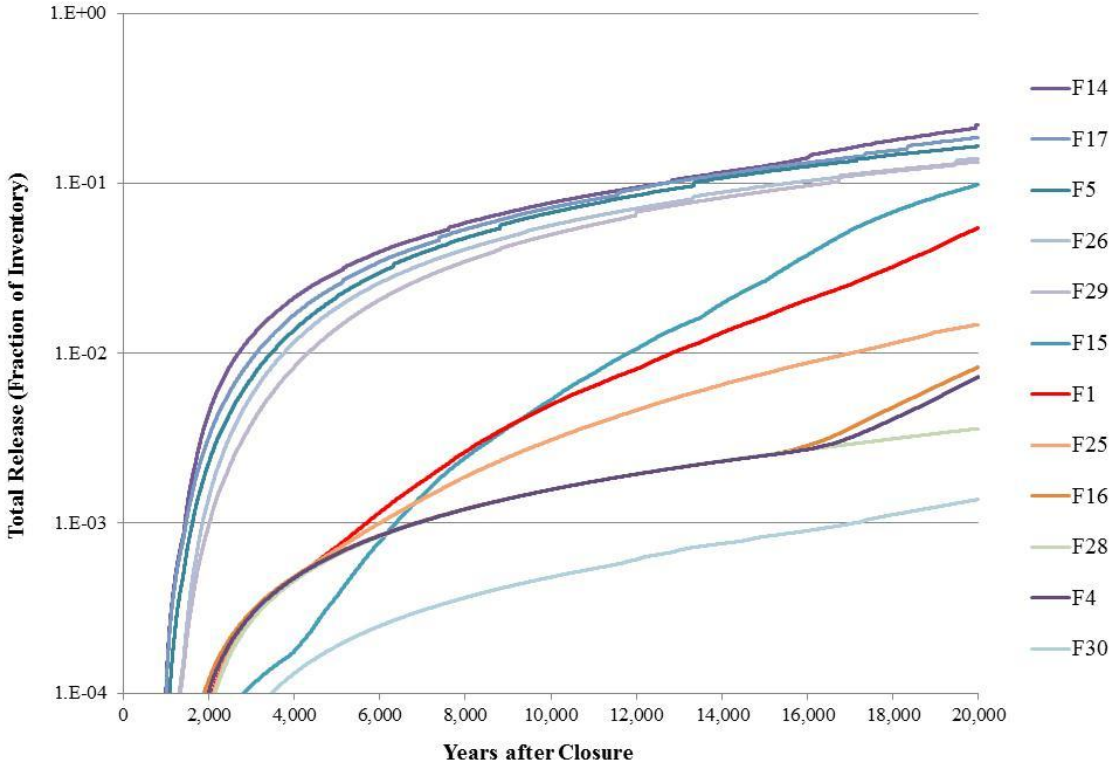

Note: Technetium solubility value of 1.0E-08 mol/L for saltstone and FDC concrete

Note that the modeling results shown in the above figures indicate that the selection of the flow cases illustrates:

(1) The probabilistic modeling results will demonstrate a wide range of potential future outcomes to provide greater insights into the sensitivities of specific modeling assumptions.

(2) The selection of these flow cases are expected to result in conservatively high doses, which may not be indicative of a more likely or expected set of modeling assumptions (e.g., the deterministic flow settings of the Evaluation Case F1).

5.6.6.8 Maximum Potential Dose to the MOP from Tc-99 Release within 10,000 Years

Previous sensitivity studies in this SA addressed the potential impact to the dose to the MOP from two flow cases (F10 and F20) as well as the Evaluation Case (Section 5.6.6.1). The flow cases are described in Table 4.4-3. Flow Case F10 was chosen to determine the potential dose to the MOP using flow parameters that could be considered as expected; that is, the best estimate degradation rate of cementitious material, the average infiltration rate, and the average, or nominal, initial saturated hydraulic conductivity of 6.4E-09 cm/s for saltstone. Flow Case F20 was selected to investigate the most pessimistic flow conditions; that is, the nominal degradation rate of cementitious material, the maximum infiltration rate, and the very large initial saturated hydraulic conductivity of 4.5E-07 cm/s for saltstone. Although Flow Case F20 provides the most pessimistic flow conditions, it may not provide the flow conditions necessary to provide the highest peak Tc-99 release rate (and associated dose) within the performance period of 10,000 years that is evaluated by the NRC in their consultation role. Of interest is how soon after SDF closure could the peak dose to the MOP occur based on the computer modeling used in this SA. A consequence of the shrinking core model is the manufacturing of spikes of Tc-99 being released when individual nodal elements release their remaining Tc-99 mass once these nodal elements become oxidized. When a nodal element is oxidized the Tc-99 release is no longer solubility controlled but rather is released with a very small K_d value of 0.5 mL/g. The timing and magnitude of these Tc-99 release spikes is an artifact of the current model which conservatively maximizes the Tc-99 dose.

This additional analysis considers the 12 flow cases identified in Section 5.6.6.7 and the three values for technetium solubility provided in Section 5.6.6.5, with the SDU concrete initially oxidized and the joints having MCCs associated with gravel. The peak Tc-99 release rates from these 36 cases (12 flow cases and three values of technetium solubility) out to 10,000 years are provided in Table 5.6-21, ranked from the highest to the lowest Tc-99 peak release rate.

Table 5.6-21: Peak Tc-99 Release Rate from a FDC within 10,000 Years

Parametric Flow Case	Solubility Value (mol/L)	Peak Tc-99 Release Rate (mol/yr)	Time of Peak Release Rate (years)
F5	1.0E-09	1.21E-01	7,892
F17	1.0E-09	1.09E-01	6,550
F5	1.0E-08	1.01E-01	7,892
F17	1.0E-08	9.25E-02	6,549
F14	1.0E-09	8.54E-02	6,762
F29	1.0E-09	7.87E-02	9,995
F14	1.0E-08	7.24E-02	6,762
F29	1.0E-08	6.58E-02	9,995
F14	1.0E-07	2.68E-02	2,901
F5	1.0E-07	2.54E-02	5,001
F17	1.0E-07	2.51E-02	5,501
F26	1.0E-09	2.47E-02	7,992
F26	1.0E-07	2.39E-02	5,201
F29	1.0E-07	2.20E-02	8,032
F26	1.0E-08	2.17E-02	7,992
F15	1.0E-07	5.90E-03	9,814
F1	1.0E-07	4.42E-03	9,928
F25	1.0E-07	2.04E-03	9,941
F15	1.0E-08	7.59E-04	9,956
F28	1.0E-07	6.89E-04	2,401
F4	1.0E-07	6.41E-04	2,401
F16	1.0E-07	6.07E-04	2,401
F1	1.0E-08	4.72E-04	10,000
F15	1.0E-09	3.19E-04	9,958
F25	1.0E-08	2.79E-04	8,606
F1	1.0E-09	2.37E-04	8,479
F30	1.0E-07	2.02E-04	3,501
F25	1.0E-09	1.49E-04	8,609
F28	1.0E-08	6.89E-05	2,401
F30	1.0E-08	6.78E-05	10,000
F4	1.0E-08	6.41E-05	2,401
F30	1.0E-09	6.25E-05	10,000
F16	1.0E-08	6.07E-05	2,401
F28	1.0E-09	6.89E-06	2,401
F4	1.0E-09	6.41E-06	2,401
F16	1.0E-09	6.07E-06	2,401

Table 5.6-22 shows the same data as Table 5.6-21 but it is grouped by the technetium solubility value for the 10,000-year peaks. Inspection of these two tables shows that what may be "conservative" assumptions with respect to flow conditions does not necessarily result in greater Tc-99 release rates. Tables 5.6-21 and 5.6-22 indicate Flow Case F5 provides the largest Tc-99 release rate within 10,000 years for the solubility values of 1.0E-09 mol/L and 1.0E-08 mol/L. Flow Case F5 represents the average infiltration rate and the Best Estimate degradation rate (summarized in Section 4.2.5) for cementitious materials, but with the highest value for the initial saturated hydraulic conductivity for saltstone of 4.5E-07 cm/s. For the technetium solubility value of 1.0E-07 mol/L, the peak Tc-99 release rate is provided by Flow Case F14; however, this peak release rate is less than 20 % greater than the peak Tc-99 release rate associated with Flow Case F5 for the same solubility value. Note also that the peak Tc-99 release rates for flow cases with a technetium solubility value of 1.0E-07 mol/L are significantly lower than the peak release rates associated with the other two values for the technetium solubility value.

Table 5.6-22: Peak Tc-99 Release Rate from a FDC within 10,000 years (Grouped by Solubility Value)

Solubility = 1E-09 mol/L			Solubility = 1E-08 mol/L			Solubility = 1E-07 mol/L		
Flow Case	**Peak (mol/yr)**	**Time (years)**	**Flow Case**	**Peak (mol/yr)**	**Time (years)**	**Flow Case**	**Peak (mol/yr)**	**Time (years)**
F5	1.21E-01	7,892	F5	1.01E-01	7,892	F14	2.68E-02	2,901
F17	1.09E-01	6,550	F17	9.25E-02	6,549	F5	2.54E-02	5,001
F14	8.54E-02	6,762	F14	7.24E-02	6,762	F17	2.51E-02	5,501
F29	7.87E-02	9,995	F29	6.58E-02	9,995	F26	2.39E-02	5,201
F26	2.47E-02	7,992	F26	2.17E-02	7,992	F29	2.20E-02	8,032
F15	3.19E-04	9,958	F15	7.59E-04	9,956	F15	5.90E-03	9,814
F1	2.37E-04	8,479	F1	4.72E-04	10,000	F1	4.42E-03	9,928
F25	1.49E-04	8,609	F25	2.79E-04	8,606	F25	2.04E-03	9,941
F30	6.25E-05	10,000	F28	6.89E-05	2,401	F28	6.89E-04	2,401
F28	6.89E-06	2,401	F30	6.78E-05	10,000	F4	6.41E-04	2,401
F4	6.41E-06	2,401	F4	6.41E-05	2,401	F16	6.07E-04	2,401
F16	6.07E-06	2,401	F16	6.07E-05	2,401	F30	2.02E-04	3,501

Figure 5.6-88 illustrates the Tc-99 release rates associated with Flow Case F5 and the three values for technetium solubility. At a solubility value of 1.0E-07 mol/L, the inventory of Tc-99 is released within 16,000 years. For the other two solubility values, 1.0E-09 mol/L and 1.0E-08 mol/L, the Tc-99 release rate spikes coincide with each other as to be expected because of the common flow parameters between the cases. The Tc-99 release rate spikes are generally higher for the lower solubility value, than the higher solubility value, because there is more Tc-99 available for release once nodal regions within the model become oxidized and release the Tc-99. The nodal discretization used in the model has a significant impact on the frequency and magnitude of the spikes. A finer discretization would likely result in an increase in the number of spikes but at lower magnitudes.

Figure 5.6-88: Tc-99 Release Rates from an FDC for Flow Case F5

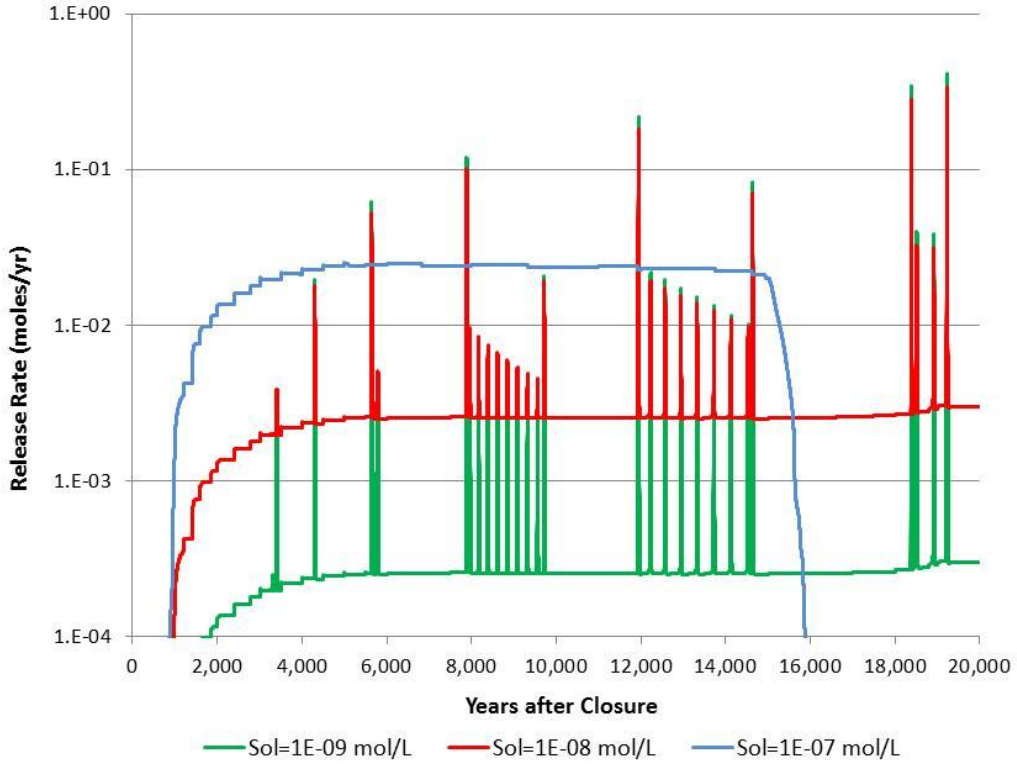

Figure 5.6-89 illustrates the Tc-99 dose profile to the MOP at 100 meters for these release scenarios at the maximum sector. Although this potential dose to the MOP exceeds 25 mrem/yr within 10,000 years at a particular spike, the dose to the MOP is expected to be less than this value due to assumptions and artifacts of the modeling. In particular, the general assumption that all of the FDCs degrade at exactly the same way at exactly the same time increases the magnitude of the estimated dose to the MOP from the potential dose spikes.

Figure 5.6-89: Maximum Dose to the MOP from Tc-99 for Flow Case F5

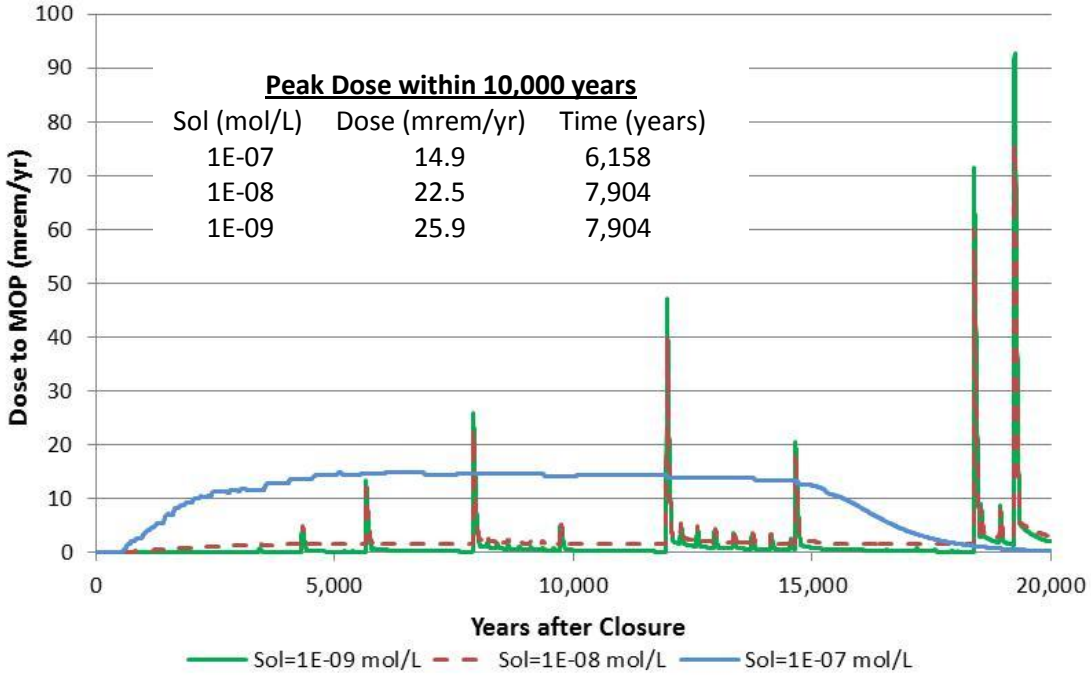

Another assumption associated with Flow Case F5 is the large initial value for the saturated hydraulic conductivity of saltstone. Flow Cases F5 and F4 differ only by the initial hydraulic conductivity of saltstone. For Flow Case F5 the initial hydraulic conductivity is 4.5E-07 cm/s and for Flow Case F4 the initial hydraulic conductivity for saltstone is 6.4E-09 cm/s. As shown in Tables 5.6-21 and 5.6-22, the peak Tc-99 release rates are orders of magnitude greater for the F5 case than for the F4 case, with the only difference between the two cases being the initial hydraulic conductivity of saltstone. Figure 5.6-90 illustrates the difference between these two flow cases on the Tc-99 release rate from a single FDC.

Figure 5.6-90: Tc-99 Release Rates from FDC for Flow Cases F4 and F5 with Assumed Solubility of 1E-09 mol/L

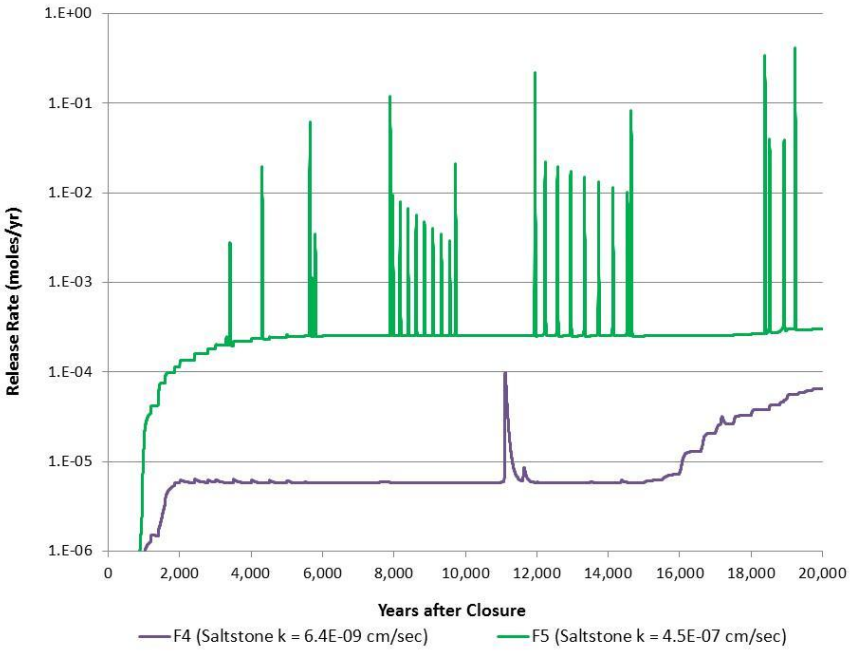

In summary, the maximum potential dose to the MOP within 10,000 years from the release of Tc-99 is shown to slightly, exceed 25 mrem/yr. However, this maximum dose is due to pessimistic assumptions; namely, an unlikely initial hydraulic conductivity of saltstone (10 times greater than the maximum reported value from recent testing, see Section 4.2.1), the degradation and Tc-99 releases of all of the FDCs in the same year. Also, the model construction has a significant impact on the Tc-99 release spikes.

Even though this current Tc-99 release model would tend to maximize the magnitude of the Tc-99 release spikes, this section is provided to identify the maximum Tc-99 spike that could occur based on this release model. The expectation of the actual result is less than the spikes indicate with the understanding that the spikes are model artifacts. Considering the goal of this special analysis is to provide confidence that performance objectives will be met, the fact that the conservative modeling results (i.e., spikes) only slightly exceed 25 mrem/yr within the 10,000 year timeframe provides that confidence.

5.6.6.9 Summary of the SA Using the Deterministic PORFLOW Model

Various sensitivity analyses were performed using the Deterministic PORFLOW Model to provide improved understanding of a number of important input parameters affecting the dose results. The modeling runs were performed to evaluate the impact of variability in multiple areas of interest (e.g., flow variability, roof slope variability, Tc-99 solubility). The various sensitivity studies performed illustrate that the Evaluation Case dose results presented in Section 5.5.1 are not significantly impacted, even using more conservative inputs, providing greater confidence that the results and conclusions remain valid. Based on these analyses, future doses are not expected to exceed performance objectives for the SDF.

5.7 ALARA Analysis

Section 5.7 of the SDF PA describes how the "as low as reasonably achievable" (ALARA) requirement of DOE O 435.1, Chg. 1 and 10 CFR 61.41 are implemented for SDF. [SRR-CWDA-2009-00017] The ALARA information presented in the SDF PA is not affected by the new information presented in this SA.

6.0 INADVERTENT INTRUDER ANALYSIS

This section will discuss the impact of the new information on the SDF inadvertent intruder analysis information presented in Section 6.0 of the SDF PA.

6.1 Groundwater Concentrations at One Meter

Radionuclide inventories for the one-meter groundwater concentrations used in this SA are presented in Table 3.4-1. The one-meter groundwater concentrations were calculated using the SDF PORFLOW Model for the Evaluation Case. Maximum groundwater concentrations are given for the modeling cell adjoining the analyzed source terms. Table B-1 (see Appendix B) shows peak 1-meter radionuclides concentrations for any of the three aquifers in the highest sector modeled in 1,000 years.

Appendix B tables also list the MCL for each constituent with the derived values for beta-gamma and photon emitters from Table II-3 of FR-00-9654. The MCLs provided in the reference are based on a beta-gamma dose of 4 mrem/yr. The peak concentration of each beta-gamma emitter is compared to a specific MCL to determine their fraction. To determine if the 4 mrem/yr beta-gamma limit is met, the sum of the fractions must be less than 1.0. The total alpha MCL includes Ra-226, but does not include radon or uranium. The radium MCL includes both Ra-226 and Ra-228. [SCDHEC R.61-58]

6.2 Acute Exposure Scenarios

Section 6.2 of the SDF PA describes how the biotic pathway doses are calculated for the Acute Exposure Scenarios. The acute exposure scenarios information presented in the SDF PA is not being revised as part of this SA.

6.3 Chronic Exposure Scenarios

Section 6.3 of SDF PA describes how doses are calculated for the chronic intruder scenario. The chronic exposure scenarios presented in the SDF PA have been revised to reflect the most recent available data. For example, applicable input parameters were updated based on the EPA's 2011 *Exposure Factors Handbook* (EPA-600-R-090-052F). A complete discussion of the revised biotic pathways, dose calculations, and related inputs is provided in the report: *Dose Calculation Methodology for Liquid Waste Performance Assessments at the Savannah River Site* (SRR-CWDA-2013-00058). An analysis of the revised approach (in Appendix A of SRR-CWDA-2013-00058) indicated that these updates do not significantly impact the dose results, relative to the approach used in the SDF PA.

6.4 Chronic Intruder Dose Results

Section 6.4 of SDF PA contains calculations of the peak total intruder doses for the chronic intruder agricultural (Post-Drilling) scenario. The peak total doses for the Chronic Intruder Agricultural (Post-Drilling) Scenario were calculated using the maximum 1-meter concentrations identified in Section 6.1. A peak dose was identified for the 10,000-year performance period.

The peak Chronic Intruder Scenario doses for the SDF were calculated in the SDF PA using the highest concentration for each radionuclide in any sector (a discussion of how peak

concentrations were determined by sector was provided in Section 6.1 of the SDF PA). These peak doses were the total dose associated with the applicable individual 1-meter well pathways identified in Section 6.3 of the SDF PA. The doses associated with direct exposure from the disposed waste form are not tied to groundwater concentration and were calculated separately. The direct exposure dose was shown to be negligible and therefore did not contribute to the peak dose.

For this SA, additional locations for the groundwater dose pathway to the chronic intruder, also identified as the IHI, are utilized. Two of the additional locations were discussed in the response to RAI II-1 (SRR-CWDA-2011-00044). These two locations were representative of the maximum groundwater concentrations associated with SDU 4 and FDCs. For SDU 4 the location of the well to obtain groundwater concentrations was chosen to maximize the concentration by radionuclide within the vicinity of SDU 4. A similar analysis was conducted for FDCs, which had the potential for more extreme values of groundwater radionuclide concentration; that is, the maximum concentration, by radionuclide was obtained from any location within the SDF boundary at the proximity of any FDC. In a similar fashion to SDU 4, the maximum groundwater concentrations associated with SDU 1 have been developed for this SA. In addition to these locations, specific well locations have been identified to estimate the dose to the IHI at strategic locations within the SDF. These well locations are discussed in Section 4.4.2.4 and shown in Figure 4.4-2. These well locations are also shown in Figure 6.4-1, identified by their grid location (I, J).

Figure 6.4-1: Well Locations for the Chronic Intruder

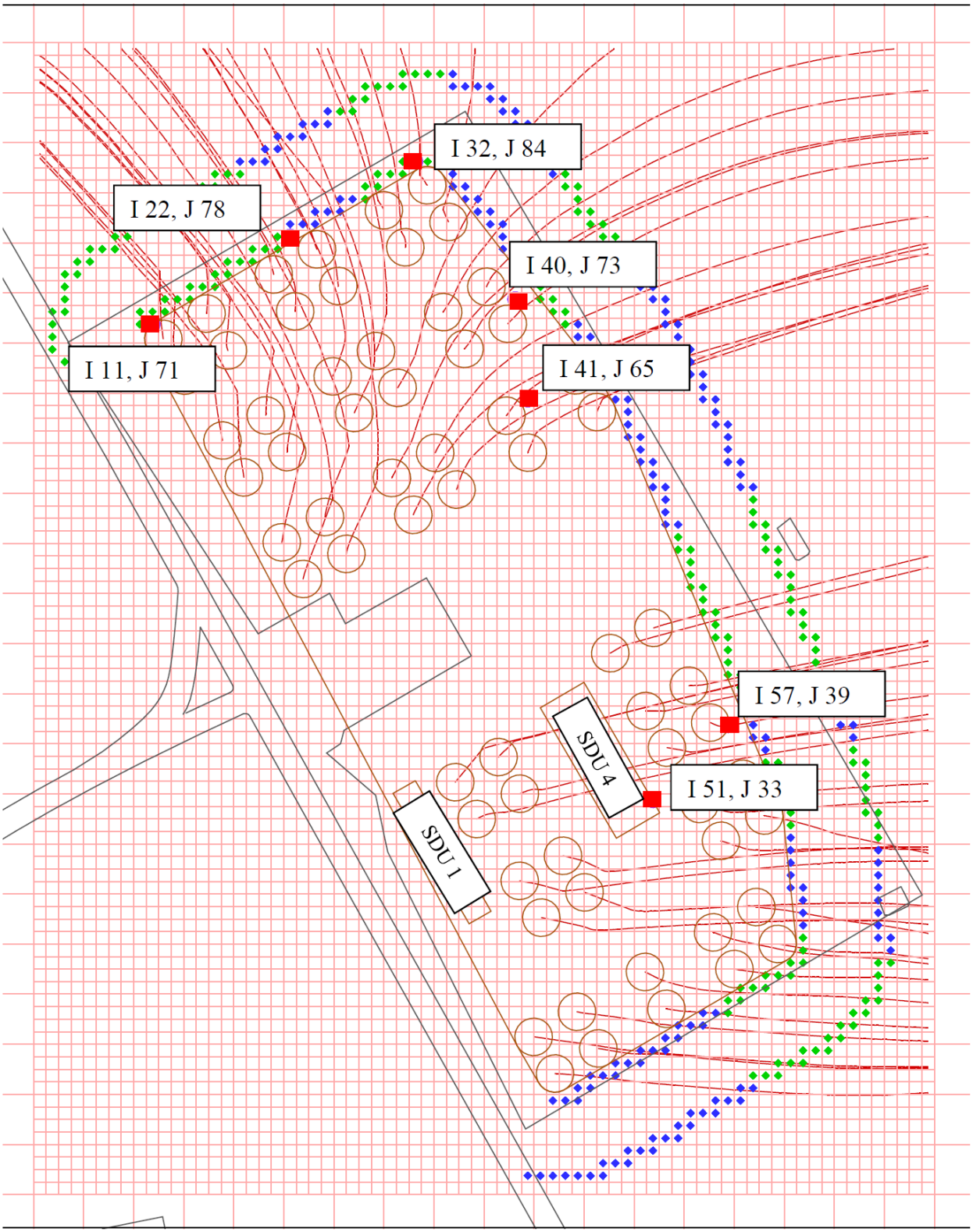

Tables 6.4-1 and 6.4-2 present the peak dose results to the chronic intruder in 1,000 years and 10,000 years, respectively, for the shown in Figure 6.4-1.

Table 6.4-1: Peak Dose to the Chronic Intruder within 1,000 Years after Closure

Location	Peak Dose and Time	Significant Radionuclides
At 1-meter boundary	0.05 mrem/yr (1,000 years)	I-129 (65 %), Tc-99 (35 %)
Near SDU 1	0.36 mrem/yr (910 years)	I-129 (74 %), Tc-99 (26 %)
Near SDU 4	0.19 mrem/yr (812 years)	I-129 (74 %), Tc-99 (26 %)
Near FDC	0.12 mrem/yr (1,000 years)	I-129 (71 %), Tc-99 (29 %)
Well 1 (I 11, J 71)	0.03 mrem/yr (1,000 years)	I-129 (79 %), Tc-99 (21 %)
Well 2 (I 22, J 78)	0.01 mrem/yr (1,000 years)	I-129 (78 %), Tc-99 (22 %)
Well 3 (I 32, J 84)	0.02 mrem/yr (1,000 years)	I-129 (79 %), Tc-99 (21 %)
Well 4 (I 40, J 73)	0.02 mrem/yr (1,000 years)	I-129 (79 %), Tc-99 (21 %)
Well 5 (I 41, J 65)	0.02 mrem/yr (1,000 years)	I-129 (79 %), Tc-99 (21 %)
Well 6 (I 57, J 39)	0.05 mrem/yr (1,000 years)	I-129 (66 %), Tc-99 (34 %)
Well 7 (I 51, J 33)	0.10 mrem/yr (816 years)	I-129 (73 %), Tc-99 (27 %)

Table 6.4-2: Peak Dose to the Chronic Intruder within 10,000 Years after Closure

Location	Peak Dose and Time	Significant Radionuclides
At 1-meter boundary	20 mrem/yr (7,672 years)	I-129 (95 %), Tc-99 (5 %)
Near SDU 1	5.4 mrem/yr (5,588 years)	I-129 (64 %), Cs-135 (22 %), Tc-99 (14 %)
Near SDU 4	13 mrem/yr (3,504 years)	I-129 (67 %), Tc-99 (32 %)
Near FDC	39 mrem/yr (7,666 years)	I-129 (95 %), Tc-99 (5 %)
Well 1 (I 11, J 71)	24 mrem/yr (7,668 years)	I-129 (98 %), Tc-99 (2 %)
Well 2 (I 22, J 78)	13 mrem/yr (7,674 years)	I-129 (98 %), Tc-99 (2 %)
Well 3 (I 32, J 84)	19 mrem/yr (7,674 years)	I-129 (98 %), Tc-99 (2 %)
Well 4 (I 40, J 73)	17 mrem/yr (7,672 years)	I-129 (98 %), Tc-99 (2 %)
Well 5 (I 41, J 65)	14 mrem/yr (7,670 years)	I-129 (98 %), Tc-99 (2 %)
Well 6 (I 57, J 39)	32 mrem/yr (7,668 years)	I-129 (96 %), Tc-99 (4 %)
Well 7 (I 51, J 33)	7.4 mrem/yr (5,264 years)	Tc-99 (50 %), Cs-135 (39 %), I-129 (11 %)

Figure 6.4-2 presents the dose to the chronic intruder out to 20,000 years for two pairs of well locations. The first pair, FDC and Well 5739, represents the dose to the chronic intruder representative of FDCs, which may include contributions from SDU 4 and/or SDU 1. The second pair, SDU 4 and Well 5133 represents the dose to the chronic intruder representative of SDU 4 with minimal influence from other SDUs and FDCs. As noted above, a maximization of the estimated dose to the chronic intruder is expected when the FDC and SDU 4 methodology, presented in the response to RAI II-1 (SRR-CWDA-2011-00044), is used. Figure 6.4-2 reinforces that conviction.

Figure 6.4-2: Dose to Chronic Intruder Representative of FDCs and SDU 4

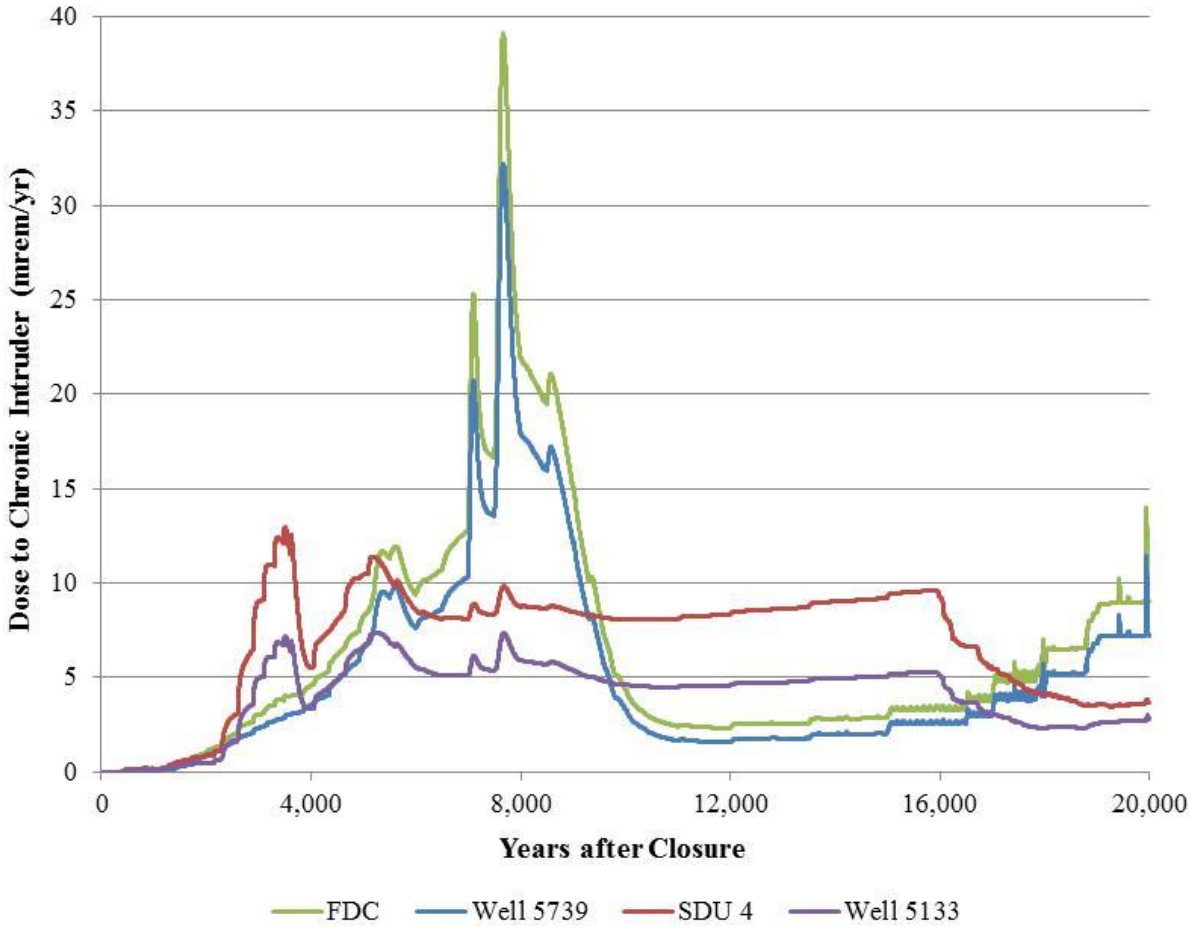

6.5 Intruder Uncertainty/Sensitivity Analysis

Section 6.5 of the SDF PA considers the effects on the inadvertent intruder analysis of uncertainties in the conceptual models used and sensitivities to the parameters used in the mathematical models. The following sections provide updated uncertainty and sensitivity analyses, using IHI model results from the Evaluation Case.

6.5.1 IHI Uncertainty Analysis: Statistics of the Peaks

As with the MOP dose results discussed in Section 5.6.4, the most direct way to communicate the uncertain nature of the modeled IHI dose results is to illustrate certain key model endpoints. Statistics for peak values are summarized in Table 6.5-1 for any time step within specific timeframes. Since it is the relevant performance metric that was analyzed in the SDF PA, peak doses to the IHI at the 100-meter boundary of the SDF is the focus of Table 6.5-1. [SRR-CWDA-2009-00017]

The table also includes data pertinent to IHI Well 4 because this well represented the peak IHI dose in nearly half of all the realizations.

Table 6.5-1: Statistics of the Peak IHI Endpoints within Any Time Step

Endpoint Evaluated	Model IDs Used [a]	Mean of the Peaks	Median of the Peaks (50th Percentile)	95th Percentile of the Peaks
All IHI Wells: IHI dose from Evaluation Case within 10,000 years (mrem/yr)	TcRS1 and TcRS2	55	27	193
All IHI Wells: IHI dose from Evaluation Case within 20,000 years (mrem/yr)	TcRS1 and TcRS2	139	35	533
IHI Well 4 dose from Evaluation Case within 10,000 years (mrem/yr)	TcRS1 and TcRS2	48	20	172

a See Table 5.6-4.

The previous Table 6.5-1 shows summary statistics for peaks of the IHI doses achieved at any time within the given time frames (e.g., 0 years to 10,000 years after closure). These are "statistics of the peak values" (e.g., mean of the peaks), regardless of when the peaks were achieved within the specific time frames. Alternatively, the information provided below examines statistics relative to each time step and offers "peak values of the statistics" (e.g., peak of mean).

As an example, Figure 6.5-1 shows the peak IHI doses (for all IHI wells) within 10,000 years for all realizations. The information presented in Table 6.5-1 gives no credit to the time of occurrence for each of these points, presenting statistics only on the magnitudes of the dose values.

Figure 6.5-1: Peak IHI Doses within 10,000 Years from SDF Uncertainty Analysis GoldSim Files (*SRS Saltstone v4.101*)

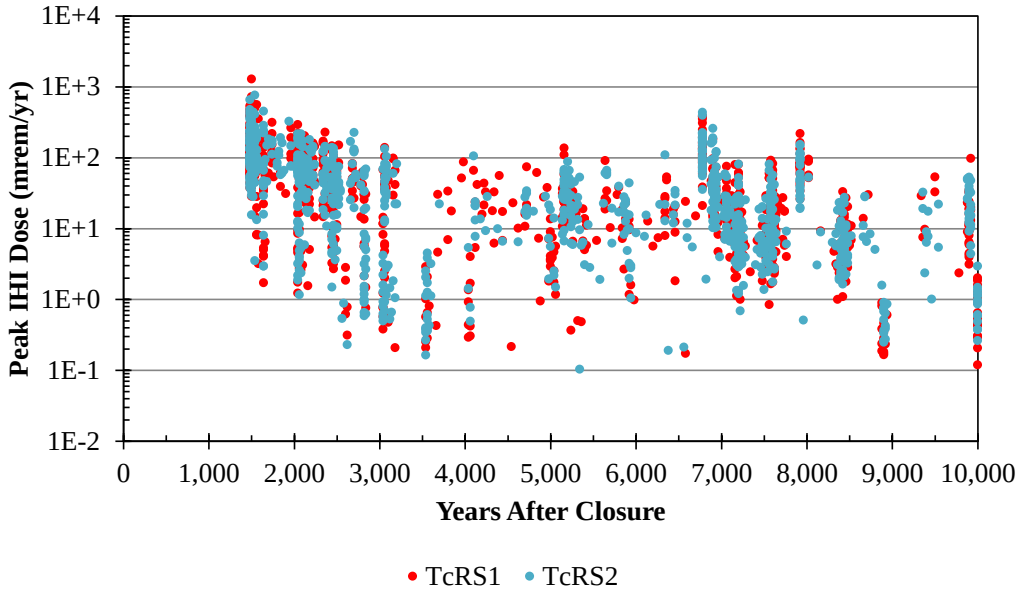

6.5.2 IHI Uncertainty Analysis: Peaks of the Statistics

Where Table 6.5-1 showed the statics of the peaks of the endpoints, regardless of timing, Table 6.5-2 shows the peaks of the statistics and identifies the timing of such peaks. Figures following this table illustrate these.

Table 6.5-2: Peaks of the IHI Endpoint Statistics

Endpoint Evaluated	Model IDs Used [a]	Peak of the Means		Peak of the Medians (50th Percentile)		Peak of the 95th Percentiles	
		Peak	Time (years)	Peak	Time (years)	Peak	Time (years)
All IHI Wells: Total IHI dose in 10,000 years (mrem/yr)	TcRS1 and TcRS2	28	1,500	5.8	3,220	152	1,500
Well 4: IHI dose (mrem/yr)	TcRS1 and TcRS2	22	1,500	5.0	7,200	133	1,500

a See Table 5.6-4.

Note that the timing of the peak of the means and the peak 95th percentile are very similar, whereas the peak of the median has a different time of occurrence. This indicates that the distributions may skew results high, as discussed below.

Figure 6.5-2 shows the statistical time histories of the total IHI dose at any intruder well, using the 2,000 realizations of data from TcRS1 and TcRS2.

Figure 6.5-2: Statistical Time Histories for IHI Total Dose, Any Intruder Well, 2,000 Realizations (*SRS Saltstone v4.101*)

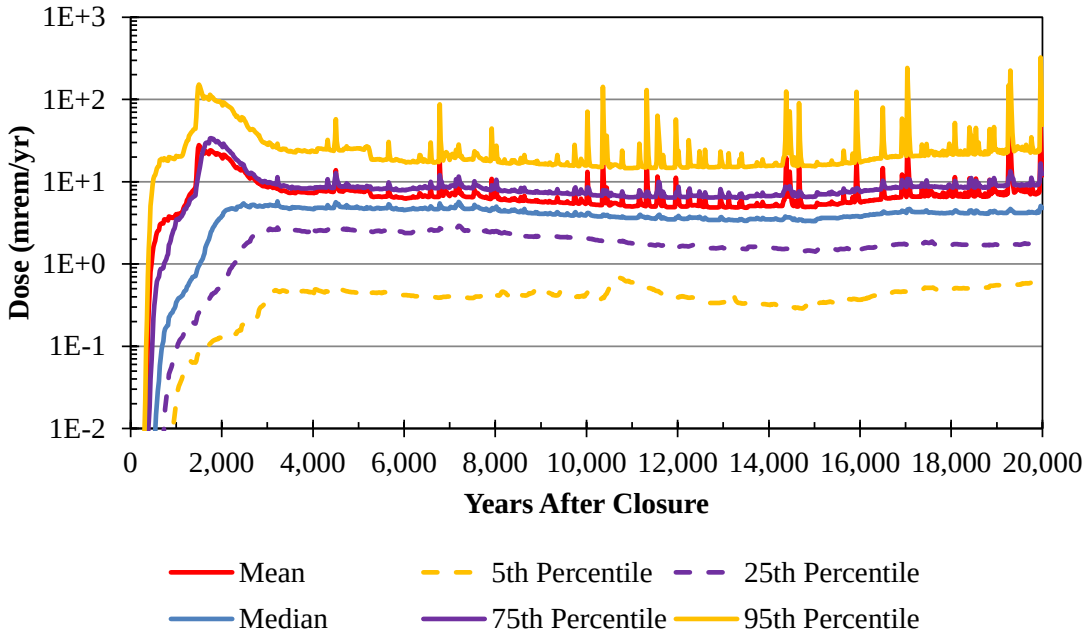

In this figure, the 5th and 95th percentiles are significantly below and above the median value, respectively. The mean values are driven higher by the uncertainty distributions of the modeled parameters, approaching (and sometimes exceeding) the 75th percentile. This indicates that the models apply distributions with long tails (e.g., lognormal distributions) or extreme values are inherent in these distributions. It is somewhat expected that the mean value is higher than the median because many of the dominant distributions were established to be reasonably conservative, resulting in the distributions being skewed to the high end. This approach inflates the variance in the uncertainty analyses, resulting in a few realizations dominating the uncertainty analysis results. The intent of Section 6.5.3 is to investigate which parameters are having the most impact on this aspect of the uncertainty analysis.

Figure 6.5-3 shows the mean value from the total dose (using only IHI Well 4), along with respective dose contributions from I-129, Cs-135, Ra-226, and Tc-99 from the *SRS Saltstone v4.101* models. This figure illustrates that at the time of the initial peak doses (between approximately 1,500 an 2,500 years after closure) the most significant radionuclide dose contributor is I-129. Then Tc-99 dominates all subsequent peaks.

Figure 6.5-3: Mean IHI Doses (Well 4), Major Radionuclide Contributors within 20,000 Years (*SRS Saltstone v4.101*)

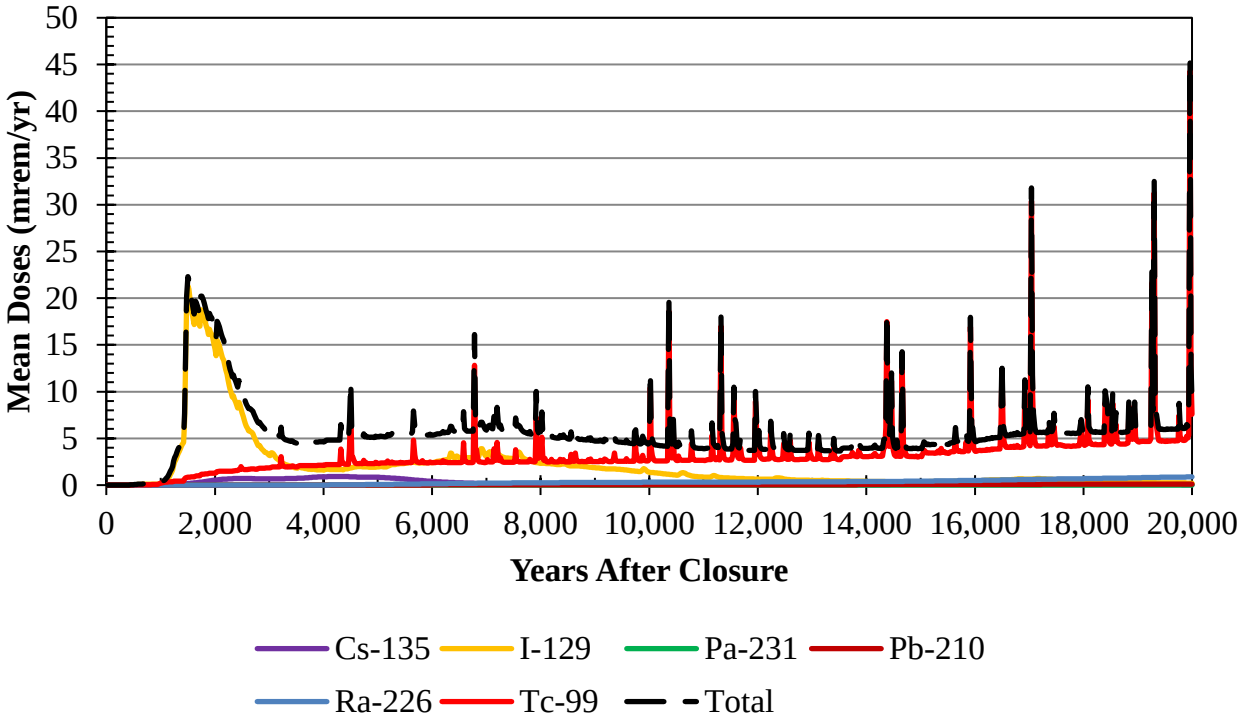

Figure 6.5-4 uses the 2,000 realizations from the *SRS Saltstone v4.101* models (TcRS1 and TcRS2), to provide the mean doses from each IHI Well over 20,000 years. Again, the peak doses are dominated by IHI Well 4.

Figure 6.5-4: Mean IHI Doses, Each Well within 20,000 Years (*SRS Saltstone v4.101*)

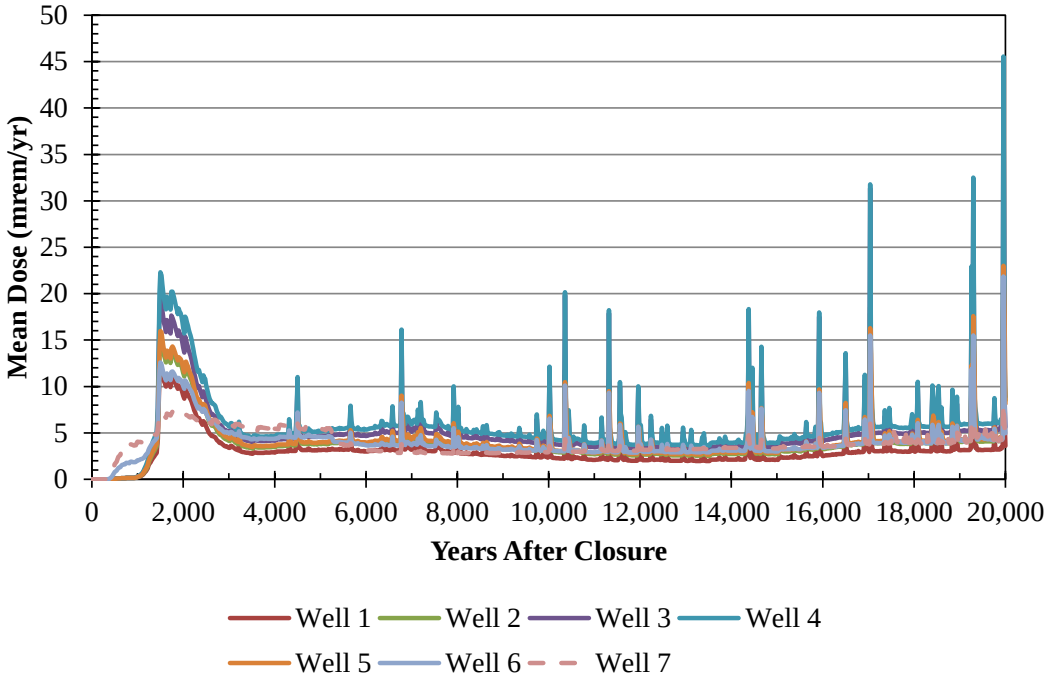

Similar to Figure 6.5-2, Figure 6.5-5 shows the statistical results of the peak doses from IHI Well 4 for *SRS Saltstone v4.101*.

Figure 6.5-5: Statistic Results for Peak IHI Doses at Intruder Well 4 (*SRS Saltstone v4.101*)

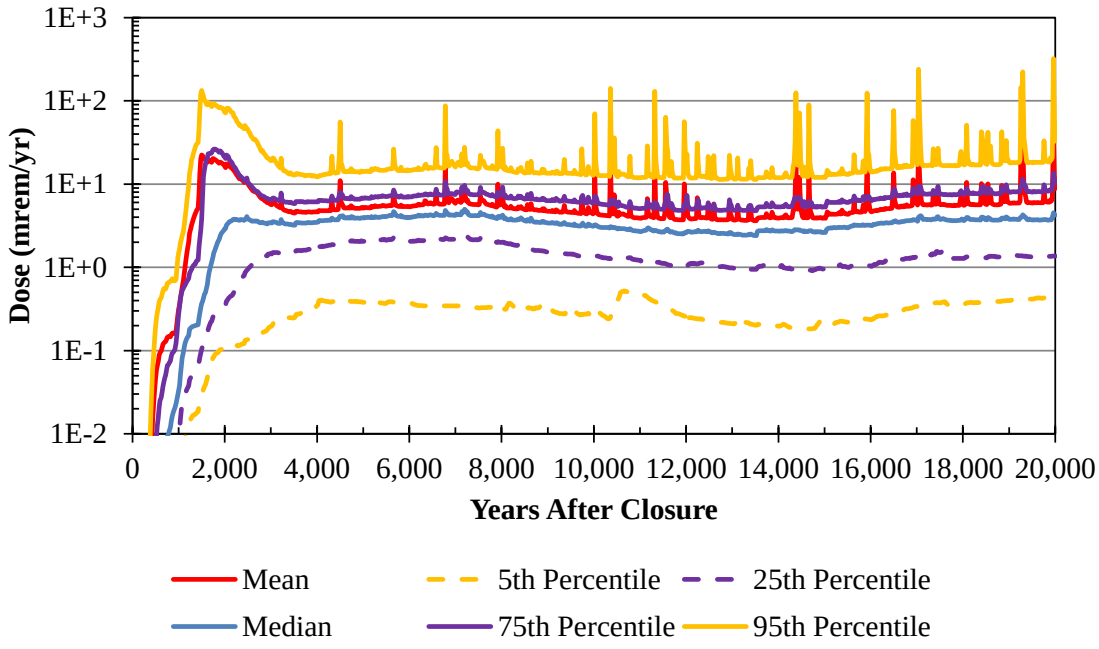

6.5.3 IHI Sensitivity Analysis Results

This section applies the same analysis methodology as was used for the sensitivity analysis of the MOP dose (described in Section 5.6.5). This section presents analysis results for the following IHI endpoints: (1) total dose to the IHI at any intruder well, (2) total dose to the IHI at intruder Well 4.

Sensitivity Analysis of the Total Dose to the IHI at Any Intruder Well

The PRCCs for total dose to the IHI at any intruder well are depicted in Figures 6.5-6 and 6.5-7. These figures show PRCC results from two separate GoldSim runs (TcRS1 and TcRS2). The order (and therefore the colors) assigned to each variable within these figures is based on the magnitude of the peak absolute value of the PRCC value expressed in each analysis. Although the order of the variables shown in these figures is slightly different, the overall results are extremely similar.

Figure 6.5-6: IHI Total Dose PRCCs, Any Intruder Well, 1,000 Realizations (Model TcRS1)

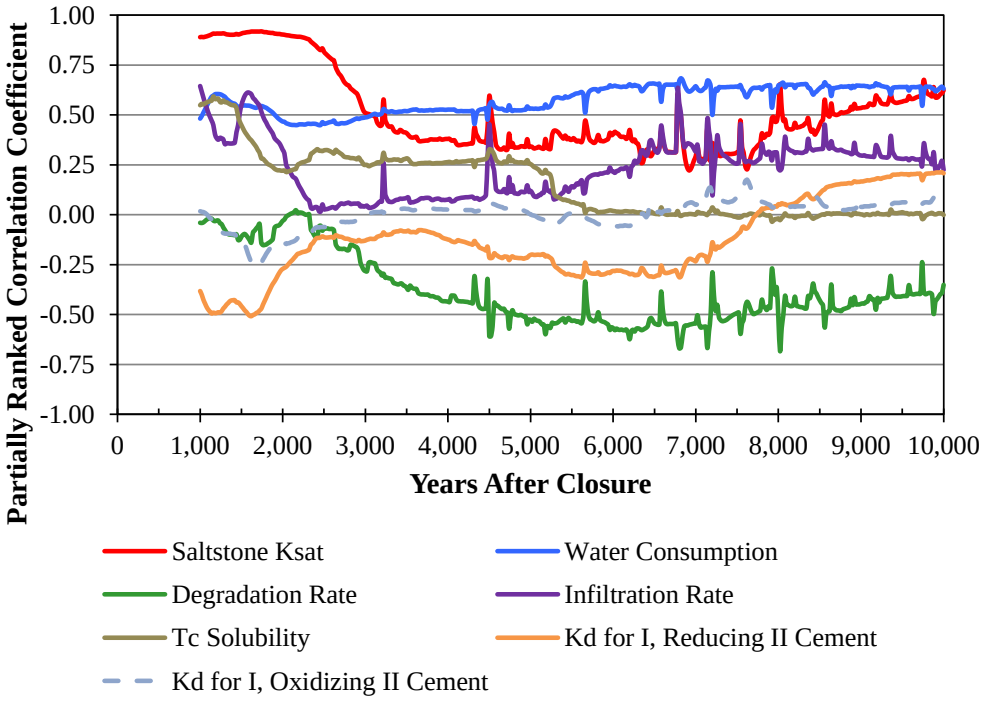

Figure 6.5-7: IHI Total Dose PRCCs, Any Intruder Well, 1,000 Realizations (Model TcRS2)

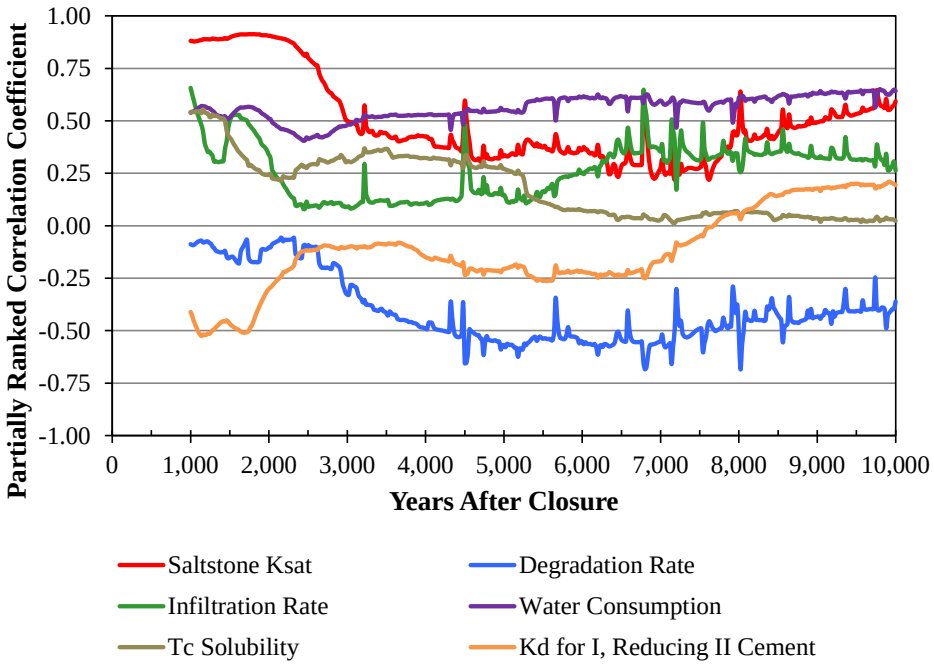

Table 6.5-3 shows the results from the stepwise regression analysis. Again, results from two 1,000-realization models (TcRS1 and TcRS2) are depicted. The table only shows the first six variables from each model as the importance of each variable quickly diminishes with each successive analysis step. In this analysis, the first four or five variables effectively dominate any influence over the dependent variable at the time of the peak of the mean.

Table 6.5-3: IHI Total Dose Top Six SRRC Results, Any Intruder Well at Time of Peak of the Mean Value

SRRCs Using 1,000 Realizations from Model TcRS1, t = 1,500 years, R^2 = 0.89			**SRRCs Using 1,000 Realizations from Model TcRS2, t = 1,500 years, R^2 = 0.86**		
Variable	**Cumulative R^2**	**SRRC**	**Variable**	**Cumulative R^2**	**SRRC**
Saltstone K_{sat}	0.66	0.79	Saltstone K_{sat}	0.64	0.81
Infiltration Rate	0.72	0.24	Infiltration Rate	0.69	0.23
Water Consumption	0.78	0.23	Water Consumption	0.74	0.24
Technetium Solubility	0.81	0.19	K_d for Iodine, Reduced Region II Cement	0.78	-0.22
K_d for Iodine, Reduced Region II Cement	0.85	-0.19	Technetium Solubility	0.82	0.19
Produce Consumption	0.85	0.06	K_d for I, Oxidizing II Cement	0.83	-0.05

Each set of realizations yielded similar variables as the top four and both with relatively similar values for the cumulative R^2 and SRRC values. This provides confidence in the identification of these four variables as important.

Sensitivity Analysis of the Total Dose to the IHI at Intruder Well 4

The PRCCs for total dose to the IHI at Intruder Well 4 are depicted in Figures 6.5-8 and 6.5-9. Table 6.5-4 shows the results from the stepwise regression analysis. Again, results from each of the 1,000-realization sets are depicted.

Figure 6.5-8: IHI Total Dose PRCCs, Intruder Well 4, 1,000 Realizations (Model TcRS1)

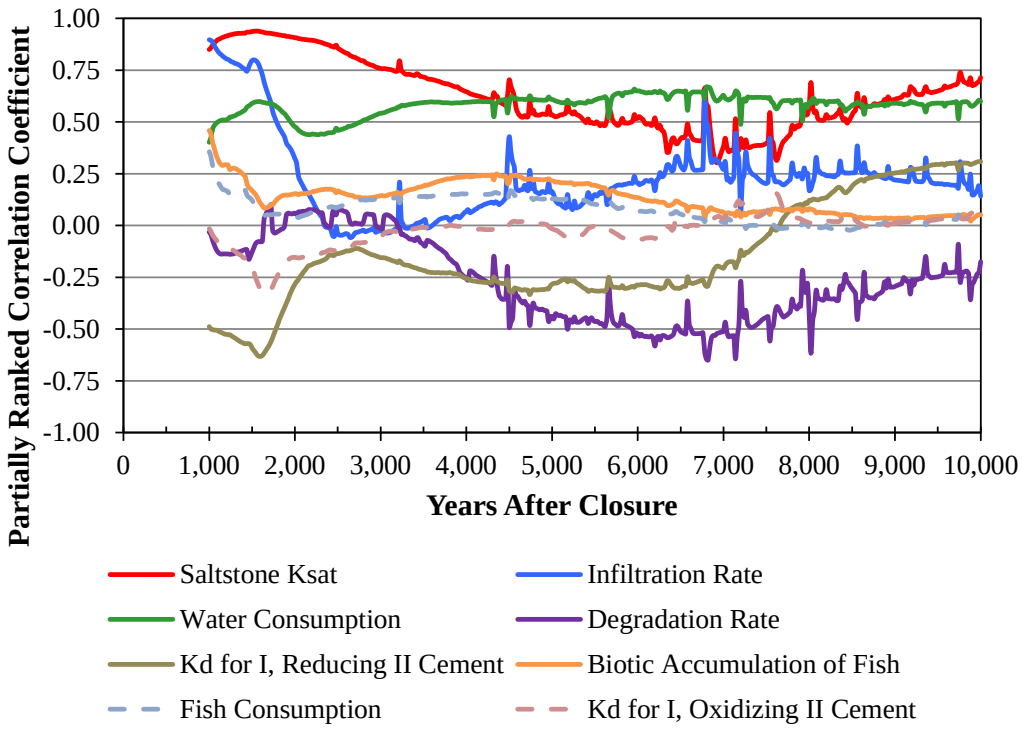

Figure 6.5-9: IHI Total Dose PRCCs, Intruder Well 4, 1,000 Realizations (Model TcRS2)

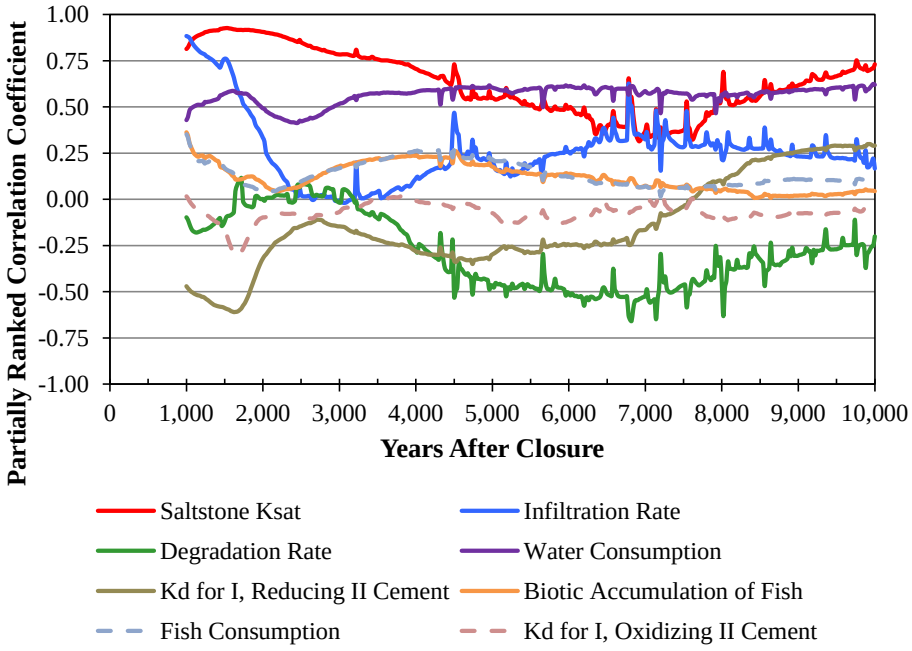

Table 6.5-4: IHI Total Dose Top Six SRRC Results, Intruder Well 4 at Time of Peak of the Mean Value

SRRCs Using 1,000 Realizations from Model TcRS1, t = 1,500 years, R^2 = 0.93			SRRCs Using 1,000 Realizations from Model TcRS2, t = 1,500 years, R^2 = 0.91		
Variable	**Cumulative R^2**	**SRRC**	**Variable**	**Cumulative R^2**	**SRRC**
Saltstone K_{sat}	0.64	0.77	Saltstone K_{sat}	0.62	0.79
Infiltration Rate	0.80	0.39	Infiltration Rate	0.75	0.39
Water Consumption	0.84	0.21	K_d for Iodine, Reduced Region II Cement	0.81	-0.23
K_d for Iodine, Reduced Region II Cement	0.88	-0.21	Water Consumption	0.86	0.23
I-129 inventory in FDC 10 (A,B,C,D)	0.89	0.10	I-129 inventory in FDC 10 (A,B,C,D)	0.88	0.12
Biotic Accumulation of Fish	0.90	0.05	K_d for Iodine, Oxidized Region II Cement	0.88	-0.06

6.5.4 Summary of the SDF Probabilistic Model Sensitivity Analysis for IHI Results

In general, the IHI sensitivity analyses reveals that the IHI results are dependent on essentially the same parameters as those identified through the MOP sensitivity analyses (see Section 5.6.5), except that the Infiltration Rate sampling shows up more prominently. This is likely caused by the shorter distance between the source term and the IHI receptor. The shorter transport distance reduces the effect of plume spreading, thus increasing the importance of infiltration.

7.0 INTERPRETATION OF RESULTS

Section 7.0 of SDF PA summarizes the conservatisms used in modeling and provides a summary and interpretation of the results presented in Section 5.0 and Section 6.0 of the SDF PA. The SDF PA conservatisms information presented in the SDF PA is not affected by the new information presented in this SA. The integrated system behavior discussion provided in the Section 7.1.1 of SDF PA remains valid irrespective of the revised parameters. The individual dose results provided in the Section 7.1.2 of SDF PA have been updated based on the Evaluation Case modeling using the updated SDU and FDC inventories and information at closure, and are summarized in the following sections. Additional sensitivity studies were performed to incorporate a revised Tc-99 waste release model and updated transport parameters.

7.1 SA Results

This section provides a summary and interpretation of the results of the Evaluation Case (Sections 7.1.1-7.1.5) and other evaluations (Sections 7.1.6-7.1.7) presented in Sections 5 and 6. The SA considered the most current understanding regarding various PA inputs (e.g., updated inventories, updated cementitious material degradation modeling, revised technetium release modeling, flow through explicit physical SDU features) through an Evaluation Case and other sensitivity analyses to confirm that the conclusions reached based on the SDF PA remain valid. The following discussions focus of a 10,000-year period since all 1,000-year doses are insignificant relative to the 10,000-year doses for all deterministic cases analyzed.

7.1.1 100-meter Groundwater Pathways Doses

The peak 100-meter groundwater pathway dose in the 10,000-year performance period is associated with Sector I (12 mrem/yr) and is dominated by the I-129 release from the FDCs. Water ingestion is the primary individual pathway. The peak 100-meter groundwater pathway dose in 10,000 years increased relative to the SDF PA. The increase is due to changes to the degradation properties of cementitious materials. The peak 100-meter groundwater pathway dose within 100,000 years comes from Sectors B and I. The dose to the MOP peaks at approximately 400 mrem/yr in Sector I and at approximately 31,000 years after closure due to Tc-99 release from the FDCs.

Movement and magnitude of the 31,000-year peak to within the 10,000-year time frame is unlikely due to several factors. The first would require the combination of multiple releases. A modeling simplification of allowing all events associated with the FDCs to occur simultaneously produces spikes in the dose results. Although this condition is understood to be unrealistic, it manufactures conservative results. Tc-99 release increases after oxidation of the saltstone material and the rate of the oxygen movement affects the release timing. The oxidation movement is primarily a function of the saltstone reduction capacity and oxygen flow, which is affected by the infiltration rate, hydraulic conductivity, and dissolved oxygen contained in the infiltrating liquid.

The saltstone reduction capacity selected was based on the most conservative result from testing of saltstone simulants. [SRNL-STI-2009-00637] Variations in flow conditions, which include infiltration rate and hydraulic conductivity, are discussed below in Section 7.1.7.1. Another factor to the oxidation rate is the amount of oxygen dissolved in the

infiltrating liquid. The dissolved oxygen content, assumed to be at the solubility limit, used in the model was conservative based on an evaluation of dissolved oxygen in water table wells at SRS. [SRNL-L3200-2011-00011]

7.1.2 All-Pathways Dose

The peak all-pathways annual dose for a MOP at 100-meter is calculated using the highest 100-meter groundwater pathways dose results during the 10,000-year performance period in combination with the air pathways results. The peak all-pathways annual dose for a MOP is 12 mrem/yr and is associated with Sector I. The air pathway dose was not affected by changes within this SA. The dose from the SDF PA was 4.0E-09 mrem/yr. Therefore, the all-pathways dose is dominated by the groundwater pathways, with the air pathway dose being negligible.

7.1.3 Intruder Dose

The peak chronic intruder scenario doses for the SDF were calculated using the highest concentration for each radionuclide in any sector (a discussion of how peak concentrations were determined by sector was provided in Section 6.1) or point within the SDF. The peak dose for the chronic intruder scenario in the 10,000-year performance period was 39 mrem/yr at the "Near FDC" well location. The intruder dose increased relative to the SDF PA. This increase is due to, similar to the groundwater pathway dose changes, the degradation properties of cementitious materials; in addition, the well location is in close proximity to an FDC versus a 1-meter facility boundary.

7.1.4 Airborne Dose

The airborne dose information presented in the SDF PA is not affected by the revised modeling approach discussed within this SA.

7.1.5 Radon Flux

The radon flux information presented in the SDF PA is not affected by the revised modeling approach discussed within this SA.

7.1.6 Probabilistic Uncertainty and Sensitivity Analysis Summary

The probabilistic SDF modeling was designed to evaluate the uncertainty and sensitivity of the calculations involving doses to MOP exposed via groundwater. Section 5.6.3 of the SDF PA describes various parameters selected for evaluation in the stochastic analyses based on modeling experience informed by the basis for the selected values and available generic and site-specific data. Given the uncertainties presented in Section 5.6.4 of this SA, the next step was to identify those input parameters and other stochastic entities in the model that led to those uncertainties. One of the goals of sensitivity analysis is to identify which independent variables have distributions that exert the greatest influence on the response.

7.1.6.1 Probabilistic Uncertainty Analysis Summary

In Section 5.6.4, Figure 5.6-40 illustrates the statistical time histories of the total dose at any sector for the MOP at the 100-meter boundary. In the figure, the 5^{th} and 95^{th} percentiles are significantly below and above the median value, respectively. The mean values are driven higher by the uncertainty distributions of the modeled parameters, approaching (and

sometimes exceeding) the 75th percentile. This indicates that the model applies distributions with long tails (e.g., lognormal distributions) or extreme values are inherent in these distributions. It is somewhat expected that the mean value is higher than the median because many of the dominant distributions were established to be reasonably conservative, resulting in the distributions being skewed to the high end. This approach inflates the variance in the uncertainty analyses, resulting in a few realizations dominating the uncertainty analysis results. Overall, mean dose results within both 1,000 and 10,000 years are less than 10 mrem/yr.

All of the realizations from TcRS1 and TcRS2 (see Table 5.6-4) were used to identify those realizations with the highest peak doses within 10,000 years of closure. The results of this review are shown in Table 5.6-7. Inspection of Table 5.6-7 indicates that even though the peak dose from the individual realizations are significantly higher than the deterministic case, the location (i.e., northern sectors), the identification of the major radionuclide contributor to the dose (I-129), and the major pathway contributors are not significantly different from the deterministic case.

In general, the detailed descriptions of the highest realizations (Section 5.6.4.3) show that the high peak doses are the result of a confluence of multiple variables being sampled such that conditions expedite the release and transport of contaminants through the system. This includes the high initial value for saturated hydraulic conductivity in saltstone, higher infiltration rates, less thickness in the unsaturated and saturated zones, and increased Darcy velocity. This is coupled with lower K_d values for iodine in cementitious materials and higher initial inventories of I-129 in FDCs that are near the 100-meter boundary. Finally, high consumption rate parameters from the dose calculation results in increased doses.

7.1.6.2 Probabilistic Sensitivity Analysis Summary

The following recurring themes appeared throughout the probabilistic sensitivity analyses:

- The primary dose contributors to the MOP dose within the first 10,000 years after closure are I-129, Tc-99, and Cs-135.
- The magnitude and timing of dose is most strongly influenced by a high initial saturated hydraulic conductivity of saltstone, wherein the more conductive the saltstone, the greater and earlier the peak dose.
- Aside from the saturated hydraulic conductivity of saltstone, iodine transport is most strongly influenced by its K_d in Reduced Region II concrete and moderately influenced by its K_d in Oxidized Region II concrete.
- The magnitude of the peak dose is strongly impacted by the amount of water consumed by the MOP.
- Technetium solubility has more control over Tc-99 doses in Sector B (where SDU 4 has a large Tc-99 inventory) than in Sector G, where the Tc-99 inventory is more distributed.
- Dose contributions from Cs-135 are influenced by the infiltration rate and dose parameters related to the fish ingestion dose pathway.

The most important parameters to the dose results were identified (hydraulic conductivity, iodine K_d, water consumption, technetium solubility, and fish ingestion pathway) as well as the primary dose contributors (in order of their importance: I-129, Tc-99, and Cs-135).

7.1.6.3 Probabilistic Uncertainty and Sensitivity Analysis Conclusion

These results confirm previous analyses and provide confidence in the parameters selected to evaluate dose impacts and in the ability of the SDF to meet performance objectives.

7.1.7 Deterministic Sensitivity Analyses Summary

Various sensitivity analyses were performed using the deterministic PORFLOW model to provide improved understanding of a number of important input parameters affecting the dose results. As discussed in Section 5.6.6, the modeling runs were performed to evaluate the impact of variability in multiple areas of interest (e.g., flow variability, roof slope variability, Tc-99 solubility). The conclusions of these analyses are provided below.

7.1.7.1 Sensitivity to Flow Variability

As discussed in Section 5.6.6.1, two flow cases (F10 and F20) were selected to investigate the impact that these flow cases would have on the potential groundwater dose to the MOP at 100 meters. Flow Case F10 was selected as the overall best representation of expected conditions. Flow Case F20 was selected to investigate the most pessimistic flow conditions; that is, the nominal degradation rate of cementitious material, the maximum infiltration rate, and a very conservative initial saturated hydraulic conductivity of 4.5E-07 cm/s for saltstone. As shown in Figure 5.6-67 (MOP Dose Profile for Flow Case F20 in 20,000 Years), even assuming the most pessimistic flow conditions resulted in peak doses in 10,000 years that were approximately 37 mrem/yr.

7.1.7.2 Roof Slope Sensitivity

As discussed in Section 5.6.6.2, the volumetric flow through saltstone was modeled for the nominal roof slope of 2 % and for roof slopes of 1.5 % and 2.5 %. The roof slope of 2.5 % caused a slight decease in the flow through saltstone as compared to the nominal case; thus further evaluation of this roof slope is not warranted since the release of radionuclides from saltstone, dependent on the flow through saltstone, would be less than the nominal case. However, for a roof slope of 1.5 % the flow through saltstone increased by approximately 33 % from the nominal case at 10,000 years as shown in Table 4.4-6. Thus, further evaluation was warranted for the 1.5 % slope.

The most significant contributors to the 10,000-year and 10,000- to 20,000-year time periods were I-129 and Tc-99. To ascertain the potential impact on the release of I-129 and Tc-99 from FDCs, the release rates to the water table of I-129 and Tc-99 were calculated and presented in Figures 5.6-71 and 5.6-72, respectively. Based on this release rate analysis, there is not significant impact on the dose results to the MOP. Thus, the results and conclusions of this SA would not be adversely impacted by a roof slope of 1.5 %.

7.1.7.3 Tc-99 Specific Sensitivity Analyses

7.1.7.3.1 Sensitivity to Technetium Solubility Variability

As discussed in Section 5.6.6.5, sensitivity cases were run where the technetium solubility was varied in saltstone and concrete. Three solubility values were considered for saltstone: 1.0E-08 mol/L (Evaluation Case), 1.0E-09 mol/L (10 times less than the Evaluation Case), and 1E-07 mol/L (10 times more than the Evaluation Case) as informed by SRNL-STI-2012-00769. These cases illustrate that the release of Tc-99 is controlled by the technetium solubility value of saltstone, as shown in Figures 5.6-78 and 5.6-79 for SDU 4 and FDCs, respectively. The results showed the release varied proportional to the solubility, as the solubility was increased 10 time, the release rate also increased 10 times, but Tc-99 release under solubility is not significant in the Evaluation Case (i.e., 10 times small value). Evaluations of dose impacts are discussed in Section 7.1.7.3.4.

7.1.7.3.2 Oxygen Sources Sensitivity Analyses

As discussed in Sections 5.6.6.4 and 5.6.6.6, sensitivity analyses were conducted where regions of non-depleting sources of oxygen are assumed to exist initially within the saltstone monolith. Five cases were considered, 1 %, 2 %, 5 %, 10 %, and 20 % of the volume of the saltstone monolith is comprised of these oxygen containing blocks that would hasten the consumption of slag within the saltstone monolith and increase the rate of Tc-99 release.

Figure 5.6-76 (SDU 4) and Figure 5.6-77 (FDCs) illustrate the total (integrated) release of Tc-99 to the water table for these cases of oxygen sources within saltstone compared to the Evaluation Case. The releases or timing of releases increases exponentially with increasing oxygen percentages. Because the total inventory of Tc-99 in SDU 4 is essentially released within 20,000 years for the Evaluation Case, these sensitivity cases have no significant impact on the total Tc-99 release from SDU-4 in 20,000 years.

At 20,000 years, the total release of Tc-99 from FDCs increases significantly for these sensitivity cases when compared to the Evaluation Case. As shown in Table 5.6-18, when saltstone is assumed to have oxygen sources comprising 20 % of the saltstone volume, the total Tc-99 release in 20,000 years is more than 10 times greater than the Evaluation Case. Evaluations of dose impacts are discussed in Section 7.1.7.3.4.

7.1.7.3.3 Sensitivity to Initially Oxidized Concrete

As discussed in Section 5.6.6.5 and 5.6.6.6, sensitivity analyses were conducted with the concrete initially oxidized. The results of these sensitivty cases are illustrated in Figures 5.6-80 to 5.6-83, for both SDU 4 and FDCs. The comparisons shown indicate that the initial chemical condition of the SDU and FDC concrete has little to no impact on the potential release of Tc-99.

7.1.7.3.4 Comparison of Technetium solubility and oxygen sources

Comparison of Figures 5.6-82 and 5.6-83 indicates that the sensitivity case of 10 times the nominal solubility value for saltstone, with initially oxidized concrete, would encompass the potential dose to the MOP for the sensitivity cases analyzed for oxygen sources within saltstone. Over the range of inputs considered, technetium solubility had a greater impact on the technetium release than the oxidized regions within the saltstone monolith. Figures 5.6-84 and 5.6-85 present dose results for 20 % oxygen at nominal solubilities and 10 times solubilities, both with oxidized concrete, and illustrate that peak doses from Tc-99 are approximately 6 mrem/yr in 10,000 years.

7.1.7.4 Deterministic Sensitivity Analyses Conclusions

The various sensitivity studies performed illustrate that the Evaluation Case dose results presented in Section 5.5.1 are not significantly impacted even using more conservative inputs, providing greater confidence that the results and conclusions remain valid. The sensitivity analysis evaluated model variability (such as flow through joints modeling) to confirm that the assessed variability would have minimal impact on the SDF PA Base Case. Multiple sensitivity analyses were performed regarding Tc-99 release to demonstrate that the Evaluation Case peak dose in 100,000 years displayed in Figure 5.5-11 (approximately 400 mrem/yr, approximately 31,000 years after closure) would not move into the 10,000-year time period even assuming more conservative Tc-99 release assumptions. The results also support a conclusion that performance objectives will be met for the SDF.

8.0 PERFORMANCE ASSESSMENT MAINTENANCE

Section 8.0 of the SDF PA describes intended use and future work to be done to support its maintenance. The SDF PA use and future work information presented in the SDF PA are not adversely impacted by the new information documented in this SA, which will be used for further information during future SDF PA maintenance activities, captured in an SRS LW Facilities PA Maintenance Program Implementation Plan. This program implementation plan is prepared annually and submitted to the DOE. The preparation and execution of the Implementation Plan is consistent with the *Maintenance Guide for U.S. Department of Energy Low-Level Waste Disposal Facility Performance Assessments and Composite Analysis* (DOE_11-10-1999) as reflected in DOE M 435.1-1. The most recent approved version of the program implementation plan as of the publication of this SA is *Savannah River Site Liquid Waste Facilities Performance Assessment Maintenance Program FY2013 Implementation Plan* (SRR-CWDA-2013-00049).

DOE recognizes that importing Tc-99 SDU release rates from PORFLOW simulation results invokes certain constraints on the stochastic model (e.g., the inability to sample Tc-99 inventories). For this reason, DOE is evaluating the development of an abstraction model to evaluate the Tc-99 releases from SDUs as part of its PA Maintenance Plan. Presently, two courses of action are being considered. First, the development of a highly simplified GoldSim shrinking-core model which simulates the major features of SDUs but eliminates smaller features such as joints will be considered. If possible, this model would also assume some simplified release mechanism for diffusion of radionuclides into the cells across the outer perimeter of the saltstone. The second course of action is to develop a numerical model that can import a windowed portion of the PORFLOW model and run the Tc-99 simulation based on PORFLOW exported cell-by cell transition times. This model would be called by an external pathway in the SDF GoldSim model. Note that either proposed methodology would still need flow and coupled (oxygen/slag) PORFLOW flow and transport simulations to provide flow and transition time input.

9.0 CONCLUSION

This SA for the SDF PA provides updated individual dose results based on the Evaluation Case modeling using the updated SDU and FDC radiological inventories and information following closure regarding radiological modeling. Additional sensitivity studies were performed based on a revised technetium waste release model and updated radiological transport parameters.

Requirements in both DOE O 435.1 and its associated manual and guide and 10 CFR 61 stipulate that a PA should provide reasonable expectation/assurance that LLW disposal will comply with specified performance objectives. DOE O 435.1 and 10 CFR 61 both require assessments of impacts to hypothetical inadvertent intruders. These assessments were performed to address the DOE M 435.1-1 1,000-year compliance period. [DOE M 435.1-1, 10 CFR 61] An evaluation of a 10,000-year performance period after facility closure is included to assist in the evaluation of compliance with performance objectives.

The results of this SA can be used in concert with the SDF PA in subsequent documents to demonstrate that there is reasonable expectation/assurance that applicable performance objectives will be met within the DOE Manual 435.1-1 1,000-year compliance period. The NRC typically uses a 10,000-year performance period when evaluating the 10 CFR 61 performance objectives. Evaluations to 10,000 years and beyond are included in the SA for additional information. Table 9.0-1 provides a summary of dose results.

Table 9.0-1: Comparison of SA Dose Results with Performance Objectives

Performance Objective			Peak Dose
DOE M 435.1-1	All-Pathways Dose	25 mrem/yr	0.04 mrem/yr
DOE M 435.1-1	Intruder Dose-chronic	100 mrem/yr	0.4 mrem/yr
10 CFR 61.41	All-Pathways Dose	25 mrem/yr	12 mrem/yr
10 CFR 61.42	Intruder Dose	Normally 500 mrem/yr	39 mrem/yr

The radiological results presented in Sections 5 and 6 considered the most current understanding regarding various PA inputs (e.g., updated radiological inventories, updated cementitious material degradation modeling, revised technetium release modeling, flow through joints modeling) through an Evaluation Case and other studies to confirm that the conclusions reached based on the SDF PA remain valid. The various uncertainty and sensitivity analyses performed illustrate that the SDF dose results presented in Section 5.5.1 are not significantly impacted even using more conservative inputs, providing greater confidence that the results and conclusions remain valid.

The SA results provide reasonable expectation/assurance that compliance is maintained with the specific requirements of DOE M 435.1-1 and 10 CFR 61 listed above. The additional sensitivity and uncertainty analyses performed using the lessons learned regarding radiological waste release modeling provide further confidence. The results presented in the SDF PA reflecting SDF final operational closure radiological inventories are not significantly impacted by new information and parameters presented in this SA, therefore, there should be no additional restrictions on the disposed inventory of Tc-99.

10.0 REFERENCES

08084SD, *2.9-MG Saltstone Storage Tanks 2A & 2B Design Drawings,* Savannah River Site, Aiken, SC, November 18, 2008.

10 CFR 61, *Licensing Requirements for Land Disposal of Radioactive Waste*, U.S. Nuclear Regulatory Commission, Washington DC, December 22, 2011.

B-SQP-C-00002, Hommel, S., *Software Quality Assurance Plan for GoldSim for Savannah River Site's Liquid Waste Program*, Savannah River Site, Aiken, SC, Rev. 0, April 23, 2012.

B-SQP-C-00003, Lester, B., *Software Quality Assurance Plan for ReadPORFLOWFiles.dll for the Savannah River Site's Liquid Waste Program*, Savannah River Site, Aiken, SC, Rev. 1, June 4, 2013.

B-SQP-C-00005, Hommel, S., *Software Quality Assurance Plan for mView*, Savannah River Site, Aiken, SC, Rev. 0, January 22, 2013.

C-CS-Z-0002, *Saltstone Vault 4, Permanent Roof Steel Sections & Details (Sh.2),* Savannah River Site, Aiken, SC, Rev. 2, July 7, 1998.

DHEC_09-09-2008, *Modified Permit for the Savannah River Site (SRS) Z-Area Saltstone Disposal Facility (SDF), Facility ID No. 025500-1603, Aiken County, (Class 3 Landfill Permit),* SC Department of Health and Environmental Control, Columbia, SC, September 9, 2008.

DOE M 435.1-1, Change 1, *Radioactive Waste Management Manual,* U.S. Department of Energy, Washington DC, June 19, 2001.

DOE O 435.1, Change 1, *Radioactive Waste Management*, U.S. Department of Energy, Washington DC, August 28, 2001.

DOE_11-10-1999, *Maintenance Guide for U.S. Department of Energy Low-Level Waste Disposal Facility Performance Assessments and Composite Analyses,* U.S. Department of Energy, Washington DC, November 10, 1999.

DOE-STD-1196-2011, *DOE Standard Derived Concentration Technical Standard*, U.S. Department of Energy, Washington, DC, April 2011.

EPA-600-R-090-052F, *Exposure Factors Handbook, 2011 Edition*, U.S. Environmental Protection Agency, Washington DC, September 2011.

FR-00-9654, Federal Register/Vol. 65, No. 78, *National Primary Drinking Water Regulations; Radionuclides; Notice of Data Availability; Proposed Rule*, U.S. Environmental Protection Agency, Washington DC, April 21, 2000.

ML073510127, *Recommended Site-Specific Sorption Coefficients for Reviewing Non-High-Level Waste Determinations at the Savannah River Site and Idaho National Laboratory*, U.S. Nuclear Regulatory Commission, Washington DC, October 2007.

ML100820097, *Request for Additional Information on the 2009 Performance Assessment for the Saltstone Disposal Facility at the Savannah River Site*, U.S. Nuclear Regulatory Commission, Washington DC, March 31, 2010.

ML103400571, *Second Request for Additional Information on the 2009 Performance Assessment for the Saltstone Disposal Facility at the Savannah River Site, Docket Number PROJ0734*, U.S. Nuclear Regulatory Commission, Washington DC, December 15, 2010.

ML120650576, Satorious, M. to Gilbertson, M., *Letter of Concern (Type IV) Regarding U.S. Department of Energy Disposal Activities at the Savannah River Site Saltstone Disposal Facility*, U.S. Nuclear Regulatory Commission, Washington DC, April 30, 2012.

ML121170309, *Technical Evaluation Report (TER) For the Revised Performance Assessment for the Saltstone Disposal Facility at the Savannah River Site, South Carolina*, U.S. Nuclear Regulatory Commission, Office of Federal and State Materials and Environmental Management Programs, Washington, DC, April 2012.

NDAA_3116, *Public Law 108-375, Ronald W. Reagan National Defense Authorization Act for Fiscal Year 2005, Section 3116, Defense Site Acceleration Completion*, October 28, 2004.

Q-SQP-A-00008, Flach, G.P., and Butcher, B.T., *Software Quality Assurance Plan for PORFLOW Flow-Field Extraction Tool (GoldSimFlows)*, Savannah River Site, Aiken, SC, Rev. 0, June 2013.

SCDHEC R.61-58, *State Primary Drinking Water Regulation*, SC Department Of Health and Environmental Control, Columbia, SC, August 28, 2009.

SRNL-L3200-2011-00011, *Summary Dissolved Oxygen in Water Table Wells at SRS*, Savannah River Site, Aiken, SC, December 21, 2011.

SRNL-L3200-2013-00022, Smith, F.G., Butcher, B.T., and Flach, G.P., *Design Checking of PORFLOW Modeling Supporting the Saltstone FY13 Special Analysis*, Savannah River Site, Aiken, SC, Rev. 0, June 2013.

SRNL-STI-2009-00115, Flach, G.P., et al., *Numerical Flow and Transport Simulations Supporting the Saltstone Disposal Facility Performance Assessment*, Savannah River Site, Aiken, SC, Rev. 1, June 17, 2009.

SRNL-STI-2009-00473, Kaplan, D.I., *Geochemical Data Package for Performance Assessment Calculations Related to the Savannah River Site*, Savannah River Site, Aiken, SC, Rev. 0, March 15, 2010.

SRNL-STI-2009-00637, Kaplan, D.I. and Roberts, K., *Reduction Capacity of Saltstone and Saltstone Components*, Savannah River Site, Aiken, SC, Rev. 0, November 30, 2009.

SRNL-STI-2010-00035, Langton, C.A., *Chemical Degradation Assessment for the H-Area Tank Farm Concrete Tanks and Fill Grouts*, Savannah River Site, Aiken, SC, Rev. 0, January 29, 2010.

SRNL-STI-2010-00493, Seaman, J.C. and Kaplan, D.I., *Chloride, Chromate, Silver, Thallium, and Uranium Sorption to SRS Soils, Sediments, and Cementitious Materials*, Savannah River Site, Aiken, SC, Rev. 0, September 29, 2010.

SRNL-STI-2010-00515, Langton, C.A., *Saltstone Characterization and Parameters for Performance Assessment Modeling*, Savannah River Site, Aiken, SC, Rev. 0, August 27, 2010.

SRNL-STI-2010-00667, Almond, P.M., and Kaplan, D.I., *Distribution Coefficients (Kd) Generated from a Core Sample Collected from the Saltstone Disposal Facility*, Savannah River Site, Aiken, SC, Rev. 0, April 29, 2011.

SRNL-STI-2011-00011, Kaplan, D.I., *Estimated Neptunium Sediment Sorption Values as a Function of pH and Measured Barium and Radium K_d Values*, Savannah River Site, Aiken, SC, Rev. 0, January 23, 2011.

SRNL-STI-2011-00661, Dixon, K.D., *Moisture Retention Properties of High Temperature Cure ARP/MCU Saltstone Grout*, Savannah River Site, Aiken, SC, Rev. 0, January 20, 2012.

SRNL-STI-2011-00672, Almond, P.M., et al., *Variability of K_d Values in Cementitious Materials and Sediments*, Savannah River Site, Aiken, SC, Rev. 0, January 2012.

SRNL-STI-2012-00558, Reigel, M., et al., *Process Formulations and Curing Conditions that Affect Saltstone Properties*, Savannah River Site, Aiken, SC, Rev. 0, September 30, 2012.

SRNL-STI-2012-00596, Kaplan, D.I., et al., *Technetium Sorption by Cementitious Materials Under Reducing Conditions*, Savannah River Site, Aiken, SC, Rev. 0, September 30, 2012.

SRNL-STI-2012-00769, Kaplan, D.I. and Dien, L., *Solubility of Technetium Dioxides (TcO2-c, TcO2 1.6H2O and TcO2 2H2O) in Reducing Cementitious Material Leachates: A Thermodynamic Calculation*, Savannah River Site, Aiken, SC, Rev. 1, February 1, 2013.

SRNL-STI-2013-00118, Flach, G.P. and Smith, F.G., *Degradation of Cementitious Materials Associated with Saltstone Disposal Units*, Savannah River Site, Aiken, SC, Rev. 0, March 2013.

SRNL-STI-2013-00280, Jordan, J.M., and Flach, G.P., *PORFLOW Modeling Supporting the FY13 Saltstone Special Analysis*, Savannah River Site, Aiken, SC, May 2013.

SRNL-TR-2008-00283, Denham, M., *Estimation of Eh and pH Transitions in Pore Fluids During Aging of Saltstone and Disposal Unit Concrete*, Savannah River Site, Aiken, SC, December 31, 2008.

SRNL-TR-2010-00213, Whiteside, T., *Software Testing and Verification of PORFLOW Versions 6.30.1 and 6.30.2*, Savannah River Site, Aiken, SC, Rev. 0, July 2010.

SRR-CWDA-2009-00017, *Performance Assessment for the Saltstone Disposal Facility at the Savannah River Site*, Savannah River Site, Aiken, SC, Rev. 0, October 29, 2009.

SRR-CWDA-2010-00033, *Comment Response Matrix for NRC Requests for Additional Information (RAIs) on the Saltstone Disposal Facility Performance Assessment (SRR-CWDA-2009-00017, Revision 0, dated October 29, 2009)*, Savannah River Site, Aiken, SC, Rev. 1, July 23, 2010.

SRR-CWDA-2010-00128, *Performance Assessment for the H-Area Tank Farm at the Savannah River Site*, Savannah River Site, Aiken, SC, Rev. 1, November 2012.

SRR-CWDA-2011-00044, *Comment Response Matrix for Nuclear Regulatory Commission RAI-2009-02 Second Request for Additional Information (RAI) on the Saltstone Disposal Facility Performance Assessment (SRR-CWDA-2009-00017, Revision 0, dated October 29, 2009)*, Savannah River Site, Aiken, SC, Rev. 1, August 25, 2011.

SRR-CWDA-2011-00178, *Saltstone Disposal Facility Stochastic Fate and Transport Model*, Savannah River Site, Aiken, SC, Rev. 0, January 10, 2012.

SRR-CWDA-2012-00103, *Sensitivity Analysis for Disposal Operations into Saltstone Disposal Facility Vault 1, Vault 4, and SDUs 2, 3 and 5*, Savannah River Site, Aiken, SC, Rev. 1, July 2012.

SRR-CWDA-2013-00049, *Savannah River Site Liquid Waste Facilities Performance Assessment Maintenance Program FY2013 Implementation Plan*, Savannah River Site, Aiken, SC, Rev. 1, May 2013.

SRR-CWDA-2013-00058, Hommel, S., *Dose Calculation Methodology for Liquid Waste Performance Assessments at the Savannah River Site*, Savannah River Site, Aiken, SC, Rev. 0, May 2013.

SRR-CWDA-2013-00064, Sheppard, R.E. to Rosenberger, K.H., *PORFLOW Input to Support the Development of the SDF FY13 Special Analysis*, Savannah River Site, Aiken, SC, Rev. 1, April 2013.

SRR-CWDA-2013-00073, *Updates to the Saltstone Disposal Facility Fate and Transport Model*, Savannah River Site, Aiken, SC, Rev. 0, June 2013.

SRR-CWDA-2013-00087, *SDF FY2013 Special Analysis for the Performance Assessment for the Saltstone Disposal Facility at the Savannah River Site Quality Assurance Report*, Savannah River Site, Aiken, SC, Rev. 0, June 2013.

WDPD-12-49, *Disposal Authorization Statement for the Savannah River Site Saltstone Disposal Facility*, United States Department of Energy, Washington, DC, Rev. 1, May 22, 2012.

WDPD-12-66, *Disposal Authorization Statement for the Savannah River Site Saltstone Disposal Facility - Prestart Corrective Actions Complete*, United States Department of Energy, Washington, DC, July 31, 2012.

W780625, *Saltstone Surface Disposal Vault Foundation and Floor Plan, Elevation and Sections*, Savannah River Site, Aiken, SC, Rev. 7, February 24, 2004.

W828992, *Saltstone Vault 4 Plan, Sections and Details Concrete*, Savannah River Site, Aiken, SC, Rev. 3, May 12, 2010.

WSRC-STI-2007-00607, Langton, C.A., *Chemical Degradation Assessment of Cementitious Materials for the HLW Tank Closure Project*, Savannah River Site, Aiken, SC, Rev. 0, September 14, 2007.

WSRC-STI-2008-00244, Jones, W.E., and Phifer, M.A., *Saltstone Disposal Facility Closure Cap Concept and Infiltration Estimates*, Savannah River Site, Aiken, SC, May 2008.

X-CLC-Z-00050, Dixon, K.D., *Analysis of Saltstone Water-to-Premix Ratio During Pre-ELAWD Operation*, Savannah River Site, Aiken, SC, Rev. 2, October 10, 2012.

APPENDIX A

PEAK RADIOLOGICAL 100-METER CONCENTRATION TABLES BY SECTOR IN 1,000 YEARS

Table A-1: Peak Radiological 100-Meter Concentrations for Sectors A through E in 1,000 Years

Radionuclide	MCL (pCi/L)**	Sector A Concentration		Sector B Concentration		Sector C Concentration		Sector D Concentration		Sector E Concentration	
		(pCi/L)	Year Peak Occurs	(pCi/L)	Year Peak Occurs	(pCi/L)	Year Peak Occurs	(pCi/L)	Year Peak Occurs	(pCi/L)	Year Peak Occurs
Ac-227	NC	1.64E-28	1,000	2.37E-28	1,000	2.67E-28	1,000	5.00E-29	1,000	<1.0E-30	1,000
Al-26	NC	<1.0E-30	1,000	<1.0E-30	1,000	<1.0E-30	1,000	<1.0E-30	1,000	<1.0E-30	1,000
Am-241	Total α	<1.0E-30	1,000	<1.0E-30	1,000	<1.0E-30	1,000	<1.0E-30	1,000	<1.0E-30	1,000
Am-242m	Total α	<1.0E-30	1,000	<1.0E-30	1,000	<1.0E-30	1,000	<1.0E-30	1,000	<1.0E-30	1,000
Am-243	Total α	<1.0E-30	1,000	<1.0E-30	1,000	<1.0E-30	1,000	<1.0E-30	1,000	<1.0E-30	1,000
Ba-137m	NC	3.47E-16	1,000	8.16E-16	1,000	1.85E-15	1,000	2.00E-16	1,000	3.73E-19	1,000
C-14	2,000	1.22E-24	1,000	2.50E-24	1,000	4.54E-24	1,000	6.02E-25	1,000	1.84E-27	1,000
Cf-249	Total α	<1.0E-30	1,000	<1.0E-30	1,000	<1.0E-30	1,000	<1.0E-30	1,000	<1.0E-30	1,000
Cf-251	Total α	<1.0E-30	1,000	<1.0E-30	1,000	<1.0E-30	1,000	<1.0E-30	1,000	<1.0E-30	1,000
Cl-36	700	4.77E-04	692	5.63E-04	808	5.62E-04	674	2.90E-04	816	3.27E-05	800
Cm-243	Total α	<1.0E-30	1,000	<1.0E-30	1,000	<1.0E-30	1,000	<1.0E-30	1,000	<1.0E-30	1,000
Cm-244	Total α	<1.0E-30	1,000	<1.0E-30	1,000	<1.0E-30	1,000	<1.0E-30	1,000	<1.0E-30	1,000
Cm-245	Total α	<1.0E-30	1,000	<1.0E-30	1,000	<1.0E-30	1,000	<1.0E-30	1,000	<1.0E-30	1,000
Cm-247	Total α	<1.0E-30	1,000	<1.0E-30	1,000	<1.0E-30	1,000	<1.0E-30	1,000	<1.0E-30	1,000
Cm-248	Total α	<1.0E-30	1,000	<1.0E-30	1,000	<1.0E-30	1,000	<1.0E-30	1,000	<1.0E-30	1,000
Co-60	100	<1.0E-30	278	<1.0E-30	264	<1.0E-30	220	<1.0E-30	244	<1.0E-30	294
Cs-135	900	8.09E-11	1,000	1.87E-10	1,000	4.13E-10	1,000	4.58E-11	1,000	9.01E-14	1,000
Cs-137	200	3.47E-16	1,000	8.16E-16	1,000	1.85E-15	1,000	2.00E-16	1,000	3.73E-19	1,000
Eu-152	200	<1.0E-30	1,000	<1.0E-30	1,000	<1.0E-30	918	<1.0E-30	994	<1.0E-30	1,000
Eu-154	60	<1.0E-30	510	<1.0E-30	484	<1.0E-30	420	<1.0E-30	470	<1.0E-30	578
Gd-152	NC	<1.0E-30	1,000	<1.0E-30	1,000	<1.0E-30	1,000	<1.0E-30	1,000	<1.0E-30	1,000
H-3	20,000	2.06E-08	376	2.50E-08	376	2.46E-08	376	4.55E-09	376	1.32E-10	386
I-129	1	1.42E-01	848	1.80E-01	850	1.76E-01	646	9.65E-02	1,000	3.93E-02	1,000
K-40	NC	2.14E-09	1,000	3.24E-09	1,000	3.84E-09	1,000	7.03E-10	1,000	4.44E-12	1,000
Nb-93m	1,000	<1.0E-30	1,000	<1.0E-30	1,000	<1.0E-30	1,000	<1.0E-30	1,000	<1.0E-30	1,000
Nb-94	NC	<1.0E-30	1,000	<1.0E-30	1,000	<1.0E-30	1,000	<1.0E-30	1,000	<1.0E-30	1,000

Table A-1: Peak Radiological 100-Meter Concentrations for Sectors A through E in 1,000 Years (Continued)

Radionuclide	MCL (pCi/L)**	Sector A Concentration		Sector B Concentration		Sector C Concentration		Sector D Concentration		Sector E Concentration	
		(pCi/L)	Year Peak Occurs	(pCi/L)	Year Peak Occurs	(pCi/L)	Year Peak Occurs	(pCi/L)	Year Peak Occurs	(pCi/L)	Year Peak Occurs
Ni-59	300	1.28E-18	1,000	2.52E-18	1,000	4.25E-18	1,000	6.04E-19	1,000	2.14E-21	1,000
Ni-63	50	6.15E-20	1,000	1.21E-19	1,000	2.06E-19	1,000	2.91E-20	1,000	1.02E-22	1,000
Np-237	Total α	1.87E-23	1,000	2.69E-23	1,000	3.02E-23	1,000	5.66E-24	1,000	4.09E-26	1,000
Pa-231	Total α	1.24E-25	1,000	1.80E-25	1,000	2.02E-25	1,000	3.79E-26	1,000	2.70E-28	1,000
Pb-210	NC	<1.0E-30	1,000	<1.0E-30	1,000	<1.0E-30	1,000	<1.0E-30	1,000	<1.0E-30	1,000
Pd-107	NC	1.30E-19	1,000	2.55E-19	1,000	4.31E-19	1,000	6.12E-20	1,000	2.17E-22	1,000
Pt-193	3,000	2.05E-23	1,000	4.06E-23	1,000	6.92E-23	1,000	9.74E-24	1,000	3.38E-26	1,000
Pu-238	Total α	<1.0E-30	1,000	<1.0E-30	1,000	<1.0E-30	1,000	<1.0E-30	1,000	<1.0E-30	1,000
Pu-239	Total α	<1.0E-30	1,000	<1.0E-30	1,000	<1.0E-30	1,000	<1.0E-30	1,000	<1.0E-30	1,000
Pu-240	Total α	<1.0E-30	1,000	<1.0E-30	1,000	<1.0E-30	1,000	<1.0E-30	1,000	<1.0E-30	1,000
Pu-241	300	<1.0E-30	1,000	<1.0E-30	1,000	<1.0E-30	1,000	<1.0E-30	1,000	<1.0E-30	1,000
Pu-242	Total α	<1.0E-30	1,000	<1.0E-30	1,000	<1.0E-30	1,000	<1.0E-30	1,000	<1.0E-30	1,000
Pu-244	Total α	<1.0E-30	1,000	<1.0E-30	1,000	<1.0E-30	1,000	<1.0E-30	1,000	<1.0E-30	1,000
Ra-226	Total α/Ra	<1.0E-30	1,000	<1.0E-30	1,000	1.39E-29	1,000	1.38E-30	1,000	<1.0E-30	1,000
Ra-228	Total Ra	<1.0E-30	1,000	<1.0E-30	1,000	<1.0E-30	1,000	<1.0E-30	1,000	<1.0E-30	1,000
Rn-222	NC	<1.0E-30	1,000	<1.0E-30	1,000	1.39E-29	1,000	1.38E-30	1,000	<1.0E-30	1,000
Se-79	NC	<1.0E-30	1,000	<1.0E-30	1,000	<1.0E-30	1,000	<1.0E-30	1,000	<1.0E-30	1,000
Sm-151	1,000	<1.0E-30	1,000	<1.0E-30	1,000	<1.0E-30	1,000	<1.0E-30	1,000	<1.0E-30	1,000
Sn-126	NC	<1.0E-30	1,000	<1.0E-30	1,000	<1.0E-30	1,000	<1.0E-30	1,000	<1.0E-30	1,000
Sr-90	8	3.24E-18	1,000	5.23E-18	1,000	7.11E-18	1,000	1.20E-18	1,000	6.24E-21	1,000
Tc-99	900	1.17E+01	1,000	1.42E+01	1,000	1.40E+01	1,000	6.48E+00	1,000	1.85E+00	1,000
Th-229	Total α	<1.0E-30	1,000	<1.0E-30	1,000	<1.0E-30	1,000	<1.0E-30	1,000	<1.0E-30	1,000
Th-230	Total α	<1.0E-30	1,000	<1.0E-30	1,000	<1.0E-30	1,000	<1.0E-30	1,000	<1.0E-30	1,000

Table A-1: Peak Radiological 100-Meter Concentrations for Sectors A through E in 1,000 Years (Continued)

Radionuclide	MCL (pCi/L)**	Sector A Concentration		Sector B Concentration		Sector C Concentration		Sector D Concentration		Sector E Concentration	
		(pCi/L)	Year Peak Occurs	(pCi/L)	Year Peak Occurs	(pCi/L)	Year Peak Occurs	(pCi/L)	Year Peak Occurs	(pCi/L)	Year Peak Occurs
Th-232	Total α	<1.0E-30	1,000	<1.0E-30	1,000	<1.0E-30	1,000	<1.0E-30	1,000	<1.0E-30	1,000
U-232	Total U*	<1.0E-30	1,000	<1.0E-30	1,000	<1.0E-30	1,000	<1.0E-30	1,000	<1.0E-30	1,000
U-233	Total U*	2.27E-29	1,000	3.28E-29	1,000	3.69E-29	1,000	6.90E-30	1,000	<1.0E-30	1,000
U-234	Total U*	<1.0E-30	1,000	<1.0E-30	1,000	<1.0E-30	1,000	<1.0E-30	1,000	<1.0E-30	1,000
U-235	Total U*	<1.0E-30	1,000	<1.0E-30	1,000	<1.0E-30	1,000	<1.0E-30	1,000	<1.0E-30	1,000
U-236	Total U*	<1.0E-30	1,000	<1.0E-30	1,000	<1.0E-30	1,000	<1.0E-30	1,000	<1.0E-30	1,000
U-238	Total U*	<1.0E-30	1,000	<1.0E-30	1,000	<1.0E-30	1,000	<1.0E-30	1,000	<1.0E-30	1,000
Y-90	60	3.24E-18	1,000	5.23E-18	1,000	7.11E-18	1,000	1.20E-18	1,000	6.24E-21	1,000
Zr-93	2,000	<1.0E-30	1,000	<1.0E-30	1,000	<1.0E-30	1,000	<1.0E-30	1,000	<1.0E-30	1,000
Total alpha	**15**	**1.88E-23**		**2.71E-23**		**3.04E-23**		**5.70E-24**		**4.12E-26**	
Total Ra	**5**	**<1.0E-30**		**<1.0E-30**		**1.39E-29**		**1.38E-30**		**<1.0E-30**	
Sum of beta-gamma MCL fractions		**1.55E-01**		**1.95E-01**		**1.92E-01**		**1.04E-01**		**4.13E-02**	

** MCL values for beta and photon emitters are calculated in Table II-3 of FR-00-9654 based on a beta-gamma dose of 4 mrem/yr
NC = Not Calculated

Table A-2: Peak Radiological 100-Meter Concentrations for Sectors F through J in 1,000 Years

Radionuclide	MCL (pCi/L)**	Sector F Concentrations		Sector G Concentrations		Sector H Concentrations		Sector I Concentrations		Sector J Concentrations	
		(pCi/L)	Year Peak Occurs	(pCi/L)	Year Peak Occurs	(pCi/L)	Year Peak Occurs	(pCi/L)	Year Peak Occurs	(pCi/L)	Year Peak Occurs
Ac-227	NC	<1.0E-30	1,000	<1.0E-30	1,000	<1.0E-30	1,000	<1.0E-30	1,000	<1.0E-30	1,000
Al-26	NC	<1.0E-30	1,000	<1.0E-30	1,000	<1.0E-30	1,000	<1.0E-30	1,000	<1.0E-30	1,000
Am-241	Total α	<1.0E-30	1,000	<1.0E-30	1,000	<1.0E-30	1,000	<1.0E-30	1,000	<1.0E-30	1,000
Am-242m	Total α	<1.0E-30	1,000	<1.0E-30	1,000	<1.0E-30	1,000	<1.0E-30	1,000	<1.0E-30	1,000
Am-243	Total α	<1.0E-30	1,000	<1.0E-30	1,000	<1.0E-30	1,000	<1.0E-30	1,000	<1.0E-30	1,000
Ba-137m	NC	1.55E-25	1,000	6.65E-27	1,000	6.05E-27	1,000	1.36E-27	1,000	5.26E-29	1,000
C-14	2,000	<1.0E-30	1,000	<1.0E-30	1,000	<1.0E-30	1,000	<1.0E-30	1,000	<1.0E-30	1,000
Cf-249	Total α	<1.0E-30	1,000	<1.0E-30	1,000	<1.0E-30	1,000	<1.0E-30	1,000	<1.0E-30	1,000
Cf-251	Total α	<1.0E-30	1,000	<1.0E-30	1,000	<1.0E-30	1,000	<1.0E-30	1,000	<1.0E-30	1,000
Cl-36	700	3.71E-06	1,000	7.61E-06	1,000	7.66E-06	1,000	6.74E-06	1,000	4.64E-06	1,000
Cm-243	Total α	<1.0E-30	1,000	<1.0E-30	1,000	<1.0E-30	1,000	<1.0E-30	1,000	<1.0E-30	1,000
Cm-244	Total α	<1.0E-30	1,000	<1.0E-30	1,000	<1.0E-30	1,000	<1.0E-30	1,000	<1.0E-30	1,000
Cm-245	Total α	<1.0E-30	1,000	<1.0E-30	1,000	<1.0E-30	1,000	<1.0E-30	1,000	<1.0E-30	1,000
Cm-247	Total α	<1.0E-30	1,000	<1.0E-30	1,000	<1.0E-30	1,000	<1.0E-30	1,000	<1.0E-30	1,000
Cm-248	Total α	<1.0E-30	1,000	<1.0E-30	1,000	<1.0E-30	1,000	<1.0E-30	1,000	<1.0E-30	1,000
Co-60	100	<1.0E-30	318	<1.0E-30	582	<1.0E-30	578	<1.0E-30	600	<1.0E-30	414
Cs-135	900	3.86E-20	1,000	5.22E-22	1,000	4.76E-22	1,000	1.09E-22	1,000	4.46E-24	1,000
Cs-137	200	1.55E-25	1,000	6.65E-27	1,000	6.05E-27	1,000	1.36E-27	1,000	5.26E-29	1,000
Eu-152	200	<1.0E-30	1,000	<1.0E-30	1,000	<1.0E-30	1,000	<1.0E-30	1,000	<1.0E-30	1,000
Eu-154	60	<1.0E-30	568	<1.0E-30	748	<1.0E-30	748	<1.0E-30	748	<1.0E-30	746
Gd-152	NC	<1.0E-30	1,000	<1.0E-30	1,000	<1.0E-30	1,000	<1.0E-30	1,000	<1.0E-30	1,000
H-3	20,000	5.08E-11	436	1.07E-10	440	1.07E-10	438	1.05E-10	444	7.48E-11	446
I-129	1	2.12E-02	1,000	4.54E-02	1,000	4.54E-02	1,000	4.41E-02	1,000	3.09E-02	1,000
K-40	NC	1.19E-16	1,000	2.35E-16	1,000	2.26E-16	1,000	9.01E-17	1,000	1.42E-17	1,000
Nb-93m	1,000	<1.0E-30	1,000	<1.0E-30	1,000	<1.0E-30	1,000	<1.0E-30	1,000	<1.0E-30	1,000
Nb-94	NC	<1.0E-30	1,000	<1.0E-30	1,000	<1.0E-30	1,000	<1.0E-30	1,000	<1.0E-30	1,000

Table A-2: Peak Radiological 100-Meter Concentrations for Sectors F through J in 1,000 Years (Continued)

Radionuclide	MCL (pCi/L)**	Sector F Concentrations		Sector G Concentrations		Sector H Concentrations		Sector I Concentrations		Sector J Concentrations	
		(pCi/L)	Year Peak Occurs	(pCi/L)	Year Peak Occurs	(pCi/L)	Year Peak Occurs	(pCi/L)	Year Peak Occurs	(pCi/L)	Year Peak Occurs
Ni-59	300	1.41E-27	1,000	<1.0E-30	1,000	<1.0E-30	1,000	<1.0E-30	1,000	<1.0E-30	1,000
Ni-63	50	6.54E-29	1,000	<1.0E-30	1,000	<1.0E-30	1,000	<1.0E-30	1,000	<1.0E-30	1,000
Np-237	Total α	<1.0E-30	1,000	<1.0E-30	1,000	<1.0E-30	1,000	<1.0E-30	1,000	<1.0E-30	1,000
Pa-231	Total α	<1.0E-30	1,000	<1.0E-30	1,000	<1.0E-30	1,000	<1.0E-30	1,000	<1.0E-30	1,000
Pb-210	NC	<1.0E-30	1,000	<1.0E-30	1,000	<1.0E-30	1,000	<1.0E-30	1,000	<1.0E-30	1,000
Pd-107	NC	1.40E-28	1,000	<1.0E-30	1,000	<1.0E-30	1,000	<1.0E-30	1,000	<1.0E-30	1,000
Pt-193	3,000	<1.0E-30	1,000	<1.0E-30	1,000	<1.0E-30	1,000	<1.0E-30	1,000	<1.0E-30	1,000
Pu-238	Total α	<1.0E-30	1,000	<1.0E-30	1,000	<1.0E-30	1,000	<1.0E-30	1,000	<1.0E-30	1,000
Pu-239	Total α	<1.0E-30	1,000	<1.0E-30	1,000	<1.0E-30	1,000	<1.0E-30	1,000	<1.0E-30	1,000
Pu-240	Total α	<1.0E-30	1,000	<1.0E-30	1,000	<1.0E-30	1,000	<1.0E-30	1,000	<1.0E-30	1,000
Pu-241	300	<1.0E-30	1,000	<1.0E-30	1,000	<1.0E-30	1,000	<1.0E-30	1,000	<1.0E-30	1,000
Pu-242	Total α	<1.0E-30	1,000	<1.0E-30	1,000	<1.0E-30	1,000	<1.0E-30	1,000	<1.0E-30	1,000
Pu-244	Total α	<1.0E-30	1,000	<1.0E-30	1,000	<1.0E-30	1,000	<1.0E-30	1,000	<1.0E-30	1,000
Ra-226	Total α/Ra	<1.0E-30	1,000	<1.0E-30	1,000	<1.0E-30	1,000	<1.0E-30	1,000	<1.0E-30	1,000
Ra-228	Total Ra	<1.0E-30	1,000	<1.0E-30	1,000	<1.0E-30	1,000	<1.0E-30	1,000	<1.0E-30	1,000
Rn-222	NC	<1.0E-30	1,000	<1.0E-30	1,000	<1.0E-30	1,000	<1.0E-30	1,000	<1.0E-30	1,000
Se-79	NC	<1.0E-30	1,000	<1.0E-30	1,000	<1.0E-30	1,000	<1.0E-30	1,000	<1.0E-30	1,000
Sm-151	1,000	<1.0E-30	1,000	<1.0E-30	1,000	<1.0E-30	1,000	<1.0E-30	1,000	<1.0E-30	1,000
Sn-126	NC	<1.0E-30	1,000	<1.0E-30	1,000	<1.0E-30	1,000	<1.0E-30	1,000	<1.0E-30	1,000
Sr-90	8	5.24E-27	1,000	2.38E-29	1,000	2.27E-29	1,000	8.34E-30	1,000	1.09E-30	1,000
Tc-99	900	9.25E-01	1,000	2.32E+00	1,000	2.38E+00	1,000	2.60E+00	1,000	2.16E+00	1,000
Th-229	Total α	<1.0E-30	1,000	<1.0E-30	1,000	<1.0E-30	1,000	<1.0E-30	1,000	<1.0E-30	1,000
Th-230	Total α	<1.0E-30	1,000	<1.0E-30	1,000	<1.0E-30	1,000	<1.0E-30	1,000	<1.0E-30	1,000

Table A-2: Peak Radiological 100-Meter Concentrations for Sectors F through J in 1,000 Years (Continued)

Radionuclide	MCL (pCi/L)**	Sector F Concentrations		Sector G Concentrations		Sector H Concentrations		Sector I Concentrations		Sector J Concentrations	
		(pCi/L)	Year Peak Occurs	(pCi/L)	Year Peak Occurs	(pCi/L)	Year Peak Occurs	(pCi/L)	Year Peak Occurs	(pCi/L)	Year Peak Occurs
Th-232	Total α	<1.0E-30	1,000	<1.0E-30	1,000	<1.0E-30	1,000	<1.0E-30	1,000	<1.0E-30	1,000
U-232	Total U*	<1.0E-30	1,000	<1.0E-30	1,000	<1.0E-30	1,000	<1.0E-30	1,000	<1.0E-30	1,000
U-233	Total U*	<1.0E-30	1,000	<1.0E-30	1,000	<1.0E-30	1,000	<1.0E-30	1,000	<1.0E-30	1,000
U-234	Total U*	<1.0E-30	1,000	<1.0E-30	1,000	<1.0E-30	1,000	<1.0E-30	1,000	<1.0E-30	1,000
U-235	Total U*	<1.0E-30	1,000	<1.0E-30	1,000	<1.0E-30	1,000	<1.0E-30	1,000	<1.0E-30	1,000
U-236	Total U*	<1.0E-30	1,000	<1.0E-30	1,000	<1.0E-30	1,000	<1.0E-30	1,000	<1.0E-30	1,000
U-238	Total U*	<1.0E-30	1,000	<1.0E-30	1,000	<1.0E-30	1,000	<1.0E-30	1,000	<1.0E-30	1,000
Y-90	60	5.24E-27	1,000	2.38E-29	1,000	2.27E-29	1,000	8.34E-30	1,000	1.09E-30	1,000
Zr-93	2,000	<1.0E-30	1,000	<1.0E-30	1,000	<1.0E-30	1,000	<1.0E-30	1,000	<1.0E-30	1,000
Total alpha	**15**	**<1.0E-30**		**<1.0E-30**		**<1.0E-30**		**<1.0E-30**		**<1.0E-30**	
Total Ra	**5**	**<1.0E-30**		**<1.0E-30**		**<1.0E-30**		**<1.0E-30**		**<1.0E-30**	
Sum of beta-gamma MCL fractions		**2.22E-02**		**4.80E-02**		**4.81E-02**		**4.70E-02**		**3.33E-02**	

** MCL values for beta and photon emitters are calculated in Table II-3 of FR-00-9654 based on a beta-gamma dose of 4 mrem/yr

NC = Not Calculated

Table A-3: Peak Radiological 100-Meter Concentrations for Sectors K through L in 1,000 Years

Radionuclide	MCL (pCi/L)**	Sector K Concentrations		Sector L Concentrations	
		(pCi/L)	Year Peak Occurs	(pCi/L)	Year Peak Occurs
Ac-227	NC	<1.0E-30	1,000	<1.0E-30	1,000
Al-26	NC	<1.0E-30	1,000	<1.0E-30	1,000
Am-241	Total α	<1.0E-30	1,000	<1.0E-30	1,000
Am-242m	Total α	<1.0E-30	1,000	<1.0E-30	1,000
Am-243	Total α	<1.0E-30	1,000	<1.0E-30	1,000
Ba-137m	NC	1.47E-27	1,000	5.58E-21	1,000
C-14	2,000	<1.0E-30	1,000	4.80E-29	1,000
Cf-249	Total α	<1.0E-30	1,000	<1.0E-30	1,000
Cf-251	Total α	<1.0E-30	1,000	<1.0E-30	1,000
Cl-36	700	6.19E-06	1,000	6.83E-06	1,000
Cm-243	Total α	<1.0E-30	1,000	<1.0E-30	1,000
Cm-244	Total α	<1.0E-30	1,000	<1.0E-30	1,000
Cm-245	Total α	<1.0E-30	1,000	<1.0E-30	1,000
Cm-247	Total α	<1.0E-30	1,000	<1.0E-30	1,000
Cm-248	Total α	<1.0E-30	1,000	<1.0E-30	1,000
Co-60	100	<1.0E-30	374	<1.0E-30	326
Cs-135	900	3.50E-22	1,000	1.42E-15	1,000
Cs-137	200	1.47E-27	1,000	5.58E-21	1,000
Eu-152	200	<1.0E-30	1,000	<1.0E-30	1,000
Eu-154	60	<1.0E-30	786	<1.0E-30	572
Gd-152	NC	<1.0E-30	1,000	<1.0E-30	1,000
H-3	20,000	9.55E-11	444	9.59E-11	438
I-129	1	4.05E-02	1,000	4.05E-02	1,000
K-40	NC	5.29E-17	1,000	2.86E-13	1,000
Nb-93m	1,000	<1.0E-30	1,000	<1.0E-30	1,000
Nb-94	NC	<1.0E-30	1,000	<1.0E-30	1,000
Ni-59	300	4.81E-29	1,000	6.48E-23	1,000
Ni-63	50	<1.0E-30	1,000	3.04E-24	1,000
Np-237	Total α	<1.0E-30	1,000	3.82E-27	1,000
Pa-231	Total α	<1.0E-30	1,000	2.46E-29	1,000
Pb-210	NC	<1.0E-30	1,000	<1.0E-30	1,000
Pd-107	NC	4.87E-30	1,000	6.56E-24	1,000
Pt-193	3,000	<1.0E-30	1,000	9.94E-28	1,000
Pu-238	Total α	<1.0E-30	1,000	<1.0E-30	1,000
Pu-239	Total α	<1.0E-30	1,000	<1.0E-30	1,000
Pu-240	Total α	<1.0E-30	1,000	<1.0E-30	1,000
Pu-241	300	<1.0E-30	1,000	<1.0E-30	1,000
Pu-242	Total α	<1.0E-30	1,000	<1.0E-30	1,000
Pu-244	Total α	<1.0E-30	1,000	<1.0E-30	1,000

Table A-3: Peak Radiological 100-Meter Concentrations for Sectors K through L in 1,000 Years (Continued)

Radionuclide	MCL (pCi/L)**	Sector K Concentrations		Sector L Concentrations	
		(pCi/L)	Year Peak Occurs	(pCi/L)	Year Peak Occurs
Ra-226	Total α/Ra	<1.0E-30	1,000	<1.0E-30	1,000
Ra-228	Total Ra	<1.0E-30	1,000	<1.0E-30	1,000
Rn-222	NC	<1.0E-30	1,000	<1.0E-30	1,000
Se-79	NC	<1.0E-30	1,000	<1.0E-30	1,000
Sm-151	1,000	<1.0E-30	1,000	<1.0E-30	1,000
Sn-126	NC	<1.0E-30	1,000	<1.0E-30	1,000
Sr-90	8	4.86E-28	1,000	3.13E-22	1,000
Tc-99	900	2.38E+00	1,000	1.94E+00	1,000
Th-229	Total α	<1.0E-30	1,000	<1.0E-30	1,000
Th-230	Total α	<1.0E-30	1,000	<1.0E-30	1,000
Th-232	Total α	<1.0E-30	1,000	<1.0E-30	1,000
U-232	Total U	<1.0E-30	1,000	<1.0E-30	1,000
U-233	Total U	<1.0E-30	1,000	<1.0E-30	1,000
U-234	Total U	<1.0E-30	1,000	<1.0E-30	1,000
U-235	Total U	<1.0E-30	1,000	<1.0E-30	1,000
U-236	Total U	<1.0E-30	1,000	<1.0E-30	1,000
U-238	Total U	<1.0E-30	1,000	<1.0E-30	1,000
Y-90	60	4.86E-28	1,000	3.13E-22	1,000
Zr-93	2,000	<1.0E-30	1,000	<1.0E-30	1,000
Total alpha	**15**	**<1.0E-30**		**3.85E-27**	
Total Ra	**5**	**<1.0E-30**		**<1.0E-30**	
Sum of beta-gamma MCL fractions		**4.31E-02**		**4.27E-02**	

** MCL values for beta and photon emitters are calculated in Table II-3 of FR-00-9654 based on a beta-gamma dose of 4 mrem/yr

NC = Not Calculated

APPENDIX B

PEAK RADIOLOGICAL 1-METER CONCENTRATION TABLES IN 1,000 YEARS

Table B-1: Peak Radiological 1-Meter Concentrations in 1,000 Years

Radionuclide	MCL** (pCi/L)	Peak Concentration in 1,000 years	
		(pCi/L)	Year Peak Occurs
Ac-227	NC	8.76E-28	1,000
Al-26	NC	<1.0E-30	1,000
Am-241	Total α	<1.0E-30	1,000
Am-242m	Total α	<1.0E-30	1,000
Am-243	Total α	<1.0E-30	1,000
Ba-137m	NC	1.83E-14	1,000
C-14	2,000	3.03E-23	1,000
Cf-249	Total α	<1.0E-30	1,000
Cf-251	Total α	<1.0E-30	1,000
Cl-36	700	6.84E-04	774
Cm-243	Total α	<1.0E-30	1,000
Cm-244	Total α	<1.0E-30	1,000
Cm-245	Total α	<1.0E-30	1,000
Cm-247	Total α	<1.0E-30	1,000
Cm-248	Total α	<1.0E-30	1,000
Co-60	100	<1.0E-30	186
Cs-135	900	3.90E-09	1,000
Cs-137	200	1.83E-14	1,000
Eu-152	200	<1.0E-30	808
Eu-154	60	<1.0E-30	346
Gd-152	NC	<1.0E-30	1,000
H-3	20,000	3.39E-08	374
I-129	1	2.10E-01	836
K-40	NC	1.35E-08	1,000
Nb-93m	1,000	<1.0E-30	1,000
Nb-94	NC	<1.0E-30	1,000
Ni-59	300	2.52E-17	1,000
Ni-63	50	1.23E-18	1,000
Np-237	Total α	1.01E-22	1,000
Pa-231	Total α	6.92E-25	1,000
Pb-210	NC	1.74E-29	1,000
Pd-107	NC	2.55E-18	1,000
Pt-193	3,000	4.18E-22	1,000
Pu-238	Total α	<1.0E-30	1,000
Pu-239	Total α	<1.0E-30	1,000
Pu-240	Total α	<1.0E-30	1,000
Pu-241	300	<1.0E-30	1,000
Pu-242	Total α	<1.0E-30	1,000
Pu-244	Total α	<1.0E-30	1,000

Table B-1: Peak Radiological 1-Meter Concentrations in 1,000 Years (Continued)

Radionuclide	MCL** (pCi/L)	Peak Concentration in 1,000 years	
		(pCi/L)	Year Peak Occurs
Ra-226	Total α/Ra	3.56E-27	1,000
Ra-228	Total Ra	<1.0E-30	1,000
Rn-222	NC	3.56E-27	1,000
Se-79	NC	<1.0E-30	1,000
Sm-151	1,000	<1.0E-30	1,000
Sn-126	NC	<1.0E-30	1,000
Sr-90	8	3.02E-17	1,000
Tc-99	900	1.71E+01	1,000
Th-229	Total α	<1.0E-30	1,000
Th-230	Total α	<1.0E-30	1,000
Th-232	Total α	<1.0E-30	1,000
U-232	Total U	<1.0E-30	1,000
U-233	Total U	1.18E-28	1,000
U-234	Total U	<1.0E-30	1,000
U-235	Total U	<1.0E-30	1,000
U-236	Total U	<1.0E-30	1,000
U-238	Total U	<1.0E-30	1,000
Y-90	60	3.02E-17	1,000
Zr-93	2,000	<1.0E-30	1,000
Total alpha	**15**	**1.02E-22**	
Total Ra	**5**	**3.56E-27**	
Sum of beta-gamma MCL fractions		**2.29E-01**	

** MCL values for beta and photon emitters are calculated in Table II-3 of FR-00-9654 based on a beta-gamma dose of 4 mrem/yr

NC = Not Calculated